Department of Experimental and Health Sciences

Faculty of Health and Life Sciences

Universitat Pompeu Fabra

Doctoral Thesis 2020

Endothelial Snail1 in angiogenesis and tumorigenesis

Dissertation presented by

David CABRERIZO GRANADOS

For the degree of Doctor in Biomedical Sciences

Work carried out under the supervision of Dr Antonio GARCÍA DE HERREROS and Dr Raúl PEÑA ARRANZ in the Mechanisms of tumorigenesis and tumor progression in the Cancer Research Program in the Insititut Hospital del Mar d'Investigacions Mèdiques (IMIM)

Barcelona 2020

Dr Antonio GARCÍA DE HERREROS (Thesis co-director and tutor)

Dr Raúl PEÑA (Thesis co-director)

David CABRERIZO GRANADOS (PhD student)

A mi abuela Isabel.

ABSTRACT

Snail1 is a transcriptional factor with a great relevance in tumor development as it is required for epithelial to mesenchymal transition and activation of cancer-associated fibroblasts (CAF). In this thesis, we reported that tumor endothelial cells did also express Snail1, being key for angiogenesis, by promoting endothelial cell migration, invasion and tubulogenesis *in vitro*. Those roles are associated to Snail1 induction by FGF2 and VEGF-A, leading to gene expression profile change in endothelial cells and modulation of their activation status. Specific Snail1 depletion in the endothelium of adult mice does not promote an overt phenotype; however, it controls angiogenesis and vessel morphology in Matrigel plug assay. Moreover, endothelium-specific Snail1 depletion in the MMTV-PyMT breast cancer murine model delays the initiation of neoplasms, being less advanced and with a papillary morphology, which was corroborated by orthotopic breast tumor inoculation model. These *in vivo* effects are associated to the inability of Snail1-deficient endothelial cells to promote a full *in vitro* and *in vivo* activation of fibroblasts through a reduced FGF2 and CXCL12 signaling; as well as to sustain a complete *in vivo* angiogenesis, with wider and less invasive neo-vessels. Similar changes on tumor onset and morphology are observed by the pretreatment of MMTV-PyMT mice with the angiogenic inhibitor bevacizumab. Checking those results in human breast tumor samples, papillary carcinomas are less advanced and exhibit lower levels of Snail1 expression, both in vessels and in associated stromal cells, compared to no special type breast carcinomas. Furthermore, TCGA consortium breast tumors datasets show a strong correlation between vasculature and stromal activation, as well as better survival and prognosis in tumors mimicking the molecular profile of breast tumor endothelium-Snail1 depletion mice. Altogether, these findings establish a new role for Snail1 in endothelial cells, not only in angiogenesis but also in tumor onset, development and phenotype.

RESUMEN

Snail1 es un factor de transcripción con una gran relevancia en el desarrollo tumoral, siendo necesario para la transición epitelio-mesénquima y la activación de fibroblastos asociados al cáncer (CAF). En esta tesis, hemos descrito la expresión de Snail1 en células endoteliales de tumor, teniendo un papel fundamental durante la angiogénesis y promoviendo su migración, invasión y creación de túbulos *in vitro*. Estas funciones están asociadas a la inducción de Snail1 por FGF2 y VEGF-A, que generan un cambio en el patrón de expresión génica en las células endoteliales y modulan su nivel de activación. La depleción específica de Snail1 en el endotelio de ratones adultos no provoca un cambio fenotípico evidente; sin embargo, sí controla la angiogénesis y la morfología de los vasos en ensayos de *plugs* de Matrigel. Además, la eliminación específica de Snail1 en el endotelio del modelo murino de los tumores de mama espontáneos MMTV-PyMT provoca el retraso en la iniciación de tumores, siendo éstos menos avanzados y con una morfología papilar. Estos efectos *in vivo* están asociados a la incapacidad de las células endoteliales sin Snail1 de promover una activación completa de fibroblastos *in vitro* e *in vivo*, debido a una reducida señalización de las vías de FGF2 y CXCL12; ni de generar una angiogénesis completa *in vivo*, con *neovasos* más anchos y menos invasivos. Cambios similares en la iniciación de los tumores y en su morfología se observaron en ratones MMTV-PyMT pretratados con el antiangiógenico bevacizumab. En muestras de pacientes de cáncer de mama, los carcinomas papilares son menos avanzados y muestran menores niveles de expresión de Snail1, tanto en vasos como en el estroma, comparados con los carcinomas sin tipo especial. Asimismo, la base de datos de tumores de mama del consorcio TCGA muestra una fuerte correlación entre la vasculatura y la activación estromal, al igual que una mayor supervivencia y mejor prognosis en tumores con un perfil molecular semejante a los tumores de mama murinos sin Snail1 en su endotelio. En resumen, estos hallazgos establecen un nuevo papel para Snail1 en las células endoteliales, no solo durante la angiogénesis, sino también en la iniciación, desarrollo y fenotipo tumoral.

TABLE OF CONTENTS

LIST OF FIGURES

INTRODUCTION

MATERIALS & METHODS

RESULTS

DISCUSSION

LIST OF TABLES

INTRODUCTION

MATERIALS & METHODS

ACRONYMS AND ABBREVIATIONS

αSMA	α Smooth Muscle Actin
AKT	Protein Kinase B (PKB)
BBB	Blood-Brain Barrier
BMP	Bone Morphogenetic Protein
BSA	Bovine Serum Albumin
CAF	Cancer Associated Fibroblasts
CCL2	Chemokine Ligand 2
CD10	Cluster of Differentiation 10
CD31	Cluster of Differentiation 31
cDNA	complementary DesoxyriboNucleic Acid
CK14	CytoKeratin 14
CK5	CytoKeratin 5
Cre	Circular recombinase especific
CTGF	Connective Tissue Growth Factor
CXCL12	C-X-C motif chemokine Ligand 12
DAPI	5', 6-DiAmidino-2-PhenylIndole
DLL4	DeLta-Like-4
DMEM	Dulbecco's Modified Eagle's Medium
DMSO	DiMethyl SulfOxide
E-Cadh	E-Cadherin / Cadherin 1
ECM	ExtraCellular Matrix
EDTA	EthyleneDiamineTetra-Acetic acid
EGF	Epidermal Growth Factor
EMT	Epithelial to Mesenchymal Transition
EndoMT/EndMT	Endothelial to Mesenchymal Transition
EpCAM	Epithelial Cellular Adhesion Molecule
ePyMT	epithelial cells derived from PyMT tumors
ER	Estrogen Receptor
ERK	Extracellular signal-Regulated Kinase
FBS	Fetal Bovine Serum
FGF2	Fibroblast Growth Factor 2
FGFR	Fibroblast Growth Factor Receptors
FN1	Fibronectin 1
FW	ForWard
GM-CSF	Granulocyte Macrophage Colony-Stimulating Factor
H&E	Hemtoxylin and Eosin

HA	Human influenza hemagglutinin
HEK-293	Human Embryonic Kidney 293 cells
HER2	Human Epidermal growth factor Receptor 2
HGF	Hepatocyte Growth Factor
HIF-1α	Hypoxia-Inducible Factor 1 α
HUVEC	Human Umbilical Vein Endothelial Cells
IF	ImmunoFluorescence
IgG	Immunoglobulin G
IHC	ImmunoHistoChemistry
IL	InterLeukin
KO	Knock-Out
LoxP	Locus of x-over P1
LSD1	Lysine-Specific Demethylase 1
Lyve-1	Lymphatic vessel endothelial hyaluronan receptor 1
MEF	Mouse Embryonic Fibroblasts
MMP	Matrix MetalloProteinases
MMTV	Mouse Mammary Tumor Virus
mRNA	messenger RiboNucleic Acid
MSC	Mesenchymal Stem Cells
MTT	3-(5, 5-diMeThylThiazol-2-yl)-2,5-diphenyltetrazolium bromide
N-Cadh	N-Cadherin
NES	Nuclear Export Signal
NES	Normalized Enrichment Score
NMuMG	Normal Murine Mammary Gland epithelial cells
NST	No Specific Type
OptiMEM	Opti-minimal Essential Medium
p-AKT	phosphorylated AKT
PBS	Phosphate Buffered Saline
PCR	Polymerase Chain Reaction
PDGF	Platelet-Derived Growth Factor
PD-L1	Programmed Death-Ligand 1
PDX	Patient Derived Xenograft
p-ERK	phosphorylated ERK
PFA	ParaFormAldehyde
PGE_2	ProstaGlandin E2
Plat-E	Platinum-E cells
PPP	Pentose Phosphate Pathway
PR	Progesterone Receptor
PyMT	Polyoma virus Middle T antigen

qPCR	quantitative Polymerase Chain Reaction
RT	Room Temperature
RV	ReVerse
S100A4	S100 Calcium Binding Protein A4
SDS	Sodium Dodecyl Sulfate
SEM	Standard Error of the Mean
shRNA	short hairpin RiboNucleic Acid
siRNA	small interfering RiboNucleic Acid
TBS	Tris Buffered Saline
TBS-T	Tris Buffered Saline-Tween
Tet	Tetracycline
TGF-β	Transforming Growth Factor β
TNBC	Triple Negative Breast Cancer
VE-Cadh	Vascular Endothelial Cadherin
VEGF-A	Vascular Endothelial Growth Factor A
VEGFR	Vascular Endothelial Growth Receptors
VVO	Vesiculo-Vacuolar Organelles
WB	Western Blot
WT	Wild Type

INTRODUCTION

1. Breast Cancer

Cancer is a tissue-specific disease. It is characterized by an abnormal uncontrolled growth of cells, causing the halt of the normal function of the organ, with what it entails in the whole physiology.[1] In the particular case of breast cancer, it is a highly predominant and diverse disease.

1.1 Demographics, incidence and mortality

Worldwide, in 2018, 18 million people have been diagnosed with cancer, and 10 million cases were recorded, being one of the leading causes of mortality.[2] In Spain, it is estimated that during 2018, 32.000 patients were diagnosed with cancer and 6.600 died because of it.[3]

In fact, if we take a deeper look in the statistics of the most diagnosed cancers, we find that lung and breast share the first position of the charts. Breast cancer can be found in women and men, but the incidence in men does not reach 1% of all breast cancer patients.[4] Among women, breast cancer is the most common one, representing 25% of all tumors diagnosed in women around the world. Even though breast cancer mortality has decreased significantly in western societies during the past 20 years, nowadays, it is still one of the most important causes of death among them.[4,5] In Spain, breast cancer is the most frequent type of cancer diagnosed in women, being the leading type of cancer mortality.[3]

Therefore, breast cancer can be considered a challenge in terms of incidence and mortality, thus, it needs to be addressed by extensive research on it.

1.2 Morphology of the breasts

First, we need to explore the morphology of the normal breasts, specifically women breasts, to put this thesis into context. Anatomically, women have more developed breasts than men since they undergo very important physiological changes, related to

pregnancy. This is the main reason why the incidence of breast cancer is higher in women than in men. Women breasts are composed of two main tissues:

- **Adipose tissue**. This tissue consists of white adipocytes that wrap and intermingle the glandular tissue in variable amounts. Its proportion varies under several conditions, such as obesity, age, pregnancy or lactation.[6] Normally, this tissue is not the cradle of tumors.
- **Glandular tissue**. It is composed of lobules (acinar cells grouped in clusters) connected by ducts, formed by a process called branching morphogenesis, converging on the nipple.[7] During lactation, the acini of the lobules produce milk that is secreted to the empty lumens found in the ducts, to be finally expelled by the nipple. The glandular tissue does not distribute uniformly among the breast, being more abundant in the axillar region, where there is a greater frequency of neoplasias.[6] The glandular tissue suffers more changes than the adipose one, mainly due to puberty and pregnancy, associated to tissue remodeling. That bombardment of hormones is thought to trigger most breast tumors, mainly in the glandular section.[8]

1.3 Classification of breast tumors

Physicians have known for decades that breast cancer cannot be grouped as a single disease, but it is rather a complex, heterogenous illness. Therefore, there was a need for classifying the different breast tumor types to treat them adequately. Over time, the classification of breast neoplasias has evolved. Firstly, a simple staging of the tumors was sufficient; however, nowadays, it is compulsory a deep histological and molecular analysis in order to treat them properly.

1.3.1 Classical staging

Between 1943 and 1952, Pierre Denoix mastered and stated a method to classify solid tumors using their size and extension, lymph nodes invasion and metastatic status.[9] Up

to today, this method is the most used worldwide and it is known as TNM system, which refers to: [10]

- **T**: Size and extent of the primary tumor. In this case, we find the following categories:
    - **TX**: primary tumor cannot be measured.
    - **T0**: primary tumor cannot be found.
    - **Tis**: primary tumor has not started growing into healthy breast tissue.
    - **T1, T2, T3, T4**: the higher the number, the bigger the tumor is or the more it has infiltrated surrounding tissues. In this category, a, b or c can be added in order to subdivide each degree in subtle changes of the primary tumor size.
- **N**: degree of spread to regional lymph nodes.
    - **NX**: tumors in surrounding lymph nodes cannot be measured.
    - **N0**: tumors in surrounding lymph nodes cannot be found.
    - **N1, N2, N3**: the higher the number, the more lymph nodes that contain tumors.
- **M**: presence of distant metastases.
    - **MX**: metastasis cannot be measured.
    - **M0**: tumor has not spread to other parts of the body.
    - **M1**: tumor has spread to distant parts of the body.

In some cases, TNM classification can be grouped into five stages which comprise similar information: [11]

- **Stage 0**: abnormal cells are present but have not spread to surrounding tissues. It is not considered cancer, although it has the potential.
- **Stage 1, 2, 3:** the higher the number, the bigger and the more spread to remote tissues is the primary tumor.
- **Stage 4**: the primary tumor has spread to distant parts of the body.

The TNM method provides a standardized system to classify solid tumors providing some hints of its severity. Nevertheless, it does not deepen sufficiently in the tumor,

lacking some other analysis to manage the disease properly, such as its histology. Currently, the histological and molecular classifications are mainly used to determine the treatment of breast cancer patients.[8]

1.3.2 Histological subtypes

As mentioned before, one of the classifications with highly clinical relevance is the histotype of the tumors. This method started in the early 90's and it is used up to these days. In this case, breast tumors can be broadly classified in preinvasive or invasive tumors:[8,12–14]

- **Preinvasive tumors.** They represent a minority of breast tumors. They are characterized by the confinement of tumoral cells in the basement membrane of the glandular tissue. According to the location of the tumor, we are able to distinguish two subtypes:
    - **Ductal Carcinoma *In Situ* (DCIS).** Tumoral cells spread along the ducts misshaping its architecture.
    - **Lobular Carcinoma.** Tumoral cells grow within the lobules instead of the duct, without altering its architecture.
- **Invasive tumors.** This category represents the majority of breast tumors. In this case, tumoral cells extend beyond the basement membrane of the breast duct epithelia. These invasive tumors evolve from their preinvasive precursors, hence, we can also distinguish two subtypes: [15]
    - **Invasive Ductal Carcinoma (IDC).** The majority of breast tumors are IDCs. They can cause a fibrotic response, leading to a detectable mass during palpable examination. IDC can be further subclassified reflecting from low to high aggressiveness of the tumor:
        - **Grade 1** – Well differentiated tumors.
        - **Grade 2** – Moderately differentiated tumors.
        - **Grade 3** – Poorly differentiated tumors.

- **Invasive Lobular Carcinoma (ILC).** They represent a very residual set of breast tumor cases. They cause such a minimal fibrotic response that they are hardly detected at palpable examination.

Regardless of the basement membrane status, DCIS and IDC can be further subclassified based on the morphological features of the tumors, since they are more heterogenous compared to the lobular tumors. The main morphological subtypes, from more to less frequent, shown in Figure I-1, are: [16,17]

- **No specific type (NST).** They do not have any specific differentiating feature. Most of tumors are included on it and share most of its features with the solid type.
- **Solid**. Tumor cells grow filling completely the duct in which they are, forming a compact, dense mass. Solid tumors tend to be highly aggressive.
- **Comedo**. Similarly to the solid, tumor cells grow forming a compact mass, but they present considerable areas of necrosis. They tend to be highly aggressive.
- **Cribiform**. Neoplastic cells have angulated epithelial nests in a sieve-like pattern, leaving spaces between the cancer cells within the duct. They tend to be mildly aggressive.
- **Papillary**. Tumor cells form finger like projections, called papules, around the fibrovascular axis, leaving clear spaces between those epithelial columns. Many papillary tumors are non-aggressive.
- **Micropapillary**. These tumors look like papillary, but they lack the fibrovascular cores. They are composed by tumor cells arranged in solid nests or tubules, surrounded by clear spaces. They tend to be very aggressive.
- **Mixed**. They encompass different morphological types in a single tumor.

Histology offers very valuable information in terms of aggressiveness.[13] Unfortunately, tumors arising from a common mutation can evolve into diverse morphologies, with different clinical outcomes.[18] Therefore, there was a need to unravel a method by which aggressiveness could be firmly stated and systematized. In light of this necessity, a molecular profile of breast tumors arose as a plausible solution.[13]

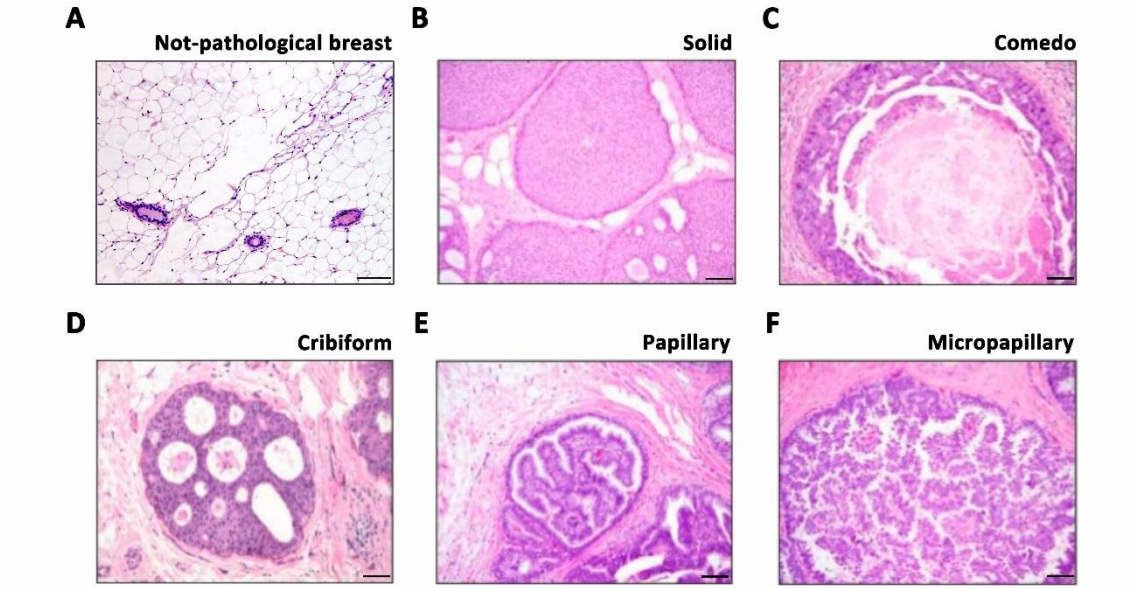

Figure I-1. Breast morphology in not-pathological and tumoral stages. A-F, Representative images of hematoxylin and eosin staining of not-pathological breast (A), solid carcinoma (B), comedo carcinoma (C), cribiform carcinoma (D), papillary carcinoma (E) and micropapillary carcinoma (F). Scale bar: 200 μm. Adapted from [19].

1.3.3 Molecular subtypes

The biology of breast tumors remained poorly understood until the 90's, when some light was brought to it. Expression of estrogen receptor (ER),[20,21] progesterone receptor (PR)[20] and protooncogenes like ERBB2, which synthetizes HER2/neu,[21,22] were discovered to have a link in the prognosis of breast tumors.

However, physicians found several drawbacks at classifying tumors since some of them did not completely fit with the known prognostic markers ER, PR and HER2. In the early 2000's, Perou, Sørlie and others began a revolution in terms of breast tumor classification, since they started to classify breast tumors analyzing their mRNA profile on microarrays.[23,24] Based on their studies, Cheang and colleagues developed the PAM50 classification.[25] This is a microarray-based gene expression analysis of the 50 more distinctive genes that Perou and Sørlie stated. Once performed, and following an unbiased hierarchical clustering, five intrinsic molecular subtypes of breast cancer were identified, recapitulated in Table I-1.[25]

Table I-1. Molecular classification of breast tumors.

Name	Frequency	Classical markers	Tumor cell proliferation	Main altered genes	Prognosis
Luminal A	40%	ER^{high} PR^{high} $HER2^{low}$	Low	ERS1, GATA3, FOXA1, XBP1	Good
Luminal B	20%	ER^{low} PR^{low} $HER2^{low}$	High	PI3KCA, ESR1, ERBB2 ERBB3	Intermediate
TNBC (triple negative)	15%	ER^{-} PR^{-} $HER2^{-}$	High	TP53, BRCA	Poor
HER2 enriched	15%	ER^{-} PR^{-} $HER2^{high}$	High	HER2, GRB7, PI3KCA	Intermediate
Claudin low	10%	ER^{-} PR^{-} $HER2^{-}$	High	CLDN3/4/7 SNAI1 ZEB1 CDH1 VIM	Poor

Adapted from [8,13].

Apart from having a proper classification of the breast tumors that help physicians in their decisions, there is still a huge need of basic and clinical research in the field of breast cancer, motivated by its high incidence, mortality and complexity.

1.4 Murine models of breast cancer

In order to research cancer development and test antitumoral therapies, *in vivo* murine models became an essential tool.[26] The fact that mice physiology resembles to the humans, that they can be easily genetically modified and that they are affordable to use prospective therapies, makes mice ideal for this objective. In the case of breast cancer, the first attempt to use mice as breast tumor models dates from 1903, when the first human breast tumor cell line was transplanted into a mouse.[27] Over time, several murine models have been generated: genetically engineered mice, syngeneic transplants, patient derived xenografts (PDX) and others.[26] Among others, we focused

our work on a genetically engineered spontaneous breast tumor mouse model, because of several advantages: [28]

- It can model all the stages of tumorigenesis, recapitulating physiologically the histopathology of human neoplasms.
- The tumor develops in a breast microenvironment, which resembles to the structure and physiology of the human breasts. Moreover, the same set of cells surrounding the tumor in mice are also found in human tumors, such as immune cells, fibroblasts and endothelial cells.
- They are able to generate genetically heterogeneous tumors, simulating human breast neoplasms.

Among several breast tumor mouse models, we chose the genetically modified MMTV-PyMT mouse model to be the main murine model of our research.

1.4.1 MMTV-PyMT model

The MMTV-PyMT mice were firstly generated in 1992 by Chantale Guy and colleagues.[29] In this model, the Polyomavirus Middle T antigen (PyMT) is expressed under the promoter of the Mouse Mammary Tumor Virus (MMTV) long terminal repeat. In particular, this mouse model mimics the tumorigenic events of the human breast tumors, reflected in Figure I-2, such as:

- **Molecular induction of tumorigenesis**. PyMT is a transmembrane protein that activates several signaling pathways, such as PI3K/AKT or ERK, which are altered in many human breast cancer cases.[30,31] Moreover, this activation leads to an increase of expression of several protooncogenes such as c-Myc, Bcl-2 or cyclin D1, resulting in an upregulation of proliferation and survival of cancer cells.[29,32]
- **Tissue specificity.** The expression of PyMT is controlled by the MMTV promoter, which is induced by glucocorticoid hormones secreted after puberty (around 6 weeks old in mice), namely in luminal cells of the mammary duct.[33,34] This feature gains resemblance to human breast tumors, since no breast tumors appear

before puberty.[35] However, apart from mammary ducts, there is a residual expression of PyMT in the ovaries and the salivary glands.[29]

- **Histology.** Tumor initiation and progression is divided in four phases: premalignant ducts, and tumors at hyperplasia, adenoma or carcinoma stage; which are comparable to human breast tumor histological grades.[34,36]
- **Molecular progression of the tumor.** There is a gradual loss of hormone receptors (ER and PR) and an overexpression of HER2 in late stage tumors, similar to luminal B type breast tumors.[37]

For those reasons, the MMTV-PyMT model fits properly in our research on breast tumorigenesis.

1.5 Breast cancer initiation and development

The specific mechanism by which breast cancer is initiated is currently unknown. It has been suggested that there might be several mutations in multiple cells (clonal evolution model) or in a single cell (cancer stem cell model), in which, in fact, cancer stem cells can grow in a clonal fashion.[38] However, independently of the cause of this epithelial outgrowth, non-epithelial cells that surround those cancer stem cells are extremely important for initial tumor progression. In fact, it was found that the most differential gene expression in tumor progression was in stromal cells rather than epithelial cells.[39,40] Myoepithelial cells, fibroblasts, extracellular matrix, adipocytes and endothelial cells are the most representative elements of the healthy breast tissue; therefore, they are key at the breast tumor stroma once tumor is initiated.[41]

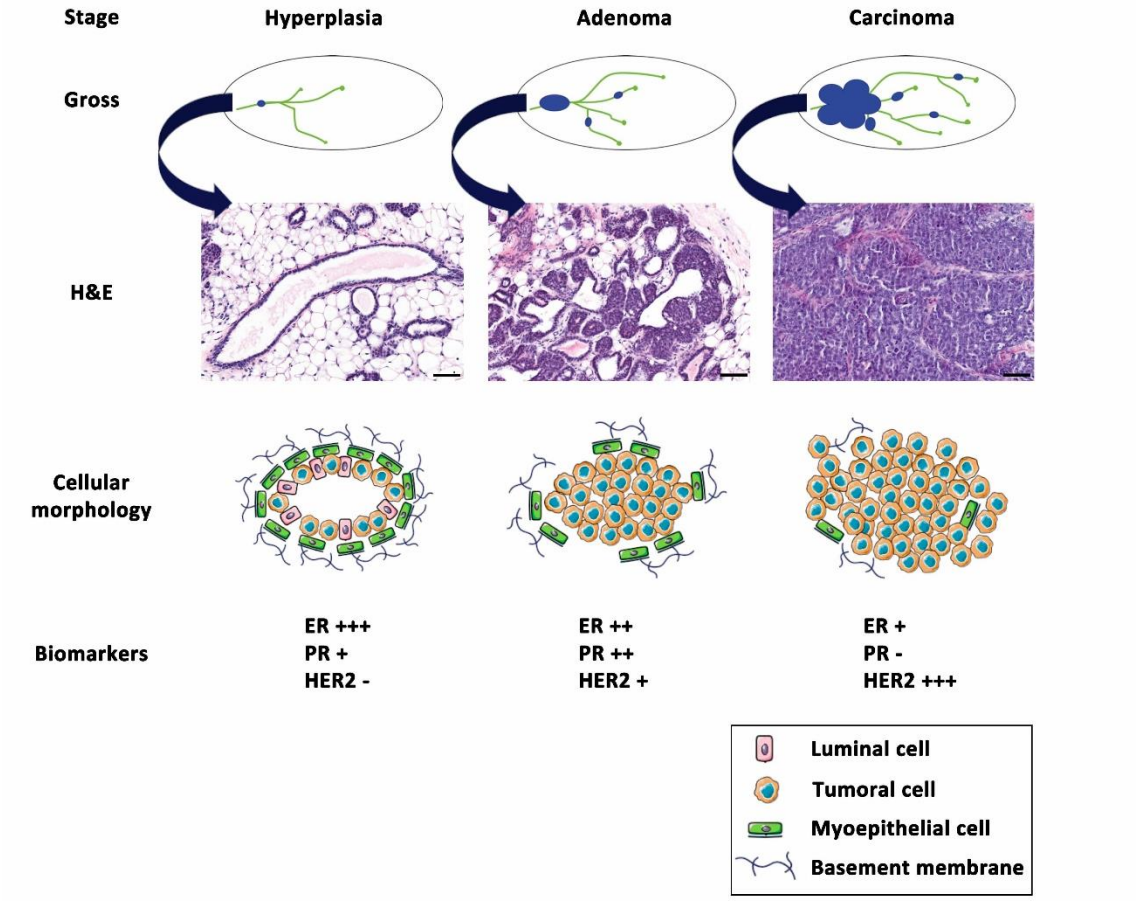

Figure I-2. Summary of tumor progression and biomarker expression in the MMTV-PyMT breast tumor mouse model.

1.5.1 Cellular composition of the breast

Among the principal structures in the breasts are lobules and ducts. Since most of cancers happen in the ducts, as well as in the MMTV-PyMT model, we are going to focus on the mammary ducts composition, reflected in Figure I-3:[42]

- **Luminal cells.** These epithelial cells are located in the apical surface of the breast ducts, closest to the lumen. During lactation, they are able to secrete milk due to the sensing of several hormones, mainly by estrogen and progesterone receptors.[43] Luminal cells can be distinguished by several markers, such as CK8/18, CK19 and EpCAM.[44]
- **Myoepithelial (or basal) cells**. They are localized surrounding the luminal cells. These myoepithelial cells are covered by a basement membrane, which is a

Laminin-rich structure that compartmentalizes luminal and myoepithelial cells from the stroma. Although they are epithelial cells, they express mesenchymal markers, such as αSMA. This special feature is essential for their function as helpers of the secretion of milk from luminal cells by contracting themselves.[45] Additionally, they do not express estrogen nor progesterone receptor. Myoepithelial cells can be detected by the distinguish expression of p63, CK5, CK14 and CD10.[44]

- **Fibroblasts.** These mesenchymal cells function as a scaffold around the myoepithelial cells by depositing extracellular matrix (ECM). Fibroblasts secrete many signaling molecules that act on epithelial cells promoting branching and ductal sprouts.[46] For instance, secreting FGF2, S100A4 or MMP3, that promote mammary epithelial cell branching and elongation.[47,48]
- **Extracellular matrix**. This structure is produced principally by fibroblasts. It is comprised mostly of fibrillar collagen and fibronectin; moreover, it contains several glycoproteins.[46] The main function of the ECM is to maintain tissue architecture by controlling the mechanical forces and regulate the cellular adhesion of the different cell types, being critical in retaining cell polarity and identity.[49]
- **Immune system**. Immune cells are also present in normal breasts, mostly myeloid progenitors. Their main function is to collaborate in the mammary duct branching.[50]
- **Adipocytes**. Apart from providing a scaffold for the whole mammary gland, adipocytes are the main reservoir of metabolites and signaling molecules which are key in the gland development and milk production.[51]
- **Endothelial cells.** Endothelial cells are the main cell type that form vasculature, encompassing blood and lymphatic vessels.[52] The mammary ducts, and the whole tissue, must be properly irrigated with vessels to provide cells with nutrients and exchange their residues. This cell type will be addressed in depth in future sections.

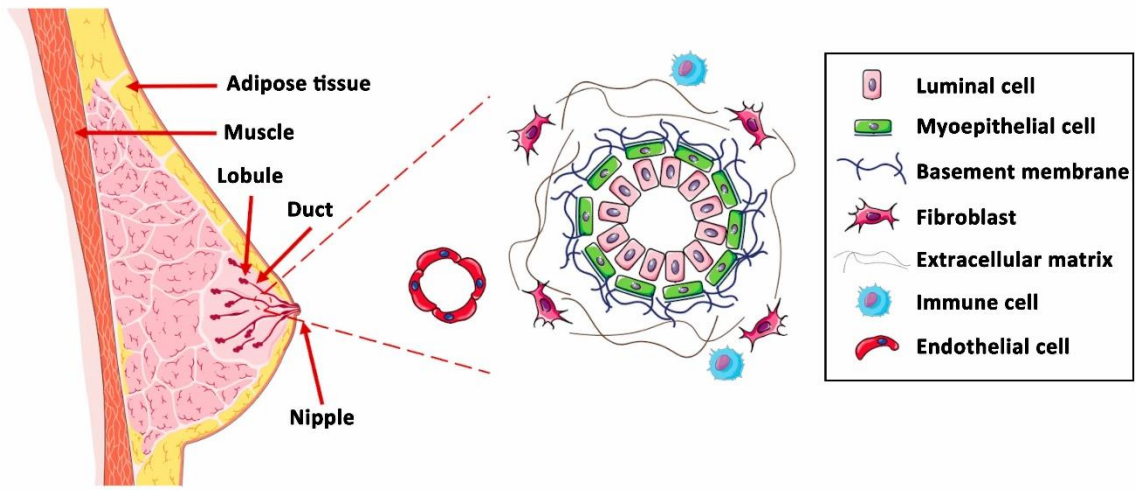

Figure I-3. Mammary duct composition. Scheme of the mammary gland and mammary duct.

1.5.2 Tumor associated stroma

Apart from the tasks of these different cell types in normal breast ducts, under tumorigenesis they are forced to acquire new roles. As mentioned before, luminal cells are the ones that usually turn malignant. The other cell types and the extracellular matrix that encompass the breast tissue are commonly known as stroma.[1] This stroma undergoes profound and intriguing changes caused by the crosstalk with the tumor cells, acquiring tumor suppressor or protumorigenic roles.[41,53] When the balance between both roles fall to protumorigenic ones, tumor progresses. Taking a deeper look into each stromal element with new acquired roles, we find:

- **Myoepithelial cells.** Myoepithelial cells are known by their tumor suppressor role.[54,55] As the tumor becomes invasive, luminal tumor cells grow massively, and can eventually cross through myoepithelial layer and the basement membrane. Moreover, as the tumor progress, myoepithelial cells disappear from invasive tumor areas, becoming an insignificant proportion in the whole tumor. However, in non-invasive tumors, as well as in certain advanced carcinomas, such as the papillary, the maintenance of myoepithelial cells is a unique trait.[56] Among their main functions as tumor suppressors, we find that myoepithelial cells interact with tumoral cells inducing morphogenic changes, avoiding their dedifferentiation; [57] myoepithelial cells secrete low amounts of MMP and high

levels of proteinase inhibitors, avoiding tumor invasiveness and progression; [58] and myoepithelial cells express angiogenic inhibitors such as soluble FGF2 receptors, blocking angiogenesis.[59]

- **Cancer-Associated Fibroblasts (CAF).** CAF are well known to have protumoral roles. CAF come mainly from those fibroblasts that remain inactive in the quiescent healthy mammary ducts. When they receive cytokines from the tumor cells, such as TGF-β, they become activated as CAF, acquiring new roles inside the tumor.[60] These CAF express high levels of their mesenchymal markers, such as αSMA, N-Cadherin or Vimentin, becoming more plastic.[61] Moreover, CAF begin to secrete signaling molecules like VEGF-A, CXCL12, FGF2, TGF-β, PGE_2 and other growth factors, keeping themselves active and, promoting many other effects, such as ECM remodeling, angiogenesis, tumor cell proliferation and cell motility and invasion in both, tumoral and non-tumoral cells.[62–65]
- **Tumor-associated ECM**. Tumorigenesis provokes a complete remodeling of the ECM, mainly supported by CAF activation. They can degrade normal ECM by the expression of several types of proteases, such as MMP, and deposit a new different ECM.[41] It is important to highlight that, among the components of this new ECM, proteoglycans play an important role, since they are sticky proteins that can sequester many growth factors, chemokines and cytokines. This hijack increases the concentration of those tumorigenic factors, which are released by MMP activity.[66] Furthermore, apart from modifying the composition of the ECM, CAF also align and stiffen the matrix due to the action of cross-linking enzymes. This property confers tumor protection against the immune system,[67] as well as protein tracks that activate tumor cells inducing them to grow and migrate, promoting eventual metastasis.[68,69] Therefore, tumoral ECM has a key role in tissue architecture and biochemistry, influencing deeply tumor initiation, growth, immune evasion and metastasis.
- **Immune system**. The immune cells undergo a dual process, mainly regulated by an intimate crosstalk with the tumor cells and tuned by other cell types. Firstly, they exert mostly as tumor suppressors, via active $CD4^+$ and $CD8^+$ T cells, NK cells

and tumor associated M1 macrophages. Nevertheless, the expression of PD-L1 by tumoral cells, as well as some other cytokines, turns the immune system to protumorigenic, in which mostly T regulatory cells and myeloid-derived stromal cells suppress all activity against tumor cells.[70]

- **Adipocytes.** This type of cell acquires protumoral roles in tumors. Adipocytes have more than just their basal function as scaffold. During tumorigenesis, adipose stromal cells are known as a source of multipotent mesenchymal stem cells (MSC).[71] In fact, MSC derived from adipose tissue may contribute to the progression of tumorigenesis, boosting tumor growth and invasion.[72]
- **Tumor endothelial cells**. Overgrowth of tumor cells lead to an increase in the demand of nutrients in order to fuel their progression.[73] This growth is supported by incrementing the number of blood vessels around the tumor, in a process called angiogenesis.[1] This phenomenon will be explained in detail in following sections.

All of this above explain how breast tumors promote their growth by causing the reprogramming and remodeling of the stroma surrounding them. In fact, it could be stated that tumor cells exploit the weaknesses of a normal microenvironment for their individual benefit.

2. Endothelial cells in basal and tumoral environments

One of the features that characterize the tumor microenvironment is the endothelial cells and, namely, the angiogenic process that undergo due to tumorigenesis, essential to provide nutrients to tumor cells. Nevertheless, we have to start addressing the outset of vasculature.

2.1 Vasculogenesis and vascular system

Vasculogenesis can be defined as the differentiation of endothelial precursor cells, or angioblasts, into endothelial cells and *de novo* formation of a primitive vascular network.[74] Vasculogenesis starts at embryogenesis, in particular after gastrulation, when there are three germ layer: ectoderm, endoderm and mesoderm. This last one will

give rise to hemangioblasts, a transient cell that has the ability to rapidly differentiate into a hematopoietic stem cell or an angioblast. Although FGF signaling is crucial for mesoderm induction, for the subsequent morphogenesis of the vascular system, VEGF signaling rules.[75] Specifically, the hemangioblast to angioblast transition is supported by the VEGF secretion of the endoderm, which induces VEGFR2 expression in the mesoderm by Snail1.[76] Following the vasculogenesis process, an accumulation of angioblasts generates the blood islands, considered the earliest perceptible vascular structures in the embryo.[77] Growth and fusion of multiple blood islands in the yolk sac of the embryo finally give rise to a primitive capillary network. Finally, once the vascular tone is settled, this primitive capillary network differentiates into an arteriovenous vascular system, resulting in a mature vasculature.[78]

Vasculature is essential for homeostasis. Animals depend on the blood supply to provide with nutrients and oxygen to the whole organism. In vertebrates, this blood supply occurs through blood vessels, which are formed by endothelial cells lined. The larger blood vessels are arteries, followed by veins. Arterioles and venules can be distinguished from both previous categories, as thinner versions of arteries or veins, respectively. Arteries and veins are formed by a layer of endothelial cells and a basal lamina, covered with smooth muscle cells, elastic fibers and connective tissue, thicker in arteries than in veins. Moreover, in the case of the arteries, pericytes do also cover them. Finally, capillaries are the smaller blood vessels structures formed uniquely by endothelial cells and pericytes.[79] I would like to remark that pericytes are mural cells embedded in the basement membrane throughout certain blood vessels, supporting vascular tone and vessel contraction.[80]

Blood vessels are quite unique, in fact, the endothelium can be physiologically different, behaving distinctively, depending on their location. For instance, liver, spleen, and bone marrow vasculature is formed by discontinuous endothelial cells that facilitate intercellular trafficking; whereas endocrine glands and kidney vasculature is composed by fenestrated endothelial cells that allow selective permeability.[81] However, they all share some common characteristics. For instance, the main role of the endothelium is to act as a semipermeable barrier that regulates the mobility of several molecules and

cells, out- and inwards the vessel lumen. For that, there are two different types of transport, the paracellular pathway (in which the intercellular tight junctions between endothelial cells are key) and transcellular pathway (based mainly in invaginations of the cell membrane called caveolae and pinocytic vesicles).[82] Apart from it, the endothelium has other roles, such as a mediator in inflammation by the secretion of interleukins, antithrombotic and procoagulant modulator and matrix production.[82] In fact, endothelial cells have polarity, which implicates the formation of a basal lamina surrounding them, which is mainly formed by Laminin and Col4a1.[82] It would be important to highlight that endothelial cells have some unique markers, being CD31 and VE-Cadherin the most known ones, which are intercellular junction proteins.[82]

In order to generate new vessels, essential for tissue growth and repair, endothelial cells have a remarkable capacity to adjust their number and rearrange themselves, following a process called angiogenesis.[83]

2.2 Tumor angiogenesis

Back in 1787, Dr John Hunter described blood vessels growing in the reindeer antler, coining the term angiogenesis for the first time.[84] Angiogenesis refers to the growth of new vessels from preexisting ones, which in the adult occurs restrictively during the ovarian cycle and in physiological repair processes, such as wound healing.[85] However, tumors are the most relevant scene of angiogenesis at adult age.

Tumors need to get vascularized due to its huge demand on oxygen and nutrients. This vascularization can occur through vessel co-option or angiogenesis. In the vessel co-option process, the preexisting vessels are hijacked by the tumor cells, growing along them.[83] On the other hand, angiogenesis is a process by which new blood vessels are formed from preexisting ones. [85]

In 1865, the formation of new capillaries in tumors was already reported.[86] In 1970, Dr Judah Folkman hypothesized that tumor growth might be dependent of new vessels formation.[87] Lately, in the mid-20th century, Greenblatt and colleagues observed that the vascular ramification depended on several secreted factors, among them, the

tumoral cells and a determined tumor environment.[88] Hitherto, tumor angiogenesis is seen as one of the key process of tumor sustenance, even named as one of the hallmarks of cancer stated by Hanahan and Weinberg.[1]

To analyze and understand properly angiogenesis, it can be divided in five different stages, commented below with a special scope on tumors, resumed in Figure I-4.

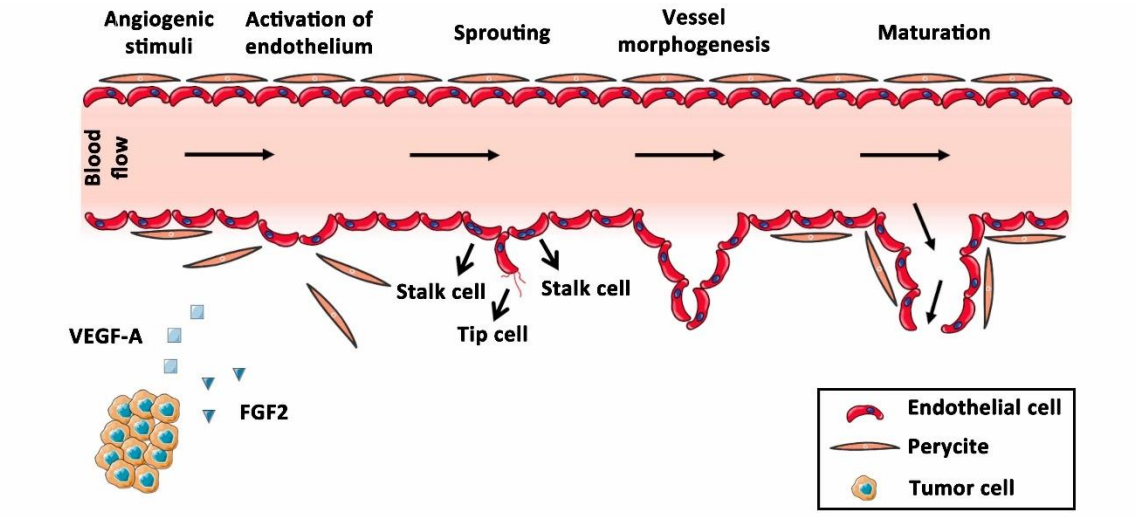

Figure I-4. Angiogenic process. Scheme of the different steps of angiogenesis.

2.2.1 Angiogenic stimuli

In 1968, Greenblatt and colleagues and Ehrmann and colleagues were the first ones to investigate the process of angiogenesis.[88,89] They observed that injecting subcutaneously tumor cells promoted the formation of new blood vessels, even when they put a filter between the tumor cells and the host. This was the first experimental outcome that led to think that there might be soluble factors that promoted this tumor angiogenic process.

From then, a vast set of experiments have been performed to bring some light into it. There has been reported that there are some specific proangiogenic molecules that initiate this process, as well as some specific inhibitory molecules that block it.[90] In fact, based on the actual knowledge, tumor angiogenesis is a balance between them. The main proangiogenic factors are the vascular endothelial growth factor (VEGF) family, angiopoietins, the members of the fibroblast growth factor (FGF) superfamily, platelet-

derived growth factor family (PDGF), transforming growth factors beta family members (TGF-β), tumor necrosis factor-alpha (TNF-α) and interleukins (IL). Regarding antiangiogenic factors, the main ones are thrombospondins (TSP), angiostatin and endostatin.[91] Apart from those, to a lesser extent some other factors, such as cell-matrix or cell-cell interaction, can also play a role regulating angiogenesis.[73]

Specifically, tumors start to awake endothelial cells, inducing the denominated 'angiogenic switch', in which the levels of some proangiogenic factors increase dramatically, being the main ones: [92]

- **VEGF**. There are five members of this cytokine: A, B, C, D and E, as well as several isoforms: VEGF121 VEGF145, VEGF165, VEGF183, VEGF189 and VEGF206. Nonetheless, VEGF-A_{165} (referred from now on as VEGF-A) is the most predominant one in solid tumors.[93]
- **FGF.** There are two members of this cytokine family directly related with angiogenesis, FGF1 and FGF2. Even though both are highly relevant in angiogenesis, FGF2 seem to be the major contributor in tumor angiogenesis, being accumulated in the ECM and being released by the action of MMP.[94,95]

These angiogenic factors are mainly produced by tumor cells when they sense low levels of oxygen, condition called hypoxia. In that particular case, tumoral cells overexpress and stabilize Hypoxia-inducible factor 1-alpha (HIF-1α), which is a very potent transcription factor that induces the expression of several angiogenic factors.[96,97] Apart from tumor cells, CAF and macrophages are also considered as providers of those cytokines, as well as other angiogenic factors.[73]

2.2.2 Activation of endothelium

During the 'angiogenic switch', cells forming vessels get activated: endothelial cells and pericytes. In the case of pericytes, they lose the contact with endothelial cells, to allow them to undergo a full activation process.[80] Endothelial cells are normally quiescent, which stands for a challengeless situation characterized by a static state.

Nevertheless, endothelial cells can initiate angiogenesis by proangiogenic factors at any moment.[92] Endothelial cells sense their presence by some specific receptors in their plasma membrane; the main ones are:

- **VEGF Receptors (VEGFR).** These transmembrane tyrosine kinase receptors are VEGFR1 (Flt-1), VEGFR2 (KDR) and VEGFR3 (Flt-4). VEGFR1 and VEGFR2 are closely related to angiogenesis, whereas VEGFR2 and VEGFR3, to lymphangiogenesis.[98] When VEGF-A is present in the tumor microenvironment, mainly VEGFR1 and VEGFR2 are able to sense it, which subsequently, activate VEGFR3 expression. These three receptors activate a cascade of phosphorylation, mainly through AKT and ERK pathways.[93]
- **FGF Receptors (FGFR).** There are four different FGFR, from 1 to 4. FGF2 binds to extracellular domain of these transmembrane tyrosine kinase receptors, which causes receptor dimerization and autophosphorylation of their tyrosine residues on their cytoplasmic domain, triggering the activation of ERK, AKT and STAT3 pathways.[99,100]

Regarding the hierarchy of FGF and VEGF pathways, some data suggest that FGF signaling lies upstream of VEGF; for instance, FGF2 is able to induce the expression of VEGF-A in endothelial and stromal cells.[101] Other data suggests the opposite; VEGF-A induces FGF2 production in endothelial cells.[102] Therefore, endothelial activation hinges upon a complex crosstalk between different angiogenic factors, numerous receptors and several signaling cascades.

2.2.3 Sprouting

The activation of VEGFR and FGFR provokes a change in the endothelial expression profile. In this context, the endothelial cells that sense more rapidly these angiogenic factor gradients gain some specific features, such as an increase of VEGFR2 and VEGFR3. That turns them in a highly specific type of endothelial cell, known as tip cells.[85,103]

Tip cells generate filopodia, with functional VE-Cadherin, acquiring a motile and invasive phenotype. They partially lose their EC-to-EC contacts degrade basal lamina, and generate new extracellular matrix proteins, guiding new blood vessel formation towards an angiogenic gradient, predominantly to tumor cells.[102] These tip cells overexpress Notch receptor Delta-like-4 (DLL4) ligand, provoking an increase of Notch signaling in their neighbor endothelial cells, blocking them to turn into tip cells and becoming stalk cells.[102,104]

Stalk cells follow tip cells and branch out from the preexisting vessel, establishing the vascular lumen and junctional connections to ensure the stability of the forming sprout. Stalk cells tend to be more proliferative and with fewer filopodia, compared to the tip cells. In this case, instead of high expression of VEGFR2 or VEGFR3, stalk cells express high levels of VEGFR1.[105]

This new structure, leaded by a unique tip cell and followed by some other stalk cells, forms a solid cord of endothelial cells, is designated as sprout. It will give rise to the new vessels, being responsible of the neo-angiogenesis.[102]

2.2.4 Vessel morphogenesis

Once sprouts are formed, a vessel lumen starts to be generated. Stalk cells are in charge of this lumen formation, which is key for the proper gaining of vascular tone. The first step for this process is the wrap of the planar endothelial cell sheet. Afterwards, cells in the middle of the 'cord' get eliminated in a process called cavitation. Finally, the cord gets hollowed by the flattening of the endothelial cells among the sprout.[106] Moreover, during the vascular lumen generation, endothelial vacuoles formation and fusion are crucial.[107]

At the end of this process, vessels may connect to each other in a process called anastomosis, which is based on the contact and fusion of endothelial cells with neighboring vessels.[108] Finally, there is an increase of the vascular network, although its functionality is compromised. The vascular tone is established but neo-vessels are highly permeable.[109] In terms of permeability, it can be inter or intracellular. In the case of the

intercellular trafficking, molecules or even whole cells, such as immune cells, can surpass the loose intercellular contacts of endothelial cells. On the other hand, regarding the intracellular trafficking, it is enhanced by an increase of vesiculo-vacuolar organelles (VVO), which are Caveolin 1 positive.[110,111]

2.2.5 Maturation

Finally, the new vessels might undergo a process of maturation. Even though the vessels are functional, they are still leaky and unstable.[109] That feature is partially solved by pericyte coverage, which provides a coverage to the vessels, making them more stable. That process is mainly orchestrated by Platelet Derived Growth Factor subunit B (PDGFb). Nevertheless, tumor vessels end with very few pericytes covering them, compared to normal capillaries, as a characteristic of aberrant tumor angiogenesis.[112]

Regarding tumor lymphangiogenesis, which is the formation of new lymphatic vessels from preexisting ones, the process is remarkably similar to tumor angiogenesis. In this case, the process is fueled due to the increase of the secretion of several growth factors and cytokines, which stimulate tumor cell growth and metastasis.[113] Moreover, VEGF-C and VEGF-D are the most relevant activator cytokines and VEGFR3 gain prominence as the main receptor in lymphatic endothelial cells.[114]

2.3 Crosstalk between endothelium and tumoral cells

Once formed, vessels interact mutually with the tumor cells in several ways. Needless to say, vessels interact with tumor cells by providing them with nutrients and oxygen. However, endothelial cells divide at a slower rate than tumor cells and angiogenesis cannot respond to tumor growth at the same rate,[112] emerging tumor areas characterized by low levels of nutrients and oxygen deficiency (hypoxia).[115,116] Altogether, that causes a profound modification on tumoral cells, mainly in their metabolism by an increase of glycolysis.[117]

On the other way around, tumor cells can further interact with the vessels, for instance, in the regulation of vessel morphology. Vessels adapt their morphology to the tissue. It is generally known that tumor vessels are highly irregular and aberrant, molecularly and morphologically. In fact, vessels present a highly variable lumen size and morphology in tumors.[118] Generally, intratumor vessels are comprised by the mechanical force executed by the proliferating tumor cells, causing the typical tortuosity and aberrancy of the tumor associated vessel.[119]

Moreover, blood and lymphatic vessels are the gate for tumor cells to evade from tumor primary sites to colonize other tissues (metastasis) and for immune cells to invade neoplasms and modulate their immune surveillance status. For example, at the first steps of metastasis, tumor cells weaken the adherent junctions of endothelial cells by the secretion of MMP, promoting their intravasation to the lumen of the vessels and, hence, their dissemination.[120,121] Moreover, tumor endothelial cells, by the effect of tumor cells, reduce their expression of adhesion molecules, such as Intercellular Adhesion Molecule 1 (ICAM1), limiting T-cell infiltration and modifying the immune response in the tumors.[122]

Apart from those interactions in tumors, it would be important to highlight that endothelial cells have been reported to have a paracrine role in fibrotic processes. Cao and colleagues demonstrated that lung chronic injury causes a recruitment of perivascular macrophages that secrete high levels of Wnt ligands, increasing Jagged1 in endothelial cells and, subsequently, activating Notch pathway in perivascular fibroblasts, and therefore inducing pulmonary fibrosis.[123] The same group published that hepatocyte growth factor (HPG) produced by endothelial cells diminishes the expression of profibrotic NOX4 protein in perivascular fibroblasts.[124] A few years later, Sanchez and colleagues discovered that upon proinflammatory stress, human dermal endothelial cells increased their expression of chemokine ligand 2 (CCL2), IL-6 and IL-8, which activate dermal fibroblasts.[124]

All of those roles dispel the traditional thought that endothelial cells are only relevant for delivery of nutrients and oxygen to the tumor cells, gaining a more intriguing and complex character.

2.4 Murine models to study endothelial cells

For the purpose of analyzing in depth the effects of vasculature, several mice models have been established. To analyze the effects of specific gene modifications in endothelial cells, two models have been stablished: transitory or permanent alterations in gene expression.[125] By using tetracycline (Tet) dependent strategies with a specific endothelial promoter, a repetitive switching of induction and suppression of gene expression can be obtained.[126] On the other hand, by using Cre recombinase dependent strategies, a permanent effect can be obtained. Among many options described in the literature, we chose a mouse strain that had the construct Cre-ERT2 under the promoter of VE-Cadherin (CDH5), specific for endothelial cells. Upon administration of tamoxifen, Cre-ERT2 is translocated to the nucleus where it can mediate Cre-loxP site-specific recombination of a certain floxed gene.[127] Therefore, this mouse model allows endothelia specific permanent gene expression abrogation in a temporally controlled manner.

2.5 Vasculature as a target in tumor suppressor therapies

Vasculature, indeed, has been targeted in the therapies against tumor progression. The first antiangiogenic drug approved for cancer treatment was bevacizumab, which was firstly used in advanced-stage colorectal cancer.[128] Bevacizumab is an antibody that recognizes VEGF-A and captures it, blocking angiogenesis. Nevertheless, bevacizumab did not show a clear effect in reverting tumorigenesis in several advanced tumor types.[129] Other more general antineoplasms drugs can be also considered antiangiogenic due to indirect effects on vascular development, such as sorafenib, pazopanib or sunitinib, among others. These molecules affect broadly tyrosine kinases receptors, such as VEGFR, FGFR or PDGFR, known as key proangiogenic activators in

endothelial cells. Nevertheless, due to their questionable effect in tumors, these treatments have not been extensively used alone against tumor progression.[130] However, it was observed that certain antiangiogenic drugs turn the abnormal structure and dysfunction of tumor vasculature into a functionally normal one, in a process called tumor vasculature normalization. That process results in an improvement of the tumor vessels in the delivery of, not only oxygen, but drugs.[131] In fact, antiangiogenics, such as bevacizumab, are currently used as neo-adjuvants or adjuvants with antimitotic drugs, such as paclitaxel or docetaxel, to improve the outcome of patients with breast cancer.[132]

Whereas as a single treatment or in combination with other drugs, antiangiogenic treatments need to increase their efficiency and specificity; therefore, more studies need to be performed in this field, in order to have further treatments approved by the drug regulatory agencies.

3. Snail1

3.1 Snail family transcription factors: structure and cellular function

The first time a member of the Snail superfamily was described, snail, was in 1984, in *Drosophila melanogaster*, where it was shown to be essential for the formation of the mesoderm.[133,134] It would not be until 1999, when Snail1 was described in *Homo sapiens*.[135] The Snail superfamily is divided into the Snail and Scratch families. Among the members of Snail family we find: Snail1, Snail2 (Slug) and Snail3; however, the most common ones are Snail1 and Snail2, since Snail3 has only been predicted *in silico*.[136] All Snail proteins are zinc-finger transcription factors. They all share a common structure, being composed of a highly conserved carboxy-terminal region, which contains from four to six zinc fingers.[137,138] Their zinc fingers correspond to the C2H2 type, which bind specifically to the E-box DNA sequence (CAGGTG). Moreover, these zinc fingers have nuclear translocation signals.[139–141] In the N-terminal region, there is a conserved SNAG domain that functions as a molecular hook for recruiting lysine-specific histone demethylase 1A (LSD1) to repress gene expression.[142] In conjunction, SNAG domain and

zinc fingers are key for the transcriptional repressor activity of Snail. To find the divergences between Snail1 and Snail2, we have to look in the central region of the protein. Snail1 has a regulatory domain containing a nuclear export signal (NES)[143] and a destruction box domain,[144] whereas Snail2 presents the SLUG domain, required for the efficiency of Snail2-mediated repression.[145]

Snail transcription factors are key in the epithelial to mesenchymal transition (EMT) process, by which static epithelial cells transform into motile and invasive mesenchymal cells.[146] This transformation occurs mainly by the repression of epithelial genes, mostly E-Cadherin, principally orchestrated by Snail family members.[139,146] Despite inducing a common expression profile of EMT genes, Snail1 and Snail2 have some differential gene expression patterns, implicating also a differential role in several physiological processes, such as embryonic development or tumorigenesis.[147–149]

Focusing our attention on Snail1, apart from the repression activity, it can act as a transcription activator depending on its acetylation or binding to different cofactors.[150,151] Furthermore, Snail1 activates AKT and ERK kinases.[152] Thanks to this activity, Snail1 in epithelial cells induces gain of expression of mesenchymal markers, such as Fibronectin, Vimentin, α-Smooth Muscle Actin or Matrix Metalloproteinases.[151,153,154]

Apart from EMT, Snail1 also boosts other features associated to this conversion. Upon its expression, tumor cells become more resistant to apoptotic insults such as several chemotherapeutic agents, reprogram their metabolism regulating glucose flux between glycolysis and pentose phosphate pathway (PPP), gain some characteristics typical of stem cells (such as telomere transcription and stability) and secrete cytokines (such as Granulocyte Macrophage Colony-Stimulating Factor, GM-CSF) that protect them from an immune attack.[155–160]

3.2 Snail1 regulation

Snail1 expression and function is regulated at multiple levels, from gene transcription to protein modifications, modulating its interaction with specific cofactors and, thus, its activity.[161] In terms of cytokines, Snail1 is rapidly induced by some of them, such as epidermal growth factor (EGF), hepatocyte growth factor (HGF), and several members of the following protein families: bone morphogenetic proteins (BMPs), TGF-β, Wnt and Notch.[162,163] Focusing on FGF and VEGF, as main angiogenic factors, both were shown to increase Snail1 levels in epithelial cells.[164,165] Moreover, tumoral conditions like hypoxia increases Snail1 levels.[166]

3.3 Physiological and pathological roles of Snail1

As previously stated, Snail1 is key at the induction of EMT. This process is fundamental during embryogenesis. In fact, Snail1 is highly expressed during gastrulation, as well as in the epithelial cells of the neural crest and in most mesenchymal cells.[167] Indeed, Snail1 expression is necessary for a proper gastrulation in murine embryos,[168] for left–right asymmetry determination[169] and for mesenchymal activation.[170]

Apart from its role at the very early stages of development, Snail1 is not expressed in adult tissues at quiescent state. Nonetheless, Snail1 is expressed during inflammatory processes. For instance, Snail1 accelerates wound healing and, its overexpression induces fibrosis in liver, lung and kidney.[151,171–173] Regarding inflammatory processes, tumors are described as a chronic inflammatory site; thus, Snail1 was prone to have a distinct role in cancer.[174]

In fact, Snail1 have several roles in different tumor cell populations. For instance, in epithelial cells, Snail1 is essential for tumor cell clonogenicity and metastasis, through the gain of motility and invasion abilities.[159] However, Snail1 is mostly expressed by CAF, whereas its expression in epithelial cells is confined to areas of invasion.[175] In CAF, Snail1 is induced by cytokines that promote fibroblast activation, such as TGF-β or PDGFb, reinforcing their role on CAF activation.[170,175] In accordance with this dual role in EMT and fibroblast activation, Snail1 depletion in adult transgenic mice retards tumor

development and prevents metastasis.[65,176] Due to all of this, expression of Snail1 has been analyzed in multiple tumors and it has been consistently related with poor prognosis.[177]

3.4 Snail1 in endothelial cells

Apart from being expressed in epithelial cells and CAF, Snail1 can also be expressed in endothelial cells.[178] Previous research stated that Snail1 is expressed in vascular cells during development, where is essential for the formation of a correct interconnected vascular network, necessary for the embryo viability.[179] Later research stated that the hemangioblast to angioblast conversion during vasculogenesis is governed through miR-200 repression by Snail1.[180] In fact, the effect of Snail1 in $Tie2^+$ endothelial cells over embryo viability occurs through the Snail1-Dll4/Notch1 axis.[181] However, recent research did not show that embryonic alterations in viability due to lack of Snail1 in $Tie1^+$ or VE-$Cadherin^+$ endothelial cells.[182] Apart from that, Snail1 is essential for a proper development of the heart valve.[183,184] Similarly, Snail1 was proved to be essential for ocular neovascularization, in terms of depth and branching formation, potentially through the gain of motility and invasion abilities of endothelial cells and the upregulation of VEGFR3.[185,186]

In adult tissues, Snail1 also plays a role in the Blood-Brain Barrier (BBB). The BBB is an extremely special layer of endothelial cells that control tightly the circulation of solutes into the extracellular fluid of the central nervous system.[187] During bacterial infections, the BBB loses their contacts increasing their permeability, so *E. coli* or *S. agalactiae* can pass through it easily. This loss of connection between endothelial cells is mediated by Snail1, whose presence is key for the permanence of tight junction proteins, such as occludin, claudins and ZO-1.[188,189]

At this point, it would be interesting to point out that Snail2 has also been reported to have a role in angiogenesis. Concretely, in endothelial cells, miR-151a controls Snail2 enhancing sprouting, associated with an alteration in the expression of membrane type 1 matrix metalloproteinase (MT1-MMP).[190,191]

Finally, both Snail1 and Snail2 have been reported to regulate the mesenchymal transition from endothelial cells, called Endothelial to Mesenchymal Transition (EndoMT or EndMT).[192] This process has been investigated by some laboratories, differentiating a complete EndoMT from a partial one, in which the identity of endothelial cells is not completely lost and presents a coexistence of endothelial and mesenchymal markers. This partial EndoMT is predicted to be essential for angiogenesis, since a gain of motility and invasion, due to the transition, are essential for the formations of sprouts. In case this partial EndoMT persists, endothelial cells might undergo a complete EndoMT.[192] This complete EndoMT has been proposed to contribute to the CAF population in tumors, up to 40% of total activated fibroblasts.[192–194] Regarding Snail1 and EndoMT, several laboratories reported a relation between them. For instance, it was stated that Snail1 is induced under low shear stress conditions, as well as by IL-1β, being an essential driver of EndoMT.[195,196] Moreover, recently, it has been published a relevant function on endothelial Snail1 inducing EndoMT, which contributes to renal fibrosis, reinforcing the role of Snail1 in this process.[182]

Regardless of the previous research performed, further investigation on Snail1 in endothelial cells and its role in angiogenesis and tumorigenesis needs to be performed, in order to develop better treatments for patients.

OBJECTIVES

Based on the previously exposed background research, we stated the main hypothesis that interlace this doctoral thesis:

Snail1 plays a key role in endothelial cells during the angiogenesis, required for tumor development.

In order to confirm this hypothesis, we asked ourselves several questions that guided this PhD:

- Could Snail1 modify endothelial cell identity?
- Could Snail1 regulate the expression profile and the sensing and response to angiogenic stimuli in endothelial cells?
- Could Snail1 expression be essential in endothelial cells for the process of angiogenesis?
- Could endothelial Snail1 expression have an effect in quiescent vasculature or in the physiology of the adult organism?
- Could Snail1 expression in endothelial cells be necessary for tumorigenesis?
- Could we translate our *in vitro* and *in vivo* results into a clinically relevant breast cancer treatment?
- Could we reproduce our results in human breast tumor physiology?

MATERIALS & METHODS

1. Reagents

The following reagents were used in this thesis: Alexa conjugated secondary antibodies (Life Technologies), Alexa Fluor 647 Phalloidin (Lifetechnology, A22287), Bevacizumab (Avastin, Roche), Biotin microbeads (MACS Miltenyi Biotec, 130-090-485), Blasticidin S (Merck-Sigma, 203350), Carboxymethylcellulose (Merck-Sigma, C4888), Cell Recovery Solution (Corning, 354253), DAPI (Merck-Sigma, D9542), DC Protein Assay (Bio-Rad, 5000116), DharmaFECT transfection agent (Dharmacon, 77T-2001-03), DMEM (Dulbecco's modified Eagle medium, Invitrogen), EpiCult-B culture media (Stemcell Technology, 05610), Epon LX112 (Ladd Research Industries), Evans blue (Merck-Sigma, E2129), FBS (Fetal Bovine Serum, GIBCO), goat mouse $F(ab')_2$ fragments (Jackson-Immunoresearch, 115-007-003), Fluoromount-G (Southern Biotech, 0100-01), GenElute Mammalian Total RNA Miniprep Kit (Merck-Sigma, RTN70), Hoescht 33342 (ThermoFisher, H3570), Hoeschst-33358 (ThermoFisher, H3569), human recombinant FGF2 (Merck-Sigma, GF003), human recombinant Insulin (ThermoFisher, 12585014), human recombinant TGF-β1 (Prepotech, 100-21), human recombinant VEGF-A (Peprotech, 100-20), Lenti-X Concentrator (Clontech, 631231), LightCycler 480 SYBR Green I Master (Roche, 04887352001), Lipofectamin 2000 (ThermoFisher, 11668019), Matrigel Growth Factor Reduced (Corning, 354230), mouse recombinant CXCL12/SDF1 (RND System, 460-SD-010), mouse recombinant FGF2 (PeproTech, 450-33), MTT (3-(4,5-Dimethylthiazol-2-yl)-2,5-Diphenitetrazolium Bromide, Merck-Sigma, M5655), Non-Essential Aminoacids 100x (ThermoFisher, 11140050), Opti-MEM Reduced Serum Medium (Thermo, 11058021), Plerixafor (Selleckchem, S3013), Puromycin dihydrochloride (Merck-Sigma, P8833), rat tail Collagen type 1 (ThermoFisher, 354236), RBC Lysis Buffer (Affymetrix, 00-4333), Retro-X Concentrator (Clontech, 631455), RPMI media 1640 (Invitrogen), siRNA control (Dharmacon, ON-TARGETplus control siRNA, D-001810-02-50), siRNA Snail1 (Dharmacon, SNAI1-targeting ON-TARGETplus siRNA pool, L-010847-01-0005), shRNA control (Merck-Sigma, SHC002V), shSnail1 (Merck-Sigma, TRCN0000063818 and TRCN0000063822, hereafter designated as shRNA 680 and shRNA 684, respectively), Tamoxifen (Merck-Sigma, T5648), Toluidine blue (Merck-Sigma, 115930), Transcription Factor Buffer Set (Pharmigen, 562574), Transcriptor First

Strand cDNA Synthesis kit (Roche, 0489703001), Trichrome Stain (Masson) Kit (Merck-Sigma, HT15), Tumor Dissociation Kit mouse (MACS Miltenyi Biotec, 130-096-730) and SU5402 (Merck-Sigma, 572630).

2. Ethical statements

Human tumor samples were obtained from Parc de Salut MAR Biobank (MARBiobanc) Barcelona. This study was approved by the Ethical Committee for Clinical Research from PRBB (reference code 2019/8663/I).

Animal experimental procedures were approved by the Animal Research Ethical Committee from the Parc de Recerca Biomèdica de Barcelona (Barcelona, Spain) and by the Generalitat de Catalunya (CEEA: AGH-19-0028-P1).

3. Immunohistochemistry

Human tumor samples were fixed 16 hours with formol at room temperature (RT). Mice tissues or tumors were fixed 16 hours with para-Formaldehyde (PFA, 4%) in PBS at 4°C. Collagen I embedded HUVEC spheroid and *in vivo* Matrigel plugs were fixed two hours with formol at RT. Fixed samples were dehydrated and paraffin embedded at the Anatomy Dpt. of the Hospital del Mar. When required, 2.5μm sections were done with a microtome (Leica, RM-2255) for immunohistochemical analysis. Routinely, a hematoxylin and eosin staining was performed for histological evaluation of tumor samples.

After standard deparaffination and rehydration of the samples, heat mediated retrieval was done for antigen unmasking in Tris-EDTA buffer (pH 9) or Citrate buffer (pH 6) for 15 minutes. Additionally, Collagen I or Matrigel containing samples were permeabilized with Triton X-100 (1%) and Tween-20 (1%) in PBS for 45 minutes at RT. Later, tissues were blocked during two hours in FBS (1%) and BSA (1%) in TBS and incubated with primary antibodies (listed in Table MM-1) for 16 hours. PowerVision$^+$ Poly-HRP IHC Detection system was used for signal amplification and DAB$^+$ kit for signal detection. Finally, hematoxylin counterstain was done.

For the indicated samples, Trichrome Stain (Masson) Kit was done following the manufacturer's instructions.

4. Cell culture

Cell lines, their culture medium and where they were obtained from, are recapitulated in Table MM-2. Standard medium was made of Dulbecco's Modified Eagle's medium (DMEM) supplemented with FBS (10%), L-Glutamine (2mM), sodium pyruvate (1mM), penicillin (100U/mL) and streptomycin (100µg/mL). All cell lines were cultured at 37°C with CO_2 (5%) in a humidified incubator (Heracell™ 150). Culture was performed in a BioSafety Level 1 Room (BSL-1, P1), except for lentivirus and retrovirus generation and cell infection, which was performed in a BioSafety Level 2 Room (BSL-2, P2).

5. Cell lysis, protein quantification and western blot

Cell extracts were obtained in SDS lysis buffer [SDS (2%), Tris-HCl (50mM) and glycerol (10%)]. Protein concentration was measured using the DC Protein Assay. For protein detection, SDS–PAGE was run and proteins were transferred to PVDF membranes. After specific primary antibodies incubation (listed in Table MM-1), HRP conjugated secondary antibodies and ECL, for signal development, were used. ECL signal was imaged in Alliance Q9 (UVITEC) chemiluminescence imager and, when indicated, intensity was quantified by ImageJ software.[197,198] Routinely, phosphorylated and non-phosphorylated versions of the same protein were detected in the same membrane, after membrane stripping during 15 minutes at 55°C with stripping buffer [SDS (4%), Tris 500mM pH=6,8, β-Mercaptoethanol (0.7%)].

6. Reverse transcription and real-time quantitative PCR

Total RNA was extracted using a GenElute Mammalian Total RNA Miniprep Kit. Up to 1µg of RNA per sample was translated to cDNA with the Transcriptor First Strand cDNA Synthesis kit. Finally, mRNA expression levels were determined using the LightCycler 480

SYBR Green I Master and specific primers, listed in Table MM-3, in a LightCycler 480 II (Roche) analyzer.

The relative quantification value for each target gene as compared with the calibrator for that target was expressed as 2−(Ct-Cc) (where Ct and Cc are the mean threshold cycle differences after normalizing to HPRT expression). All results were normalized to HPRT expression.

7. Immunofluorescence

Cells in culture were fixed by PFA (4%) in PBS during 10 minutes at 4°C and permeabilized during 10 minutes with Triton X-100 (1%) and Tween-20 (1%) in PBS at RT. Afterwards, cells were blocked with BSA (2%) in PBS during one hour at RT. Primary antibodies and corresponding Alexa conjugated secondary antibodies were diluted in blocking solution and incubated sequentially during one hour at RT. DAPI was used for counterstain nuclei and Fluoromount-G as mounting media.

Matrigel induced tubulogenesis samples were treated for one hour with Cell Recovery Solution at 4°C. Afterwards, cells were fixed with PFA (4%) in PBS during 20 minutes at RT and permeabilized with Triton X-100 (0.5%) in PBS during 10 minutes at 4°C. Later, samples were blocked with normal goat serum (10%) and goat anti-mouse $F(ab')_2$ fragments (20µg/mL) in IF buffer [NaCl (130nM), Na_2HPO_4 (7mM), NaH_2PO_4 (3.5mM), BSA (0.1%), Triton X-100 (0.2%) and Tween-20 (0.05%)] during one hour. Primary antibodies were diluted in IF buffer and incubated overnight at 4°C with gentle agitation. Corresponding Alexa conjugated secondary antibodies were diluted in IF buffer and incubated during two hours at RT with gentle rocking. DAPI was used for counterstain nuclei and Fluoromount-G as mounting media.

When indicated, Alexa 647 conjugated Phalloidin was incubated in a dilution 1/200 in IF buffer with secondary antibodies for Actin cytoskeleton staining.

Leica SP5 confocal microscope was used for imaging at Advanced Light Microscopy Unit of Centre Regulaciò Genòmica (Barcelona).

8. Snail1 induction in HUVEC

1.5x10^5 HUVEC were seeded per plate in 60mm plates in standard medium. The next day, the medium was changed to standard medium FBS (0%) for 3 days. Cells were trypsinized and 1.5x10^5 HUVEC were seeded per well in 24well plates with standard medium FBS (0%). 24 hours later, VEGF-A (50ng/mL) or FGF2 (100ng/mL) was added and protein or RNA was collected at indicated time points.

9. Snail1 knock down by siRNA transfection

3.3 x 10^5 HUVEC were seeded per plate in a 60mm plates. One day later, culture medium was exchanged to 3.5mL and cells were transfected using DharmaFECT transfection agent with 0.2nmoles of siRNA Control (siCtl) or siRNA against SNAI1 mRNA (siSnail1), according to manufacturer's instructions. Typically, cells were detached by trypsinization 24 or 48 hours later to be used in the referred experiments. Snail1 knock down by siRNA, at mRNA and protein levels, was confirmed in HUVEC at 24 hours (Figure MM-1A, B). Similar results were obtained at 48 hours (data not shown).

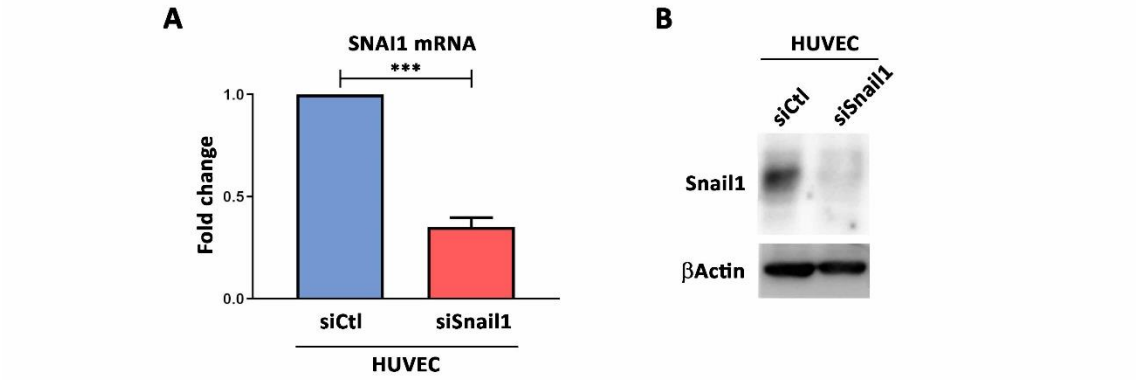

Figure MM-1. Silencing Snai1 gene by siRNA transfection in HUVEC on monolayer. A, Quantification of SNAI1 mRNA in HUVEC 24h after siCtl and siSnail1 transfection. **B**, Western blot analysis of Snail1 in HUVEC 24h after siCtl and siSnail1 transfection. Data in A represent mean values (± SEM) of at least three independent experiments. ***p<0.001.

10. Snail1 knock down by shRNA transfection

3.3 x 10^5 HUVEC were seeded per plate in a 60mm plates. One day later, culture medium was exchanged to Opti-MEM Reduced Serum Medium and cells were transfected using Lipofectamin 2000 with 5µg of Snail1 shRNA 680, Snail1 shRNA 684 or shRNA Scramble as a control, using manufacturer's instructions. Six hours after transfection, medium was exchanged to standard medium. Typically, cells were detached by trypsinization 48 hours later to be used in the determined experiments. Snail1 knock down by shRNA, at mRNA and protein levels, was confirmed in HUVEC (Figure MM-2A, B).

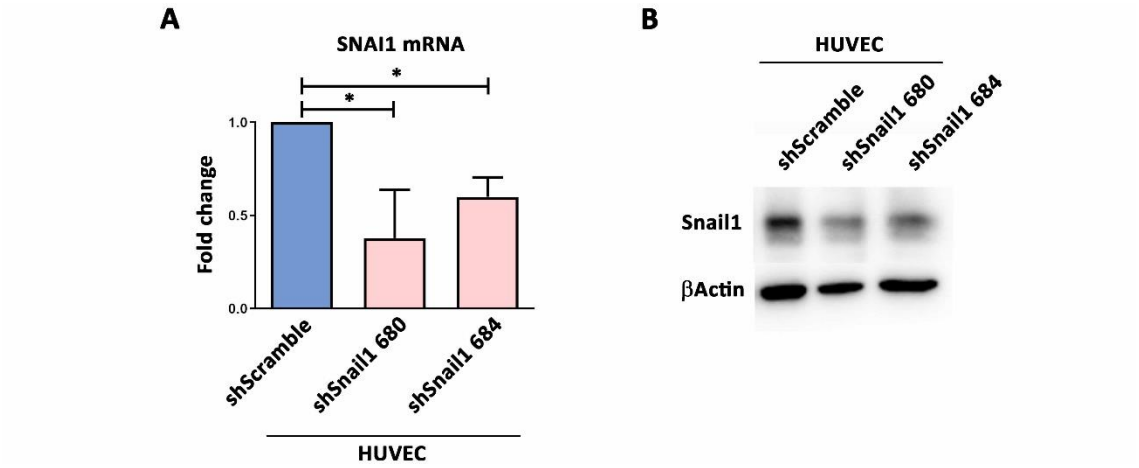

Figure MM-2. Silencing Snai1 gene by shRNA transfection in HUVEC on monolayer. A, Quantification of SNAI1 mRNA in HUVEC 24h after shScramble, shSnail1 680 or shSnail1 684 transfection. **B**, Western blot analysis of Snail1 in HUVEC 24h after shScramble, shSnail1 680 and shSnail1 684 transfection. Data in A represent mean values (± SEM) of at least three independent experiments. *p<0.05.

11. Virus production and cell infection

For lentivirus production, HEK-293T were plated in a 100mm plate and cultured to 90% of confluence. A mix of 3 vectors (3µg of pMDLg/pRRE, 1µg pRSV, 1µg pVSV-G) plus 5µg of pBABE vector carrying or not GFP was incubated with Lipofectamin 2000 in Opti-MEM Reduced Serum Medium, according to manufacturer's instructions. Then, these mixtures were added to HEK-293T in Opti-MEM medium, which was changed to standard medium five hours later. After 24 hours, medium was changed again to standard medium. At 48 and 72 hours after transfection, cultured medium was collected and filtered with 0.45µm low protein binding filters and mixed with Lenti-X Concentrator

in 1:3 proportions for one hour at 4°C. Afterwards, the mixture was centrifuged at 1500 g for 45 minutes at 4°C. Supernatant was discarded, the pellet was resuspended in 1mL of standard medium and stored at 4°C for no longer than 5 days.

For retrovirus production, Plat-E were plated in a 150mm plate, cultured to 90% of confluence. 5µg of pBABE vector carrying or not Snail1-HA, pRV vector carrying Snail2-HA-GFP or GFP (obtained from Alberto Muñoz's lab)[199], was incubated with Lipofectamin 2000 in Opti-MEM medium, according to manufacturer's instructions. Then, these mixtures were added to Plat-E in Opti-MEM medium, which was changed to standard medium five hours later. After 24 hours, medium was changed again to standard medium. At 48 and 72 hours after transfection, cultured medium was collected and filtered with 0.45µm low protein binding filters and mixed with Retro-X Concentrator in 1:3 proportions for 16 hours at 4°C. Afterwards, the mixture was centrifuged at 1500 g for 45 minutes at 4°C. Supernatant was discarded, the pellet was resuspended in 1mL of standard medium and stored at 4°C for no longer than 5 days.

HUVEC Snail1^{+} and Ctl cell line were generated by retroviral infection of pBABE vector carrying or not Snail1-HA in HUVEC WT, respectively (Figure MM-3A). One day after infection, puromycin (0.5µg/ml) was added to culture medium for three days for cell selection (Figure MM-3A). Clones were obtained by limiting dilution and their Snail1 and HA expression was checked at protein levels (Figure MM-3B-D).

HUVEC Snail2^{+} and Ctl cell line were generated by retroviral infection of pRV vector carrying Snail2-HA-GFP or GFP in HUVEC WT, respectively. Five days after infection, cells were single cell sorted through FACSAria II SORP (BD) to obtain clones.

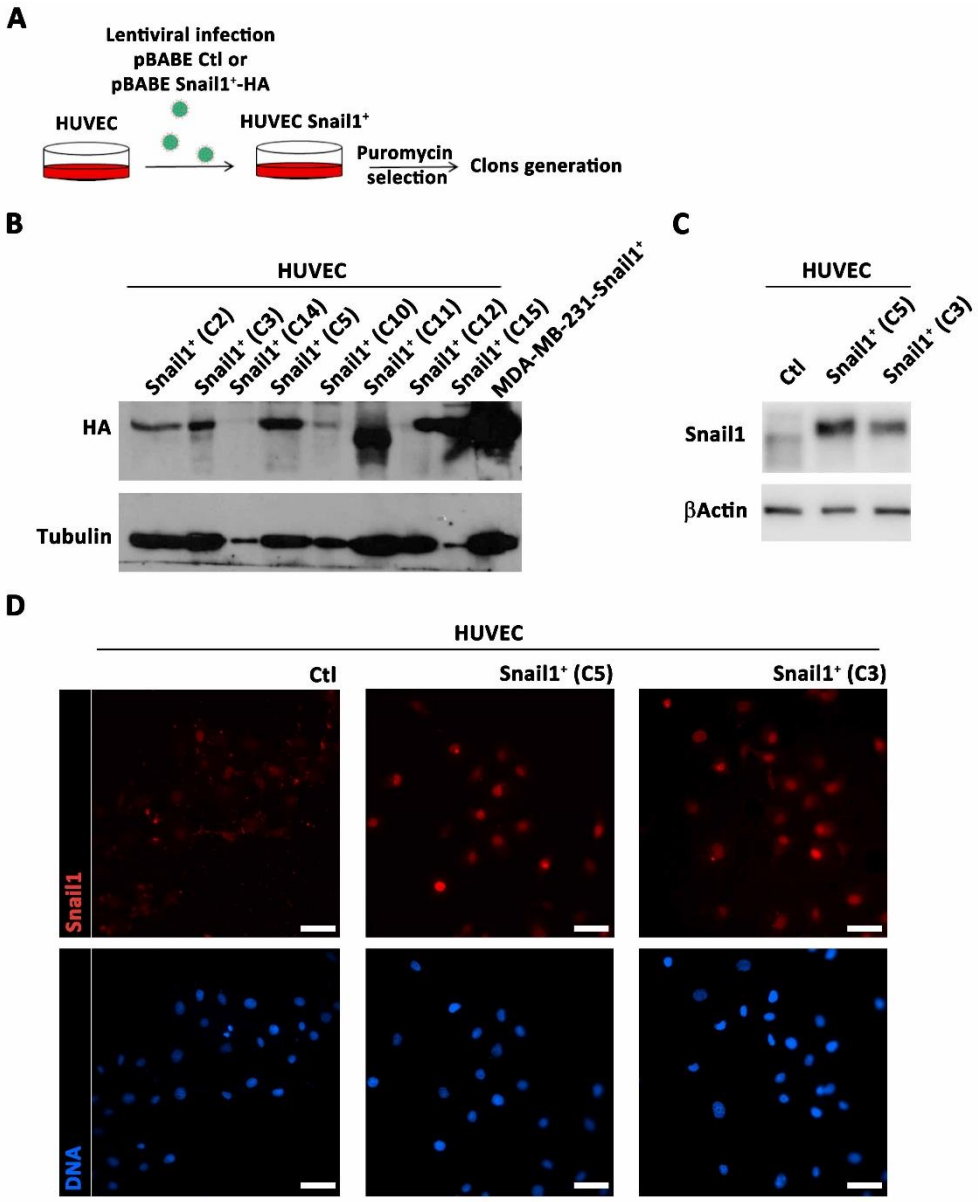

Figure MM-3. Generation of Snail1⁺ transfectants in HUVEC. A, Scheme of pBABE ctl or Snail1-HA lentiviral infection in HUVEC. **B**, Western blot analysis of HA in HUVEC Snail1⁺ clones and MDA-MB-231-Snail1⁺, as a positive control. **C**, Western blot analysis of Snail1 in HUVEC Ctl, Snail1⁺ (C5) and Snail1⁺ (C3). **D**, Snail1 immunofluorescence (red) in HUVEC Ctl, Snail1⁺ (C5) and Snail1⁺ (C3). Nuclei were counterstained with DAPI (blue). Scale bar: 30 μm.

12. Matrigel induced tubulogenesis assay

Fifty µL of Matrigel per well were polymerized at 37°C in 24-well plate. After 30 minutes, 1.1 × 10^5 HUVEC were seeded per well in 24well plates in standard medium. 500µL of standard medium, supplemented or not with VEGF-A (50ng/mL), FGF2

(100ng/mL), bevacizumab (0.5mg/mL) or conditioned medium from different cell lines in a proportion 1:1, was added when indicated. Wells were photographed at indicated time points using a Leica DMIL Led microscope. Angiogenesis Analyzer plug-in for ImageJ was used for automatic quantification of master segments (linear aggregates of endothelial cells between nodes) and master junctions (nodes connecting three segments) (Figure MM-4).[200]

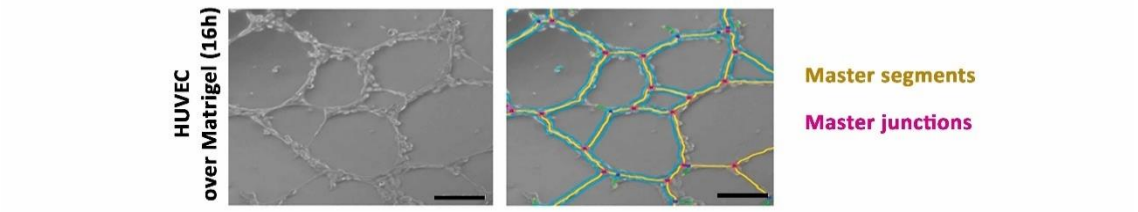

Figure MM-4. Quantification patterns of tubulogenesis. A, Images of tubulogenesis and details of master segments (yellow) and junctions (pink). Scale bar: 200 μm.

13. Spheroid based sprouting assay

Spheroids were generated by the hanging drop technique.[201] Briefly, 500 HUVEC were dispensed in 30 μl of carboxymethylcellulose (0.25% wt/vol) in standard medium on the lid of non-adherent plates and incubated upside down overnight. Afterwards, spheroids were embedded into Collagen type I (2mg/mL) and cultured in standard medium. VEGF-A (20μg/mL) or FGF2 (100ng/mL) were added to standard medium when indicated. Spheroids were fixed 24 hours later with glutaraldehyde (3%) during 5 minutes at RT and stained with Toluidine Blue (0.01%) in ethanol (30%) during 15 minutes at RT. Sprouting was quantified by measuring the number of sprouts per spheroid. A minimum of 10 spheroids per condition were analyzed in three independent experiments for statistical analysis.

14. *In vitro* wound healing assay

1.5 x 10^5 HUVEC, CAF or MEF per well were seeded in 24-well plates with standard medium. After arriving to high confluence, usually in 24 hours, medium was changed to FBS (0%) standard medium. Next day, TGF-β (0.1 or 1ng/mL, or 5ng/mL when not

specified), Plerixafor (25nM), SU5402 (5µM) or FBS (0%) conditioned medium from different cell lines, was added, when indicated, supplementing it with FBS (2%).

Afterwards, manual wound was performed with a tip and culture medium formulation was maintained during the healing process. The wounds were photographed when done and at indicated time points. After aligning both images, the space within the gap, in the same area, was measured and the migrated distance from the initial time was calculated with ImageJ software. A minimum of three areas per wound were quantified for statistical analysis.

15. Proliferation assay based on MTT

1000 HUVEC or NMuMG per well were seeded in triplicates in 96-well plates, with MCF10A conditioned or culture medium when indicated. Proliferation was determined up to the fourth, fifth or seventh day, when indicated. To measure it, culture medium was removed and 100µL of standard medium with MTT (1µg/mL) was added per well. After 3.5 hours of incubation, medium was removed, and the precipitates were solubilized by mixing with 100µL of isopropanol and DMSO in 1:4 proportion. Finally, absorbance was measured at 570nm using TECAN infinite M200 spectrophotometer.

16. Conditioned medium collection

1.3 x 10^5 HUVEC per well were seeded in a 24-well plate with 1 mL of standard medium or FBS (0%) standard medium. In the case of tumoral and myoepithelial cells, 1.3 x 10^5 cells per well were seeded in a 6-well plate with 1 mL of standard medium. After an overnight, conditioned medium was filtered with 0.22µm low protein binding filters and stored at -20°C.

17. Fibroblast activation by HUVEC conditioned medium

1.3 x 10^5 CAF or MEF per well were seeded in 24-well plates in standard medium. 24 hours later, medium was changed to FBS (0%) standard medium. The day after, FBS (0%) conditioned medium from HUVEC siCtl, siSnail1, Ctl or Snail1$^+$ (C5) was added, supplemented with FBS (0.5%) and with FGF2 (100ng/mL), TGF-β (0.1 or 1ng/mL, or

5ng/mL when not specified), Plerixafor (25nM) or SU5402 (5µM) when indicated. Two days or two hours, when indicated, cell lysates were collected to check their activation status at mRNA or protein levels.

18. *In vitro* cell cycle analysis

HUVEC on monolayer were trypsinized, and later, fixed and permeabilized using Transcription Factor Buffer Set, according to manufacturer's instructions. Hoeschst-33358 (0.5mg/mL) was added for 15 minutes at 4°C.

In the case of epithelial cells, 1.2 x 10^5 NMuMG-GFP$^+$ were seeded per well in 6-well plates. After 24 hours, medium was changed to 1mL of standard medium FBS (0%) to synchronize cells. 24 hours later, 1.88 x 10^5 MCF10A were added in half NMuMG culture medium, respectively, and half MCF10A culture medium. After other 24 hours, Hoescht 33342 (0.5mg/mL) was added to the well for 1 hour. Afterwards, cells were trypsinized and Hoescht 33342 (0.5mg/mL) was added to 1mL PBS for 90 minutes incubated at 37°C in a water bath.

Hoescht staining was analyzed in an LSR II cytometer (BD) and data was processed using BD FACSDIVA software at CRG/UPF FACS Unit at PRBB (Barcelona). Cells with 'n' amount of DNA, determined as phase G, were included in the non-proliferating category; whereas, cells with more than 'n' amount of DNA, determined as S, G2 and M phases, were included in the proliferating category.

19. Animals

Animals were housed in a specific pathogen-free (SPF) area and fed *ad libitum* at Parc de Recerca Biomèdica de Barcelona animal facility.

The generation of the murine line with Snail1 floxed (Snail1 flox) and Snail1 wild-type (Snail1) or Snail1 deleted (Snail1 del) alleles was described previously (Figure MM-5A).[170] This mouse line was crossed with C57/Bl6 background Cdh5(PAC)-CreERT2 mouse line[127] to generate endothelium specific Snail1 control and knock-out mice, referred as VE-Cadh^{Snail1CT} and VE-Cadh^{Snail1KO}, respectively (Figure MM-5B).

Depletion of Snail1 allele was performed by five daily doses of tamoxifen by intraperitoneal administration (0.2mg/g) in 6 weeks old mice. For characterization, three VE-Cadh^{Snail1CT} and VE-Cadh^{Snail1KO} mice weight was monitored during three weeks and, finally, euthanized. Their organs and tissues were processed for histological and other analysis when indicated.

Mice were genotyped as described previously.[202] After tamoxifen administration, endothelial cells knocked out SNAI1 but not non-endothelial cells (Figure MM-5C). To confirm the specificity of SNAI1 deletion, VE-Cadh^{Snail1CT} and VE-Cadh^{Snail1KO} livers were disaggregated and stained for endothelial cell isolation by FACS sorting in FACSAria II SORP (BD) as explained in Population analysis section (Figure MM-5D). A SNAI1 genotyping PCR in endothelial and non-endothelial sorted populations was performed, observing in endothelial cells a partial floxed from VE-Cadh^{Snail1CT} mice and a total floxed from VE-Cadh^{Snail1KO} mice. (Figure MM-5E). In the case of non-endothelial cells, only in VE-Cadh^{Snail1KO} mice was observed the predicted floxed of one SNAI1 allele (Figure MM-5E).

In order to generate reporter mice of the CDH5(PAC)-CreERT2 expression, they were crossed with an Enhanced Green Fluorescent Protein (eGFP) gene inserted into the constitutive Gt(ROSA)26Sor locus with a STOP codon flanked by LoxP sequences (Rosa26 LoxP STOP LoxP eGFP) mice, generating the VE-Cadh^{GFP} mouse line;[203] therefore, eGFP was expressed in endothelial cells following Cre-mediated recombination, corroborating the specificity of the CDH5 promoter (Figure MM-5F).

VE-Cadh^{Snail1} mouse line were mated with C57/Bl6 MMTV-PyMT mice[29] to obtain PyMT VE-Cadh^{Snail1CT} and PyMT VE-Cadh^{Snail1KO} mice, which develop spontaneously luminal B breast cancer tumors, and, after tamoxifen induction, an endothelium specific deletion of Snail1 allele (Figure MM-6A). Moreover, PyMT VE-Cadh mice were crossed with (Rosa26 LoxP STOP LoxP eGFP) mice, generating PyMT VE-Cadh^{GFP} (Figure MM-6B). After tamoxifen administration, expression of eGFP, as a subrogated marker of CreERT2 expression, was checked in the tumor vessels of PyMT VE-Cadh^{GFP} (Figure MM-6B).

In PyMT VE-Cadh^{Snail1CT} and PyMT VE-Cadh^{Snail1KO} mice, apart from an initial tamoxifen administration of five daily doses (0.2mg/g) injected intraperitoneally in 6 weeks old

mice, an additional dose every three weeks was administrated until animals reached the indicated time points. Mice were palpated twice per week to set the tumor onset and the bigger dimension of the tumors was measured using a caliper to monitor the tumor growth. Middle size tumors were designated as 0.5cm of diameter and big size tumors, 1cm of diameter. When tumors reached 1cm of diameter, animals were euthanized to establish the survival rate.

As MMTV-PyMT mice could develop breast tumors in any of the ten breast of the mice, tumors next to the neck and over the inferior limbs, as well as the bigger one in each animal, when these were not located in the previous positions, were processed for histological and immunohistochemical analysis.

For survival and tumor onset study, twelve MMTV-PyMT mice per condition were used. For tumor burden analysis and distinct quantifications by immunohistochemistry or FACS, three mice per condition were used. In all experiments, only female mice were used, except for characterization, where male mice were also used as indicated.

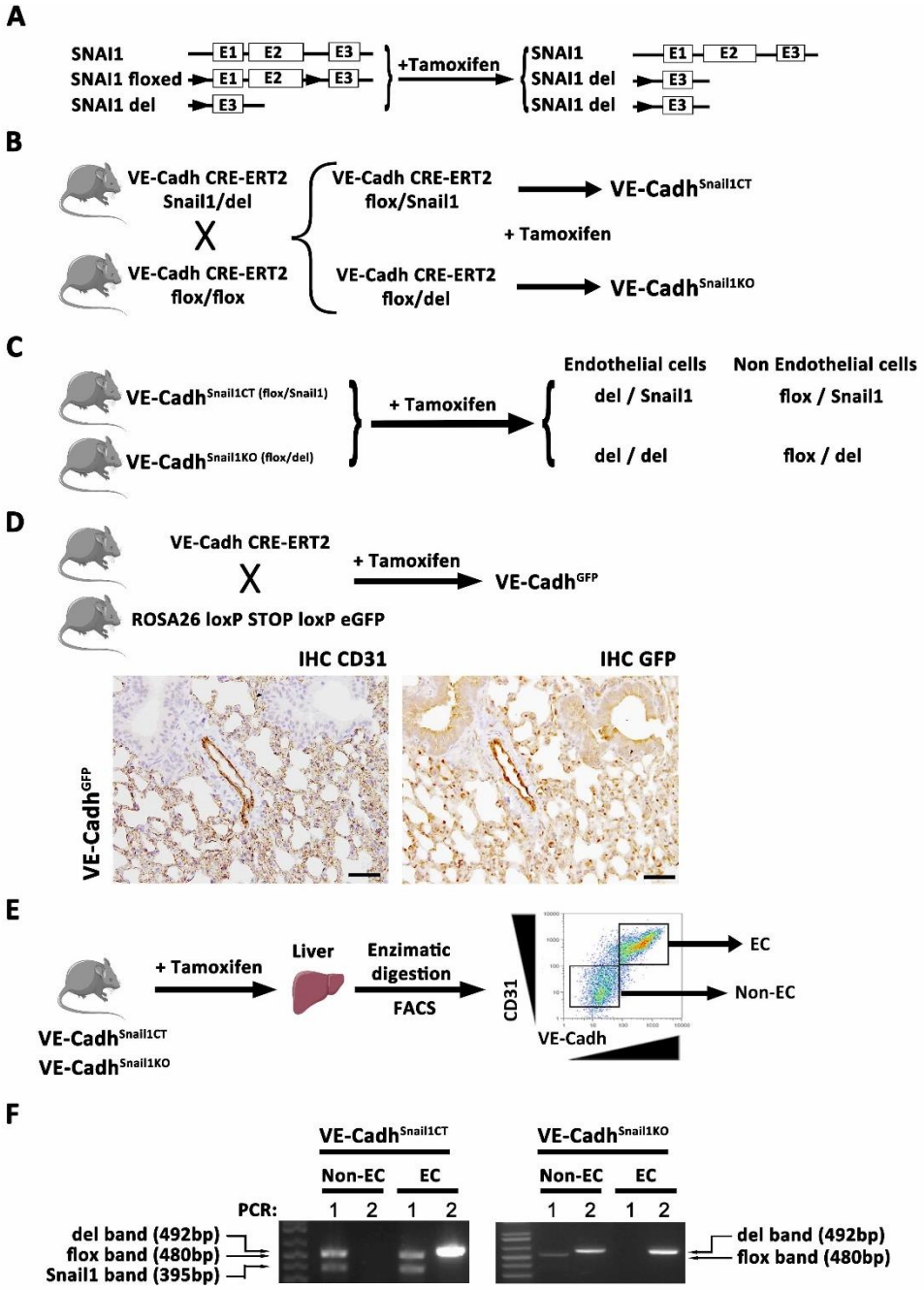

Figure MM-5. VE-Cadh^{Snail1} mice generation and confirmation. A, Scheme of SNAI1 allele depletion after tamoxifen. **B**, Scheme of mice crossing for VE-Cadh$^{Snail1CT/KO}$ mice generation. **C**, Scheme of SNAI1 recombination in endothelial and non-endothelial cells in VE-Cadh$^{Snail1CT/KO}$ mice after tamoxifen administration. **D**, Scheme of workflow and gating strategy of non-endothelial and endothelial cells for sorting from VE-Cadh$^{Snail1CT/KO}$ livers. **E**, PCR results of genotyping of non-endothelial (Non-EC) and endothelial cells (EC) in liver of VE-Cadh$^{Snail1CT/KO}$ mice after tamoxifen induction. (1), PCR to detect flox and Snail1 allele. (2), PCR to detect del allele. **F**, Scheme of mice crossing for VE-Cadh^{GFP} mice generation and tamoxifen induction (upper). Images of anti CD31 and anti GFP immunohistochemistry in VE-Cadh^{GFP} mice (lower). Scale bar: 50 μm.

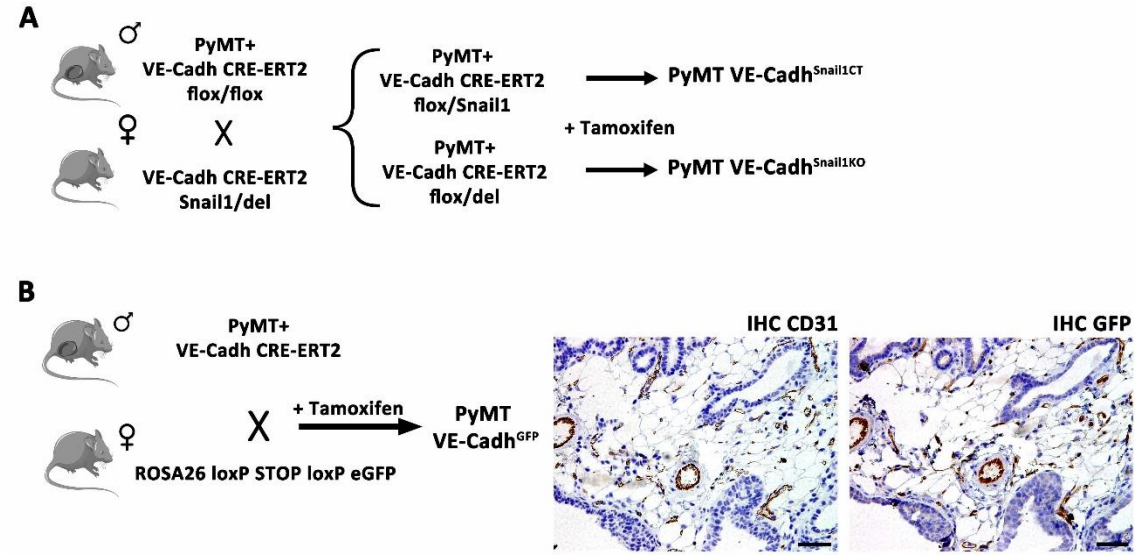

Figure MM-6. PyMT VE-Cadh^{Snail1} spontaneous luminal breast tumor mouse model. A, Scheme of mice crossing for PyMT VE-Cadh$^{Snail1CT/KO}$ generation. **B**, Scheme of mice crossing for PyMT VE-Cadh^{GFP} mice generation and tamoxifen induction (left). Images of anti CD31 and anti GFP immunohistochemistry of PyMT VE-Cadh^{GFP} tumors (right). Scale bar: 50 μm.

20. *In vivo* vasculature permeability assay

9 weeks old VE-Cadh^{Snail1CT} and VE-Cadh^{Snail1KO} mice, which were administrated with tamoxifen 3 weeks before, were intraperitoneally injected with 3μL/g of Evans blue (0.2%) in saline buffer. After two hours, mice were perfused using a perfusion pump with PBS for 10 minutes to remove the dye contained within the vessels and, afterwards, with PFA (4%) for 5 minutes to fix the tissues. Pieces of breast, lung and liver were removed and dried at 60°C for 16 hours. Evans blue of the dehydrated tissues was extracted with 1mL of formamide at 55°C for 16 hours. Dye content was quantified by measuring the solution at 610nm in a spectrophotometer and concentration was obtained by comparing to Evans blue diluted in formamide standards. Mean values of each group was represented as grams of Evans blue per mL of formamide per gram of dehydrated tissue. Three mice of each condition were used for statistical analysis.

21. *In vivo* Matrigel plug angiogenesis assay

9 weeks old VE-Cadh^{Snail1CT} and VE-Cadh^{Snail1KO} mice, which were administrated with tamoxifen 3 weeks before, were subcutaneously injected in their flanks (two injection sites per mouse) with 200 μl of Matrigel alone or containing VEGF-A (250ng/mL) or FGF2 (1μg/mL). Three mice of each condition were used for statistical analysis. One week later, mice were euthanized and Matrigel plugs were recovered and paraffin embedded for analysis, as described previously. Two medial sections of each plug were stained with anti CD31 antibody by immunohistochemistry and slides were scanned with Aperio CS2 Scan (ScanScope) at the Anatomy Dpt. of the Hospital del Mar. CD31$^+$ stained area was quantified using ImageJ software and mean values for each group were represented as the percentage of CD31$^+$ area per Matrigel plug area.

22. Population analysis

VE-Cadh^{Snail1CT} and VE-Cadh^{Snail1KO} lungs and livers and PyMT VE-Cadh^{Snail1CT} and PyMT VE-Cadh^{Snail1KO} tumors from three mice per condition, previously administrated with tamoxifen, were collected in PBS and dissected into 1 mm^3 pieces. Afterwards, enzymatic disaggregation was performed with the Tumor Dissociation Kit mouse at 37°C for 30 minutes. Further tissue disruption was made by gentleMACS Dissociator (MACS Miltenyi Biotec, 130-093-235) and RBC Lysis Buffer incubation was used to remove red blood cells. Next, solution was passed through a 70μm filter. Cells were blocked with horse serum (20%) and FBS (10%) in PBS during one hour at 4°C. Primary antibodies listed in Table MM-1 specified as FACS were diluted in blocking solution and incubated during 40 minutes at 4°C. DAPI staining was used as a viability marker. Cell staining was analyzed by LSR II cytometer (BD) and data was processed using BD FACSDIVA software.

Lung and liver endothelial cells were considered as VE-Cadherin$^+$, and CD31$^+$ when indicated.

Tumor cells were classified in these population categories depending on their staining: epithelial cells (EpCAM$^+$ CD45$^-$), immune cells (EpCAM$^-$ CD45$^+$), endothelial cells (EpCAM$^-$ CD45$^-$ CD31$^+$) and other cells (EpCAM$^-$ CD45$^-$CD31$^-$).

23. Purification of tumor endothelial cells

Big size tumors from three PyMT VE-Cadh^{Snail1CT} and PyMT VE-Cadh^{Snail1KO} mice, previously administrated with tamoxifen, were disaggregated as described in Population analysis section (Figure MM-7A). Once the red blood cells were disrupted, cells were blocked in Buffer A [HBSS supplemented with BSA (0.5%), EDTA 2mM, horse serum (10%) and FBS (10%)] during 30 minutes at 4°C. Afterwards, cells were stained with biotin anti VE-Cadherin in Buffer A during 30 minutes at 4°C. Sample was filtered through 25µm nylon mesh and incubated with anti biotin microbeads for 25 minutes at 4°C. Finally, LS columns (MACS Miltenyi Biotec, 130-042-401) were located on a MidiMACS™ Separator (MACS Miltenyi Biotec, 130-042-301), samples passed through them and bound fractions were collected for RNA extraction, as well as a small fraction of input (Figure MM-7A). Purification of bound fraction of each animal was corroborated since there was an increase of CDH5 mRNA expression compared to each corresponding input fraction (Figure MM-7B). Furthermore, upregulation of SNAI1 mRNA expression was detected in VE-Cadherin enriched samples from PyMT VE-Cadh^{Snail1CT}, compared to PyMT VE-Cadh^{Snail1KO} (Figure MM-7C).

In fact, tumor vessels from PyMT VE-Cadh^{Snail1CT} mice were analyzed by immunohistochemistry, corroborating their expression of Snail1, but not in PyMT VE-Cadh^{Snail1KO} mice (Figure MM-7D).

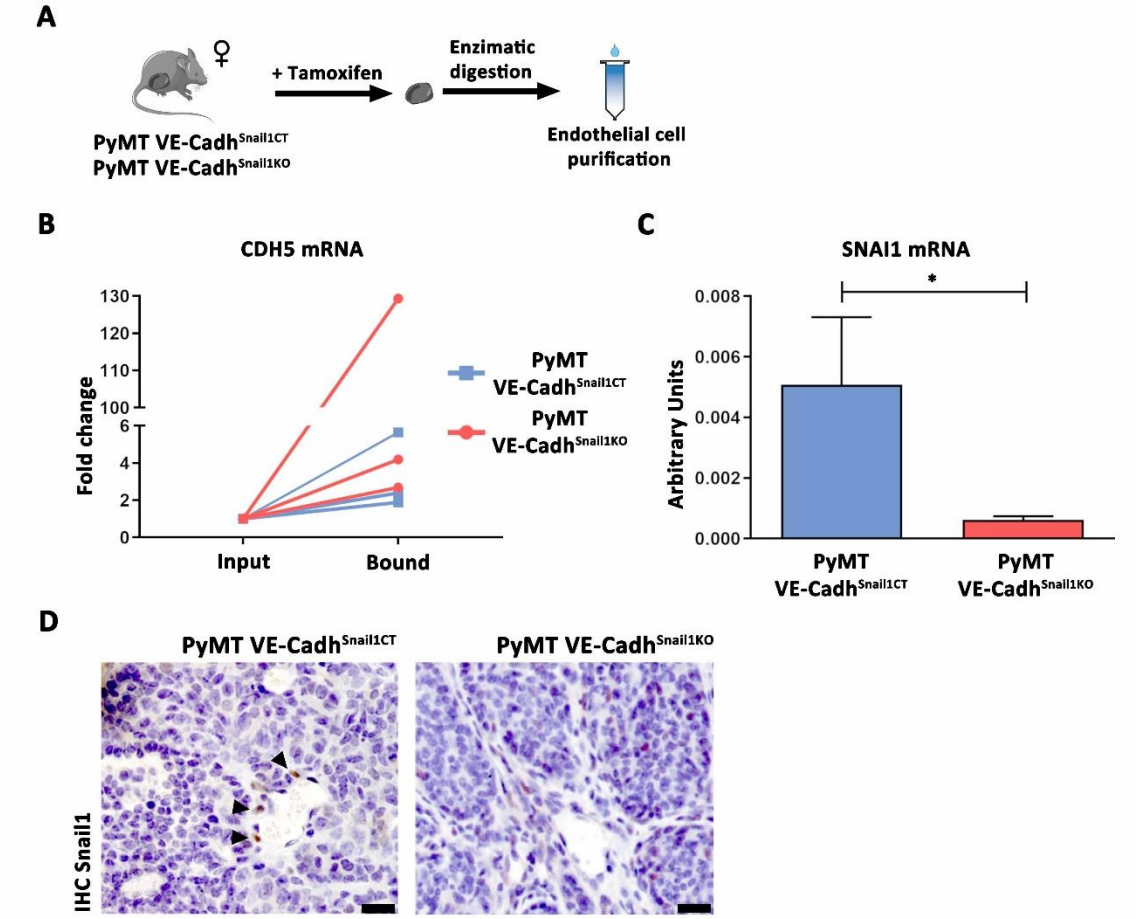

Figure MM-7. Endothelial Snail1 expression in PyMT VE-Cadh$^{Snail1CT/KO}$ tumors. A, Scheme of workflow for endothelial cell purification from PyMT VE-Cadh$^{Snail1CT/KO}$ tumors. **B**, Quantification of CDH5 mRNA in input and bound fraction of tumor cell disaggregation from PyMT VE-Cadh$^{Snail1CT/KO}$ mice. **C,** Quantification of SNAI1 mRNA expression in VE-Cadherin enriched fraction of PyMT VE-Cadh$^{Snail1CT/KO}$ tumors. **D**, Images of anti Snail1 immunohistochemistry of PyMT VE-Cadh$^{Snail1CT/KO}$ tumor vessels. Black arrowheads point Snail1^{+} cells in tumor vessels. Scale bar: 50 μm. Data in B represent a mean value of each animal and data in C represent mean values (± SEM) of at least three mice purified fractions. *p<0.05.

24. *In vivo* cell cycle analysis

Lungs and livers of three VE-Cadh^{Snail1CT} and VE-Cadh^{Snail1KO} mice, previously administrated with tamoxifen, were digested and stained for endothelial cell analysis as described in Population analysis section. Staining and analysis of endothelial cell cycle was performed using the protocol for Hoescht 33342 stain described in *in vitro* cell cycle analysis section.

25. Vasculature analysis

Two nonconsecutive sections of medial plane of three different tumors of at least three mice in the indicated groups, were stained by immunohistochemistry with an anti CD31 antibody, as described previously.

Minimum of five randomized areas of each CD31 stained slide were captured using an Olympus BX61 microscope. CD31 stained area was quantified using ImageJ software and angiogenesis was showed as the percentage of $CD31^+$ stained area per tumor area.

Vessel were manually delimited, and their lumen size and perimeter were measured using ImageJ software. Mean values of individual vessel lumen size and perimeter were represented in each condition.

26. Transmission electron microscopy

Four tumors of different sizes from PyMT VE-$Cadh^{Snail1CT}$ and PyMT VE-$Cadh^{Snail1KO}$ mice, previously administrated with tamoxifen, were dissected and fixed with a PFA (2%)/glutaraldehyde (2%) solution in cacodylate (0.2M) buffer. Samples were stored in cacodylate buffer until processing. After postfixation with osmium tetroxide (2%), samples were dehydrated and embedded in Epon LX112. Semi-thin sections (approximately 1µm thick) were cut and stained with toluidine blue. Ultrathin sections (60-80nm) were obtained with an ultramicrotome, placed on parlodion/carbon-coated nickel grids and stained with lead citrate and uranyl acetate. The grids were examined using a Phillips CM100 electron microscope at the anatomy Dpt. of the Hospital del Mar.

27. Necrosis quantification

Tumors at carcinoma stage from PyMT VE-$Cadh^{Snail1CT}$ and VE-$Cadh^{Snail1KO}$ mice, previously administrated with tamoxifen, were selected. Two nonconsecutive sections of each tumor medial plane were stained with hematoxylin and eosin. Slides were scanned using an Aperio CS2 Scan (Leica) at the Anatomy Dpt. of the Hospital del Mar. Necrotic areas were identified visually and measured by ImageJ software. At least three tumors from six mice of each condition were used for statistical analysis.

28. PyMT tumor cell isolation and orthotopic transplantation

C57/Bl6 MMTV-PyMT mice were euthanized and tumors of middle size, when indicated, were dissected into 1mm^3 pieces and enzymatically disaggregated by the Tumor Dissociation Kit mouse for 30 minutes at 37°C (Figure MM-8A). Afterwards, RBC Lysis Buffer was used to remove red blood cells. Tumor cell mixture was filtered by a 70μm pore filter and individualized cells were plated in EpiCult-B medium supplemented with mEGF (10ng/mL), mFGF2 (10ng/mL) and FBS (2%). 24 hours later, culture medium was exchanged to a serum-free medium with the rest of supplemented factors (Figure MM-8A). Cell population of the culture was analyzed as previously stated, observing a clear enrichment in epithelial cells, thus, they were called epithelial PyMT cells (ePyMT) (Figure MM-8B). ePyMT were not used after the seventh day of their isolation.

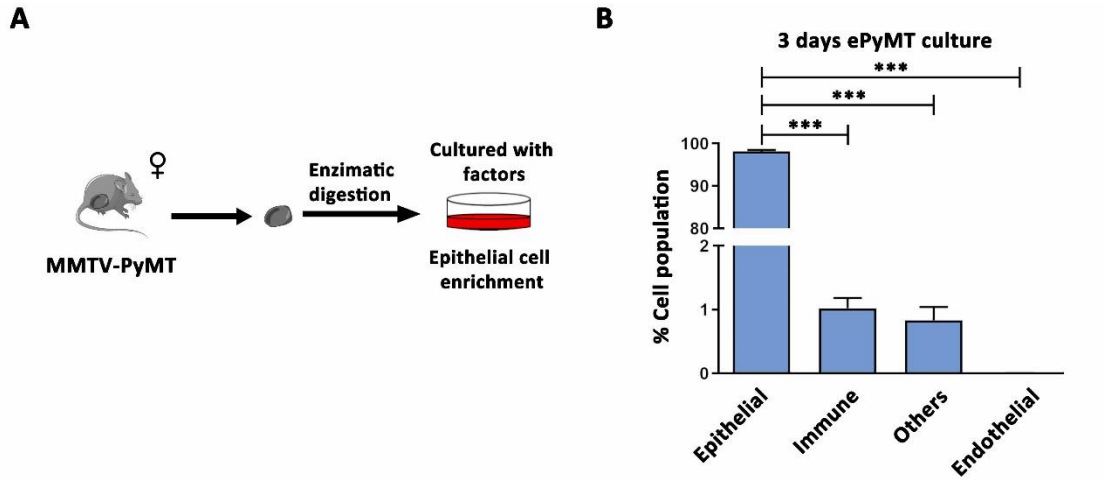

Figure MM-8. ePyMT isolation. **A**, Scheme of workflow for ePyMT isolation from MMTV-PyMT tumors. **B**, Percentage of epithelial, immune, endothelial and other stromal cells cultured for 3 days, determined by FACS. Data in B represent mean values (± SEM) of at least three independent experiments. ***p<0.001.

6 weeks old syngeneic C57/Bl6 VE-Cadh^{Snail1CT} and VE-Cadh^{Snail1KO} mice were inoculated intraperitoneally with tamoxifen (0.2mg/g) to delete SNAI1 gene in their vasculature. Four mice of each condition were used for statistical analysis. Three weeks later, mice were anesthetized with isoflurane and both inguinal mammary fat pads were injected with 0.5x10^6 ePyMT embedded in Matrigel from middle or big size tumors, when indicated. When recipient VE-Cadh^{Snail1CT} mice tumors arrived to 1cm of diameter,

primary tumors from VE-Cadh^{Snail1CT} and VE-Cadh^{Snail1KO} mice, were resected and processed for histological analysis as described.

29. Bevacizumab treatment in PyMT mice

C57/Bl6 MMTV-PyMT mice were intraperitoneal treated with PBS or bevacizumab (50mg/kg) diluted in PBS twice per week from 6 weeks old until their biggest tumor reached 1cm of diameter. Four mice of each condition were used for statistical analysis. For the morphology analysis, tumors next to the neck and over the inferior limbs, as well as the bigger ones when they were not located in the previous positions, were paraffin embedded and processed for histological analysis, as described.

30. Human tumor dataset analysis

TCGA Breast Invasive Carcinoma (Firehose Legacy) data in the cBioPortal public database (http://www.cbioportal.org/)[204,205] was used on May 2020, to analyze the correlation of mRNA-mRNA, mRNA-protein or protein-protein expression levels of indicated genes.

For the humanized version of PyMT VE-Cadh^{Snail1CT} and VE-Cadh^{Snail1KO} mice, the survival and disease free period and differential gene expression were analyzed. Differentially Expressed Genes, their corresponding fold change (Fc) and q-value from both groups were downloaded from the cBioPortal webpage and analyzed with GSEA software 4.0 (BROAD Institute, University of California)[206,207] against MSigDB Gene Ontology: Biological Process collection (v7.1).[208,209]

31. Statistical analysis

Data was analyzed by GraphPad Prism (v6) software (GraphPad Software, San Diego, CA, USA). For each experiment, the mean of at least three independent experiments was represented, with their Standard Error of the Mean (SEM), in each graph. Statistical significance was obtained using Student's t-test. Survival of each group were represented by a Kaplan Meier curve and p-value was obtained using log-rank test. Statistical comparisons of tumor histological subtypes, Collagen coverage of the vessels,

vessel location in premalignant ducts, transmission electron microscopy quantifications and human breast tumor stages, ERα intensity, correlation of Snail1 expression in stroma vs vessels were performed by $\chi 2$ (and Fisher's exact) test. p-value was represented in all the figures by * when p-value <0.05; **, when p-value <0.01; or ***, when p-value <0.001.

Table MM-1. Antibodies list

Antibody	Company (reference)	Method (dilution)
αSMA	Merck-Sigma (A2547)	WB (1/1000)
αTubulin	Merck-Sigma (T9026)	WB (1/10000)
βActin	ABCAM (ab8227)	WB (1/2000)
total AKT	Cell Signaling (9272)	WB (1/1000)
CD31	ABCAM (ab231436)	IHC (1/200)
CD31 (PE-Cy7)	Biolegend (102515)	FACS (1/200)
CD326 (EpCAM, APC/Cy7)	Biolegend (118217)	FACS (1/100)
CD45 (CD45.1 and CD45.2, PerCP)	Pharmigen (557235)	FACS (1/200)
CK14	Abcam (ab181595)	IHC (1/500) WB (1/1000)
Cleaved Caspase-3	Cell Signaling (9661)	IHC (1/100)
E-Cadherin	Transduction Labs (610182)	WB (1/1000)
ERK1/ERK2	ThermoFisher (13-6200)	WB (1/100)
Estrogen receptor α	Santa Cruz (sc-8005)	IHC (1/50)
Fibronectin1	ABCAM (ab2413)	WB (1/1000)
GFP	ABCAM (ab6556)	IHC (1/300)
Her2/Neu	BioGenex (MU134-USE)	IHC (1/60)
Ki67	BD (550609)	IHC (1/100)
LaminB1	ABCAM (ab16048)	WB (1/20000)

Lamininα	Merck-Sigma (L9393)	IHC (1/100)
Lyve-1	R&D (AF2125)	IHC (1/300)
N-Cadherin	Transduction Labs (610920)	WB (1/1000)
p63	Santa Cruz (sc-25268)	IHC (1/40)
PDGF Receptor β	Cell Signaling (3169)	IHC (1/100)
phospho AKT (Ser473)	Cell Signaling (9271)	WB (1/1000)
phospho Erk1/2 (Thr202/Tyr204)	Cell Signalling (9101)	WB (1/1000)
phospho SMAD2 (Ser465/467)	Cell Signalling (3108)	WB (1/1000) IHC (1/100)
SMAD2/3	Cell Signaling (8685)	WB (1/1000)
Snail1	Francí et al 2006[210]	IHC (1/100)
Snail1	Cell Signaling (3879)	WB (1/2000) IF (1/150) IHC (1/100)
Snail2	Santa Cruz (sc-10436)	WB (1/500)
VE-Cadherin (Alexa 647)	Pharmigen (562242)	FACS (1/50)
VE-Cadherin (Biotin)	Biolegend (138008)	Bead separation (1/10)
VE-Cadherin	Santa Cruz (sc-52751)	WB (1/200)
Vimentin	BD (550513)	IHC (1/200) WB (1/500)
Vinculin	Santa Cruz (sc-73614)	WB (1/1000)

Table MM-2. Cell lines list

Name	Cell type	Culture Medium	Obtained from
CAF	Cancer associated fibroblast from MMTV-PyMT mice	Standard medium	Stablished in our lab[65]
HEK-293T/17	Human Embrionic Kidney 293 with SV40 T-ag	Standard medium	Cancer Cell Line Repository (IMIM, Barcelona)[211]
HUVEC	Spontaneously immortalized Human Umbilical Vein Endothelial Cell	Standard medium	Kindly given by Dr Francisco J. Muñoz[212]
MCF10A	Myoepithelial cell	MEGM™ Mammary Epithelial Cell Growth Medium BulletKit supplemented with Horse Serum (5%) and cholera toxin (100ng/mL)	Cancer Cell Line Repository (IMIM, Barcelona)[213]
MEF WT / Snail1KO	Mouse Embryonic Fibroblast from C57/Bl6 mice	Standard medium	Stablished in our lab
NMuMG	Normal Murine Mammary Gland	Standard medium supplemented with insulin (10µg/mL)	Cancer Cell Line Repository (IMIM, Barcelona)[214]
Plat-E	Retrovirus packaging cell line based on the 293T cell	Standard medium supplemented with blasticidin (10µg/mL) and puromycin (1µg/mL)	Kindly gifted by Dr Nakayama[215]

Table MM-3. Primers list

Gene	Forward	Reverse
Human		
ACTA2	5’-GCACTGCCTTGGTGTGTG-3’	5’-TCCCATTCCCACCATCAC-3’
CAV1	5’-CGCGACCCCAAGCATCTC-3’	5’-TCCCTTCTGGTTCTGCAATCAC-3’
CDH2	5’-CCATCACTCGGCTTAATGGTGA-3’	5’-TCACGCGCAGGATGGAAATA-3’
CDH5	5’-GAGACCTCATCAGCCTTGGGATAG-3’	5’- CTGGATTTGCCAGCATTTGAGA-3’
COL4A1	5’-CTCCACGAGGAGCACAGC-3’	5’-CCTTTTGTCCCTTCACTCCA-3’
CXCL12	5’-CAGTCAGCCTGAGCTACCGA-3’	5’-GCCGTGCAACAATCTGAAGG-3’
EDN1	5’-CATCATTTGGGTCAACACTCC-3’	5’-CTTCCTCTCACTAACTGCTG-3’
EDN2	5’-GCCAGCGTCCTCATCTCAT-3’	5’-GCCGTAAGGAGCTGTCTGTTC-3’
FN1	5’-AGCAAGCCTGAGCCTGAAGAG-3’	5’-GCGATTTGCAATGGTACAGCT-3’
FGF2	5’-CCAAGCAGAAGAGAGAGGAGT-3’	5’-CAGCCGTCCATCTTCCTT-3’
FGFR1	5’-TAATGGACTCTGTGGTGCCCTC-3’	5’-ATGTGTGGTTGATGCTGCCG-3’
FGFR2	5’-CGCTGGTGAGGATAACAACACG-3’	5’-TGGAAGTTCATACTCGGAGACCC-3’
FGFR3	5’-CCTCGGGAGATGACGAAGAC-3’	5’-CGGGCCGTGTCCAGTAAGG-3’
FGFR4	5’-TGCAGAATCTCACCTTGATTACA-3’	5’-GGGGTAACTGTGCCTATTCG-3’
FLT1	5’-ATAGAAGGTGCCCAGGAAAAG-3’	5’-GTCTTCAGTTCCCCTCCATTG-3’
FLT4	5’-GACAAGCACTGCCACAAGAA-3’	5’-CGGTCAAGTTCTGCGTGAG-3’
HPRT	5’-GGCCAGACTTTGTTGGATTTG-3’	5’-TGCGCTCATCTTAGGCTTTGT-3’
KDR	5’-CTCTACTCCTGAAATCTATCAGA-3’	5’-TACCATCCTGTTGTACATTTGCT-3’
MMP1	5’-TCGGCCATTCTCTTGGACTCTCC-3’	5’-TGCCATCAATGTCATCCTGAGC-3’
MMP7	5’-CATTTGATGGGCCAGGAAACACG-3’	5’-CCATCCGTCCAGCGTTCATCC-3’
MMP9	5’-TTCAGGGAGACGCCCATTTC-3’	5’-TGGGTGTAGAGTCTCTCGCT-3’
MMP13	5’-AAGGACCCTGGAGCACTCAT-3’	5’-CCTGGACCATAGAGAGACTGGA-3’
PDGFA	5’- GCAAGACCAGGACGGTCATTT-3’	5’-GGCACTTGACACTGCTCGT-3’
PDGFB	5’-CTCGATCCGCTCCTTTGATGA-3’	5’-CGTTGGTGCGGTCTATGAG-3’
PDGFC	5’-TTCTTGGCAAGGCTTTTGTT-3’	5’-TGCTTGGGACACATTGACAT-3’
PDGFD	5’-GTGGAGGAAATTGTGGCTGT-3’	5’-CGTTCATGGTGATCCAACTG-3’

SNAI1	5’-GTGCCTCGACCACTATGCC-3’	5’-GCTGCTGGAAGGTAAACTCTGG-3’
TGFB1	5’-CGTCTGCTGAGGCTCAAGTTAAA-3’	5’-CCGGTAGTGAACCCGTTGAT-3’
TGFB2	5’-TCCCAGGTTCCTGTCTTTATG-3’	5’-GATGCCATCCCGCCCACTTTC-3’
TGFB3	5’-CACCCAGGAAAACACCGAGTC-3’	5’-CTCATTGTCCCACGCCTTTGAA-3’
TWIST1	5’-GGAGTCCGCAGTCTTACGAG-3’	5’-TCTGGAGGACCTGGTAGAGG-3’
VEGFA	5’-CCAACTGAGGAGTCCAACAT-3’	5’-TTTCTTGCGCTTTCGTTTTT-3’
VIM	5’-CTCCGGGAGAAATTGCAGGA-3’	5’-GCCAGAGACGCATTGTCAAC-3’
Murine		
Cdh2	5’-GCAGGTACCATGCTGACCAC-3’	5’-CCAGTTGGCAGGATCAGAC-3’
Cdh5	5’- GGATGTGGTGCCAGTAAACC-3’	5’- ACCCCGTTGTCTGAGATGAG-3’
Cxcl12	5’-CAGTCAGCCTGAGCTACCGA-3’	5’-GCCGTGCAACAATCTGAAGG-3’
Fn1	5’-AGCAAGCCTGAGCCTGAAGAG-3’	5’-GCGATTTGCAATGGTACAGCT-3’
Hprt	5’-GGCCAGACTTTGTTGGATTTG-3’	5’-TGCGCTCATCTTAGGCTTTGT-3’
Snai1	5’- GCGCCCGTCGTCCTTCTCGTC-3’	5’-CTTCCGCGACTGGGGGTCCT-3’
Tgfb1	5’-CTGCAAGACCATCGACATGG-3’	5’-GTTCCACATGTTGCTCCACA-3’
Tgfb2	5’-CTACAGACTGGAGTCACAAC-3’	5’-CATATTGGAAAGCTGTTCGATC-3’
Tgfb3	5’- CAGAGCAGAGAATTGAGCTC-3’	5’- CCTAGATCCTGCCGGAAGTC-3’

RESULTS

1. Tumor endothelial cells express Snail1

First, we checked the presence of Snail1 in tumor endothelial cells in human and murine tumor samples. In all of them, concretely human colorectal carcinoma, pancreatic carcinoma and fibromatosis, and murine liver metastasis obtained after intrasplenic injection of MTO cells, HT29 M6 plus MEF xenograft and PDX of triple negative breast cancer, we detected Snail1 expression in cells surrounding blood vessels and closely resembling endothelial cells (Figure R-1A-F).[160] Snail1^{+} cells showed co-staining with a classical endothelial marker, CD31, but not with PDGFRb, a marker for pericytes and fibroblasts (Figure R-1A). Thus, we confirmed that those Snail1^{+} cells were endothelial cells.

2. Endothelial cells induce Snail1 expression upon angiogenic stimuli without altering their cell identity

After this observation, we wondered if Snail1 could have a role during angiogenesis in endothelial cells. To address it, we grew HUVEC on monolayer and checked if they express Snail1 (Figure R-2A). Moreover, we observed that Snail1 was localized at the nuclei of HUVEC cells (Figure R-2B).

Afterwards, we wanted to analyze if Snail1 expression in HUVEC is enhanced by angiogenic factors. Therefore, we incubated HUVEC cells on monolayer with FGF2 or VEGF-A and observed a significant increase of SNAI1 mRNA expression at 2 hours of treatment (Figure R-3A). At longer times, only FGF2 produced a higher Snail1 upregulation (Figure R-3A). Similarly, we analyzed the Snail1 protein expression in HUVEC upon FGF2 and VEGF-A, observing an increase of Snail1 protein in HUVEC (Figure R-3B, C). Interestingly, FGF2 induces a higher expression of Snail1, at mRNA and protein levels, than VEGF-A (Figure R-3A, D).

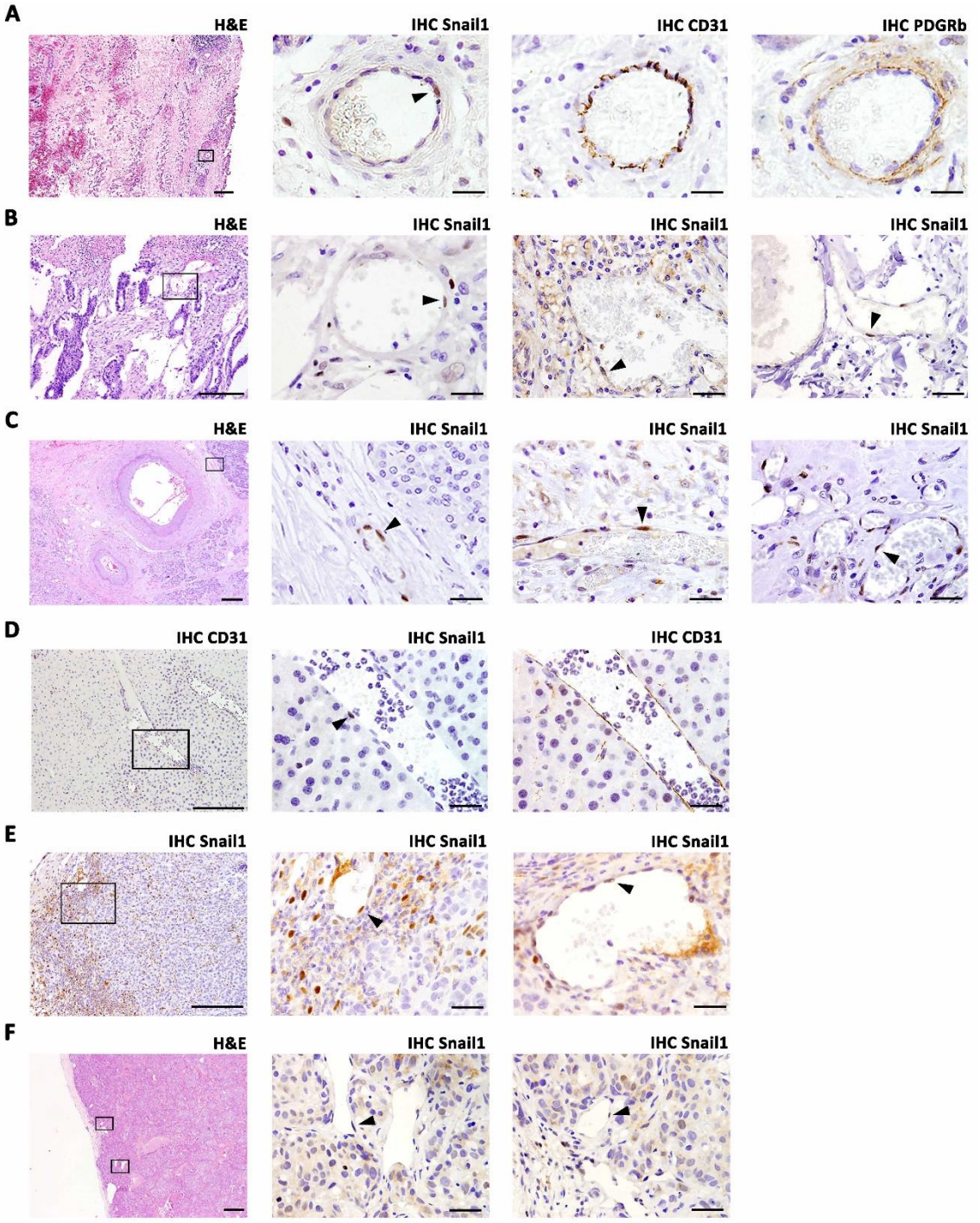

Figure R-1. Human and mouse tumors express Snail1 in their vasculature. Vasculature images of hematoxylin and eosin (H&E) staining and anti Snail1, anti CD31 or anti PDGFRb immunohistochemistry (when indicated) of human tumors **A-C**; colorectal carcinoma (A), pancreatic carcinoma (B), fibromatosis (C); murine tumors **D-F**; liver metastasis obtained after intrasplenic injection of MTO cells (D), HT29 M6 plus MEF xenograft in nude mice (E), PDX of triple negative breast cancer in nude mice (F). Black boxes represent areas magnificated. Black arrowheads point Snail1^{+} cells. Scale bars: 200 µm (H&E) and 20 µm (others).

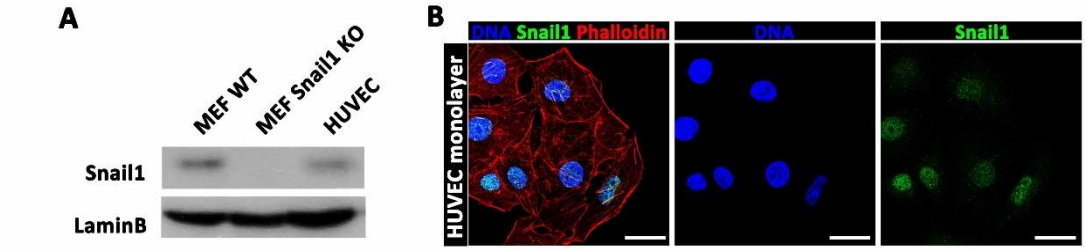

Figure R-2. Snail1 is expressed in HUVEC. A, Western blot analysis of Snail1 in MEF WT, MEF Snail1 KO and HUVEC. **B**, Snail1 (green) immunofluorescence analysis in HUVEC cells cultured on monolayer. Actin cytoskeleton was stained with Alexa 555 conjugated Phalloidin (red) and nuclei were counterstained with DAPI (blue). Scale bar: 25 μm.

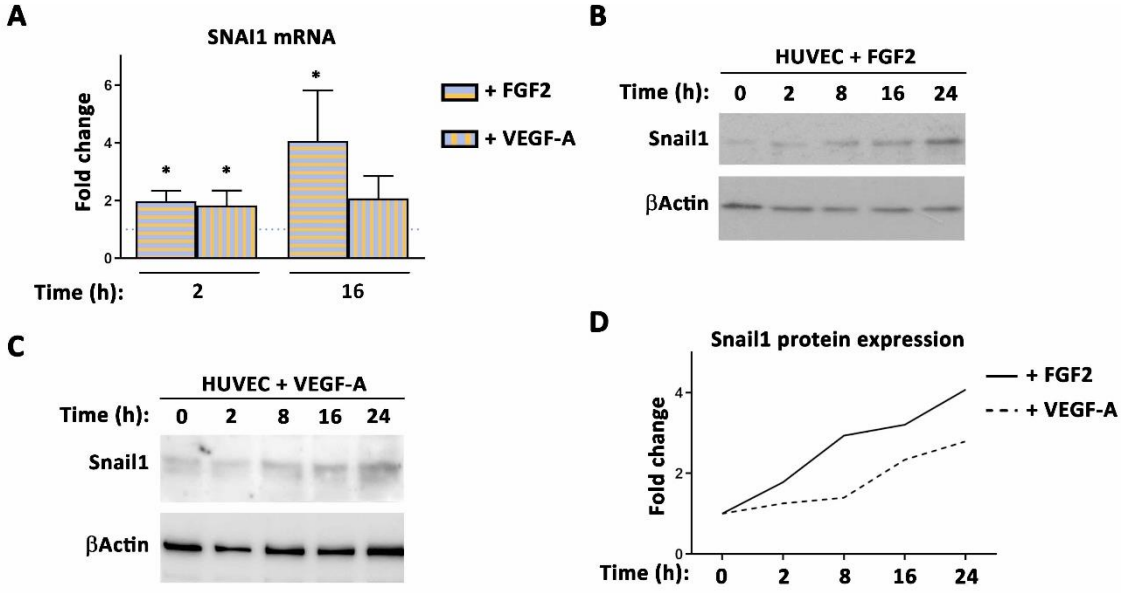

Figure R-3. Snail1 is induced upon angiogenic stimulation in HUVEC on monolayer. A, Quantification of SNAI1 mRNA in HUVEC on monolayer treated with FGF2 or VEGF-A for 2 or 16h, compared to non-treated HUVEC represented as a discontinuous line. **B-C**, Western blot analysis of Snail1 in HUVEC on monolayer treated with FGF2 (B) or VEGF-A (C) along the time. **D**, Densitometry of Snail1 expression in HUVEC on monolayer treated with FGF2 or VEGF-A along the time. Data in A represent mean values (± SEM) and data in D represent mean values, of at least three independent experiments. *p<0.05.

In order to test Snail1 expression during *in vitro* angiogenic process in HUVEC, we seeded them on wells coated with Matrigel. Over time, HUVEC elongated and interconnected among themselves, forming a honeycomb panel like structure (Figure R-4A). We observed that Snail1 mRNA and protein expression in HUVEC were increased when cultured over Matrigel for 16 hours, when compared with monolayer (Figure R-

4B, C). Over Matrigel, we observed that Snail1^{+} cells were mainly localized in the tubulogenic segments (Figure R-4D). Therefore, we could state that angiogenic *in vitro* models increase Snail1 expression in HUVEC.

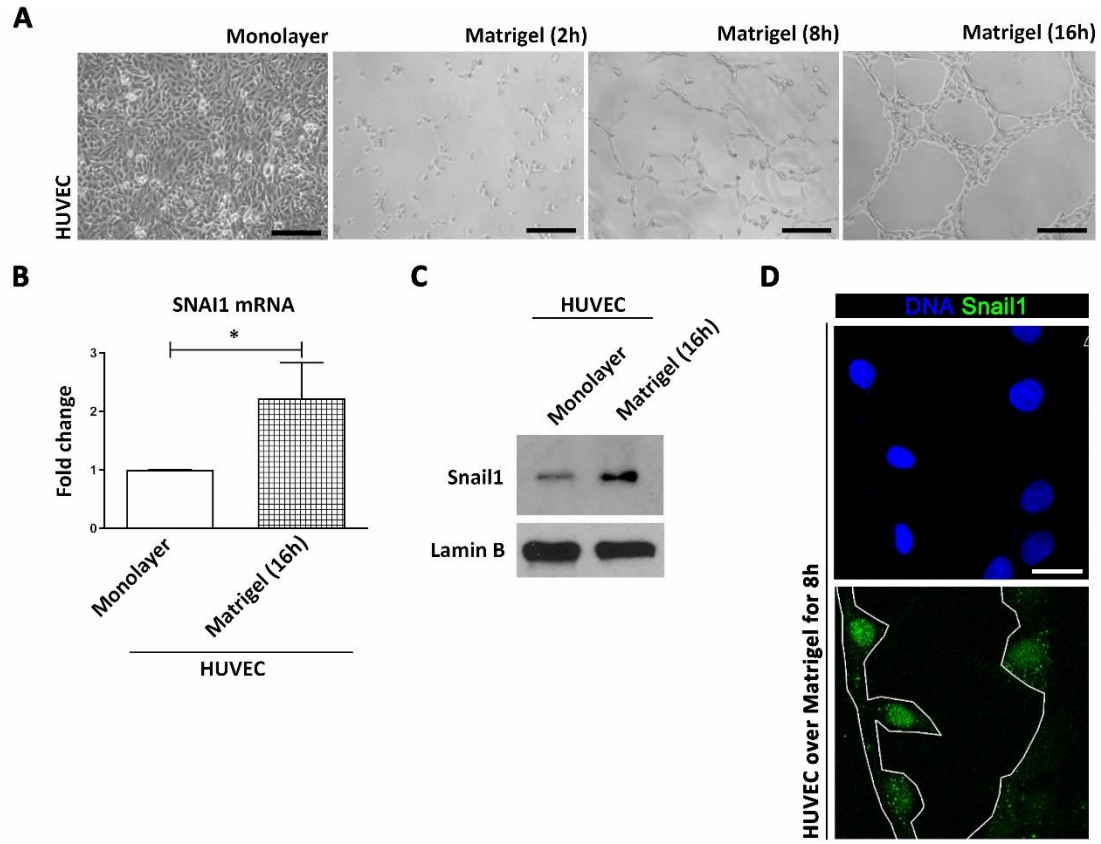

Figure R-4. Matrigel induced tubulogenesis increases Snail1 expression in HUVEC. A, Images of HUVEC on monolayer and over Matrigel at different time points. Scale bars: 200 µm. **B**, Quantification of SNAI1 mRNA in HUVEC on monolayer and over Matrigel for 16h. **C,** Western blot analysis of Snail1 in HUVEC on monolayer and over Matrigel for 16h. **D**, Snail1 (green) immunofluorescence analysis in HUVEC cells cultured on monolayer. Nuclei were counterstained with DAPI (blue). White lines delimit cells. Scale bars: 25 µm. Data in B represent mean values (± SEM) of at least three independent experiments. *p<0.05.

As Snail1 is described to promote important cell transformations such as EMT or EndoMT, we wanted to determine the effects on cell identity of HUVEC depending on their Snail1 levels. As a first glimpse, neither protein downregulation nor overexpression provoke any dramatic change in cell morphology, since they all grew as tessellate colonies, which is typical for endothelial cells (Fig R-5A). Later, we checked classical endothelial (CDH5) and mesenchymal (ACTA2, CDH2, VIM) genes mRNA expression. We

did not observe any differences in CDH5 expression but we did notice a decrease of ACTA2 and VIM in HUVEC siSnail1, and the other way around in HUVEC Snail1^{+} (C5), compared to their respective controls (Figure R-5B). These results were corroborated at protein levels. VE-Cadherin was not altered upon Snail1 level modifications, as well as N-Cadherin and only αSMA was reduced at HUVEC siSnail1, but not altered at HUVEC Snail1^{+} (C5) (Figure R-5C). Altogether, these data confirmed that Snail1 does not modify endothelial cell identity, but it does slightly regulate the expression of some mesenchymal markers.

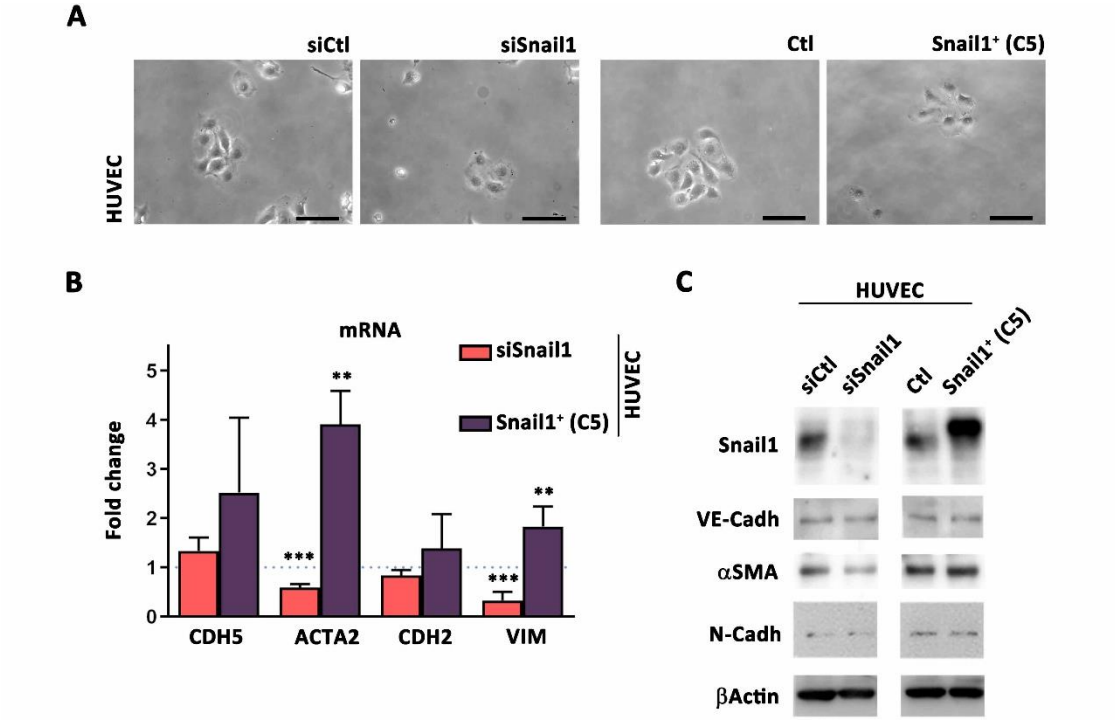

Figure R-5. Snail1 modulates mesenchymal gene expression in HUVEC without affecting their endothelial identity. A, Representative brightfield images of HUVEC siCtl, siSnail1, Ctl and Snail1 (C5) colonies growing on monolayer. Scale bars: 100 µm. **B**, Quantification of CDH5, ACTA2, CDH2 and VIM mRNA in HUVEC siSnail1 and Snail1^{+} (C5) on monolayer, compared to their respective controls represented as a discontinuous line. **C**, Western blot analysis of Snail1, VE-Cadherin, αSMA and N-Cadherin in HUVEC siCtl, siSnail1, Ctl and Snail1 (C5) on monolayer. Data in B represent mean values (± SEM) of at least three independent experiments. **p<0.01; ***p<0.001.

To complete the characterization of HUVEC with upregulated or downregulated Snail1 levels, we assessed their proliferation on monolayer. We noticed that only Snail1

downregulation affected cell proliferation by its downregulation (Figure R-6A). To corroborate this effect, we analyzed the DNA cell cycle distribution of HUVEC siCtl and siSnail1 by FACS, where we observed a slight reduction of proliferating cells (those in S, G2 and M phases) in HUVEC siSnail1 (Figure R-6B).

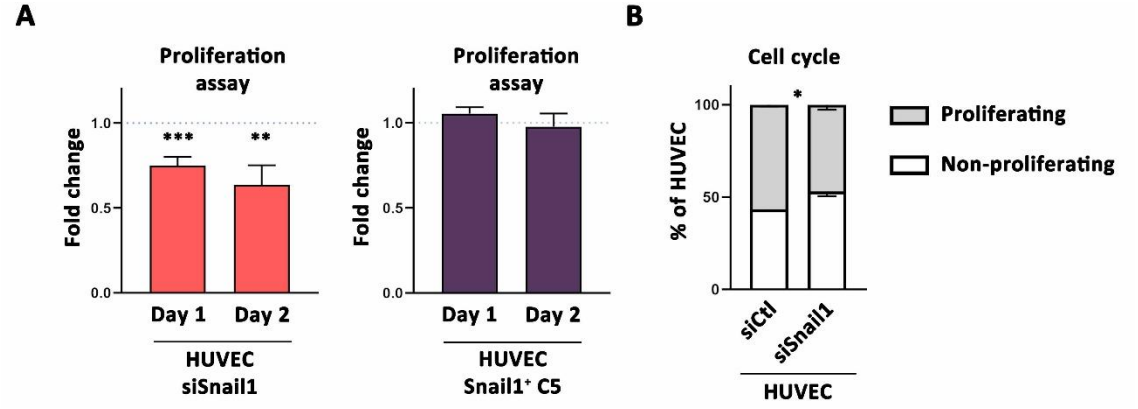

Figure R-6. Snail1 controls cell cycle progression in endothelial cells. A, Proliferation assay of HUVEC siSnail and Snail1$^+$ (C5) at day 1 and 2 on monolayer, compared to their respective controls represented as a discontinuous line. **B**, Cell cycle analysis of HUVEC siCtl and siSnail at day 1 on monolayer. Data in A and B represent mean values (± SEM) of at least three independent experiments. *p<0.05 **p<0.01; ***p<0.001.

3. Snail1 in endothelial cells is essential for *in vitro* angiogenesis

Afterwards, we studied the role of Snail1 in endothelial cells during angiogenesis performing a tubulogenesis assay. In this case, apart from HUVEC siSnail1 and Snail1$^+$ (C5), we used other approaches to manipulate Snail1 levels on HUVEC, such as short hairpin RNA or another clone of HUVEC Snail1$^+$. Snail1 knock down by siRNA or shRNA transfection leaded to a decrease of tubulogenesis, determined by a reduction of master segments and master junctions after 16 hours over Matrigel, compared to their respective controls (Figure R-7A, B). CDH5 and CDH2 mRNA levels remained unaltered after tubulogenic assay, but ACTA2 mRNA levels were diminished in HUVEC siSnail1 and increased in HUVEC Snail1$^+$ (C5), compared to their respective controls (Figure R-7C). Hence, Snail1 is highly relevant for endothelial tubulogenic ability without further cell identity alterations.

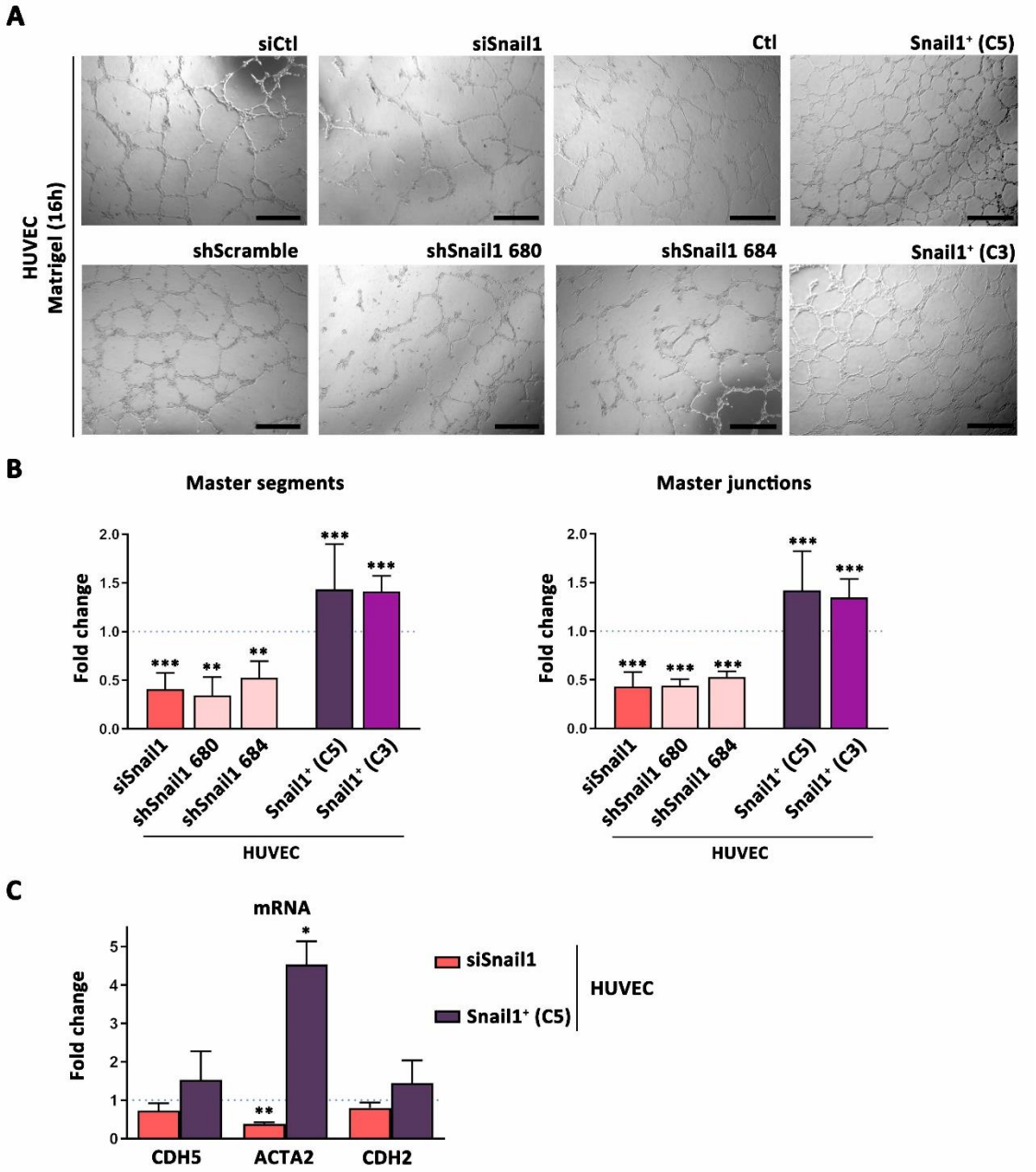

Figure R-7. HUVEC have differential tubulogenic abilities depending on Snail1 expression. A, Images of HUVEC siCtl, siSnail1, Ctl, Snail1^{+} (C5), Snail1^{+} (C3), shScramble, shSnail1 680 and shSnail1 684 over Matrigel for 16h. Scale bars: 200 µm. **B**, Quantification of HUVEC siSnail1, shSnail1 680, shSnail1 684, Snail1^{+} (C5) and Snail1^{+} (C3) master segments (left) and junctions (right), compared to their respective controls represented as a discontinuous line. **C**, Quantification of CDH5, ACTA2 and CDH2 mRNA in HUVEC siSnail1 and Snail1^{+} (C5) over Matrigel for 16h, compared to their respective controls represented as a discontinuous line. Data in B and C represent mean values (± SEM) of at least three independent experiments. *p<0.05 **p<0.01; ***p<0.001.

Apart from tubulogenesis, we addressed the angiogenic ability of endothelial cells in a sprouting assay, in which we analyzed invasion in a Collagen type I matrix of HUVEC with different Snail1 protein levels. The first step was the generation of HUVEC spheroids by hanging drop technique. After one day, those spheroids were embedded in Collagen type I. HUVEC siSnail1 spheroids generated less sprouts and HUVEC Snail1^{+} (C5) more, compared to their respective controls after 24 hours (Figure R-8A, B). Finally, we performed an immunohistochemistry against Snail1 in HUVEC spheroids after the sprouting assay, localizing Snail1^{+} cells in the base of the sprouts (Figure R-8C).

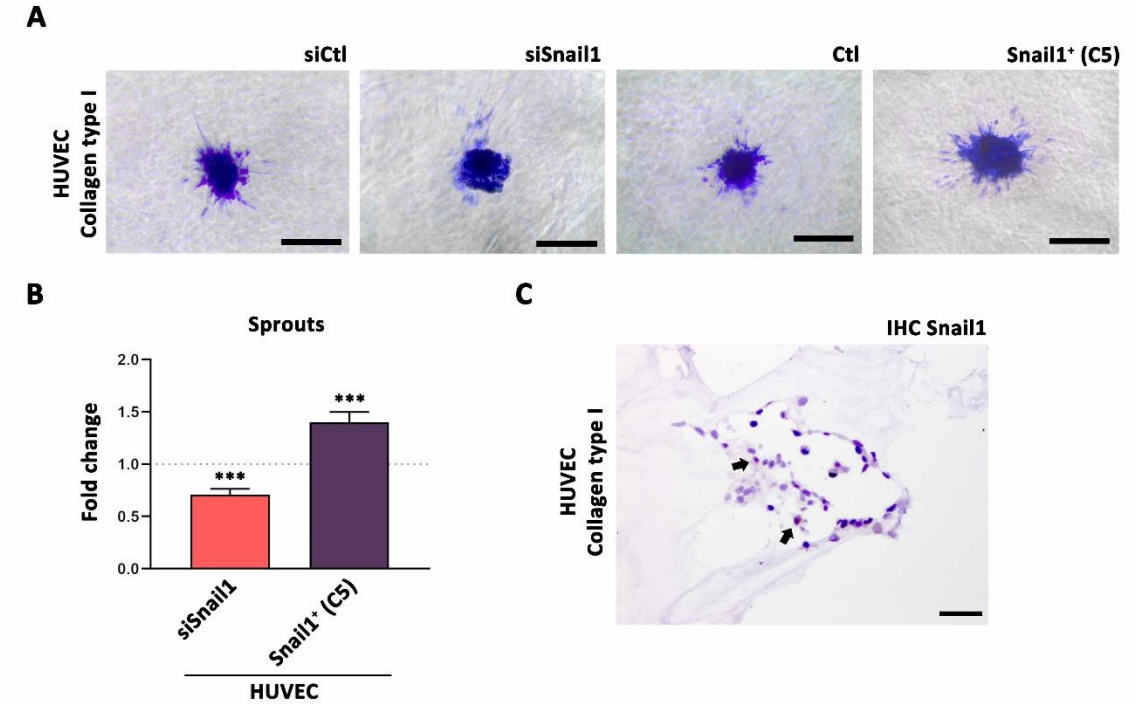

Figure R-8. HUVEC have differential sprouting abilities depending on Snail1 expression. A, Images of HUVEC siCtl, siSnail1, Ctl, Snail1^{+} (C5) spheroids on Collagen type I matrix for one day. Scale bars: 50 µm. **B**, Quantification of HUVEC siSnail1 and Snail1^{+} sprouts (C5), compared to their respective controls represented as a discontinuous line. **C**, Image of anti Snail1 immunohistochemistry in HUVEC spheroids on Collagen type I matrix for one day. Black arrows point to Snail1^{+} HUVEC. Scale bars: 40 µm. Data in B represent mean values (± SEM) of at least three independent experiments. ***p<0.001.

We also assessed the migration ability of HUVEC depending on their Snail1 levels. To address it, we performed an *in vitro* wound healing assay. HUVEC siSnail1 closed the wound slower than HUVEC siCtl, and the other way around with HUVEC Snail1^{+} (C5) compared to Ctl (Figure R-9A, B). Regarding the localization of Snail1^{+} cells in this assay, Snail1 was spotted in HUVEC siCtl at the migration front cells, but not in HUVEC siSnail1, where its signal was almost undetected (Figure R-9C).

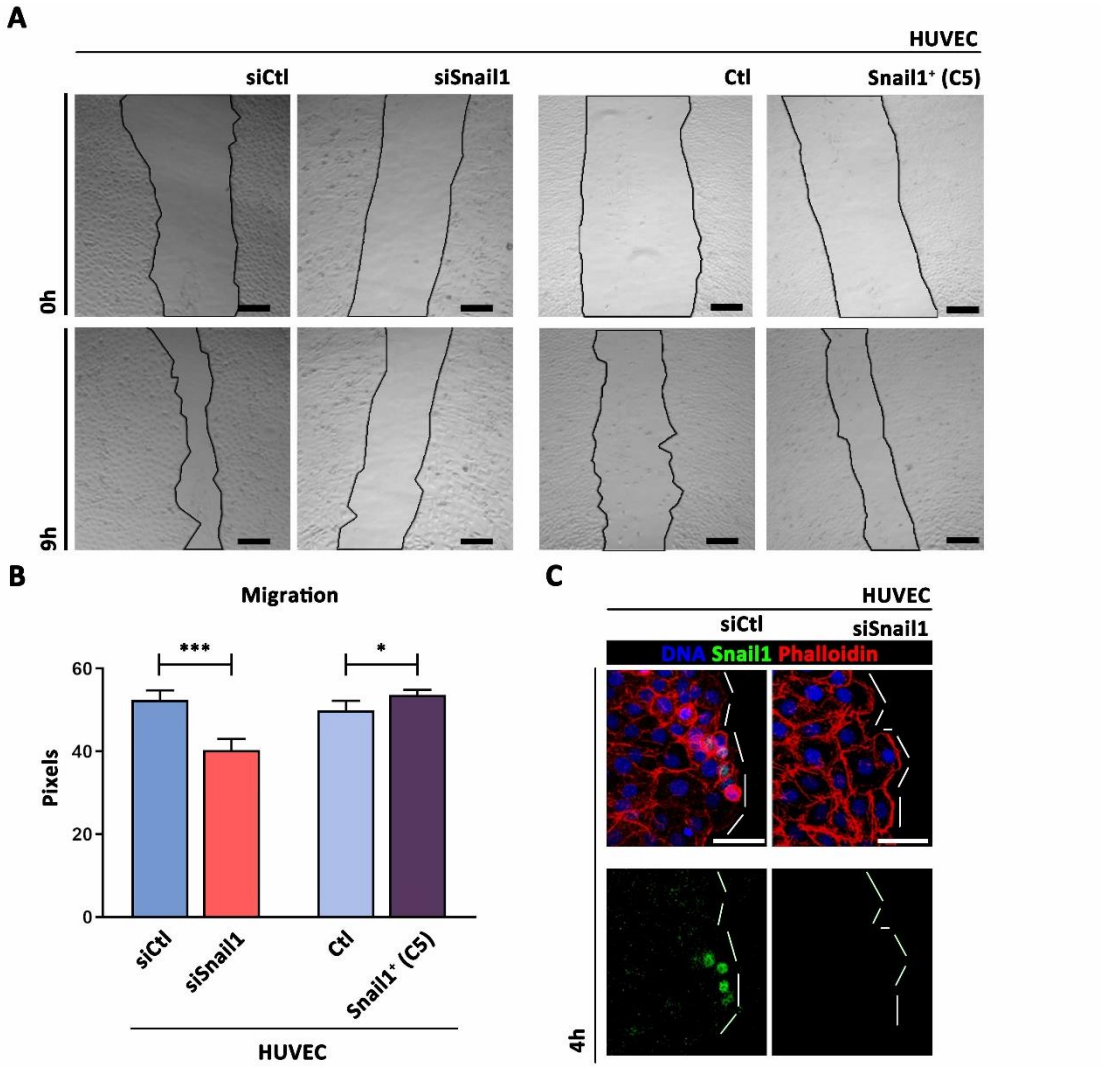

Figure R-9. HUVEC have differential migration abilities depending on Snail1 expression. A, Images of wound healing assay of HUVEC siCtl, siSnail1, Ctl and Snail1^{+} (C5) at 0 and 9h after the wound was done. Black lines delimit the wounds. Scale bars: 200 µm. **B**, Quantification of migrated pixels of HUVEC siCtl, siSnail1, Ctl and Snail1^{+} (C5) 9h after the wound was done. **C**, Snail1 (green) immunofluorescence analysis in HUVEC siCtl or siSnail1 after 4h of wound healing assay. Actin cytoskeleton was stained with Alexa 555 conjugated Phalloidin (red) and nuclei were counterstained with DAPI (blue). Scale bars: 25 µm. Data in B represent mean values (± SEM) of at least three independent experiments. *p<0.05; ***p<0.001.

4. Snail2 induces profound changes in endothelial cells compromising their angiogenic ability

As previously explained, Snail1 belongs to Snail protein family, as well as Snail2. Since Snail2 is also key in EMT, we wondered what it is role in endothelial cells. In order to properly compare, we used HUVEC Snail2^{+} (C3), which had similar levels of exogenous expression as HUVEC Snail1^{+} (C5) (Figure R-10A). Similarly to how we proceeded with the Snail1 study, we first checked how HUVEC looked like upon Snail2 protein levels upregulation. In this case, cell phenotype was strikingly different. HUVEC Snail2^{+} (C3) did not grow as tessellate colonies, but as individual cells (Figure R-10B). This gave us a clue that Snail2 might be provoking a drastic gaining of mesenchymal markers in endothelial cells. In fact, we confirmed a gain of N-Cadherin, αSMA and Vimentin at protein levels upon Snail2 overexpression (Figure R-10C). Nevertheless, VE-Cadherin remained unaltered (Figure R-10C).

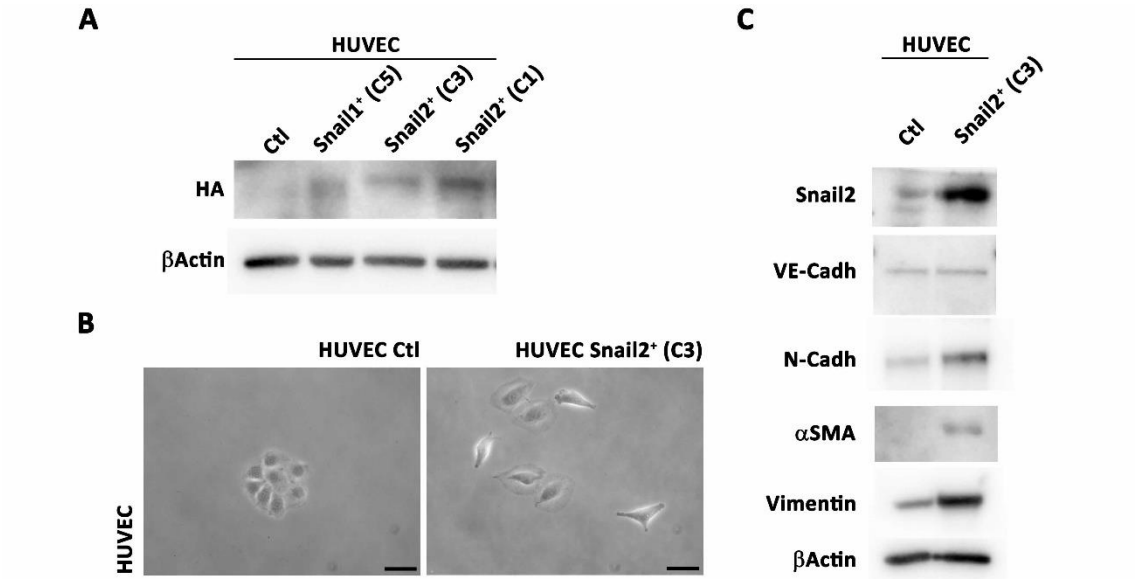

Figure R-10. Snail2 overexpression provokes a gain of mesenchymal markers expression in HUVEC without affecting their cell identity. A, Western blot analysis of HA in HUVEC Ctl, Snail1^{+} (C5) and Snail2^{+} (C3) and Snail2^{+} (C1). **B**, Representative brightfield images of HUVEC Ctl and Snail2^{+} (C3) colonies growing on monolayer. Scale bars: 100 µm. **C**, Western blot analysis of Snail2, VE-Cadherin, N-Cadherin, αSMA and Vimentin in HUVEC Ctl and Snail2^{+} (C3) on monolayer.

Regarding their tubulogenic ability, HUVEC Snail2^{+} (C3) formed a highly unstable honeycomb panel with significantly fewer master segments and junctions (Figure R-11A, B). Hence, Snail2 strongly controlled mesenchymal gene expression in endothelial cells. Even though Snail2 overexpressing cells remained as endothelial cells, they lose angiogenic properties, performing an almost full EndoMT. We did not longer keep working on Snail2, since the analysis of its function in endothelial cells would represent an entirely different project.

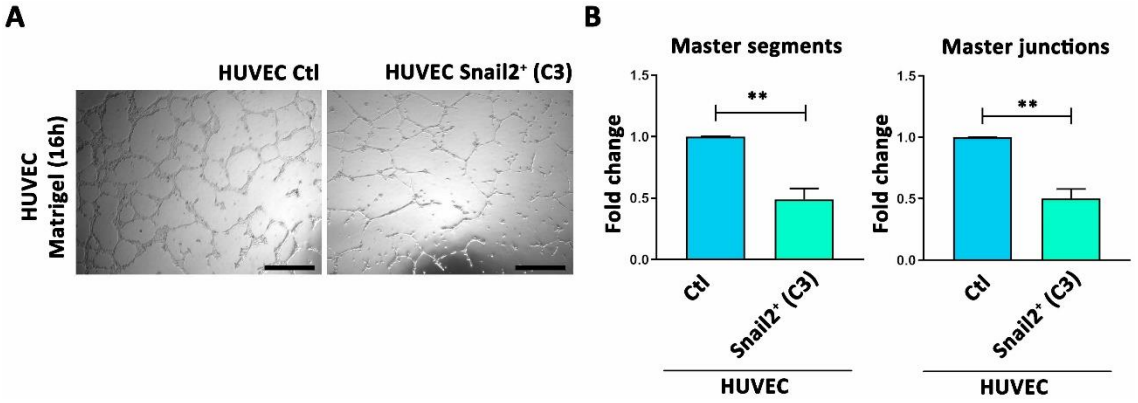

Figure R-11. Snail2 overexpression reduces HUVEC tubulogenic ability. A, Images of HUVEC Ctl and Snail2^{+} (C3) over Matrigel for 16h. **B**, Quantification of their master segments (left) and junctions (right). Scale bars: 200 µm. Data in B represent mean values (± SEM) of at least three independent experiments. **p<0.01.

5. Snail1 modulates the activation status and the expression profile of endothelial cells

Returning to Snail1 analysis, once we determined that this transcription factor had a relevant role during *in vitro* angiogenesis, we investigated the molecular events altered by Snail1 in HUVEC behind this process. We decided to focus on downstream molecular effectors of angiogenic signaling.

Firstly, we studied the angiogenic signaling cascades by analyzing the phosphorylation levels of AKT and ERK of HUVEC on monolayer. AKT and ERK showed reduced phosphorylated levels in HUVEC siSnail1 compared to siCtl, and higher in HUVEC Snail1^{+} (C5) compared to Ctl (Figure R-12A). Afterwards, we checked the FGF and VEGF receptors gene expression. On monolayer, we observed that some receptor levels showed a trend downward in HUVEC siSnail1 compared to siCtl, although the only

significant one was FGFR4 (Figure R-12B). Over Matrigel, this finding was corroborated and supported by an overexpression of FGFR4 mRNA levels in HUVEC Snail1^{+} (C5) compared to Ctl (Figure R-12C). Moreover, FGFR3 mRNA levels followed the same tendency as FGFR4 (Figure R-12C).

Finally, we checked the expression of angiogenesis related genes, which some of them presented an altered pattern. For instance, VEGFA mRNA was upregulated in HUVEC Snail1^{+} (C5) compared to Ctl, as well as FGF2, which, in this case, was also significantly downregulated in HUVEC siSnail1 compared to siCtl (Figure R-12D). COL4A1 and MMP mRNA levels were also downregulated in HUVEC siSnail1 and upregulated in HUVEC Snail1^{+} (C5), compared to their respective controls (Figure R-12D). Contrary to this trend, CAV1 mRNA levels were upregulated in HUVEC siSnail1 and downregulated in HUVEC Snail1^{+} (C5), compared to their controls (Figure R-12D). Taking everything into account, we could state that Snail1 modulate the gene expression of endothelial cells.

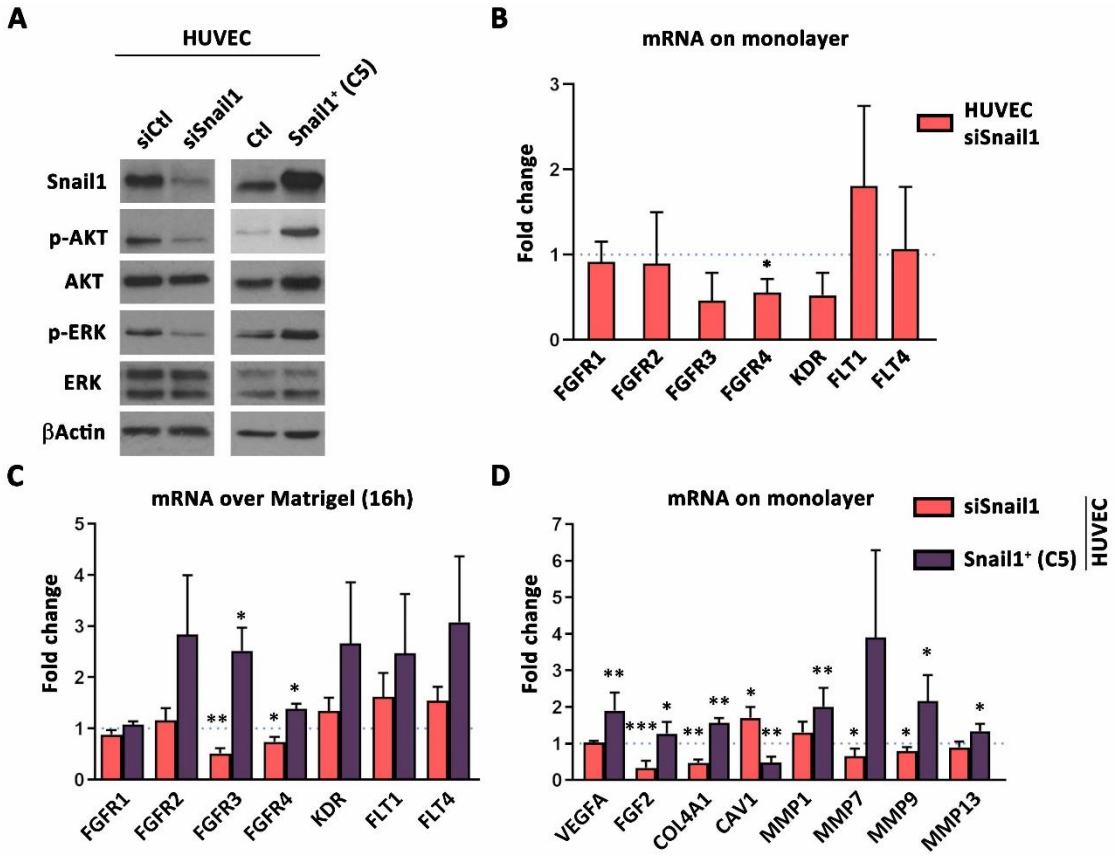

Figure R-12. HUVEC have differential activation status and expression profile depending on Snail1 expression. A, Western blot analysis of Snail1, p-AKT, AKT, p-ERK and ERK in HUVEC siCtl,

siSnail1, Ctl and Snail1^{+} (C5) on monolayer. **B**, Quantification of FGFR and VEGFR mRNA in HUVEC siSnail1 on monolayer, compared to HUVEC siCtl values represented as a discontinuous line. **C**, Quantification of FGFR and VEGFR mRNA in HUVEC siSnail1 and Snail1^{+} (C5) over Matrigel for 16h, compared to their respective controls represented as a discontinuous line. **D**, Quantification of VEGFA, FGF2, COL4A1, CAV1, MMP1, 7, 9 and 13 in HUVEC siSnail1 and Snail1^{+} (C5) over Matrigel for 16h, compared to their respective controls represented as a discontinuous line. Data in B, C and D represent mean values (± SEM) of at least three independent experiments. *p<0.05; **p<0.01; ***p<0.001.

6. Snail1 is required for a complete response to angiogenic factors in endothelial cells

After that, we addressed the effect of angiogenic factors (VEGF-A and FGF2) on HUVEC with different levels of Snail1. Both angiogenic factors increased sprouting ability of HUVEC siCtl and Ctl and to a lesser extent in HUVEC siSnail1 (Figure R-13). HUVEC Snail1^{+} (C5) did not show any significant improvement with the angiogenic factors (Figure R-13). We also performed the tubulogenesis and wound healing assays, obtaining similar results (data not shown). Summing up, these results indicated that angiogenic factors provoked an increase of angiogenic abilities in HUVEC, as long as they could express Snail1, without overexpressing it.

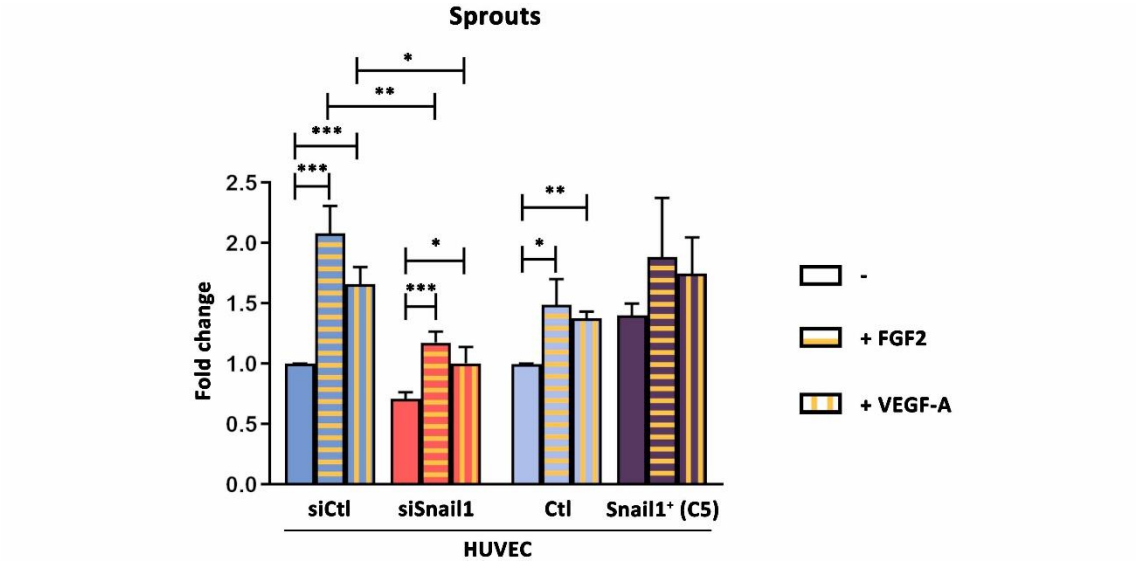

Figure R-13. HUVEC have different sprouting abilities depending on Snail1 expression upon angiogenic factors induction. Quantification of HUVEC siCtl, siSnail1, Ctl and Snail1+ (C5) sprouts, with or without FGF2 or VEGF-A treatments. Data represent mean values (± SEM) of at least three independent experiments. *p<0.05; **p<0.01; ***p<0.001.

Finally, in order to decipher the molecular causes by which HUVEC knocked down of Snail1 had an unbalanced response to angiogenic factors, we analyzed their angiogenic receptor expression and the cell activation status upon stimulation. We observed that HUVEC siCtl increased significantly FLT1 (VEGFR2) and FLT4 (VEGFR3) mRNA levels under VEGF-A administration, which did not happen in HUVEC siSnail1 (Figure R-14). Similar results were obtained in HUVEC over Matrigel (data not shown).

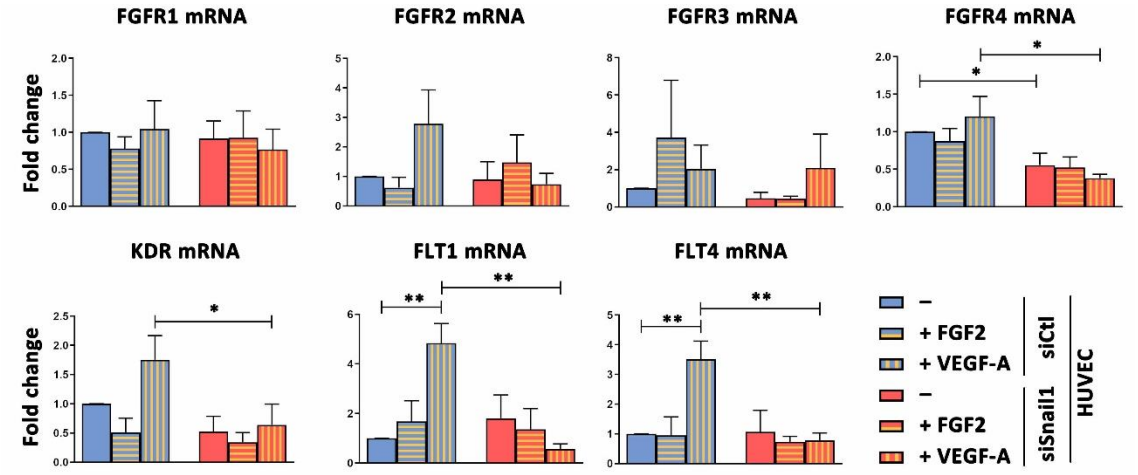

Figure R-14. HUVEC have different angiogenic receptor expression levels depending on Snail1 expression upon angiogenic factors stimulation. Quantification of FGFR and VEGFR mRNA in HUVEC siCtl and siSnail1 on monolayer with or without FGF2 or VEGF-A treatment. Data represent mean values (± SEM) of at least three independent experiments. *p<0.05; **p<0.01.

Looking for downstream effectors, we next analyzed the ERK phosphorylation response of HUVEC on monolayer under angiogenic factors. We noticed that HUVEC siCtl could response to angiogenic factors by increasing their phosphorylation of ERK, which, in contrast, was completely abolished in HUVEC siSnail1 (Figure R-15A). That indicated that the activity of the receptors in HUVEC siCtl was higher after stimulation than in the case of HUVEC siSnail1. Finally, we observed that some genes related to Snail1 activation were overexpressed upon angiogenic factors.[162,163] MMP7 and TWIST1 mRNA levels were increased upon FGF2 or VEGF-A, which was not the case in HUVEC siSnail1 (Figure R-15B). Thus, we corroborated that Snail1 is key for a proper response to angiogenic factors in endothelial cells.

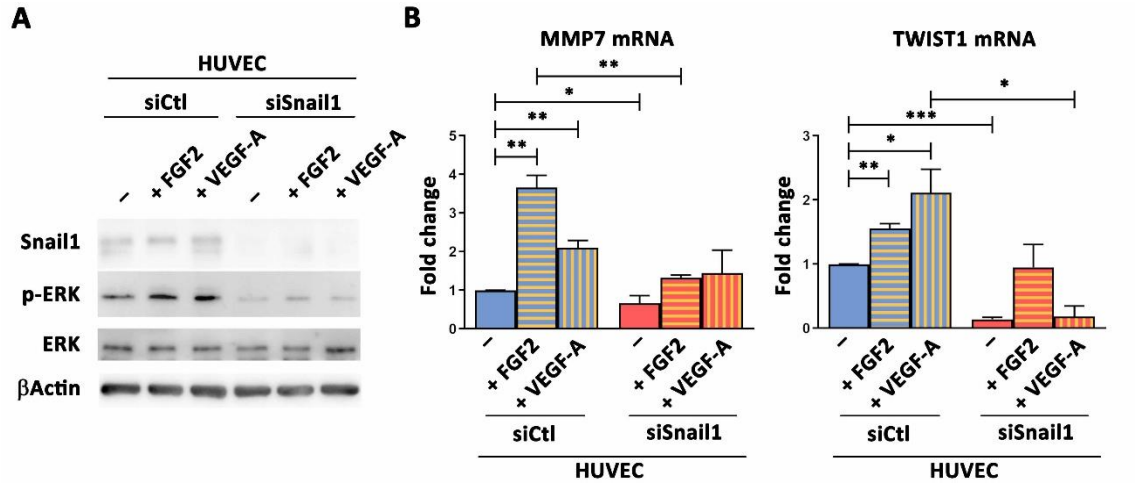

Figure R-15. HUVEC have different molecular responses depending on Snail1 expression upon angiogenic factors stimulation. A, Western blot analysis of Snail1, p-ERK and ERK in HUVEC siCtl and siSnail1 on monolayer with or without FGF2 or VEGF-A treatment for 10min. **B**, Quantification of MMP7 or TWIST1 mRNA expression in HUVEC siCtl and siSnail1 on monolayer with or without FGF2 or VEGF-A treatment. Data in B represent mean values (± SEM) of at least three independent experiments. *p<0.05; **p<0.01; ***p<0.001.

7. Breast tumor cells induce angiogenesis *in vitro* through FGF2 and VEGF-A signaling by a Snail1 dependent mechanism

Apart from the exogenous addition of VEGF-A and FGF2, we boosted endothelial cell activity with tumoral cells, which are known to induce angiogenesis.[104] To address it, we used conditioned medium from epithelial cells extracted from MMTV-PyMT mice tumors (ePyMT) over HUVEC. First, we checked that HUVEC cultured with this conditioned medium on monolayer enhanced SNAI1 mRNA levels (Figure R-16A). After that, we wondered if FGF2 or VEGF-A in the ePyMT conditioned medium were responsible for that upregulation. Thus, we used the antibody bevacizumab to neutralize VEGF-A present in the conditioned medium or the drug SU5402 to block HUVEC FGF downstream signaling. We observed that both molecules abrogated the upregulation of Snail1 at protein levels in HUVEC on monolayer upon ePyMT conditioned medium (Figure R-16B). Similar results at mRNA levels were observed in HUVEC over Matrigel (data not shown).

Next, we tested the tubulogenic ability of HUVEC with different Snail1 proteins expression levels cultured with ePyMT conditioned medium, with or without

bevacizumab or SU5402 (Figure R-16C). We found that ePyMT conditioned medium increased tubulogenesis when Snail1 could be expressed, but not when its expression was knocked down (Figure R-16C). Furthermore, we observed that both inhibitors reduced the number of master segments in HUVEC, except when Snail1 was overexpressed (Figure R-16C). Similar patterns were followed in master junctions (data not shown).

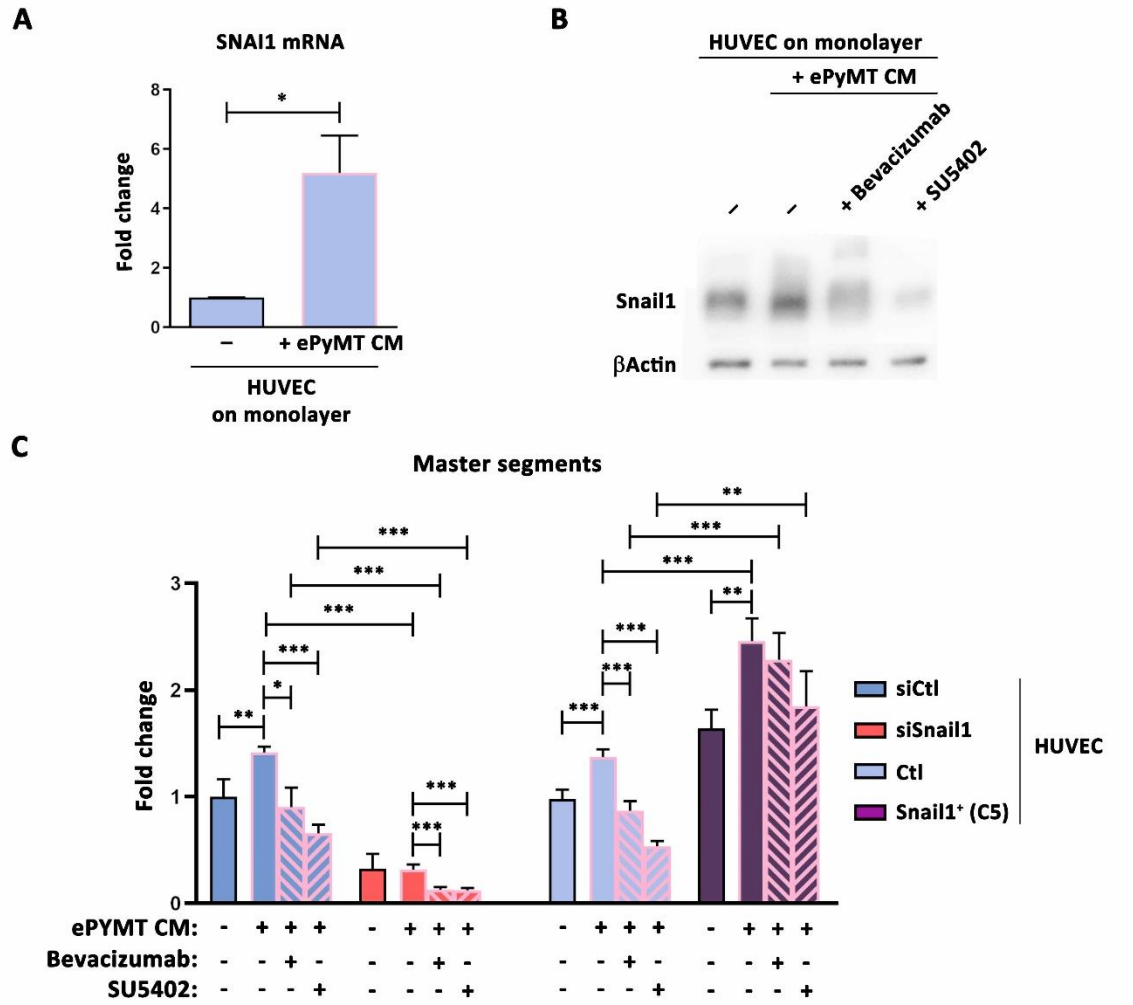

Figure R-16. ePyMT secretome induces Snail1 expression and tubulogenesis through VEGF and FGF signaling. A, Quantification of SNAI1 mRNA in HUVEC on monolayer with or without ePyMT conditioned medium. **B**, Western blot analysis of Snail1 in HUVEC cultured on monolayer with or without ePyMT conditioned medium and treated with or without bevacizumab or SU5402. **C**, Quantification of master segments in HUVEC siCtl, siSnail1, Ctl and Snail1^{+} (C5) cultured with or without ePyMT conditioned medium, treated with or without bevacizumab or SU5402. Data in A and C represent mean values (± SEM) of at least three independent experiments. *p<0.05; **p<0.01; ***p<0.001.

8. Endothelial Snail1 is required for adult angiogenesis *in vivo*, but not organ morphology nor vascularization

After an *in vitro* analysis of the role of Snail1 in endothelial cells, we wanted to decipher its role *in vivo*. First, we addressed the function of endothelial Snail1 in adult mice, generating a murine line with a specific depletion of Snail1 in their endothelium, named as VE-Cadh^{Snail1CT} and VE-Cadh^{Snail1KO}. We depleted Snail1 in endothelial cells in 6 weeks old mice by tamoxifen injection, and let these mice grew for 3 other weeks (Figure R-17A). Neither their body nor their main organs weight presented any alterations (Figure R-17B, C). Moreover, their main organs were anatomically and morphologically identical to the control (Figure R-17D).

Apart from those general effects, we focused on endothelial cells. After analyzing the number of endothelial cells by FACS in lung and liver from VE-Cadh^{Snail1CT} and VE-Cadh^{Snail1KO} mice, we did not observe any significant difference (Figure R-18A, B). Indeed, their proliferation status, studied by analyzing their DNA content by FACS, was also unaltered (Figure R-18C). Finally, we checked the basal permeability status of their vasculature by quantifying Evans Blue extravasation in breast, lung and liver (Figure R-18D). We did not find significant differences upon endothelial Snail1 depletion (Figure R-18E). Actually, we could not detect Snail1 expression in vessels at quiescent state in breasts, neither in VE-Cadh^{Snail1CT} nor VE-Cadh^{Snail1KO} mice (Figure R-19). These results leaded us to confirm that Snail1 in endothelial cells seem not to have any active role in adult mice at quiescent state.

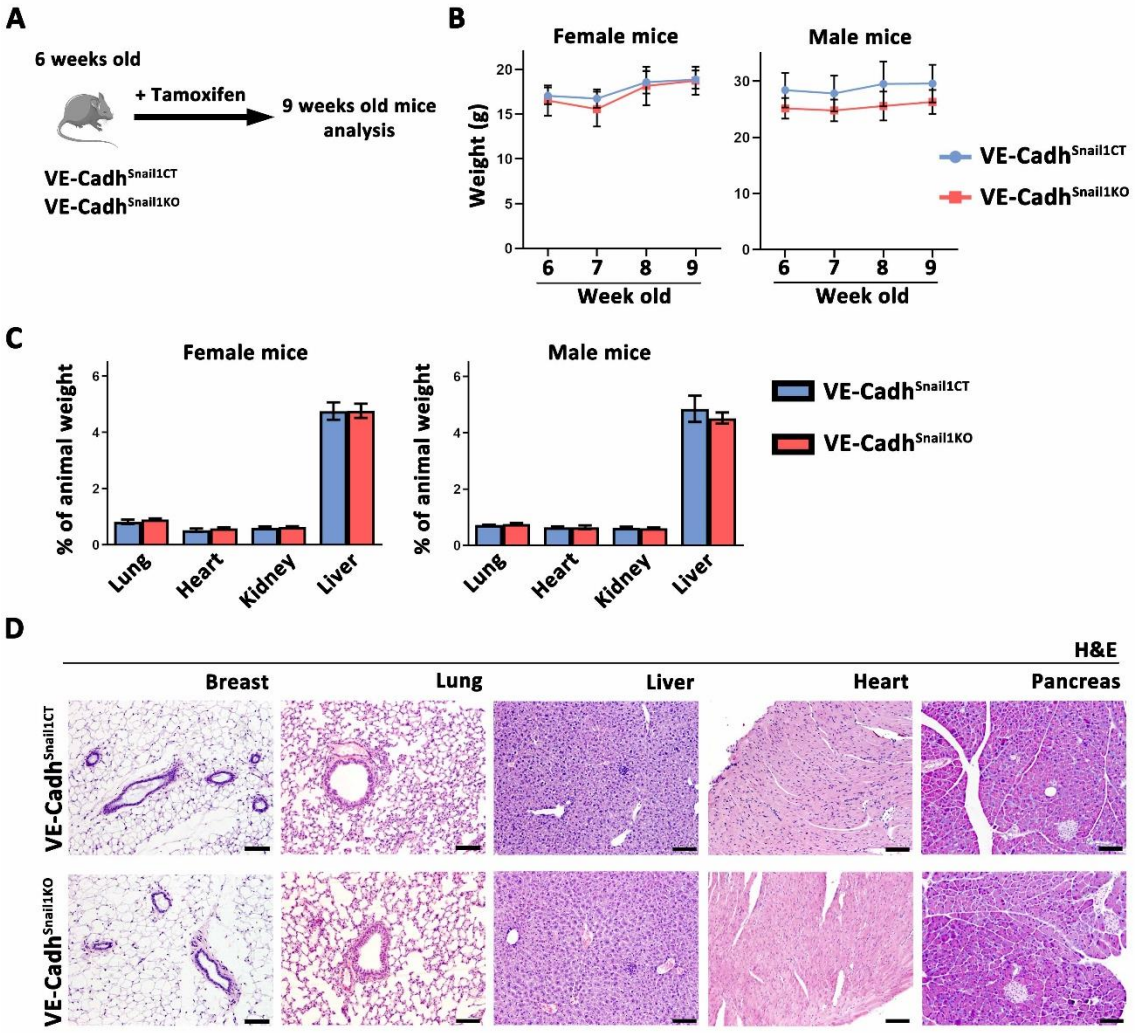

Figure R-17. Adult mice endothelial cells do not need to express Snail1 to maintain organ morphology. A, Scheme of mouse strategy used for their characterization. **B**, Body weight analysis of 6 to 9 weeks old VE-Cadh$^{Snail1CT/KO}$ mice after tamoxifen injection. **C**, Weight analysis of lung, heart, kidney and liver in 9 weeks old VE-Cadh$^{Snail1CT/KO}$ mice. **D**, Representative images of hematoxylin and eosin staining of breast, lung, liver, heart, and pancreas of 9 weeks old VE-Cadh$^{Snail1CT/KO}$ mice. Scale bar: 100 µm. Data in B and C represent mean values (± SEM) of at least three mice.

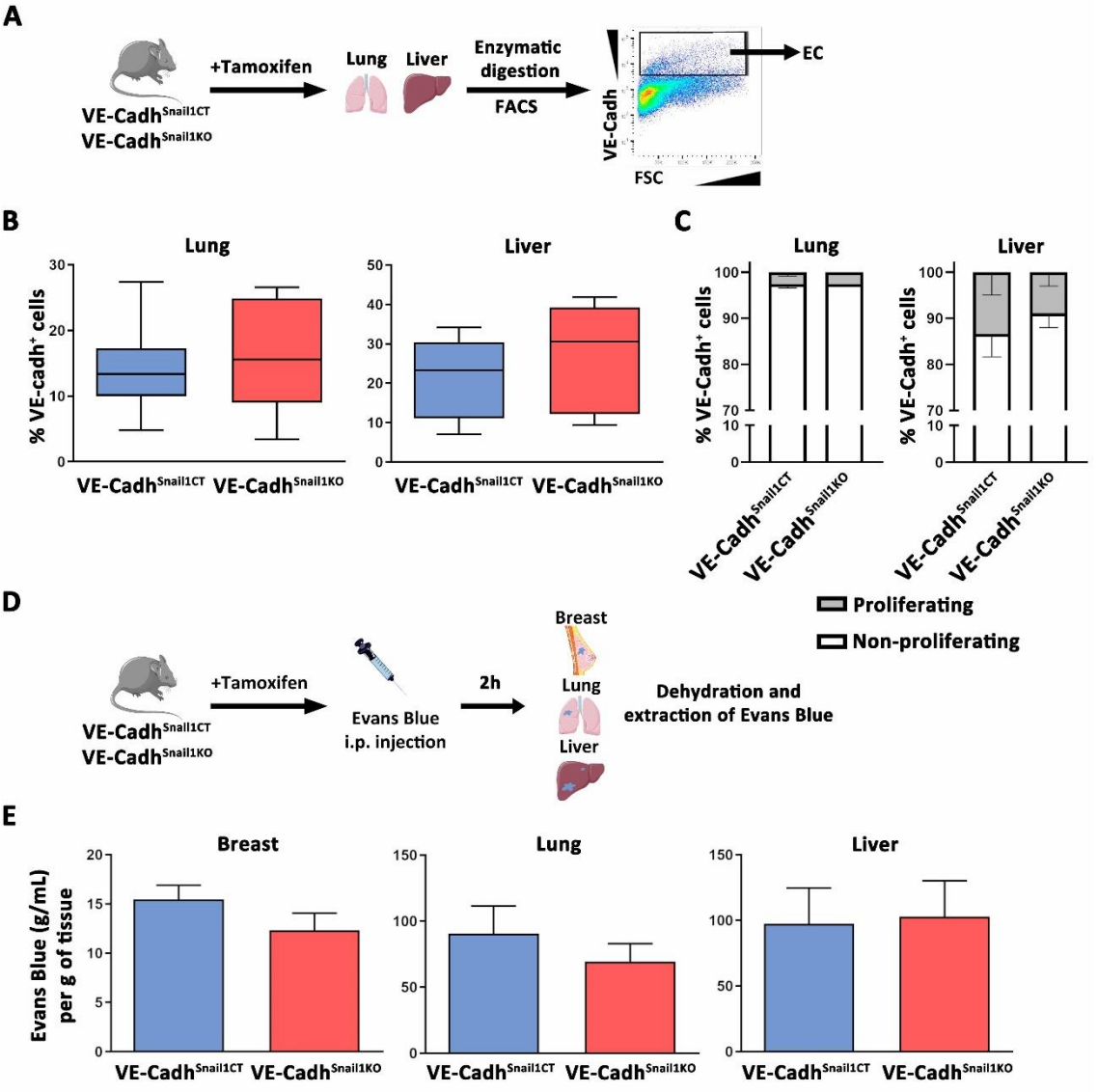

Figure R-18. Endothelial cells in adult mice do not need Snail1 for proper tissue vascularization. **A**, Scheme of workflow and gating strategy for endothelial cell analysis in lung and liver from 9 weeks old VE-Cadh$^{Snail1CT/KO}$ mice. **B**, Percentage of endothelial cells in lung (left) and liver (right) from adult VE-Cadh$^{Snail1CT/KO}$ mice. **C**, Proliferation rate of endothelial cells in lung (left) and liver (right) of 9 weeks old VE-Cadh$^{Snail1CT/KO}$ mice. **D**, Scheme of permeability assay in VE-Cadh$^{Snail1CT/KO}$ mice. **E**, Quantification of Evans Blue (g/mL) per g of dehydrated breast (left), lung (middle) and liver (right) of 9 weeks old VE-Cadh$^{Snail1CT/KO}$ mice. Data in B, C and E represent mean values (± SEM) of at least three mice.

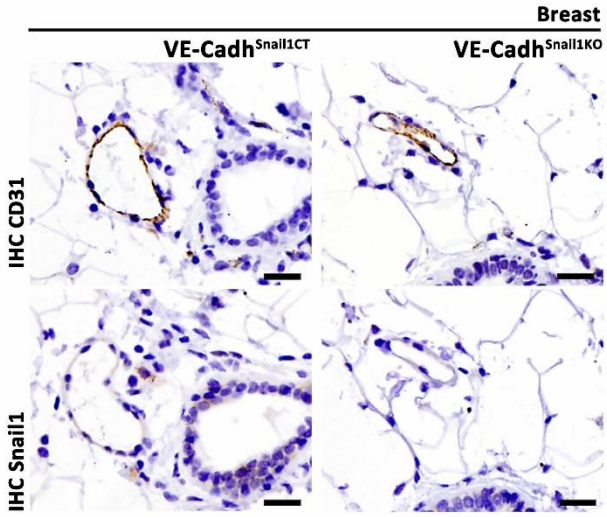

Figure R-19. Endothelial cells do not express Snail1 in adult mice vasculature at quiescent state. Images of anti CD31 (upper row) and anti Snail1 (lower row) immunohistochemistry in breasts of 9 weeks old VE-Cadh$^{Snail1CT/KO}$ female mice. Scale bar: 20 µm.

Once we certified that, at quiescent state, Snail1 was not crucial in endothelial cells, we tested the angiogenic response of VE-Cadh^{Snail1CT} and VE-Cadh^{Snail1KO} mice injecting subcutaneously Matrigel, with or without a supplemental angiogenic boost of FGF2 or VEGF-A, for 7 days (Figure R-20A). We checked the presence of Snail1 in endothelial cells migrated into the Matrigel plug, corroborating that some Snail1^{+} cells were also CD31^{+} (Figure R-20B). Later, we quantified the amount of CD31^{+} stained area, determining that VE-Cadh^{Snail1CT} had an increase of total angiogenesis, with or without the supplementation of angiogenic factors, compared to VE-Cadh^{Snail1KO} mice (Figure R-20C, D). The boost of angiogenesis caused by FGF2 or VEGF-A in VE-Cadh^{Snail1KO} Matrigel plugs was not as higher as in VE-Cadh^{Snail1CT} mice, showing an impairment of this response (Figure R-20C, D). Apart from the amount of angiogenesis, we analyzed the morphology of these neo-vessels by quantifying their area and perimeter. Without angiogenic factors supplementation, VE-Cadh^{Snail1CT} neo-vessels had decreased area and perimeter than VE-Cadh^{Snail1KO} ones (Figure R-20E, F). In the case of FGF2 addition, vessels reduced their size but VE-Cadh^{Snail1CT} vessels remained smaller than VE-Cadh^{Snail1KO} ones (Figure R-20E, F). Finally, VEGF-A supplementation induced no differences in the size of VE-Cadh^{Snail1CT} and VE-Cadh^{Snail1KO} neo-vessels (Figure R-20E, F). These results indicate that endothelial Snail1 is essential for *in vivo* angiogenesis and proper response to angiogenic factors.

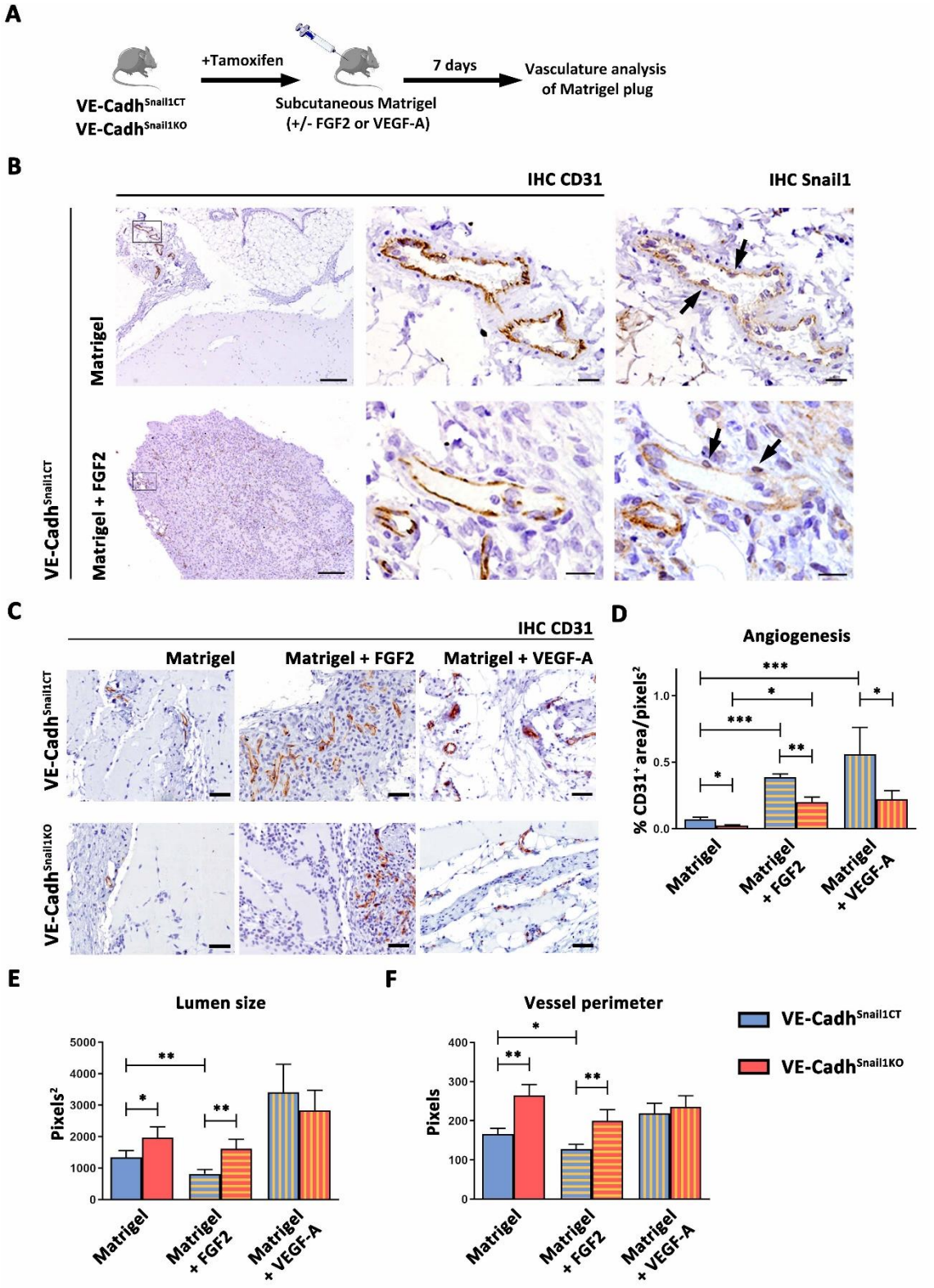

Figure R-20. Snail1 expression in endothelial cells controls *in vivo* Matrigel plug induced angiogenesis and neo-vessels morphology. A, Scheme of subcutaneous Matrigel plug assay *in vivo*. **B**, Images of anti CD31 and anti Snail1 immunohistochemistry in Matrigel plugs with or without FGF2 in VE-Cadh$^{Snail1CT/KO}$ mice. Black arrows indicate Snail1^{+} endothelial cells. **C**, Images of anti CD31 immunohistochemistry in Matrigel plug with or without FGF2 or VEGF-A in VE-

Cadh^{Snail1CT} mice. **D-F**, Quantification of CD31^{+} stained area (D), vessel lumen size (E) and vessel perimeter (F) in Matrigel plug with or without FGF2 or VEGF-A supplementation. Data in D, E and F represent mean values (± SEM) of at least three mice per condition. *p<0.05; **p<0.01; ***p<0.001.

9. Endothelial Snail1 expression activates stroma fostering breast tumor initiation

Following the Matrigel plug assay, we next worked with a breast tumor murine model. In this case, we used MMTV-PyMT mice which we crossed with our VE-Cadh^{Snail1} mice line, generating a spontaneous breast tumor mouse model with a specific conditional deletion of Snail1 in their endothelial cells. Depletion of endothelial Snail1 upon tamoxifen administration was done at 6 weeks old mice, when murine puberty begins and the PyMT oncogene starts to be expressed. One of the first phenotypes we observed was a delay in the tumor onset, since PyMT VE-Cadh^{Snail1CT} mice had a mean of 92 days, compared to PyMT VE-Cadh^{Snail1KO} mice, with a mean of 116 days (Figure R-21A).

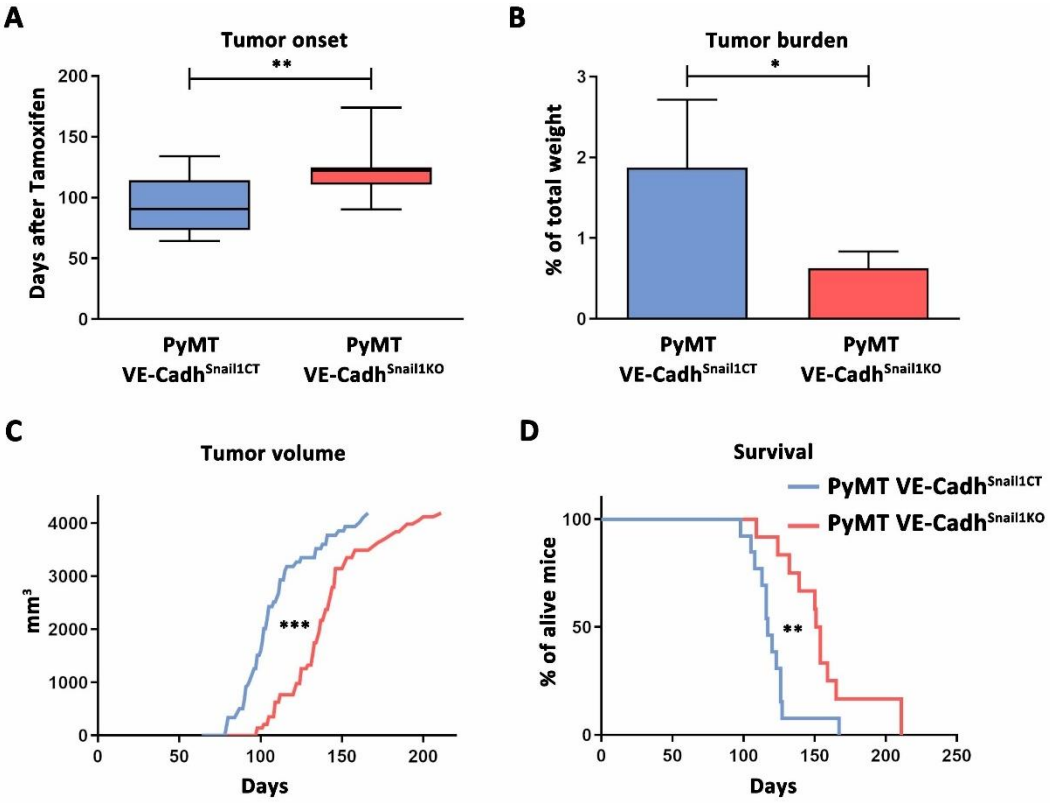

Figure R-21. Endothelial Snail1 regulates tumor development. A-D, Comparison of tumor onset (A), tumor burden at 18 weeks (B), tumor volume (C) and mice survival (D) in PyMT VE-

Cadh$^{Snail1CT/KO}$ mice. Data in A and B represent mean values (± SEM). Data in D is represented as a Kaplan–Meier curve. *p<0.05; **p<0.01; ***p<0.001.

Moreover, PyMT VE-Cadh^{Snail1CT} mice showed an increase in their tumor burden at 18 weeks of age, as well as in their tumor volume growth, compared to PyMT VE-Cadh^{Snail1KO} mice (Figure R-21B). As a consequence of it, mice survival was decreased 36 days in PyMT VE-Cadh^{Snail1CT} (Figure R-21C, D). The slowdown in the tumor growth of PyMT VE-Cadh^{Snail1KO} mice was caused by the delay in their tumor onset, since when tumors started to grow, PyMT VE-Cadh^{Snail1CT} and PyMT VE-Cadh^{Snail1KO} tumor growth curves were parallel (Figure R-21C). Due to all of these, we focused on the analysis of tumor initiation process.

First of all, we checked the proliferation and apoptosis at in the first phases of tumorigenesis, which are premalignant ducts and tumors at hyperplasia stage, in PyMT VE-Cadh^{Snail1CT} and PyMT VE-Cadh^{Snail1KO} mice. For that, we stained with an anti Ki67 to detect proliferative cells and with an anti Cleaved Caspase-3 for apoptotic ones (Figure 22A, C). We observed a significant increase of proliferation in tumors at hyperplasia stage in PyMT VE-Cadh^{Snail1CT} mice (Figure R-22A, B). Apoptosis did not present any difference (Figure R-22C, D).

In the earliest phase of tumorigenesis, premalignant ducts, we analyzed angiogenesis by an anti CD31 immunohistochemistry (Figure R-23A). More vessels were detected surrounding PyMT VE-Cadh^{Snail1CT} premalignant ducts than compared to PyMT VE-Cadh^{Snail1KO} ones (Figure R-23A, B). Moreover, these vessels were morphologically different, since PyMT VE-Cadh^{Snail1KO} vessels were bigger in area and perimeter than PyMT VE-Cadh^{Snail1CT} ones (Figure R-23C, D). Furthermore, the location of these vessels was altered. PyMT VE-Cadh^{Snail1CT} vessels tend to be closer to the premalignant ducts, compared to PyMT VE-Cadh^{Snail1KO} ones, that were prone to be outside of the extracellular matrix surrounding the premalignant ducts (Figure R-23E). Therefore, angiogenesis at early stages of tumorigenesis is already controlled by the expression of Snail1 in endothelial cells.

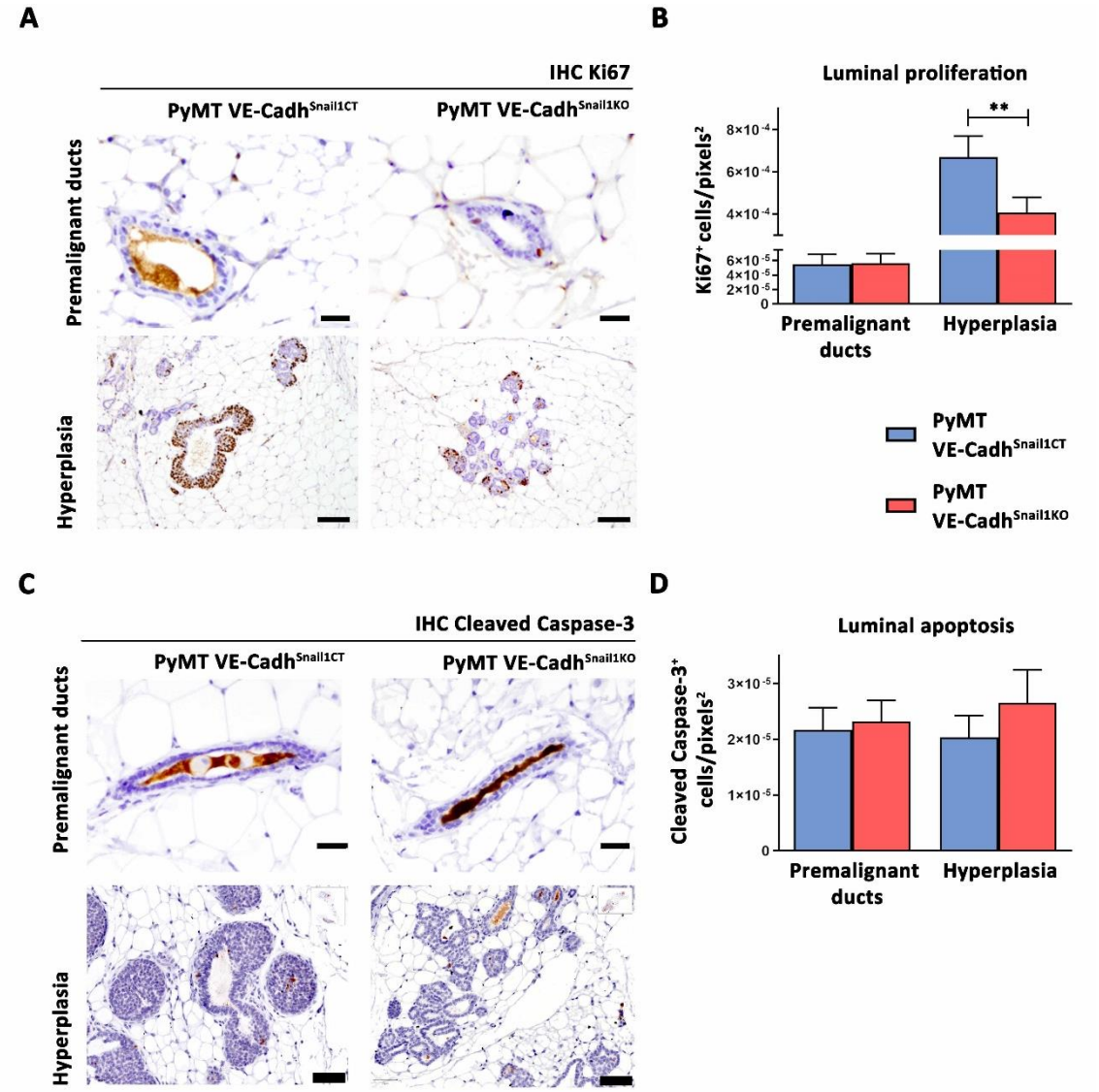

Figure R-22. Endothelial Snail1 expression regulates tumor growth at early tumor stages without affecting apoptosis. A-B, Images of anti Ki67 immunohistochemistry (A) and quantification of Ki67^{+} cells per pixels^{2} (B) in PyMT VE-Cadh$^{Snail1CT/KO}$ tumors at premalignant and hyperplasia stage. Scale bar (upper): 20 µm; (lower): 50 µm. **C-D**, Images of anti Cleaved Caspase-3 immunohistochemistry (C) and quantification of Cleaved Caspase-3^{+} cells per pixels^{2} (D) in PyMT VE-Cadh$^{Snail1CT/KO}$ mice at premalignant and hyperplasia stage. Scale bar (upper): 20 µm; (lower): 50 µm. Data in B and D represent mean values (± SEM). **p<0.01.

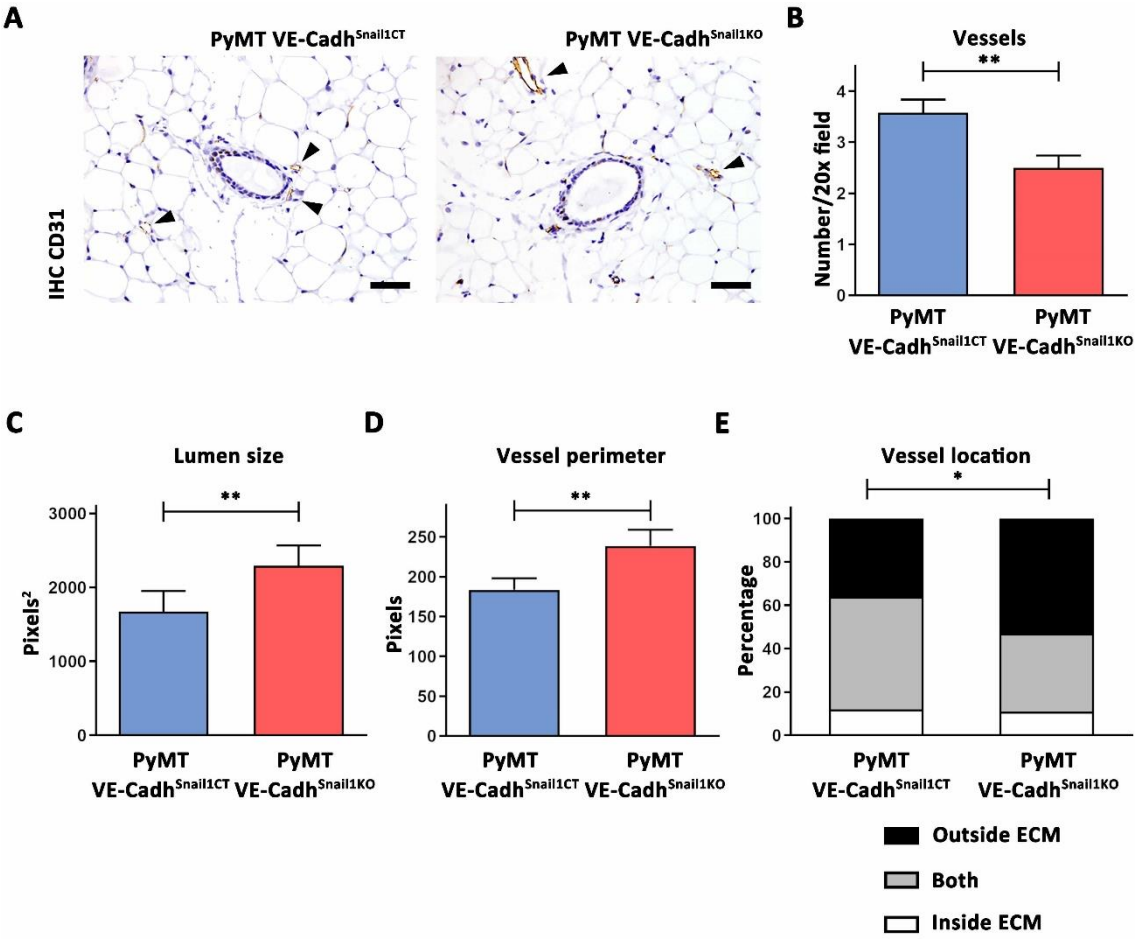

Figure R-23. Angiogenesis is altered due to Snail1 presence in endothelial cells at early tumor stages. A-E, Images of anti CD31 immunohistochemistry (A) and quantification of vessel number per 20x field (B), vessel lumen size (C), vessel perimeter (D) and vessel location (E) in PyMT VE-Cadh$^{Snail1CT/KO}$ tumors in premalignant ducts. Black arrowheads point vessels. Scale bar: 20 µm. Data in B, C and D represent mean values (± SEM). *p<0.05; **p<0.01.

Stroma activation is one of the main causes of tumor progression. For that, we hypothesized that stroma could be differentially activated depending on Snail1 in endothelial cells. In fact, p-Smad2, a subrogated marker of cell activation, strongly related to activated fibroblasts, was present in more cells close to PyMT VE-Cadh^{Snail1CT} vessels than to PyMT VE-Cadh^{Snail1KO} ones (Figure R-24A, B).

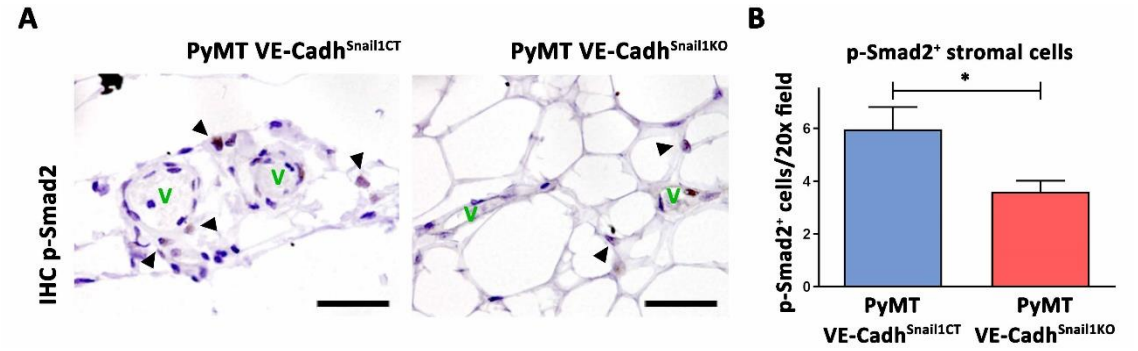

Figure R-24. Endothelial Snail1 enhances Smad2 phosphorylation of the stroma. A-B, Images of anti p-Smad2 immunohistochemistry (A) and quantification of p-Smad2$^+$ cells around vessels per 20x field (B) in adjacent healthy breast tissue of PyMT VE-Cadh$^{Snail1CT/KO}$ tumors at premalignant stage. Black arrowheads point p-Smad2$^+$ cells. Green 'V' marks vessels. Scale bar: 40 µm. Data in B represent mean values (± SEM). *p<0.05.

To further assess fibroblasts activation, we determined Vimentin expression. Premalignant ducts and tumors at hyperplasia stage from PyMT VE-Cadh^{Snail1CT} mice exhibited an enrichment of Vimentin$^+$ areas in their stroma compared to PyMT VE-Cadh^{Snail1KO} ones (Figure R-25A-D). Moreover, Snail1, which is another classical marker of fibroblast activation, was more expressed in stroma of PyMT VE-Cadh^{Snail1CT} tumors at hyperplasia stage, compared to PyMT VE-Cadh^{Snail1KO} ones (Figure R-25E, F). Moreover, in tumors at hyperplasia stage, Snail1$^+$ cells were closer to vessels in PyMT VE-Cadh^{Snail1CT} mice than in PyMT VE-Cadh^{Snail1KO} mice (Figure R-25G). Thus, we could state that Snail1 expression in endothelial cells potentiates fibroblast activation at very early stages of breast tumorigenesis.

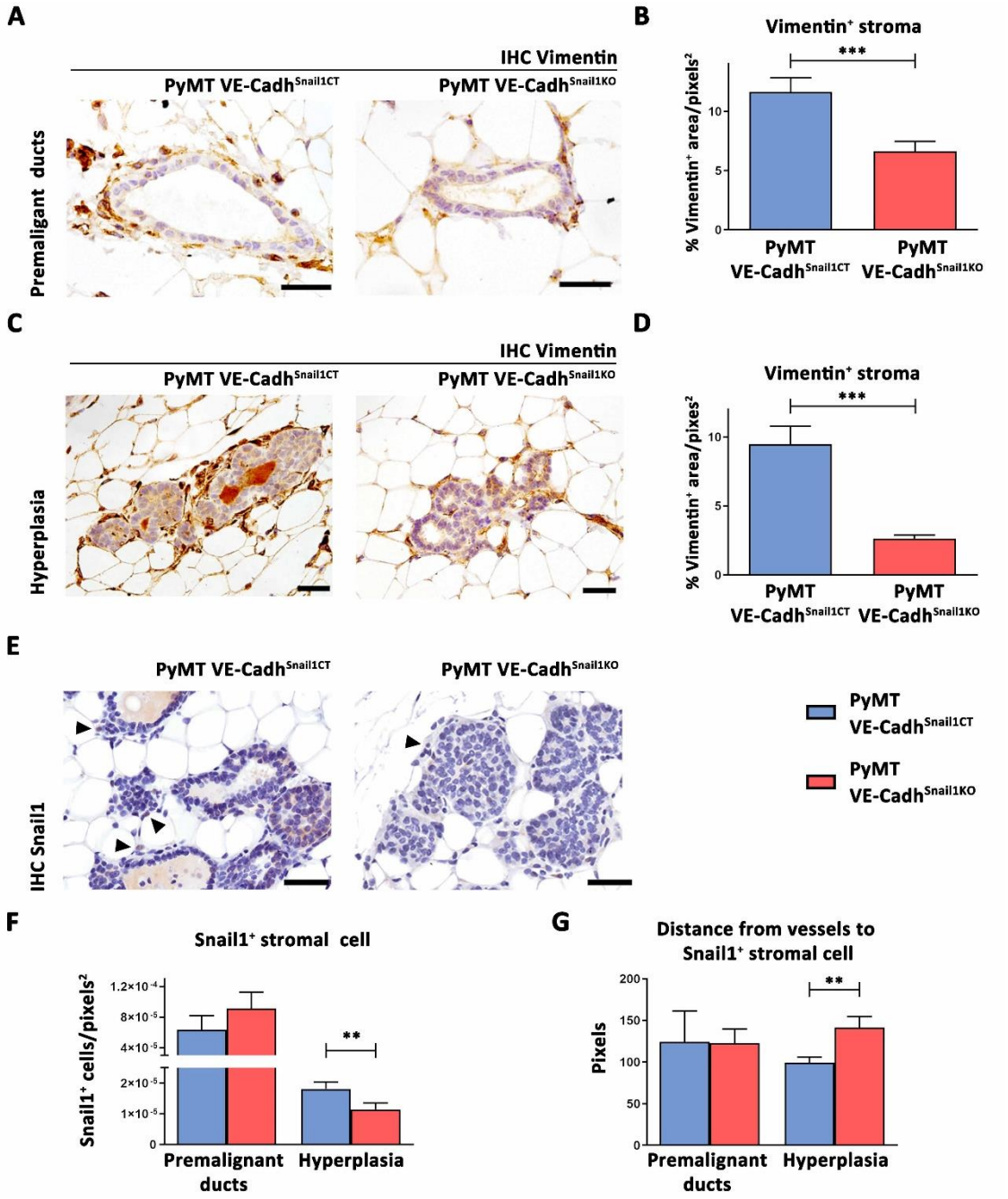

Figure R-25. Endothelial Snail1 expression activates the stroma at early tumor stages. A-B, Images of anti Vimentin immunohistochemistry (A) and quantification of Vimentin$^+$ area in stroma (B) of PyMT VE-Cadh$^{Snail1CT/KO}$ tumors in premalignant ducts. Scale bar: 40 µm. **C-D**, Images of anti Vimentin immunohistochemistry (C) and quantification of Vimentin$^+$ area in stroma (D) of PyMT VE-Cadh$^{Snail1CT/KO}$ tumors at hyperplasia stage. Scale bar: 50 µm. **E-F**, Images of anti Snail1 immunohistochemistry (E) at hyperplasia stage and quantification of Snail1$^+$ cells per pixels^2 (F) in premalignant ducts and tumors at hyperplasia stage of PyMT VE-Cadh$^{Snail1CT/KO}$ mice. Black arrowheads point Snail1$^+$ cells. Scale bar: 100 µm. **G**, Quantification of distance from Snail1$^+$ cells to its closer vessel in PyMT VE-Cadh$^{Snail1CT/KO}$ premalignant ducts and tumors at hyperplasia stage. Data in B, D, F and G represent mean values (± SEM). **p<0.01; ***p<0.001.

10. Endothelial Snail1 expression induces fibroblast activation through FGF2 and CXCL12

To further corroborate the effect of endothelial Snail1 on fibroblast activation, we cultured CAF with HUVEC siCtl, siSnail1, Ctl and Snail1^{+} (C5) conditioned medium for two days. HUVEC siSnail1 conditioned medium reduced the mRNA expression of several mesenchymal genes (FN1 and CDH2) and profibrotic cytokines genes (TGFB1, 2 and CXCL12) in CAF, compared with these cells cultured with HUVEC siCtl conditioned medium (Figure R-26A). Aversely, HUVEC Snail1^{+} (C5) conditioned medium enhanced more the expression of those genes than HUVEC Ctl conditioned medium in CAF (Figure R-26A). These effects were corroborated at protein levels. Firstly, adding conditioned medium from HUVEC, without altering their Snail1 levels, altered the expression of some mesenchymal markers in CAF (Figure R-26B). Regarding conditioned medium from HUVEC with altered Snail1 expression, CAF treated with HUVEC siSnail1 conditioned medium presented less mesenchymal genes expression, such as FN1 and N-cadherin protein expression, compared to HUVEC siCtl conditioned medium (Figure R-26B). Conversely, HUVEC Snail1^{+} (C5) conditioned medium boosted the protein expression of these markers in CAF, compared to its control (Figure R-26B). We tested another characteristic of active fibroblast, the acquisition of a promigratory phenotype. CAF decreased their migration ability when cultured with HUVEC siSnail1 conditioned medium, and, conversely, increased their migration ability with HUVEC Snail1+ (C5) conditioned medium (Figure R-26C). Actually, these effects were significantly higher over the time (Figure R-26C). CAF located at the migration leading front reflected this differential activation. HUVEC siSnail1 conditioned medium did not generate many CAF elongations; in fact, CAF were clustered, compared to HUVEC siCtl conditioned medium (Figure R-26D). Conversely, HUVEC Snail1^{+} (C5) presented more membrane elongations than HUVEC Ctl conditioned medium (Figure R-26D). Finally, we tested the activation cascades responsible for the differential activation of CAF. To address that, we cultured CAF for two hours with HUVEC conditioned medium with different levels of Snail1. We observed that CAF phosphorylation of AKT was regulated by Snail1 expression in HUVEC conditioned medium and only in Snail1 knocked down was abrogated the

phosphorylation of Smad2 (Figure R-26E). Thus, we concluded that Snail1 status in HUVEC regulated fibroblast activation by HUVEC conditioned medium.

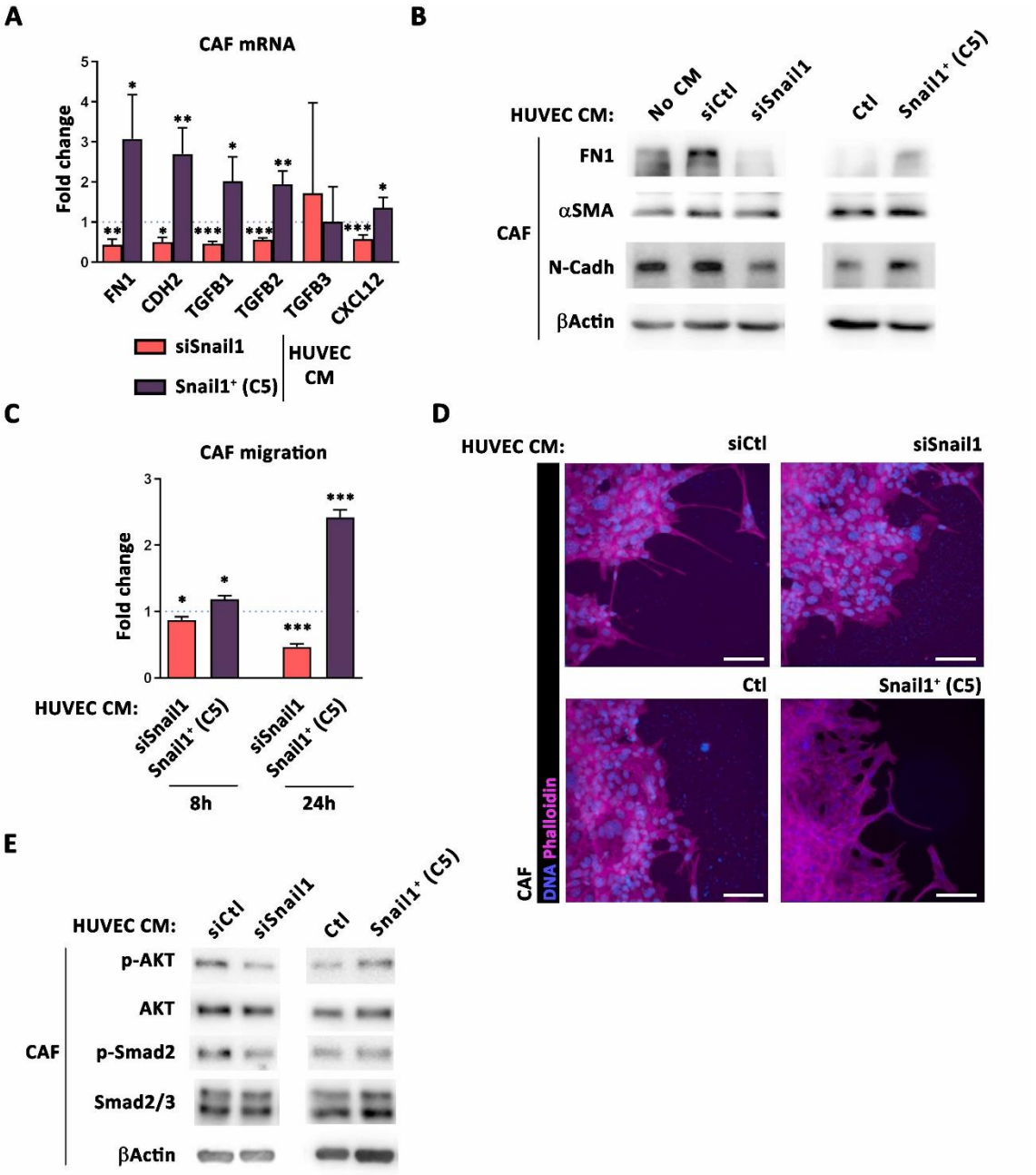

Figure R-26. HUVEC secretome activates CAF *in vitro* depending on Snail1 expression. A, Quantification of FN1, CDH2, TGFB1, 2, 3 and CXCL12 genes mRNA expression in CAF, compared to their respective controls represented as a discontinuous line. **B**, Western blot analysis of FN1, αSMA and N-Cadherin in CAF cultured for two days with no conditioned medium or HUVEC siCtl, siSnail1, Ctl or Snail1^{+} (C5) conditioned medium. **C**, Quantification of migration in CAF 8 or 24h after wound was done, cultured with siSnail1 or Snail1^{+} (C5) conditioned medium, compared to their respective controls represented as a discontinuous line. **D**, Actin cytoskeleton analysis by immunofluorescence in CAF cells in the leading front of migration. Cell were stained with Alexa

647 conjugated Phalloidin (purple) and nuclei were counterstained with DAPI (blue). **E**, Western blot analysis of p-AKT, AKT, p-Smad2 and Smad2/3 in CAF cultured for 2h with HUVEC siCtl, siSnail1, Ctl or Snail1^{+} (C5) conditioned medium. Data in A and C represent mean values (± SEM) of at least three independent experiments. *p<0.05; **p<0.01; ***p<0.001.

Apart from CAF, we also used MEF to investigate fibroblast activation by endothelial cells. In this case, we cultured MEF with HUVEC siCtl, siSnail1, Ctl and Snail1^{+} (C5) conditioned medium for two days and we determined whether their activation status varied. Similarly to CAF, HUVEC siSnail1 conditioned medium reduced the mRNA expression of several mesenchymal genes (FN1 and CDH2) but less profibrotic cytokines genes were reduced (TGFB2), compared to HUVEC siCtl conditioned medium culture (Figure R-27A). Aversely, HUVEC Snail1^{+} (C5) conditioned medium enhanced the expression of some genes compared to HUVEC Ctl conditioned medium (Figure R-27A). These effects were studied at protein levels and only with HUVEC Snail1^{+} (C5) conditioned medium we observed an upregulation of mesenchymal markers (Figure R-27B).

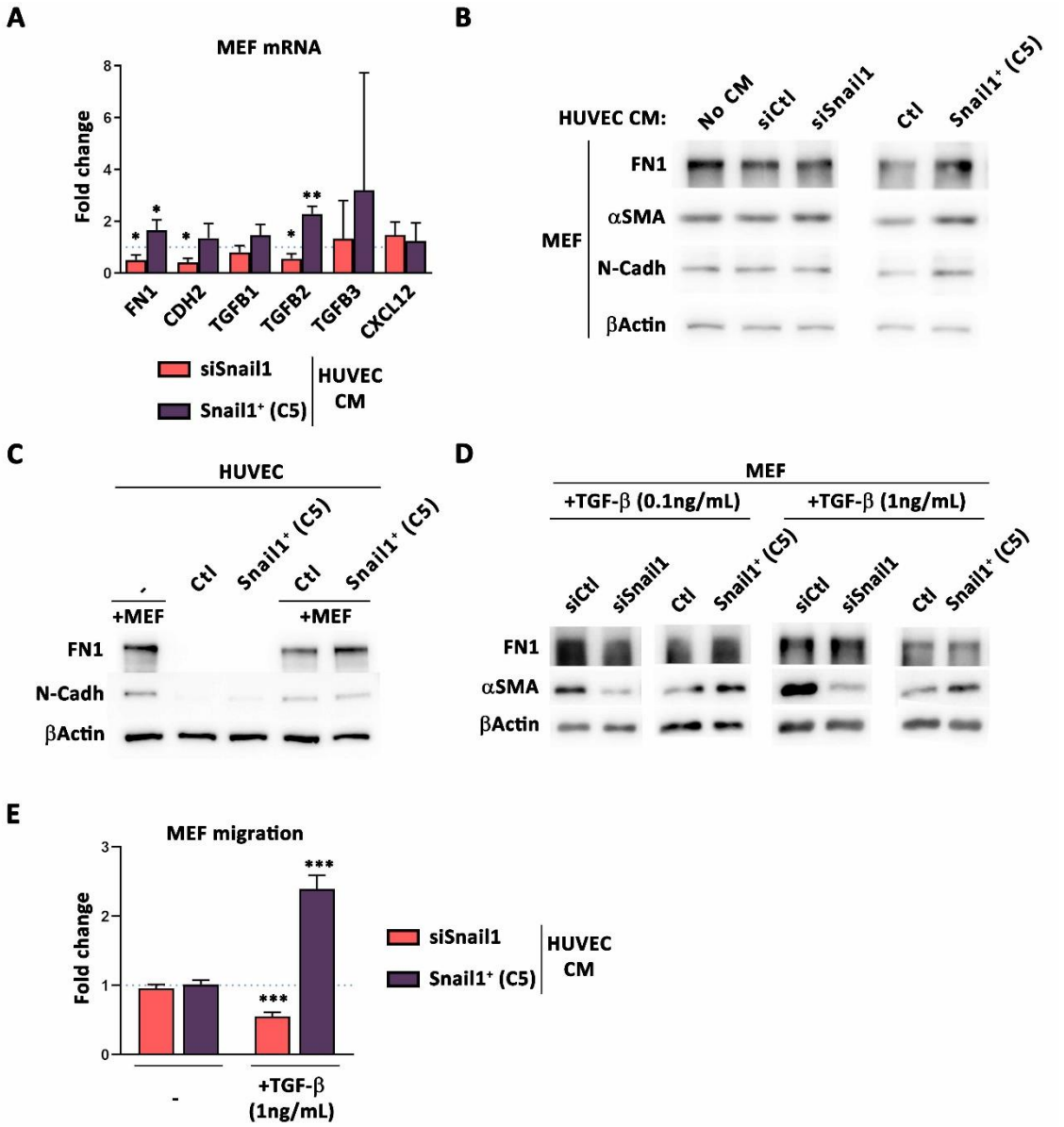

Figure R-27. HUVEC activates MEF *in vitro* depending on Snail1 expression by co-culture or TGF-β preactivation. A, Quantification of FN1, CDH2, TGFB1, 2, 3 and CXCL12 genes mRNA expression in MEF treated for two days with HUVEC siSnail1 or Snail1^{+} (C5) conditioned medium, compared to their respective controls represented as a discontinuous line. **B**, Western blot analysis of FN1, αSMA and N-Cadherin in MEF treated for two days with no conditioned medium or HUVEC siCtl, siSnail1, Ctl or Snail1^{+} (C5) conditioned medium. **C**, Western blot analysis of FN1 and N-Cadherin in MEF alone or co-cultured with HUVEC Ctl or Snail1^{+} (C5) for one day. **D**, Western blot analysis of FN1 and αSMA in MEF treated with HUVEC siCtl, siSnail1, Ctl or Snail1^{+} (C5) conditioned medium and prestimulated with 0.1 or 1ng/mL TGF-β. **E**, Quantification of migration in MEF for 24h treated with siSnail1 or Snail1^{+} (C5) conditioned medium with or without TGF-β pretreatment, compared to their respective controls represented as a discontinuous line. Data in A and E represent mean values (± SEM) of at least three independent experiments. *p<0.05; **p<0.01; ***p<0.001.

Afterwards, we focused our attention on deciphering the secreted cytokines differentially expressed in HUVEC depending on their Snail1 levels. After checking the mRNA expression of several genes involved in fibroblast activation, we found that CXCL12 and FGF2 were potential candidates (Figure R-28A). The mRNA levels of CXCL12 and FGF2 were upregulated in HUVEC Snail1^{+} (C5) and downregulated in HUVEC siSnail1 (Figure R-28A). We confirmed that CXCL12 and FGF2 induced CAF activation (Figure R-28B). We also determined if the migration ability could be potentiated with these factors. FGF2 increased the migration of CAF and MEF, whereas CXCL12 only upregulated significantly migration of MEF (Figure R-28C). All cytokines induced more elongated fibroblasts in the migration front after wound (Figure R-28D). In these sets of experiments, TGF-β was used as a positive control for obtaining fibroblast activation (Figure R-28-D).

To confirm that CXCL12 and FGF2 were the key cytokines in our model, we cultured CAF with conditioned medium from HUVEC with different Snail1 levels combined with inhibitors of the activity of these cytokines. We used SU5402 to block FGFR signaling and Plerixafor, as an antagonist of CXCL12 signaling. We noticed that treating CAF with these molecules completely abrogated the activation of mesenchymal markers expression in CAF (Figure R-29A, B). Furthermore, the migration boost by HUVEC conditioned medium was abrogated with the treatment of SU5402 and Plerixafor (Figure R-29C). Thus, we confirmed that CXCL12 and FGF2 were the cytokines responsible for the activation of fibroblasts by HUVEC paracrine activity.

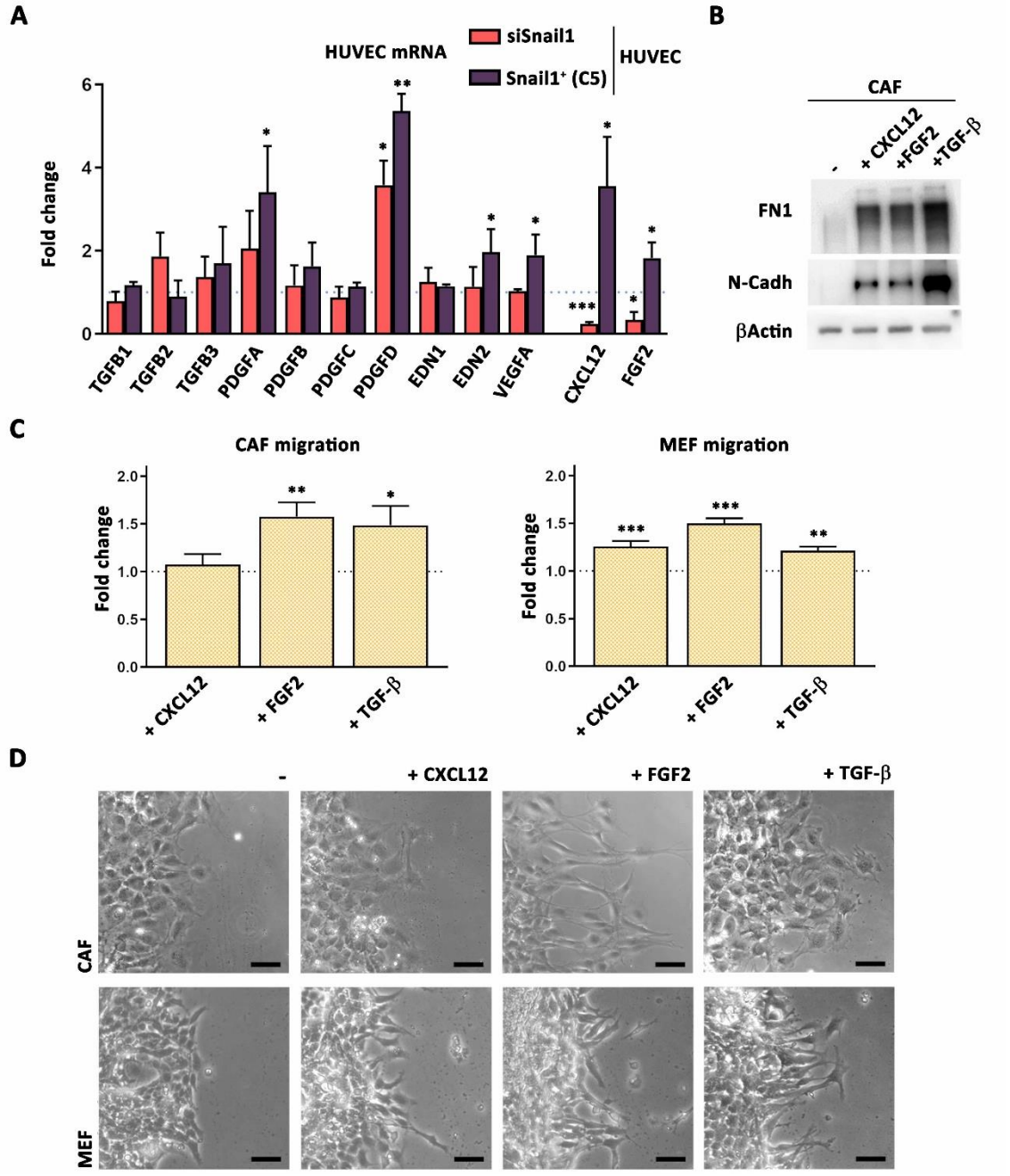

Figure R-28. HUVEC have a differential profibrotic secretome depending on their Snail1 expression. A, Quantification of TGFB1, 2, 3, PDGFA, B, C, D, EDN1, 2, VEGFA, CXCL12 and FGF2 mRNA expression in HUVEC siSnail1 or Snail1^{+} (C5), compared to their respective controls represented as a discontinuous line. **B**, Western blot analysis of FN1 and N-Cadherin in CAF treated with or without CXCL12, FGF2 or TGF-β. **C**, Quantification of migration in CAF (left) for 9h or MEF (right) for 24h with CXCL12, FGF2 and TGF-β, compared to their respective controls represented as a discontinuous line. **D**, Images of migration leading front of CAF (upper row) and MEF (lower row) with or without CXCL12, FGF2 and TGF-β. Data in A and C represent mean values (± SEM) of at least three independent experiments. *p<0.05; **p<0.01; ***p<0.001.

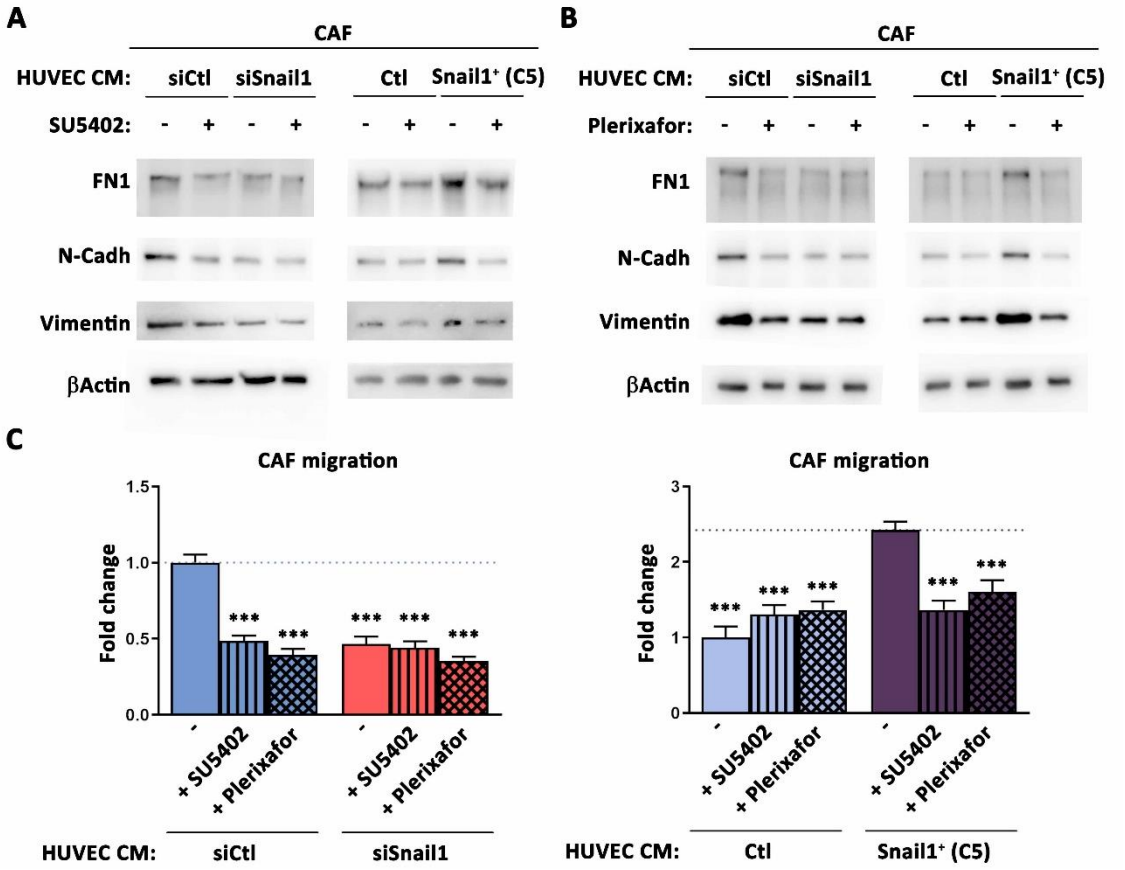

Figure R-29. Inhibition of FGFR signaling or CXCR4 activation abrogates fibroblast activation by Snail1 expressing HUVEC secretome. A, Western blot analysis of FN1, N-Cadherin and Vimentin in CAF treated with HUVEC siCtl, siSnail1, Ctl or Snail1^{+} (C5) conditioned medium, treated with or without SU5402. **B**, Western blot analysis of FN1, N-Cadherin and Vimentin in CAF treated with HUVEC siCtl, siSnail1, Ctl or Snail1^{+} (C5) conditioned medium, treated with or without Plerixafor. **C**, Quantification of migration in CAF for 24h treated with HUVEC siCtl and siSnail1 (left) or Ctl or Snail1^{+} (C5) (right) conditioned medium, treated with or without SU5402 or Plerixafor. Discontinuous line represents CAF cultured with HUVEC siCtl or Snail1^{+} (C5) conditioned medium, respectively. Data in C represent mean values (± SEM) of at least three independent experiments. ***p<0.001.

11. Endothelial Snail1 modifies the development of luminal breast tumors *in vivo*

Apart from analyzing tumor onset, we analyzed tumors at more advanced stages. We collected tumors from PyMT VE-Cadh^{Snail1CT} and PyMT VE-Cadh^{Snail1KO} mice and we performed a histological classification. Analyzing the survival curve of both groups (see Figure R-20C), we chose two time points to perform this study: 18 weeks, when PyMT VE-Cadh^{Snail1CT} mice had to be euthanized, and 22 weeks, when PyMT VE-Cadh^{Snail1KO} mice had to be euthanized. At 18 weeks, PyMT VE-Cadh^{Snail1CT} tumors were mostly at carcinoma stage and with a solid morphology, whereas, 18 weeks old PyMT VE-Cadh^{Snail1KO} tumors were mostly at adenoma stage (Figure R-30A-C). Nevertheless, at 22 weeks old PyMT VE-Cadh^{Snail1KO} mice, most of the tumors have progressed to a carcinoma stage (Figure R-30A, B) and exhibited a papillary morphology (Figure R-30A, C). Therefore, endothelial Snail1 modulated PyMT breast tumor development.

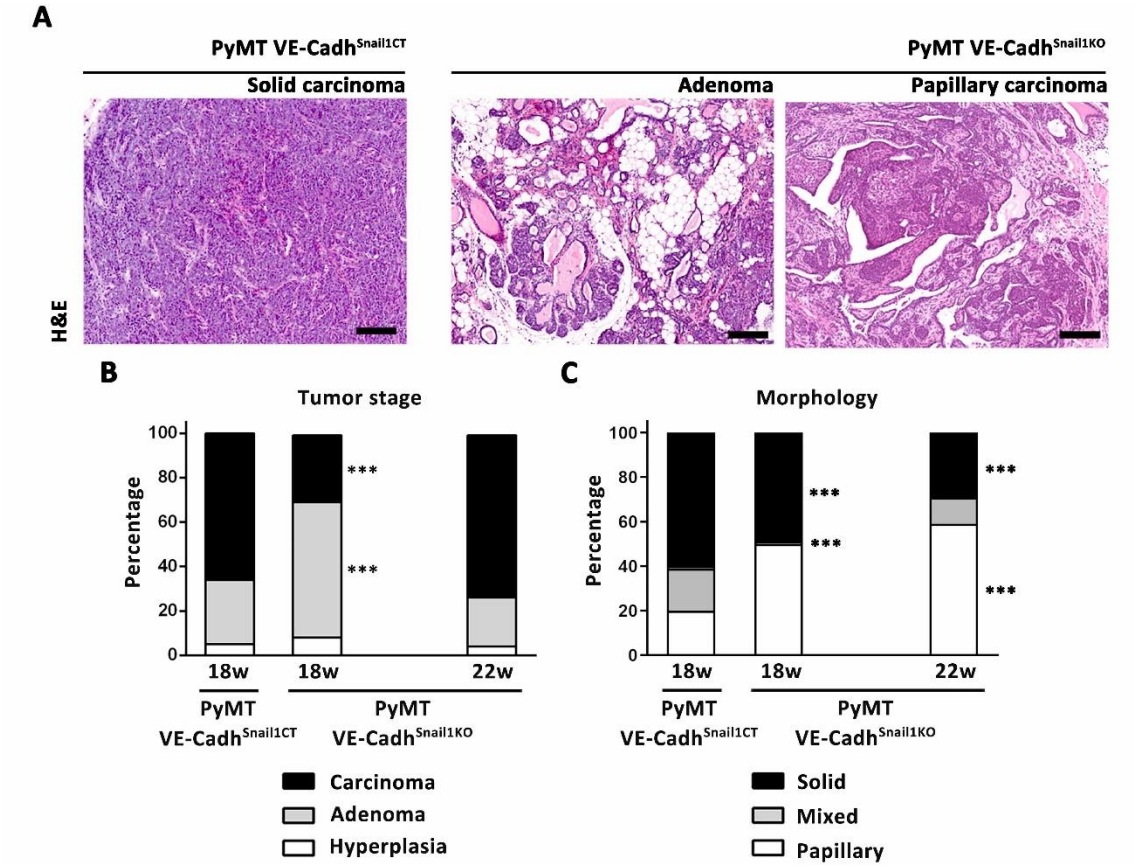

Figure R-30. Endothelial Snail1 expression promotes carcinogenesis and a differential carcinoma morphology. A, Images of hematoxylin and eosin staining of representative tumor

stages of PyMT VE-Cadh$^{Snail1CT/KO}$ tumors. Scale bar: 200 µm **B**, Quantification of tumorigenic stages of PyMT VE-Cadh$^{Snail1CT/KO}$ tumors at indicated time points. **C**, Quantification of histological type of PyMT VE-Cadh$^{Snail1CT/KO}$ tumors at carcinoma stage. Data from PyMT VE-Cadh^{Snail1KO} mice in B and C are compared statistically with PyMT VE-Cadh^{Snail1CT} mice. ***p<0.001.

Molecularly, these PyMT luminal tumors also differed. Regarding proliferation, PyMT VE-Cadh^{Snail1CT} tumors were more proliferative than PyMT VE-Cadh^{Snail1KO} tumors at carcinoma stage, since they had more Ki67^{+} cells (Figure R-31A, B). Considering the expression of hormone receptors, Estrogen Receptor α (ERα) disappeared faster from PyMT VE-Cadh^{Snail1CT} tumors over the progression of tumorigenesis, than in PyMT VE-Cadh^{Snail1KO} tumors (Figure R-31C, D). HER2 analysis showed that PyMT VE-Cadh^{Snail1CT} tumors had a higher expression than PyMT VE-Cadh^{Snail1KO} tumors at carcinoma stage (Figure R-31E, F). Thus, luminal MMTV-PyMT breast tumors had higher expression of aggressive markers when Snail1 is expressed in their vasculature.

We evaluated tumor cellular composition by FACS in PyMT VE-Cadh^{Snail1CT} and PyMT VE-Cadh^{Snail1KO} tumors, considering epithelial, immune, endothelial and other stromal cells (Figure R-32A); this last subgroup encompassed mainly fibroblasts and myoepithelial cells. There were more epithelial and fewer immune cells in PyMT VE-Cadh^{Snail1CT} tumors than in PyMT VE-Cadh^{Snail1KO} ones at carcinoma stage (Figure R-32B). In this case, endothelial cells remained unaltered (Figure R-32B). To confirm the immune cell infiltration result, we quantified the amount of CD45^{+} cells in PyMT VE-Cadh^{Snail1CT} and PyMT VE-Cadh^{Snail1KO} tumors by immunohistochemistry. Thanks to that we could confirm that there were significantly fewer immune cells in PyMT VE-Cadh^{Snail1CT} tumors, and interestingly, not only in the capsule of the tumors but also intratumorally (Figure R-32C, D). Hence, these data reflected that endothelial Snail1 expression altered the cellular composition of MMTV-PyMT breast tumors.

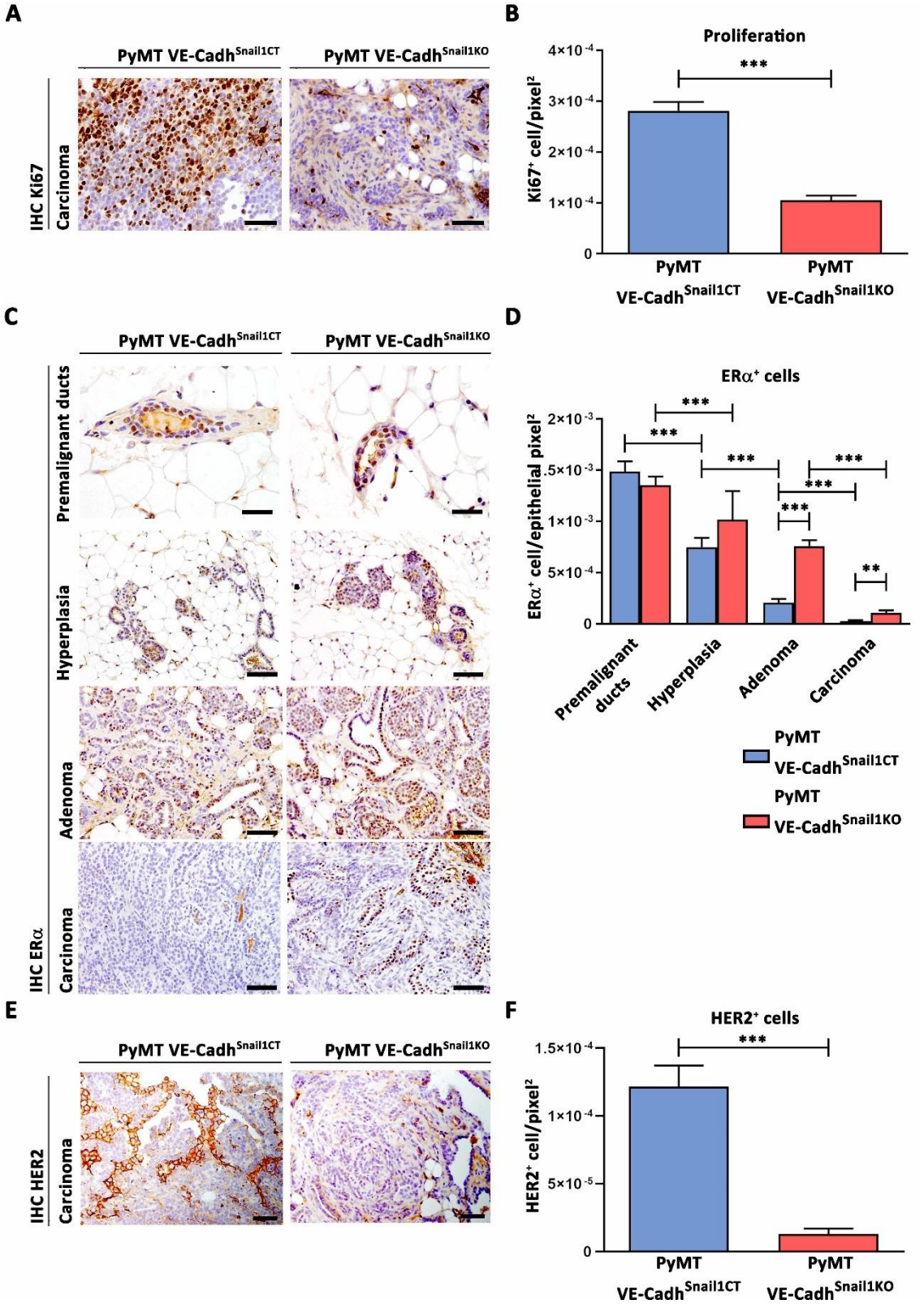

Figure R-31. Snail1 expression in endothelial cells promotes more proliferation, lower nuclear ERα signaling and higher HER2 expression in MMTV-PyMT tumors. A-B, Images of anti Ki67 immunohistochemistry (A) and quantification of Ki67$^+$ cells per pixels^2 (B) in PyMT VE-

Cadh$^{Snail1CT/KO}$ mice at carcinoma stage. Scale bar: 40 µm. **C-D**, Images of anti ERα immunohistochemistry (C) and quantification of ERα^{+} cells per pixels^{2} (D) in PyMT VE-Cadh$^{Snail1CT/KO}$ mice at premalignant ducts and hyperplasia, adenoma and carcinoma stage, when indicated. Scale bar (premalignant duct): 25 µm. Scale bar (others): 50 µm. **E-F**, Images of anti HER2 immunohistochemistry (E) and quantification of HER2^{+} cells per pixels^{2} (F) in PyMT VE-Cadh$^{Snail1CT/KO}$ mice at carcinoma stage. Scale bar: 50 µm. Data in B, D and F represent mean values (± SEM). **p<0.01; ***p<0.001.

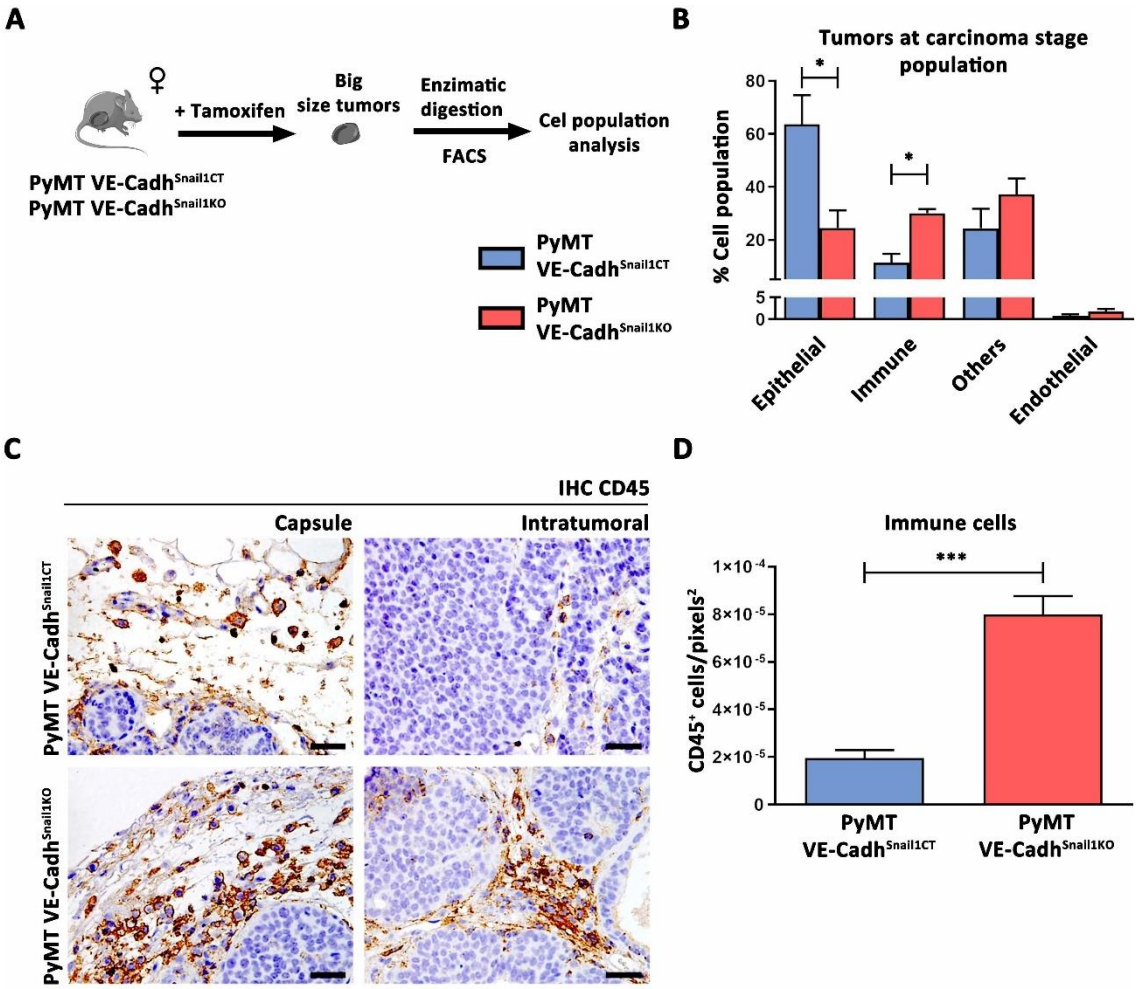

Figure R-32. Endothelial Snail1 expression provokes a different cell type content in MMTV-PyMT tumors. A, Scheme of workflow for tumor population analysis by FACS. **B**, Quantification of percentage from alive singlets of epithelial, immune, others and endothelial cells in PyMT VE-Cadh$^{Snail1CT/KO}$ tumors at carcinoma stage, determined by FACS. **C-D**, Images of anti CD45 immunohistochemistry (C) and quantification of CD45^{+} cells per pixels^{2} (D) in PyMT VE-Cadh$^{Snail1CT/KO}$ tumors at carcinoma stage. Scale bar: 50 µm. Data in B and D represent mean values (± SEM). *p<0.05; ***p<0.001.

Commonly, tumor stroma gets activated during tumor progression. We checked if Snail1 in the endothelium affected it, observing that, PyMT VE-Cadh^{Snail1CT} tumors had more presence of Vimentin than PyMT VE-Cadh^{Snail1KO} tumors (Figure R-33A, B).

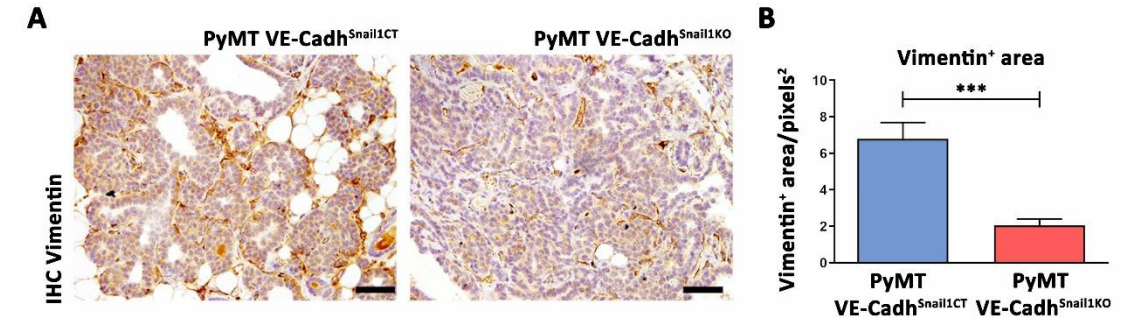

Figure R-33. Endothelial Snail1 generates more active stroma at adenoma tumor stage. A-B, Images of anti Vimentin immunohistochemistry (A) and quantification of Vimentin$^+$ area per pixels^2 (B) in PyMT VE-Cadh$^{Snail1CT/KO}$ tumors at adenoma stage. Scale bar: 50 µm. Data in B represent mean values (± SEM). ***p<0.001.

12. Endothelial Snail1 induces more invasive breast tumors with less myoepithelial cells

As stated previously, PyMT VE-Cadh^{Snail1KO} tumors at carcinoma stage tend to be papillary instead of solid. One of the described characteristics of papillary tumors is the abundance of myoepithelial cells. These cells express nuclear p63, marker that was more abundant in PyMT VE-Cadh^{Snail1KO} tumors at hyperplasia, adenoma and carcinoma stage compared to PyMT VE-Cadh^{Snail1CT} ones (Figure R-34A, B). Myoepithelial cells do also express CK14, which was increased in PyMT VE-Cadh^{Snail1KO} tumors at carcinoma stage compared to PyMT VE-Cadh^{Snail1CT} tumors (Figure R-34C). Finally, basal lamina, analyzed by Laminin α, was also increased in PyMT VE-Cadh^{Snail1KO} tumors at carcinoma stage compared to PyMT VE-Cadh^{Snail1CT} tumors (Figure R-34C). Thus, tumors with Snail1 expression in their endothelium had a lower presence of myoepithelial cells and basal lamina, being considered as invasive.

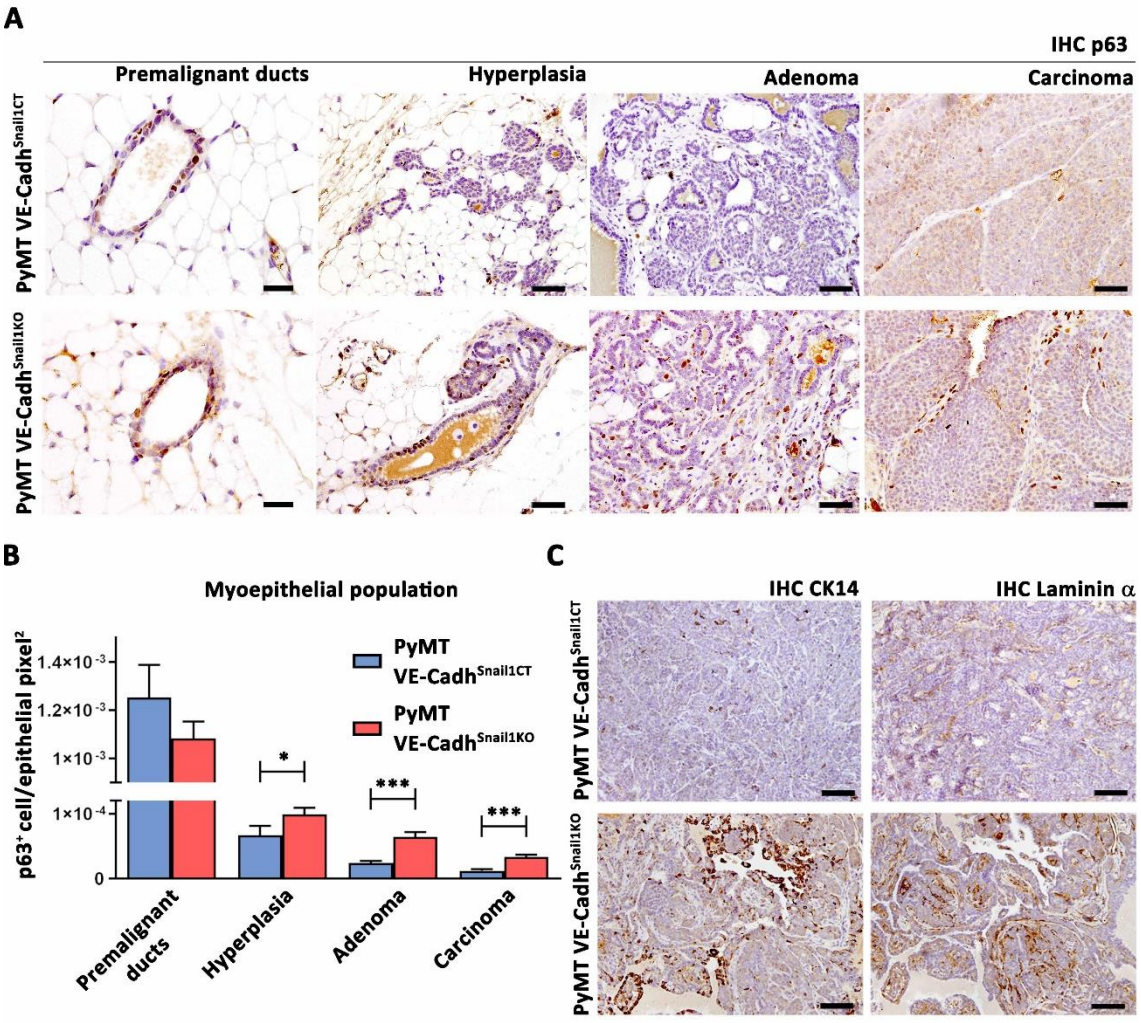

Figure R-34. Endothelial Snail1 promotes less presence of myoepithelial cells and basal lamina in breast tumors stroma. A, Images of anti p63 immunohistochemistry in PyMT VE-Cadh$^{Snail1CT/KO}$ premalignant ducts and tumors at hyperplasia, adenoma and carcinoma stage. Scale bar (premalignant duct): 25 µm. Scale bar (others): 100 µm. **B**, Quantification of p63^{+} cells per pixels^{2} in PyMT VE-Cadh$^{Snail1CT/KO}$ premalignant ducts and tumors at hyperplasia, adenoma and carcinoma stage. **C**, Images of anti CK14 and anti Laminin α immunohistochemistry in PyMT VE-Cadh$^{Snail1CT/}$KO tumors at carcinoma stage. Scale bar: 100 µm. Data in B represent mean values (± SEM). *p<0.05; ***p<0.001.

To test the effect of myoepithelial cells on epithelial population, we collected conditioned medium from MCF10A (myoepithelial cells) and we added it to NMuMG (normal mammary epithelial cells), observing a reduction in their proliferation (Figure R-35A). Afterwards, we co-cultured MCF10A cells with NMuMG-GFP^{+} cells for one day

and we checked their DNA content by FACS, showing a significant decrease of proliferating cells (those in S, G2 and M phases) of NMuMG (Figure R-35C).

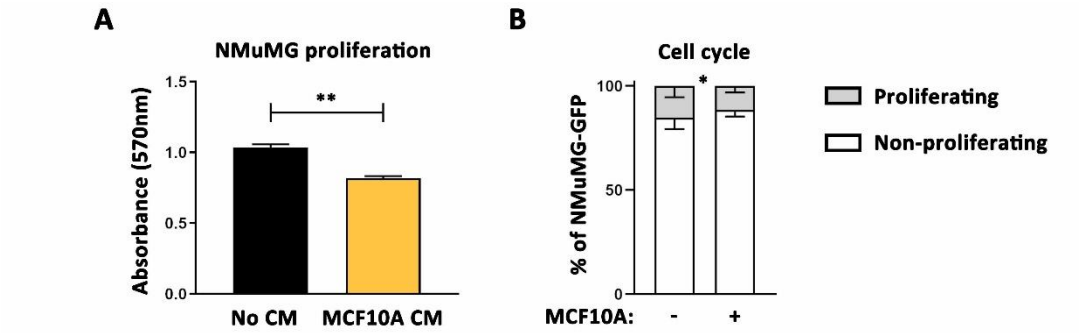

Figure R-35. Myoepithelial cells reduce breast epithelial cell proliferation. A, Proliferation assay of NMuMG after seven days with or without MCF10A conditioned medium. **C**, Cell cycle analysis of NMuMG being co-cultured with or without MCF10A for 24h. Data in A and B represent mean values (± SEM) of at least three independent experiments. *p<0.05; **p<0.01.

13. Snail1 in endothelial cells is key in tumor angiogenesis and vessel morphogenesis, location and structure

Once we characterized the main histological and clinical parameters of PyMT VE-Cadh^{Snail1CT} and PyMT VE-Cadh^{Snail1KO} mice, we focused on tumor angiogenesis. In 6 weeks old breasts from PyMT VE-Cadh^{Snail1CT} and PyMT VE-Cadh^{Snail1KO} mice, we did not find differences in the amount or morphology of the vessels (Figure R-36A-D). In 18 weeks old breast tumors from PyMT VE-Cadh^{Snail1CT} and PyMT VE-Cadh^{Snail1KO} mice, there was significantly more endothelial cells in PyMT VE-Cadh^{Snail1CT} tumors than in PyMT VE-Cadh^{Snail1KO} ones (Figure R-36A, B). Regarding the morphology of the vessels, 18 weeks old PyMT VE-Cadh^{Snail1CT} tumor vessels had bigger areas with larger perimeters (Figure R-36A, C, D). Finally, in 22 weeks old PyMT VE-Cadh^{Snail1KO} mice, tumors recovered the same level of angiogenesis than in 18 weeks old breast tumors from PyMT VE-Cadh^{Snail1CT} mice (Figure R-36A, B), although their vessels became dramatically bigger in area and perimeter, compared to PyMT VE-Cadh^{Snail1CT} ones at 18 weeks (Figure R-36A, C, D). These results confirmed the role of Snail1 in tumor angiogenesis and vessel morphology *in vivo*.

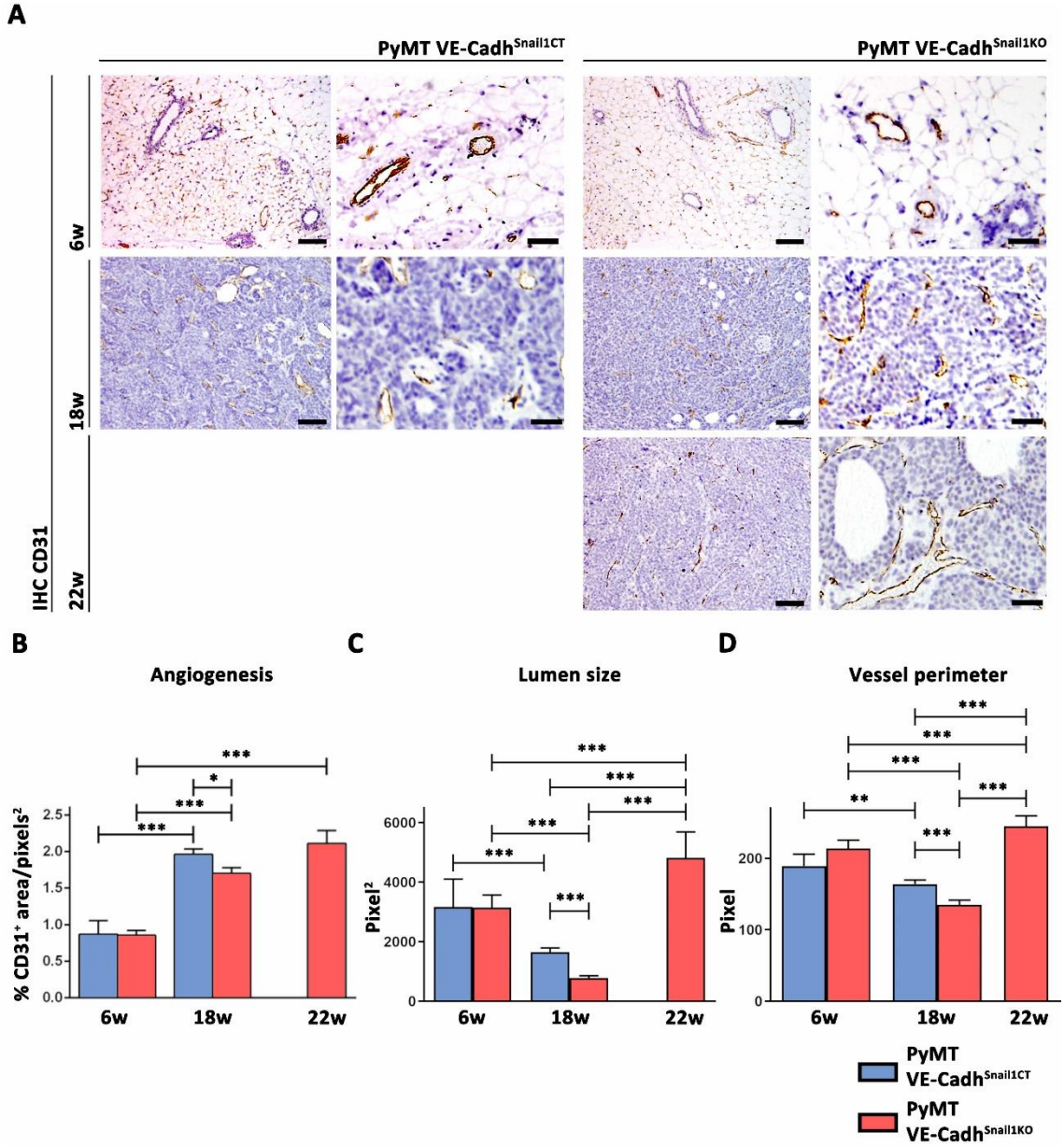

Figure R-36. Expression of Snail1 in vasculature promotes a more potent proangiogenic response and distinct vessel morphology in response to MMTV-PyMT breast tumor signaling. **A**, Images of anti CD31 immunohistochemistry in breast tissues from 6 weeks old or tumors from 18 or 22 weeks old PyMT VE-Cadh$^{Snail1CT/KO}$ mice. Scale bar (first and third column): 200 µm; Scale bar (second and fourth column): 40 µm. **B-D**, Quantification of CD31^{+} stained area (B), vessel lumen size (C) and vessel lumen perimeter (D) in breast tissues from 6 weeks old or tumors from 18 or 22 weeks old PyMT VE-Cadh$^{Snail1CT/KO}$ mice. Data in B, C and D represent mean values (± SEM). *p<0.05; **p<0.01; ***p<0.001.

Apart from angiogenesis, endothelial cells in tumors also undergo lymphangiogenesis. We wanted to check if this process was affected by endothelial Snail1, thus, we quantified Lyve-1^{+} stained area as a marker of lymphatic vessels at carcinoma stage. We did not observe any significant difference between PyMT VE-Cadh^{Snail1CT} and PyMT VE-Cadh^{Snail1KO} tumors at carcinoma stage (Figure R-37A, B).

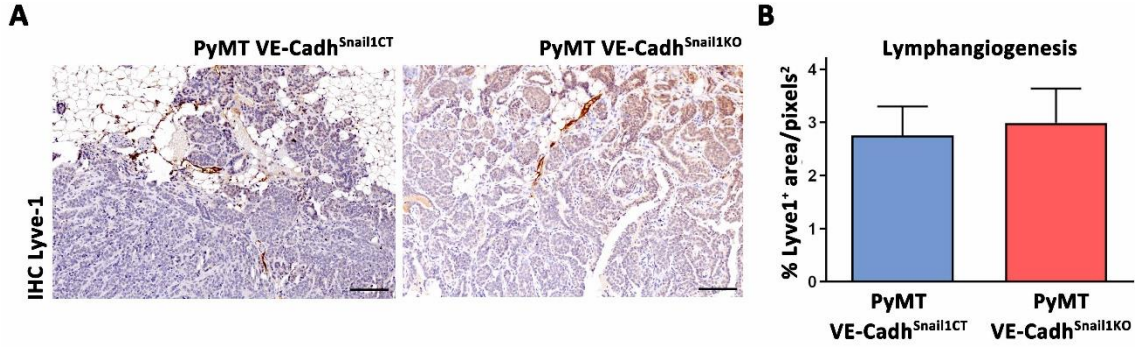

Figure R-37. Snail1 expression in endothelial cells does not alter tumor lymphangiogenesis at carcinoma stage. A-B, Image of anti Lyve-1 immunohistochemistry (A) and quantification of Lyve-1^{+} area per pixels^{2} (B) in PyMT VE-Cadh$^{Snail1CT/KO}$ tumors at carcinoma stage. Scale bar: 200 µm. Data in B represent mean values (± SEM).

To further characterize the tumoral vessels, we performed a Masson's Trichrome staining to analyze the Collagen coverage of the vessels of PyMT VE-Cadh^{Snail1CT} and PyMT VE-Cadh^{Snail1KO} tumors at hyperplasia, adenoma and carcinoma stage. We quantified the percentage of vessel perimeter covered by Collagen (Figure R-38A). We did not detect any significant differences neither at hyperplasia nor adenoma stage (Figure R-38B). However, at carcinoma stage, PyMT VE-Cadh^{Snail1CT} tumor vessels were more covered by Collagen than in PyMT VE-Cadh^{Snail1KO} ones (Figure R-38B).

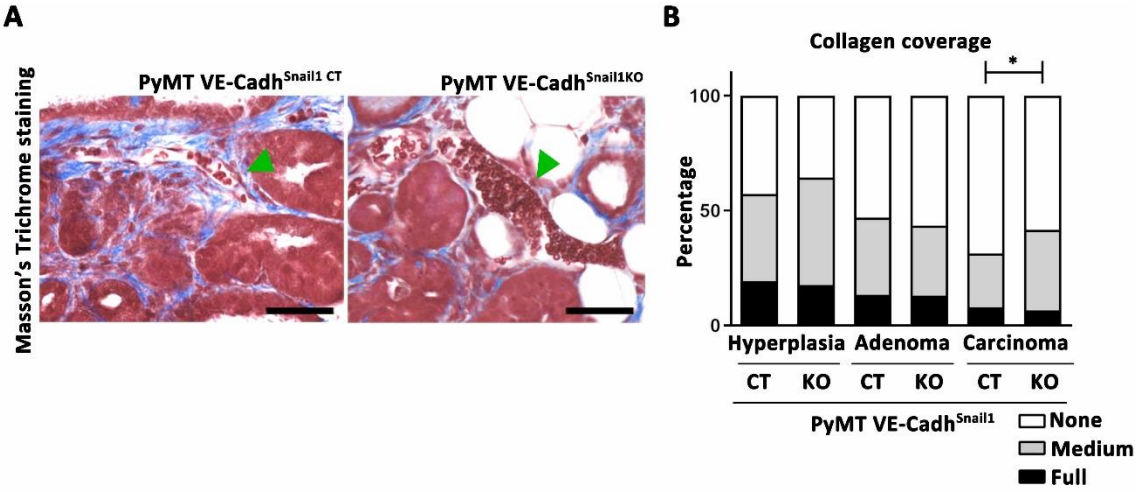

Figure R-38. Snail1 expressing vessels are localized in areas with higher content of Collagen. A, Images of Masson's Trichrome staining in PyMT VE-Cadh$^{Snail1CT/KO}$ tumors at carcinoma stage. Blue staining stays for Collagen. Green arrowheads point vessels. Scale bar: 50 µm. **B**, Quantification of Collagen coverage of vessels in of PyMT VE-Cadh$^{Snail1CT/KO}$ tumors at hyperplasia, adenoma and carcinoma stage. Data in B represent mean values (± SEM). *p<0.05.

Afterwards, we took a deeper look at tumor vessels and analyzed by transmission electron microscopy the ultrastructure of tumor vessels of PyMT VE-Cadh^{Snail1CT} and PyMT VE-Cadh^{Snail1KO} tumors at carcinoma stage. We quantified the most predominant differences found between both mice groups (Figure R-39A). Firstly, we analyzed the lumen integrity differentiating tumor vessels with restricted, fenestrated or dismantled lumen. We observed that PyMT VE-Cadh^{Snail1CT} tumor lumen vessels were more dismantled than PyMT VE-Cadh^{Snail1KO} vessels, as a signal of aberrant angiogenesis (Figure R-39B). Secondly, we studied the amount of vesiculo-vacuolar organelles (VVO) as the number of clear spheroids in the cytoplasm of endothelial cells. We noticed that PyMT VE-Cadh^{Snail1CT} tumor vessels had much less VVO inside their cytoplasm compared to PyMT VE-Cadh^{Snail1KO} tumor vessels (Figure R-39B). Finally, we quantified the amount of intraluminal filopodia, observing less number in PyMT VE-Cadh^{Snail1CT} tumor vessels than in PyMT VE-Cadh^{Snail1KO} ones (Figure R-39B). As a conclusion, these results supported the idea that endothelial Snail1 influenced in the ultrastructure of tumor vessels.

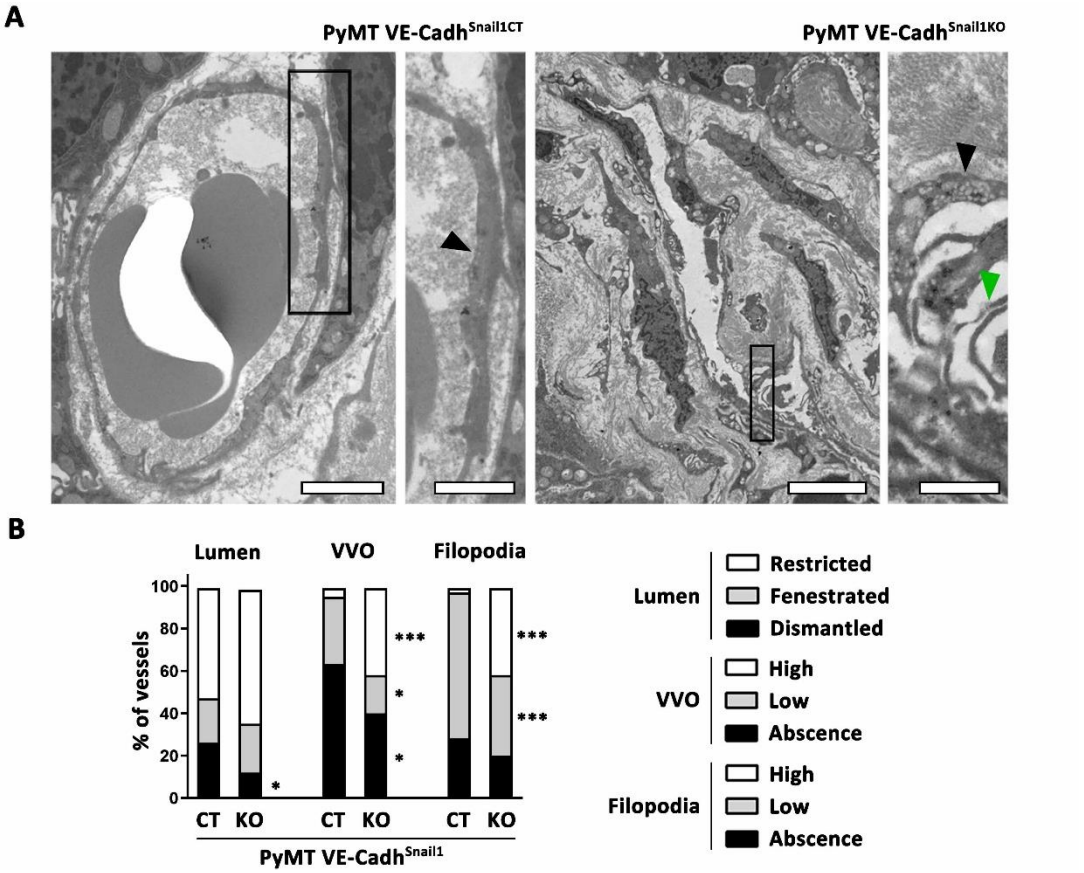

Figure R-39. Endothelial Snail1 regulates tumor vessel ultrastructure. A, Images of transmission electron microscopy of vessels in PyMT VE-Cadh$^{Snail1CT/KO}$ tumors at carcinoma stage. Box magnified in detail. Black arrowheads point VVO in endothelial cells. Green arrowhead points filopodia. Scale bar (PyMT VE-Cadh^{Snail1CT}): 2 µm; Scale bar (PyMT VE-Cadh^{Snail1KO}): 5 µm; Scale bar (magnification): 1 µm. **B**, Quantification of vessel lumen integrity, VVO and filopodia in vessels in PyMT VE-Cadh$^{Snail1CT/KO}$ tumors at carcinoma stage. *p<0.05; ***p<0.001.

Finally, we analyzed necrosis in big size tumors from PyMT VE-Cadh^{Snail1CT} and PyMT VE-Cadh^{Snail1KO} mice. We quantified these areas by a hematoxylin and eosin staining (Figure R-40A). We found that there were less necrotic areas in PyMT VE-Cadh^{Snail1CT} tumors than in PyMT VE-Cadh^{Snail1KO} tumors (Figure R-40B). As we hypothesized that necrosis could be associated to morphological changes of the tumors, we compared the necrotic areas of PyMT VE-Cadh^{Snail1CT} tumors with a solid and papillary morphology. We concluded that tumor morphology *per se* did not alter necrosis of PyMT VE-Cadh^{Snail1CT} tumors, since solid and papillary tumors in PyMT VE-Cadh^{Snail1CT} tumors presented the same proportion of necrosis (Figure R-40C). Therefore, expression of Snail1 in endothelial cells regulated necrosis in MMTV-PyMT breast tumors.

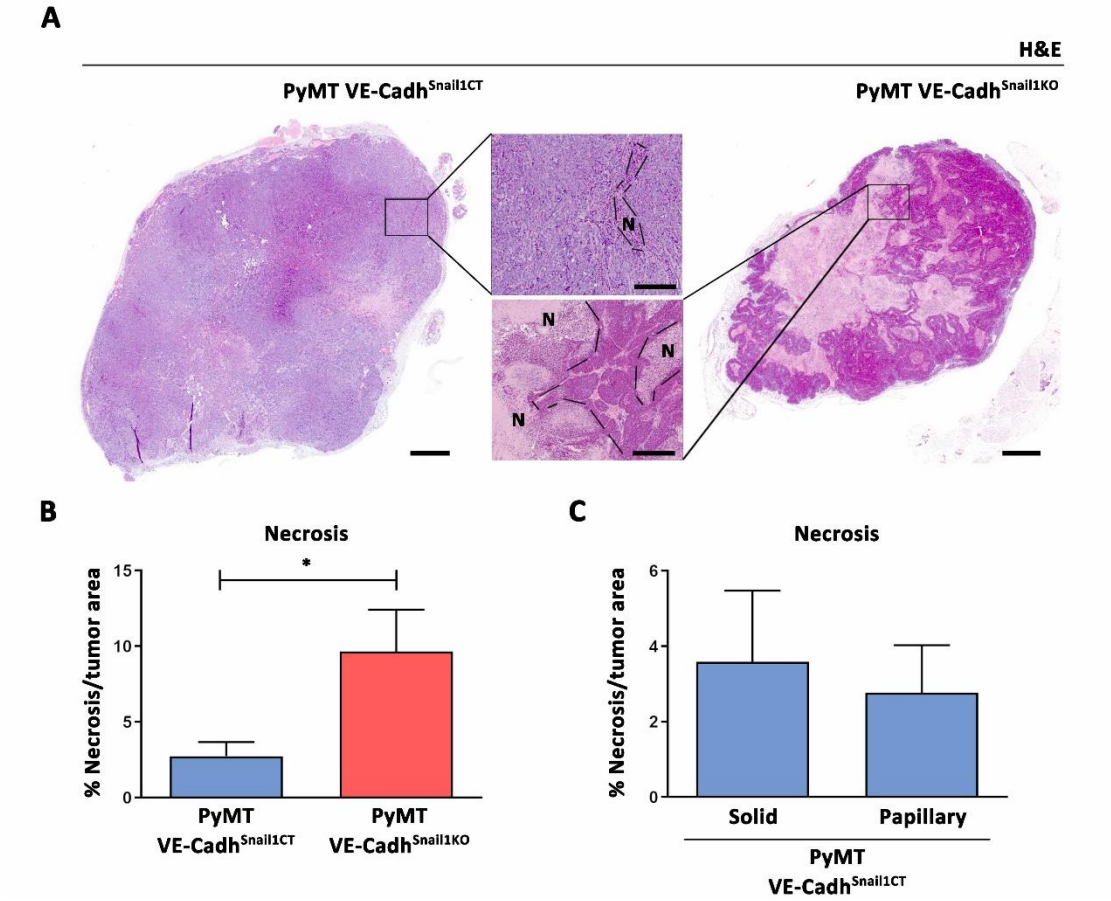

Figure R-40. Snail1 expression in endothelial cells promotes less necrotic areas at carcinoma stage. A, Hematoxylin and eosin staining in PyMT VE-Cadh$^{Snail1CT/KO}$ tumors at carcinoma stage. 'N' states for necrosis. Scale bar (whole scan): 1 mm; Scale bar (magnification): 200 µm. **B**, Quantification of necrotic areas per tumor area in PyMT VE-Cadh$^{Snail1CT/KO}$ tumors at carcinoma stage. **C,** Quantification of necrotic areas per tumor area in PyMT VE-Cadh^{Snail1CT} tumors at carcinoma stage with solid or papillary morphology. Data in B and C represent mean values (±SEM). *p<0.05.

14. Orthotopic breast tumor model confirms Snail1 vasculature effects

Apart from the spontaneous breast tumor mouse model, we used an alternative model to corroborate the role of endothelial Snail1 in tumorigenesis. For that, we isolated cells from middle size tumors and injected them orthotopically in VE-Cadh^{Snail1CT} and VE-Cadh^{Snail1KO} mice (Figure R-41A). Tumor growth was identical for both genetic backgrounds (Figure R-41B). However, tumors showed a differential progression and morphology (Figure R-41C). Morphologically, VE-Cadh^{Snail1CT} tumors at carcinoma stage had a solid morphology rather than papillary one, more common in VE-Cadh^{Snail1KO}

tumors at carcinoma stage (Figure R-41D). Thus, endothelial Snail1 affected tumor development in an orthotopic breast tumor model, similar to the spontaneous one.

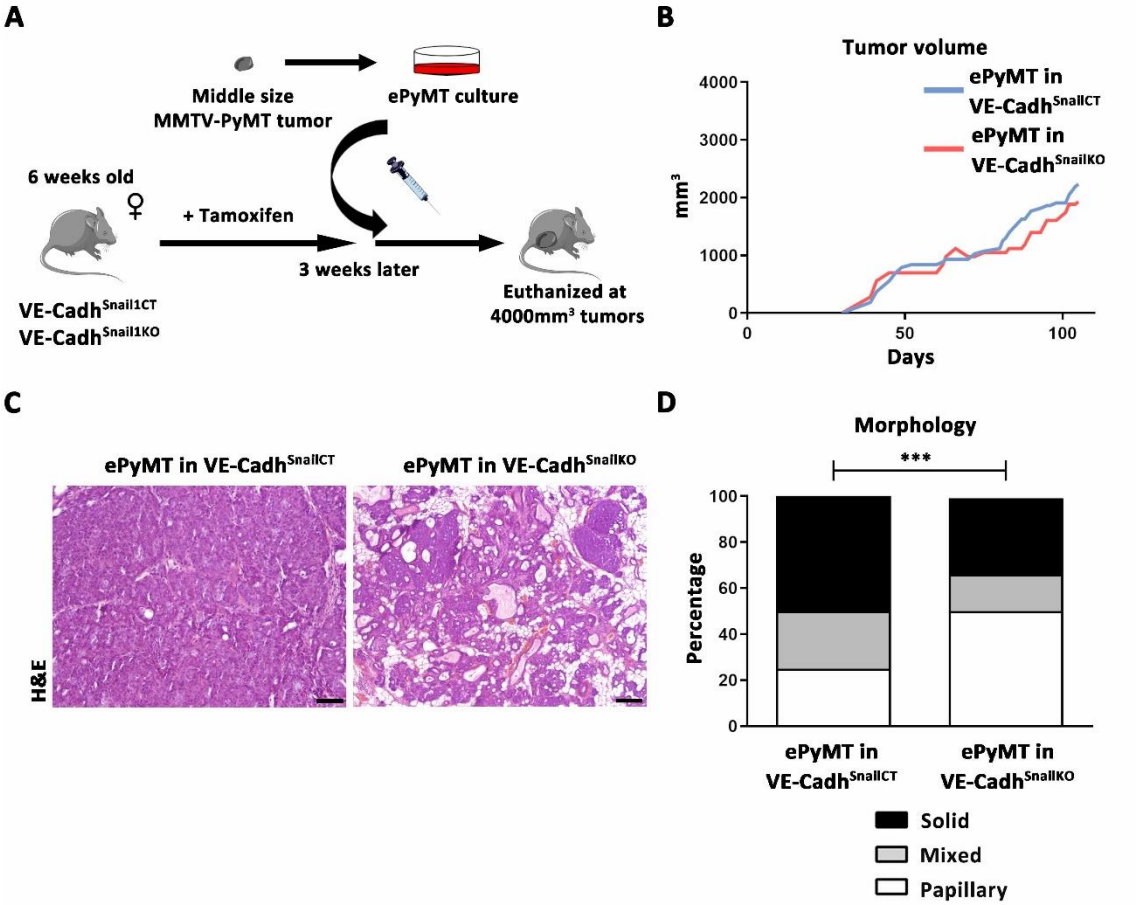

Figure R-41. Orthotopic tumors from ePyMT cells generate papillary tumors grafted in Snail1 lacking vasculature mice. A, Scheme of workflow for ePyMT cell isolation from middle size tumors and its orthotopic transplantation. **B**, Comparison of tumor volume of ePyMT tumors in VE-Cadh$^{Snail1CT/KO}$ mice. **C**, Image of hematoxylin and eosin staining of ePyMT tumors at carcinoma stage in VE-Cadh$^{Snail1CT/KO}$ mice. Scale bar: 200 µm. **D**, Comparison of morphology of ePyMT tumors at carcinoma stage in VE-Cadh$^{Snail1CT/KO}$ mice. **p<0.01; ***p<0.001.

In this model we also checked the angiogenesis status. The amount of angiogenesis showed an upward tendency in ePyMT VE-Cadh^{Snail1CT} tumors compared to ePyMT VE-Cadh^{Snail1KO} tumors, close to be significant (Figure R-42A, B). Moreover, in terms of vessel morphology, ePyMT VE-Cadh^{Snail1CT} tumor vessels had smaller areas and perimeters than ePyMT VE-Cadh^{Snail1KO} ones (Figure R-42C, D). Thus, this orthotopic model recapitulated the previously reported angiogenic effects of Snail1 in endothelial cells in spontaneous breast tumor model.

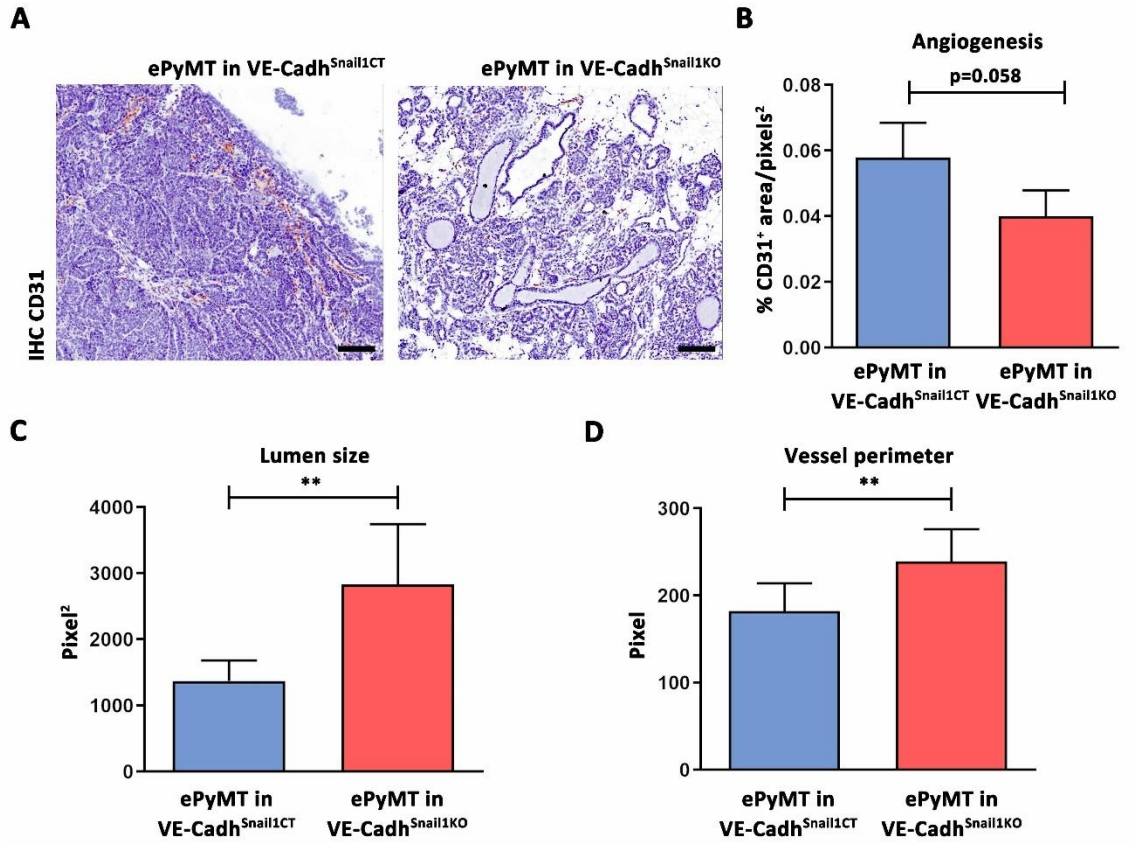

Figure R-42. Orthotopic tumors from ePyMT cells lead to a different morphology in their vessels grafted in Snail1 lacking vasculature mice. A, Images of anti CD31 immunohistochemistry of ePyMT tumors in VE-Cadh$^{Snail1CT/KO}$ mice. Scale bar: 200 µm. **B-D**, Quantification of CD31^{+} stained area (B), vessel lumen size (C) and vessel lumen perimeter (D) of ePyMT tumors in VE-Cadh$^{Snail1CT/KO}$ mice. Data in B, C and D represent mean values (± SEM). **p<0.01.

15. *In vivo* early antiangiogenic treatment of breast tumor model provokes tumor onset delay and papillary morphology tumors with differential tumor vessel morphology

After corroborating several effects of Snail1 in endothelial cells in two different breast tumor mouse models, we wondered if we could mimic our results by using a drug treatment that could be translated to the clinic. For that, we used bevacizumab, which neutralizes VEGF-A cytokine. Firstly, we checked that Snail1 protein expression on HUVEC on monolayer was decreased (Figure R-43A). Moreover, we analyzed bevacizumab effects on tubulogenesis, which was also affected. Indeed, bevacizumab reduced the tubulogenic ability of HUVEC (Figure R-43B, C).

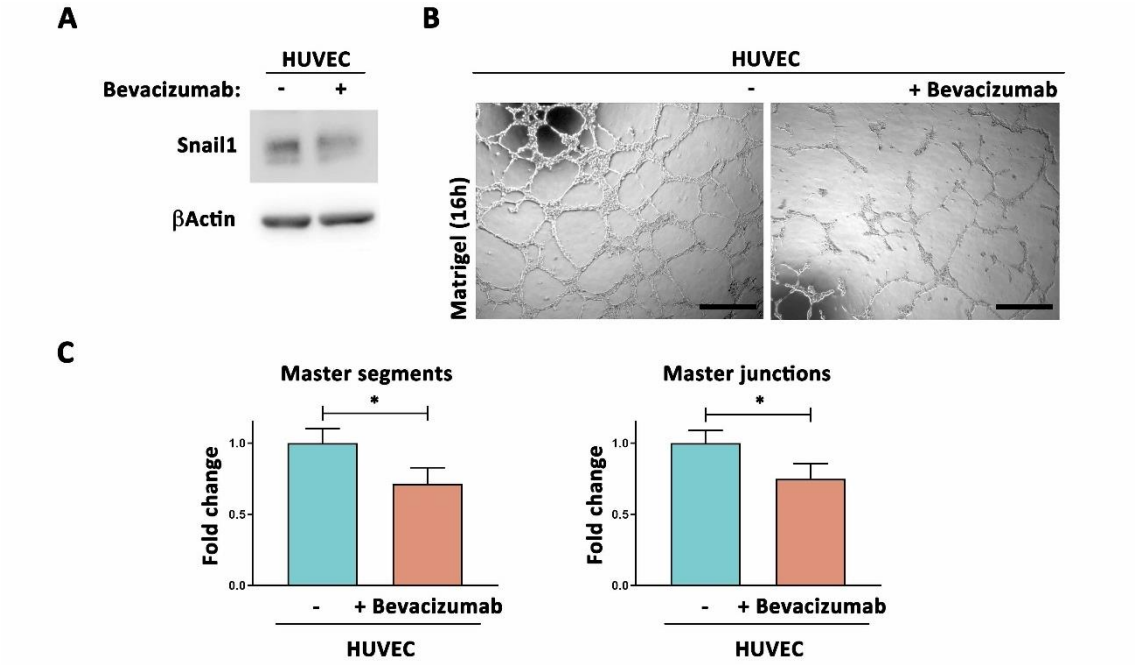

Figure R-43. Bevacizumab reduces Snail1 expression in HUVEC associated to an impairment in Matrigel induced tubulogenesis *in vitro*. A, Western blot analysis of Snail1 in HUVEC on monolayer treated with or without bevacizumab. **B**, Images of HUVEC treated with or without bevacizumab over Matrigel for 16h. Scale bars: 200 μm. **C**, Quantification of master segments (left) and junctions (right) of HUVEC treated with or without bevacizumab. Data in C represent mean values (± SEM) of at least three independent experiments. *p<0.05.

Afterwards, we treated MMTV-PyMT mice with bevacizumab or with PBS as control (Figure R-44A), starting at 6 weeks old, exactly the same age as in our Snail1 depleted *in vivo* model. Firstly, we observed a significant delay of 10 days on the tumor onset after bevacizumab treatment (Figure R-44B). Moreover, tumor growth was also delayed by bevacizumab treatment, caused by a longer tumor onset since the tumor growth curves were parallel when tumors appeared (Figure R-44C). Moreover, tumors looked morphologically different in both groups (Figure R-44D). Although there were the same proportion of tumors at carcinoma stage in both groups (Figure R-44E), bevacizumab treated mice presented a higher proportion of tumors at carcinoma stage with papillary morphology (Figure R-44F). Therefore, bevacizumab controlled breast tumorigenesis similarly to Snail1 depletion in endothelial cells.

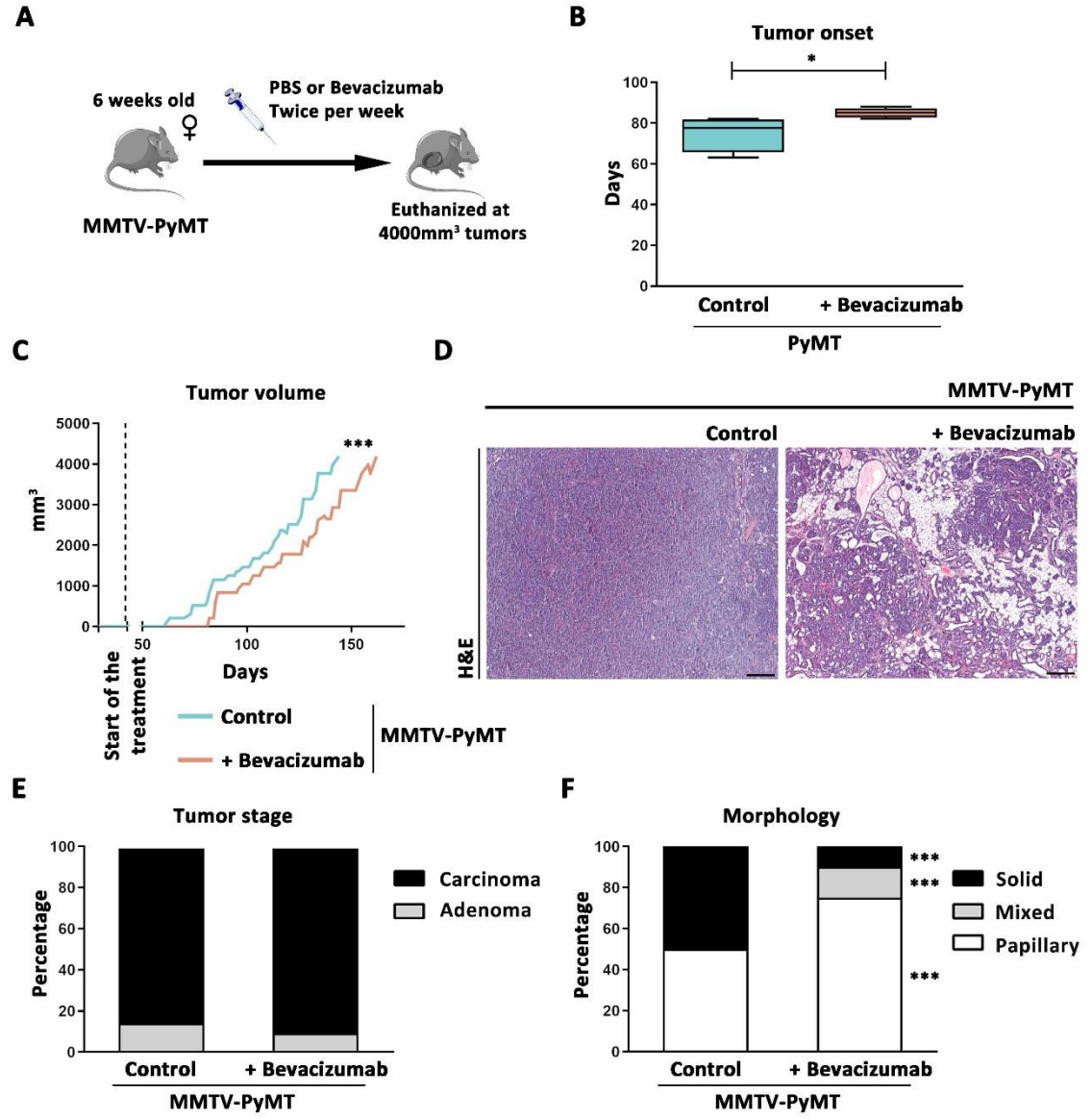

Figure R-44. Early treatment with bevacizumab *in vivo* mimics the effects of the absence of endothelial Snail1 during tumor progression and tumor morphology. A, Scheme of mouse strategy for bevacizumab treatment in MMTV-PyMT mice. **B-C**, Comparison of tumor onset (B) and tumor volume (C) in MMTV-PyMT mice treated or not with bevacizumab. **D**, Image of hematoxylin and eosin staining of tumors from MMTV-PyMT mice treated or not with bevacizumab. **E-F**, Comparison of tumor stage (E) and their morphology (F) of tumors from MMTV-PyMT mice treated or not with bevacizumab. Data in B represents mean values (± SEM). *p<0.05; ***p<0.001.

Finally, we quantified the angiogenesis of tumors at carcinoma stage being or not treated with bevacizumab. We did not observe any significant alteration in the amount of endothelial cells (Figure R-45A, B). Nevertheless, tumor vessels were bigger in area

and perimeter under bevacizumab treatment (Figure R-45C, D). Therefore, we could state that an early treatment of bevacizumab affected tumor angiogenesis morphology.

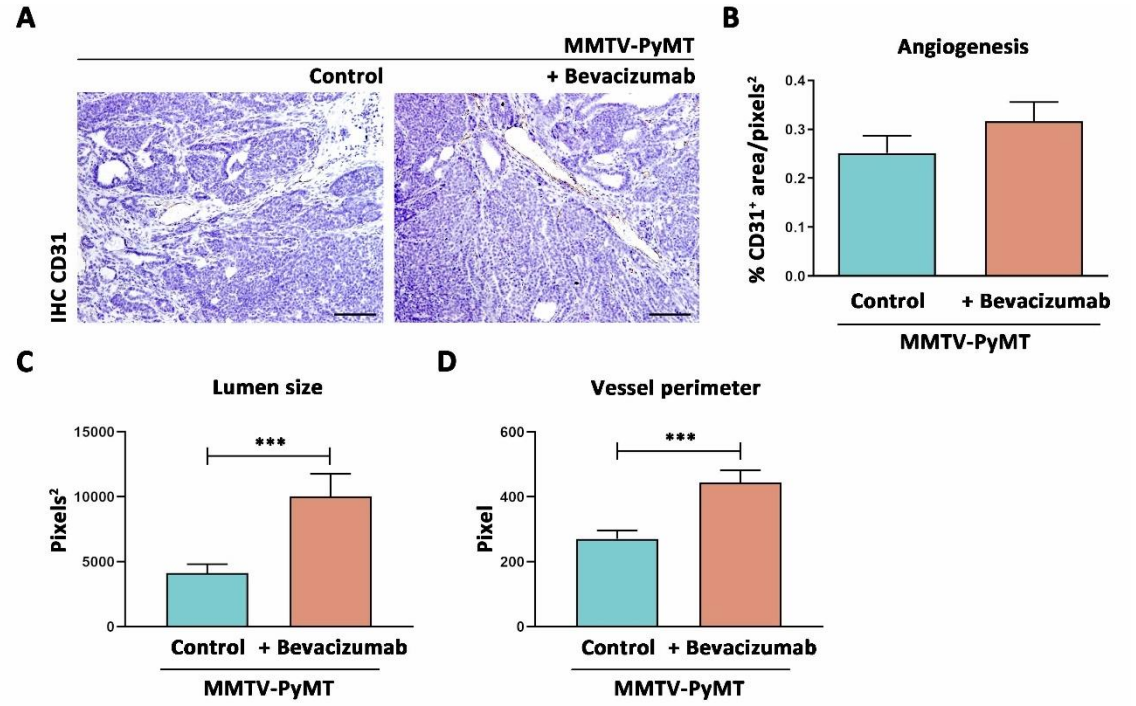

Figure R-45. Early bevacizumab treatment *in vivo* modifies tumor vasculature morphology. A, Images of anti CD31 immunohistochemistry in tumors from MMTV-PyMT mice treated or not with bevacizumab. Scale bars: 200 µm. **B-D**, Quantification of $CD31^+$ stained area (B), vessel lumen size (C) and vessel lumen perimeter (D) in tumors from MMTV-PyMT mice treated or not with bevacizumab. Data in B, C and D represent mean values (± SEM). ***p<0.001.

16. Breast human tumor samples mimic the differential tumor development, angiogenesis, vessel morphogenesis and profibrotic signaling of PyMT VE-Cadh$^{Snail1CT/KO}$ mice

After the *in vitro* and *in vivo* analysis of endothelial Snail1 in mice, we aimed to translate this study to the clinic and extrapolate our results to human samples. We analyzed human luminal breast tumors at carcinoma stage from diagnostic biopsies of non-treated patients, comparing No Specific Type (NST) and papillary morphologies, as a representation of PyMT VE-Cadh^{Snail1CT} and PyMT VE-Cadh^{Snail1KO} tumors, respectively. First of all, we clinically classified these tumors. Apart from the morphology, we observed that both NST and papillary tumors were positive for HER2, ERα and PR, similarly to our PyMT VE-Cadh^{Snail1} model (Figure R-46A). In the case of ERα, human NST

tumors had lower intensity compared to human papillary tumors (Figure R-46B). Regarding proliferation, there was an upward trend of $Ki67^+$ cells in NST tumors, compared to papillary tumors (Figure R-46C). Finally, human NST tumors at diagnosis had a bigger proportion of more advanced tumor stage than human papillary tumors (Figure R-46D).

Next, we focused on their vasculature. In these comparisons, we considered the adjacent healthy tissue from tumor samples as a non-tumorigenic condition. We quantified the amount of $CD31^+$ stained area as a signal of angiogenesis (Figure R-47A). We observed that NST and papillary tumors had an increase of angiogenesis compared to adjacent healthy tissue (Figure R-47B). We did not detect any significant difference between both tumor groups, but there was an upward tendency of angiogenesis in human NST tumors compared to papillary ones (Figure R-47B). Regarding vessel morphology, human NST tumor vessels were smaller in area and perimeter than papillary (Figure R-47C, D). Hence, human breast tumor had different tumor vessel morphology between NST and papillary morphology, mirroring the results from PyMT VE-$Cadh^{Snail1}$ model.

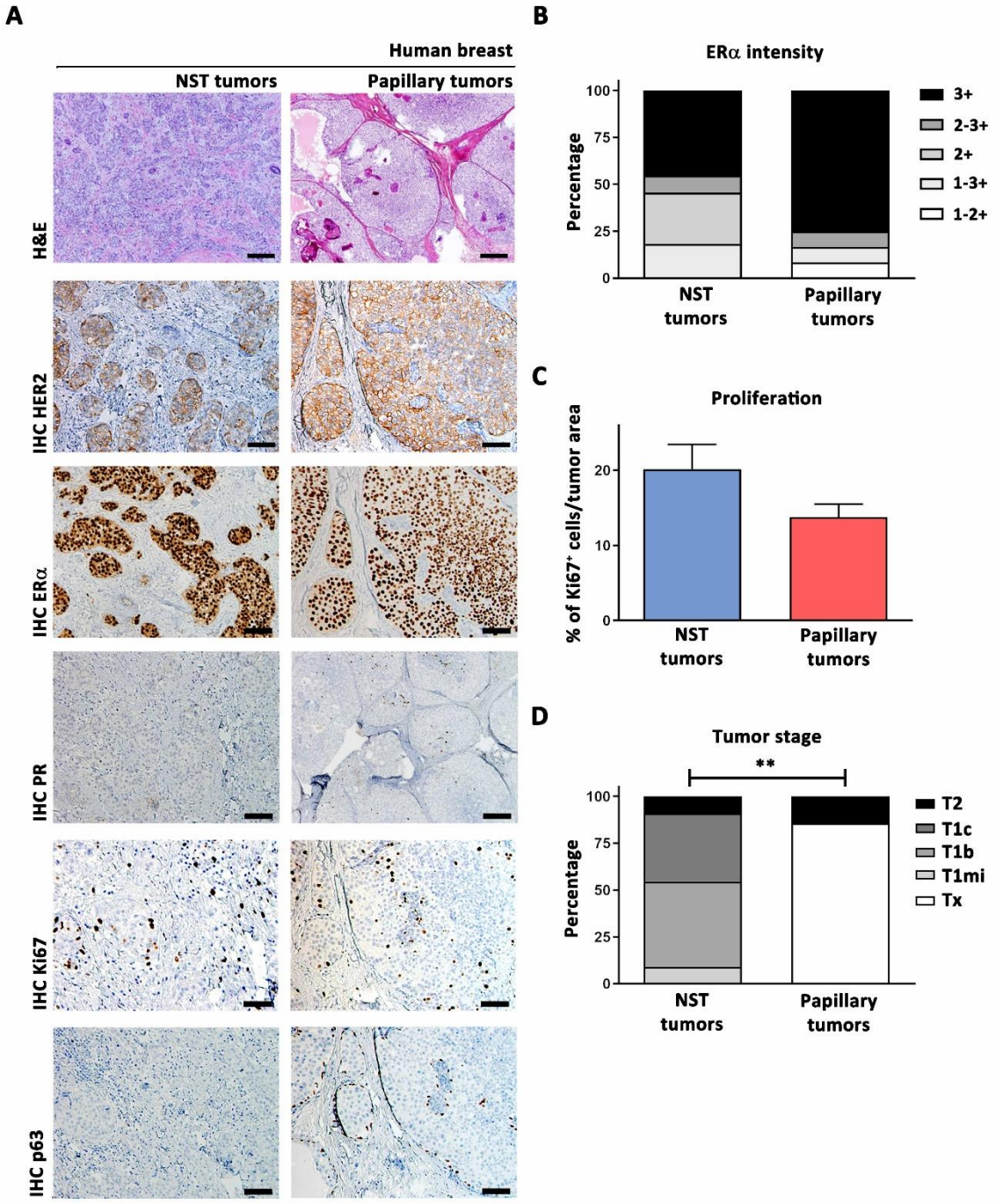

Figure R-46. Human papillary breast tumors present a higher presence of nuclear ERα, are less proliferative and less aggressive. A, Images of hematoxylin and eosin staining and anti HER2, anti ERα, anti PR, anti ki67 and anti p63 immunohistochemistry in NST (left column) and papillary (right column) human breast tumors at carcinoma stage. Scale bar (H&E): 200 µm. Scale bar (others): 100 µm. **B-D**, Quantification of percentage of ERα intensity (B), Ki67$^+$ cell per nuclei (C) and tumor stage at diagnosis (D) in NST and papillary human breast tumors at carcinoma. Data in C represent mean values (± SEM). **p<0.01.

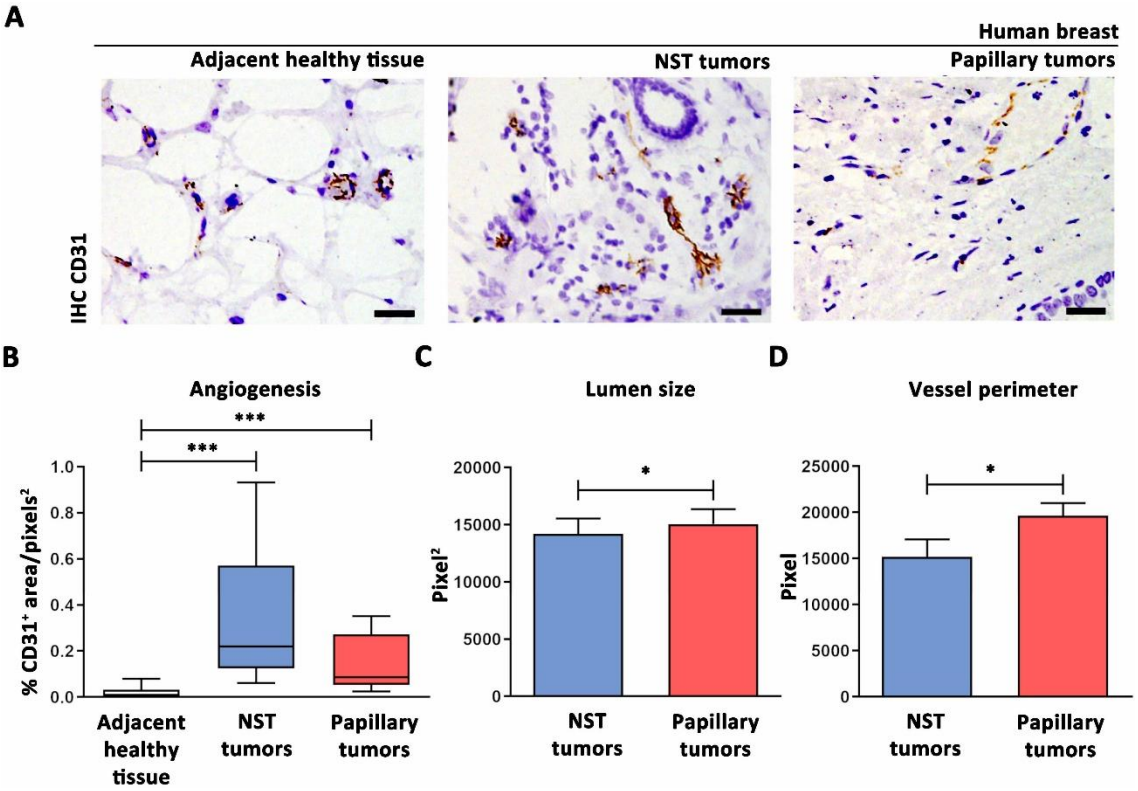

Figure R-47. Human papillary breast tumors have different vessel morphology. A, Images of anti CD31 immunohistochemistry in adjacent healthy tissue and NST or papillary human breast tumors at carcinoma stage. Scale bar: 40 µm**. B-D**, Quantification of $CD31^+$ stained area (B), vessel lumen size (C) and vessel perimeter (D) in adjacent healthy tissue and NST or papillary human breast tumors at carcinoma stage, when indicated. Data in B, C and D represent mean values (± SEM). *p<0.05; ***p<0.001.

Afterwards, we analyzed endothelial and non-endothelial Snail1 expression in these tumors (Figure 48A). We quantified the amount of $Snail1^+$ vessels in each group and we noticed that breast tumors exhibited a higher amount, compared to adjacent healthy tissue (Figure R-48B). Interestingly, there were significantly more $Snail1^+$ vessels in human NST tumors than in human papillary tumors (Figure R-48B). Furthermore, we also quantified $Snail1^+$ stroma, showing that in tumor areas there were more $Snail1^+$ cells than in adjacent healthy tissue (Figure R-48C). Moreover, in human NST tumors the presence of $Snail1^+$ stroma was higher than in papillary tumors (Figure R-48C). In all cases, $Snail1^+$ vessels were surrounded by $Snail1^+$ stroma, showing a correlation between $Snail1^+$ endothelial cells and active stroma (Figure R-48D). Summing up all

these results, we confirmed that Snail1 in vessels showed a correlation with human breast tumors with papillary morphology and active stroma.

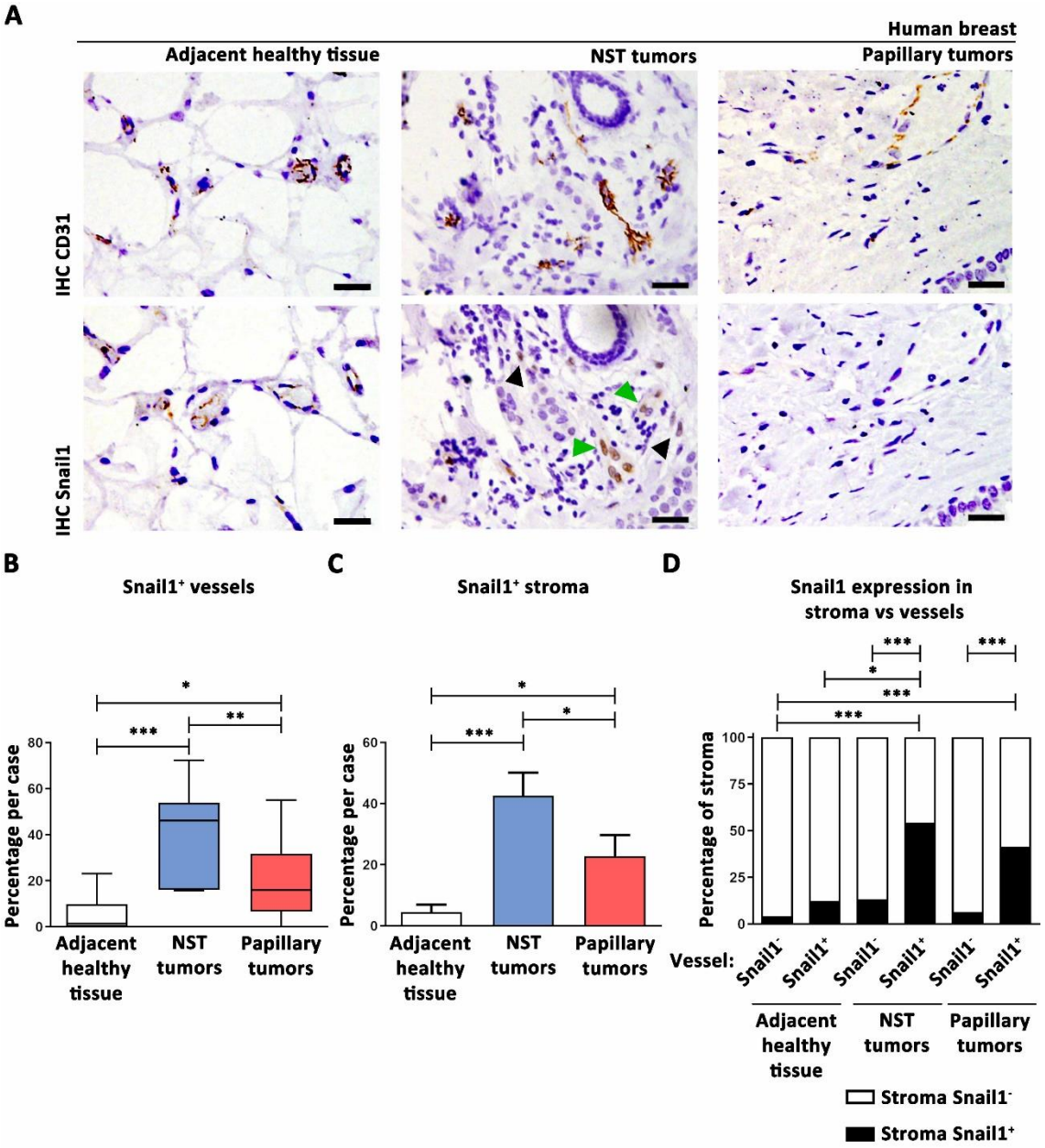

Figure R-48. Human papillary breast tumors have less Snail1⁺ endothelial cells, associated with a reduced of Snail1⁺ cells in their surrounding stroma. A, Images of anti CD31 and anti Snail1 immunohistochemistry in adjacent healthy tissue and NST or papillary carcinoma from human breast tumors. Black arrowheads point Snail1⁺ stroma cells. Green arrowheads point Snail1⁺ endothelial cells. Scale bar: 40 µm**. B-D**, Quantification of percentage of Snail1⁺ vessels per case (B), percentage of Snail1⁺ stroma per case (C) and evaluation of Snail1⁺ stroma depending on the presence of Snail1⁺ vessels (D) in adjacent healthy tissue and NST or papillary carcinoma from human breast tumors, when indicated. Data in B and C represent mean values (± SEM). *p<0.05; **p<0.01; ***p<0.001.

Next, we wanted to study some aspects in human tumor samples that required a higher number of cases. For that, we dived into the cBioPortal public database. There, we searched in the TCGA Breast Invasive Carcinoma (Firehose Legacy) database, that included a thorough dataset of clinical data, as well as mRNA and protein levels of the whole tumor of a high number of samples. Firstly, we analyzed protein and mRNA correlations in breast tumors from that database. PECAM1 (CD31) mRNA levels and protein levels correlate positively with SNAI1 mRNA and protein levels, respectively (Figure R-49A). Therefore, the more CD31, the more Snail1 in human breast tumors. Moreover, we found that PECAM1 mRNA levels correlate positively with VIM (Vimentin) mRNA levels (Figure R-49B) and SNAI1 mRNA levels with VIM mRNA levels (Figure R-49C). All Vimentin correlations showed were at mRNA level since this database did not contain data for Vimentin protein levels. Summing up, the more CD31 or Snail1, the more Vimentin in human breast tumors.

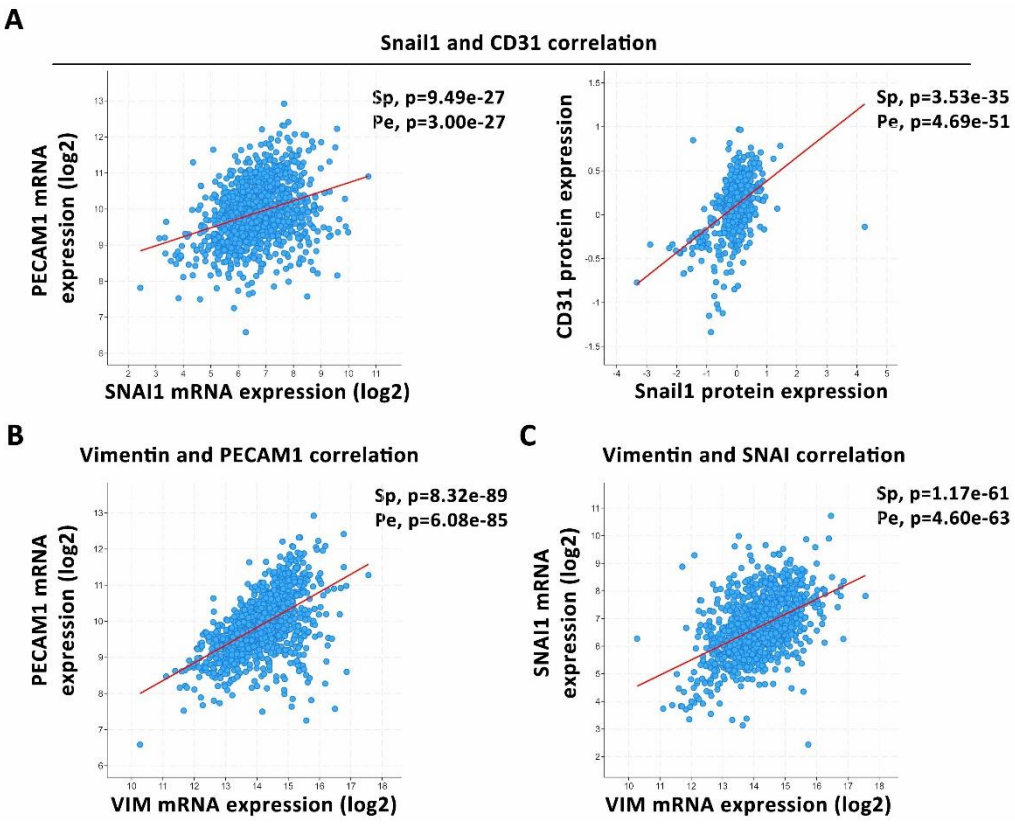

Figure R-49. Human breast cancer dataset from TCGA consortium correlates positively Snail1, CD31 and Vimentin expression among each other. A-C, Regression analysis of PECAM (CD31) mRNA expression versus SNAI1 mRNA expression (A, left), CD31 protein expression versus Snail1 protein expression (A, right), PECAM1 (CD31) mRNA expression versus VIM mRNA expression

(B) and SNAI1 mRNA expression versus VIM mRNA expression (C) in human breast cancer dataset from TCGA consortium. Regression lines between the indicated parameters and Pearson (Pe) and Spearman (Sp) correlation coefficients with their corresponding p-value are shown for each graph.

TCGA Breast Invasive Carcinoma (Firehose Legacy) database also contained clinical data of their breast samples. To get advantaged of that, we humanized our PyMT VE-Cadh^{Snail1} model, recapitulating the characteristics of PyMT VE-Cadh^{Snail1CT} and PyMT VE-Cadh^{Snail1KO} tumors. PyMT VE-Cadh^{Snail1CT} tumors had higher angiogenesis (CD31), more active stroma (Vimentin and Snail1), lower proportion of myoepithelial cells (CK14, p63, CK5) and low content of immune cells (CD45), compared to PyMT VE-Cadh^{Snail1KO} tumors. After translating these features to mRNA gene expression and mirroring it to PyMT VE-Cadh^{Snail1KO} tumors as the opposite, we obtained their humanized version (Figure R-50A). We checked the survival of both groups and, "humanized PyMT VE-Cadh^{Snail1CT}" patients had a worse survival compared to "humanized PyMT VE-Cadh^{Snail1KO}" patients (Figure R-50B). Moreover, analyzing the disease-free period of both groups, "humanized PyMT VE-Cadh^{Snail1CT}" patients had a shorter period of time free of disease (Figure R-50C). Therefore, not only the correlation of human breasts followed the same pattern as we found previously, but also clinically our PyMT VE-Cadh^{Snail1} model was corroborated.

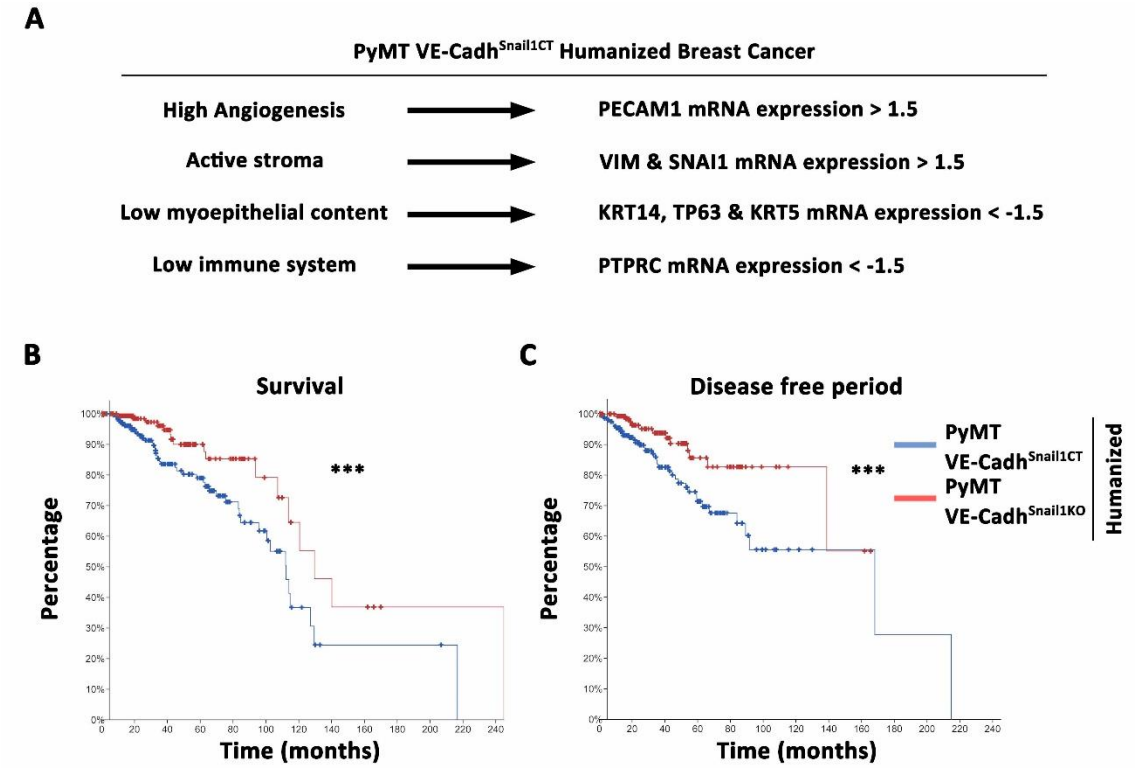

Figure R-50. Mimic of PyMT VE-Cadh$^{Snail1CT/KO}$ tumors in human breast cancer dataset from TCGA consortium reiterates survival and disease-free period trend found in mice. A, Scheme of PyMT VE-Cadh^{Snail1CT} humanized breast cancer. **B-C**, Kaplan-Meier curves of survival (B) and disease-free (C) from patients with breast tumors from public dataset TCGA consortium mimicking those obtained in PyMT VE-Cadh$^{Snail1CT/KO}$ mice. *** p<0.001.

Furthermore, using this TCGA database, we analyzed the genes that were differentially expressed in "humanized PyMT VE-Cadh^{Snail1CT}" and "PyMT VE-Cadh^{Snail1KO}" tumors. After performing a Gene Set Enrichment Analysis (GSEA) of those groups, we detected that in the top ten biological processes of "humanized PyMT VE-Cadh^{Snail1CT}" tumors, most of them were related to stromal activation and oxidative metabolism (Figure R-51). On the other hand, in "humanized PyMT VE-Cadh^{Snail1KO}" tumors, most of their biological processes were related to gene expression and chromatin remodeling (Figure R-51).

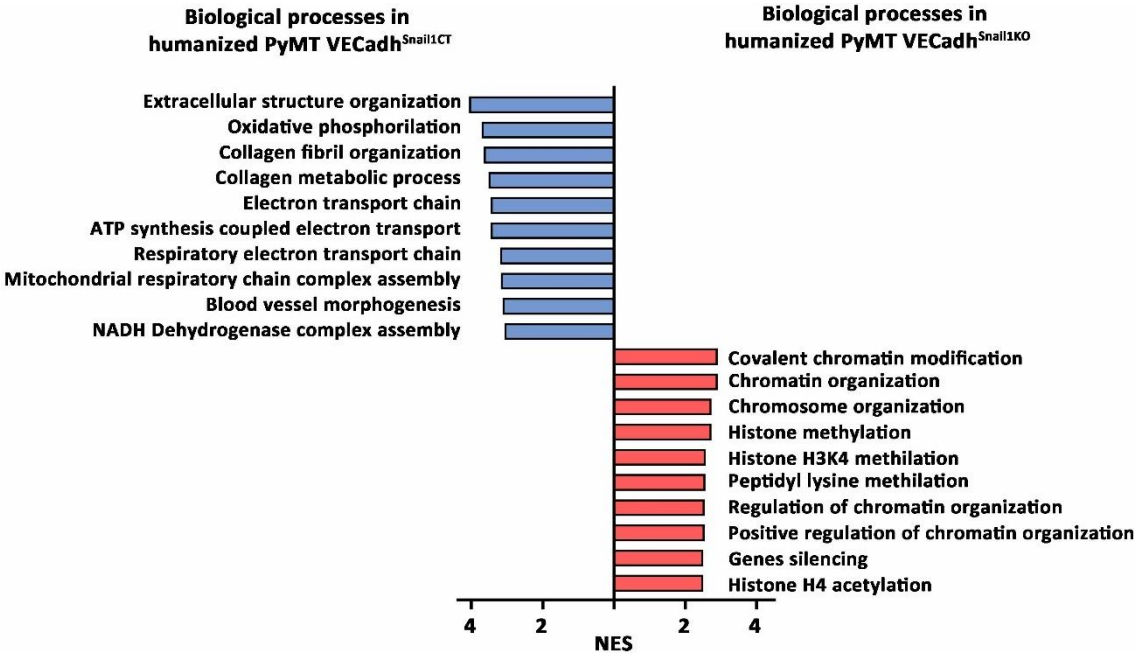

Figure R-51. GSEA analysis of "humanized PyMT VE-Cadh^{Snail1CT}" tumors in human breast cancer dataset from TCGA consortium shows that top categories are related to fibrotic remodeling and chromatin modification in the case of "humanized PyMT VE-Cadh^{Snail1KO}" tumors. Top ten biological processes of "humanized PyMT VE-Cadh^{Snail1CT}" and "humanized PyMT VE-Cadh^{Snail1KO}" mice. Normalized Enrichment Score (NES).

DISCUSSION

Snail1 is a transcription factor that has been extensively studied in tumors as a determinant of the epithelial to mesenchymal transition and in the activation of cancer-associated fibroblasts. Nevertheless, few attention has been drawn to Snail1 in the endothelium, even though previous research has stated its role in motility and plasticity in those cells. In this thesis, we sought to address this issue by exploring the biological consequences of Snail1 in the endothelial cells, *in vitro* and *in vivo*, in a quiescent state or in a tumor angiogenic environment.

1. Expression of Snail1 in endothelial cells

Firstly, *in vitro* we observed that Snail1 was expressed in the nuclei of HUVEC on monolayer and over Matrigel. Over Matrigel, most Snail1$^+$ HUVEC were localized in the segments of tubulogenesis, suggesting a necessary role for Snail1 in this process. Moreover, we detected Snail1 expression in the sprouting spheres (see Figure R-8). At this respect, Snail1$^+$ HUVEC were localized in the surface of the spheres, in the base of sprouts. That leads us to think that expression of Snail1 in HUVEC might be induced during its activation, changing the expression profile of the cell and fading from there when tip cells are specified. This assumption is supported by our data, which showed that Snail1 regulates AKT and ERK pathways in endothelial cells, which control endothelial activation status (Figure D-1). Moreover, Snail1 might induce a stalk phenotype, since Snail1 blocks Dll4 expression in endothelial cells, which is a molecular switch that determines tip/stalk fate decision.[181,216]

I*n vivo*, we did not register any expression of Snail1 in endothelial cells at quiescent state in adult tissues (see Figure R-19). That lack of expression was expected since Snail1 is described to be expressed in endothelial cells under an angiogenic challenge or during embryogenesis (vasculogenesis).[179,181] Whereas, in Matrigel plugs, in MMTV-PyMT and human breast tumors, we did detect Snail1 expression in endothelial cells. Due to the difficulty to identify an *in vivo* vessel sprout in a paraffin section, we could not determine if Snail1$^+$ cells were tip or stalk cells. Supporting this endothelial Snail1 expression, another laboratory did also report expression of Snail1 in human colorectal and pharyngeal squamous tumor vessels.[190,217]

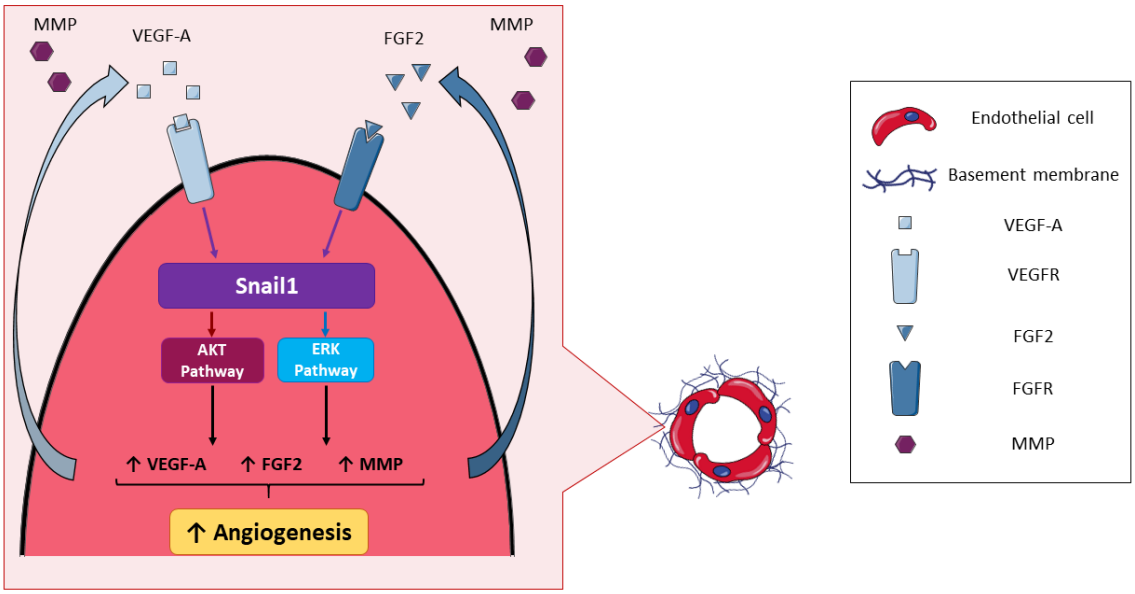

Figure D-1. Proposed model of Snail1 activity in endothelial cells. VEGF-A and FGF2 angiogenic factors are detected by endothelial cells through VEGF and FGF receptors, respectively, activating Snail1 expression and subsequently AKT and ERK pathways. That activation induces the expression of VEGF-A, FGF2 and MMP, that boosts the angiogenic pathways of the endothelial cell.

2. Endothelial Snail1 and EndoMT

Snail1 is key in the EMT process, and endothelial cells could eventually undergo in a similar process called EndoMT.[161] Thus, we presumably expected to see differences in the identity of endothelial cells depending on Snail1. Our results suggested that Snail1 does not induce a complete EndoMT. Far from that, only a partial EndoMT was observed, since there was no alteration of endothelial identity but a slight regulation of some mesenchymal markers by Snail1, without altering their morphology, on monolayer and over Matrigel. This data was supported by other laboratories.[186,218] In fact, several reviews stated that a complete angiogenesis requires a partial EndoMT;[192,219] thus, compromising this partial EndoMT could end in a deficient angiogenesis, which, is indeed, what we did observe among the entire thesis. However, other authors have reported that Snail1 affects profoundly endothelial cells identity, leading to a loss of endothelial markers and gaining remarkable levels of mesenchymal markers.[220]

On the other hand, in the case of Snail2, ours results indicated a profound alteration of endothelial cells, closed to an extensive EndoMT, since Snail2 overexpression regulated several mesenchymal genes provoking a remarkable mesenchymal phenotype in HUVEC. Due to that, Snail2 affected tubulogenic ability. However, other authors have described that Snail2 overexpression increased sprouting ability.[190] We explain that controversial result based on the fact that, they did not show how HUVEC overexpressing Snail2 behave molecularly in terms of gain of mesenchymal genes and the very limited overexpression of Snail2 in this system.

3. Induction of Snail1 in endothelial cells

Snail1 is induced by VEGF-A and FGF2 in epithelial and mesenchymal cells.[165,221] Indeed, we corroborated it in endothelial cells (see Figure D-1).[222] In fact, we noticed that FGF2 induced Snail1 more extensively and faster than VEGF-A in HUVEC. Furthermore, ePyMT conditioned medium induced Snail1 expression at mRNA and protein levels (see Figure R-16). Regarding the conditioned medium composition, tumor cells do secrete FGF2 and VEGF-A;[104] thus, we expected that blocking FGF2 and VEGF-A signaling with SU5402 or bevacizumab, respectively, we could observe an abrogation of that induction. Indeed, we did observe a decrease of Snail1 induction, accompanied by a decrease of tubulogenic abilities. SU5402 strongly abrogated Snail1 upregulation, more than bevacizumab, reaching low basal levels (see Figure R-16). It is important to state that, even though the effects are considerably higher when they are supplemented with proangiogenic conditioned medium, those drugs may also affect HUVEC without the addition of any conditioned medium. We checked that with bevacizumab, observing that basal Snail1 levels in HUVEC were reduced. Supporting that data, it was reported that blocking VEGF-A, by administrating a VEGF-antagonistic peptide in tumor epithelial cells, decreased Snail1 expression.[223] In the case of SU5402, we would expect similar and stronger results, since its effect observed in HUVEC were more intense than bevacizumab. Moreover, even though SU5402 has been extensively used in research articles as an FGF signaling inhibitor, SU5402 is a potent multi-targeted receptor tyrosine

kinase inhibitor, including other receptors apart from FGF, such as VEGFR or PDGFR.[224] Thus, the effect of SU5402 over Snail1 expression is expected to be stronger than bevacizumab.

Apart from external proangiogenic signaling, HUVEC can also support their activation status by an autocrine loop.[225] In fact, this loop is regulated by Snail1: the more Snail1, the more FGF2 and VEGF-A mRNA levels (see Figure D-1). The stricter control of Snail1 by FGF2, compared to VEGF-A, supported the above commented results; SU5402 blocks FGF2 signaling, reducing Snail1 levels, which induces less FGF2, as a repressive auto-loop.

4. Control of Snail1 over angiogenesis in HUVEC

Snail1 had a dose dependent effect on tubulogenic, sprouting and migration abilities; the more Snail1 HUVEC have, the more angiogenesis (see Figure D-1). Nevertheless, there is some controversy in the field, since some researchers reported that lack of Snail1 abrogated sprouting abilities, but its transient overexpression prevented tubulogenesis.[190,220] We expected to see a coordinated response between both assays, since both assays are complemented and not divergent.[226] Therefore, it is possible that Snail1 should get to a determined concentration and lower or higher (even higher than in our Snail1 overexpressed cells) levels disrupt their angiogenic characteristics.

Behind these effects, FGFR3 and FGFR4 seemed to be strictly controlled by Snail1 (see Figure D-1), thus, regulating the angiogenic sensing of endothelial cells. Regarding FGFR3, it compensated the activity of FGFR1 and FGFR2 when they were lacking in endothelial cells, thus, FGFR3 is a highly relevant receptor in endothelial functionality.[227] Additionally, a relation between Snail1 and FGFR3 was previously discovered; FGFR3 required Snail1 expression during bone development and disease.[221] In the case of FGFR4, it was stated that it activated an 85-kDa serine kinase, activation not detected with other FGF receptors.[228] Moreover, it was speculated that some effects of FGF2 in HUVEC may occur through FGFR4, boosting its importance in endothelial cells.[229] In terms of Snail1 regulation, FGFR4 induced Snail1 expression.[230] Thus, intertwining that

information with our data, Snail1 regulates FGFR4 expression, which might be amplificated since FGFR4 increases Snail1 expression, creating a positive loop, supporting our data. In previous researches, Snail1 was found to control VEGFR3 levels in endothelial cells, relation that we did not detect.[186] Nevertheless, it is important to notice that they used Human Retinal Endothelial Cells (HREC), different from HUVEC. Indeed, origin of endothelial cells can have different responses to Snail1 in terms of gene expression, possibly through the dependence of Snail1 on other co-factors for gene regulation.[161,218]

5. Endothelial Snail1 in vessel development and adult mice

The role of Snail1 in endothelial cells during embryogenesis recently showed a strong controversy. Summing up, Snail1 in $Tie2^+$ endothelial cells was essential for embryo viability,[179] whereas in $Tie1^+$ or VE-$Cadherin^+$ endothelial cells, was not.[182] This might be seen as a contradiction, as all those promoter are considered specific of endothelial cells; however, Tie2 starts to be expressed at E6.5, whereas Tie1 and VE-Cadherin are expressed at E8.0 or E9.5, respectively.[231,232] Between these time points, there are two main vasculogenic processes within the embryo that, presumably, need Snail1 expression. The first one covers E6.5 to E7.5 and is based on the formation of the extra-embryonic vessels by the migration of angioblasts and the generation of blood islands. The second one, which covers from E7.5 to E.8.5, is based on the formation of intra-embryonic vessels, mainly related to the formation of the endocardium (E7.5), the dorsal aorta (E7.5) and a rudimentary circulatory system from E8.0.[233]

When mice get to adult age (6 weeks old), we did not detect any expression of Snail1 in endothelial cells at quiescent state (Figure R-19), as any other literature report. That was expected since Snail1 is expressed in endothelial cells under an angiogenic challenge or during vasculogenesis.[179,181] Therefore, there was no differential phenotype regardless of the status of Snail1 in the endothelial cells, in terms of weight, organ morphology or number, proliferation status and permeability of endothelial cells in mature vessels at adult stage. Studies using adult mice lacking Snail1 in their vasculature

did not show an overt phenotype at quiescent state.[182] In the case of Twist1, another transcription factor inducer of EMT and directly regulated by Snail1,[162] after its endothelial specific deletion, mice did not present any major alteration at quiescent state, except for an increase of their vascular permeability.[182,234]

6. Endothelial Snail1 and its contribution to tumor onset and its profibrotic paracrine effect

Previous research has studied extensively the role of Snail1 in transgenic mice during embryogenesis, wound healing, fibrosis or tumoral processes.[65,69,146,167–169] On the other hand, specific role of Snail1 in endothelial cells in transgenic mice have only been studied in embryogenesis, eye vascularization and kidney fibrotic processes, but not in tumors.[179,181,183,185,186]

Spontaneous breast tumor mouse model, MMTV-PyMT, generated several differences in the behavior of tumor growth upon Snail1 expression in endothelial cells (see Figure R-21). We found that endothelial Snail1 induced faster tumor growth, and a lower survival of mice, as well as an increased of their tumor burden, compared to endothelial Snail1 knocked out tumors. In fact, MMTV-PyMT mice lacking Snail1 ubiquitously, also showed an increase of their survival and a decrease of their tumor burden.[65] However, it is difficult to compare ubiquitous to specific endothelial Snail1 depletion, since ubiquitous depletion affects multiple cell types with multiple crosstalks.

Focusing on the tumor growth rate, we observed that the main reason of this delayed was due to the tumor onset, which was delayed 36 days in the endothelial Snail1 knocked out group. Taking a look at the initial stages of tumorigenesis, we observed a retard of proliferation, but not apoptosis, in endothelial Snail1 knocked out tumors (see Figure R-22). That was expected since tumor initiation is devoid of apoptosis. Angiogenesis was already altered in the number of vessels and their lumen size at that moment, leading us to think that Snail1 in endothelial cells was already having an effect (see Figure D-2). In fact, previous research indicated that angiogenesis starts at the very early stages of breast tumorigenesis, supporting our data.[214]

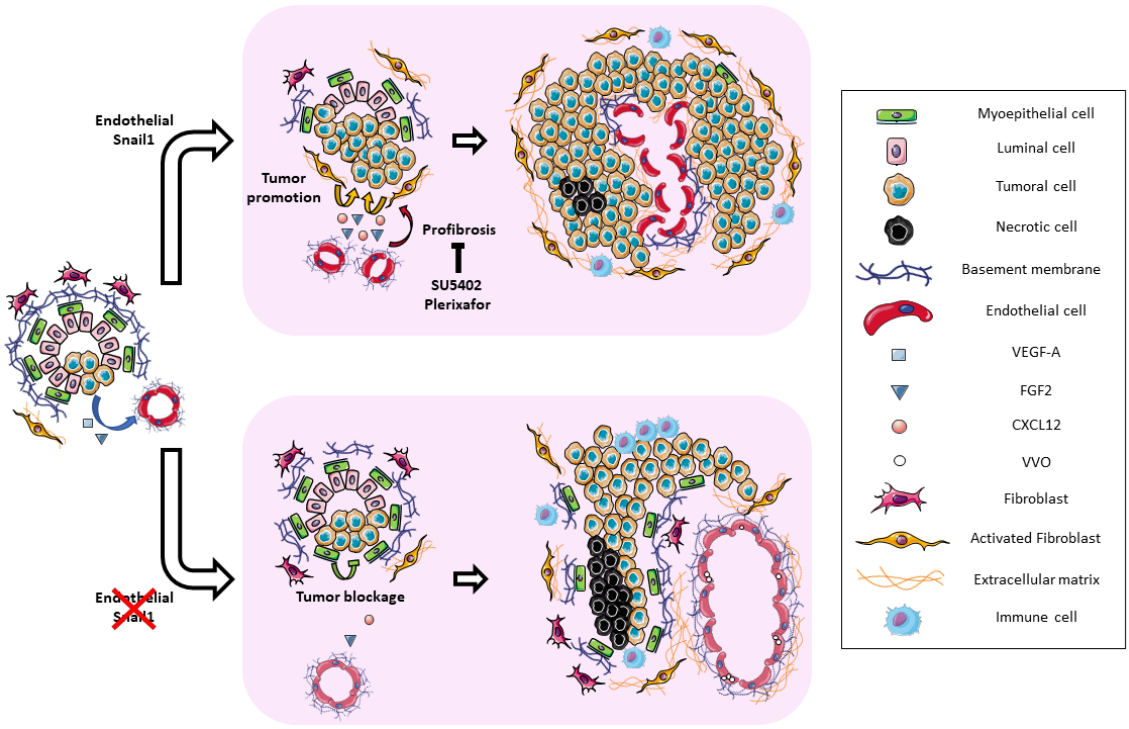

Figure D-2. Proposed model of endothelial Snail1 role in breast tumorigenesis. When breast tumor cells appear, FGF2 and VEGF-A are started to be secreted by them. Along tumor progression, when endothelial Snail1 is expressed, endothelial cells increase activation of fibroblast through CXCL12 and FGF2 cytokines, which can be blocked by SU5402 or Plerixafor. That fibroblast activation promotes tumorigenesis, leading to a solid tumor with few necrosis and disrupted vessels. When Snail1 is not expressed in endothelial cells, vessels are further from tumor cells, activation of fibroblasts is compromised and myoepithelial content is increased, provoking a tumorigenesis delay associated to a tumor blockage environment. Along time, papillary tumors with high content of immune cells and myoepithelial cells, with wider vessels and extended necrotic areas are generated.

We also observed that vessels in the control group were located closer to the premalignant ducts (see Figure D-2). That made us think that one possibility of this differential onset could reside in the lack of nutrients and oxygen that might be reaching to premalignant ducts, due to the impossibility for the vessels to reach them because of an impairment in their invasion ability.

Apart from that, stroma activation was also considered a trigger of tumor initiation.[61] Previous studies indicated the relevance of endothelial cells in the induction of fibrosis and the role of Snail1 on it.[182,220,235] An increase of Vimentin staining surrounding premalignant ducts and tumors at hyperplasia stage in the control group supported the

profibrotic paracrine contribution of endothelial Snail1 (see Figure D-2). Vimentin was reported to be a general marker of activated fibroblasts.[119] Further studies on Vimentin in CAF were associated to poor survival in pancreatic ductal adenocarcinoma, showing their relation with tumorigenesis.[236] Moreover, in a lung adenocarcinoma mouse model, a general loss of Vimentin was associated to a decrease of CAF activation and motility, affecting tumor prognosis.[237]

Furthermore, stromal Snail1 was more abundant in tumors at hyperplasia stage in the control group, reinforcing that idea, since Snail1 was a marker of activation (see Figure R-25).[65,69,170] Nevertheless, there were no significant differences around premalignant ducts, indicating that Snail1 activation in stroma might boost the already Vimentin supported tumor activation. A hypothesis based on previous research could be that Twist1 is firstly induced in stromal cells, inducing Vimentin and, afterwards, Snail1.[238,239]

Moreover, at hyperplasia stage, Snail1$^+$ stromal cells were found closer to vessels when mice expressed Snail1 in their endothelium; moreover, in human tumor samples, Snail1$^+$ stroma tend to be surrounding Snail1$^+$ vessels, showing a link between vasculature and stromal activation (see Figure D-2). That leaded us to start experimenting with conditioned medium from HUVEC with different Snail1 levels (see Figure R-26, 27), which resulted in CAF activation at mRNA and protein levels, as well as in migration and a more mesenchymal phenotype, when conditioned medium was coming from Snail1 expressing HUVEC. The activation of those CAF was through the activation of AKT pathway, and partially, through Smad2. This Smad2 activation was also seen in surrounding vessel stroma in the wild type mouse. To confirm this activation, we used MEF, which only showed a complete activation by HUVEC conditioned medium when they were pretreated with low concentrations of TGF-β in order to raise their basal activation status. Due to all of that, we assumed that instead of inducing fibroblast activation (Snail1$^+$) from scratch, Snail1 in endothelial cells modulated *in vivo* preexistent activated fibroblasts (Vimentin$^+$), reinforced by a crosstalk between endothelial and fibroblast cells.

Since the results with HUVEC conditioned medium showed a regulation of fibroblast activation status, we speculated the involvement of paracrine signaling as a main mediator of stromal activation. In terms of which cytokine might be involved in this activation, overexpression of Snail1 induced CXCL12, FGF2, PDGFA, EDN2 and VEGFA mRNA expression, which have been reported to collaborate in fibrosis.[101,240,241] Nevertheless, we proposed CXCL12 and FGF2 as candidates, since they were also inversely regulated by Snail1 overexpression and knock-down (see Figure R-28). We checked that both of them induced CAF and MEF activation, but only FGF2 increased migration in both cell types. Moreover, FGF2 and CXCL12 activity drove AKT phosphorylation, similarly to what we reported in CAF with conditioned medium from HUVEC.[242,243] Furthermore, FGF2 also activates Smad2 phosphorylation,[242] which was also detected in CAF with conditioned medium from HUVEC and *in vivo*, surrounding vessels in breast tissues. Altogether leaded us to think that FGF2 *per se* could be a candidate for this differential activation and CXCL12 could be working in conjunction with other molecules, at least in CAF. Previous studies stated that endothelial Snail1 induced a fibrotic paracrine activity in endothelial cells in hypoxic conditions, in this case through connective tissue growth factor (CTGF).[220]

7. Breast tumor morphology and Snail1 in endothelial cells

As tumors progressed, we observed that depending on the expression of Snail1 in their endothelium, they acquired striking different phenotypes. Absence of Snail1 in the endothelium provoked a delayed in tumorigenesis and a gain of papillary morphology in spontaneous breast mouse tumors (see Figure D-2). In the bibliography we found several reports in which they also found an increase of papillary morphology in breast tumors. For instance, a ubiquitous loss of amphiregulin,[244] lack of AKT2,[245] constitutive activation of Notch1 in luminal cells,[246] ubiquitous loss of Myosin 1e,[247] ubiquitous loss of Caveolin 1,[248] overexpression of prolactin within mammary epithelial cells,[249] luminal expression of Human Cripto-1,[250] or constitutively active STAT5,[251] generated a higher proportion of breast tumors with papillary morphology. In most of these researches,

angiogenesis is not characterized or varied among those articles; hence, we could not extrapolate a common molecular or cellular hypothesis for the papillary phenotype.

Interestingly, bevacizumab treatment did also increase the proportion of breast tumors with papillary morphology. In this particular case, it was previously reported that long-term bevacizumab treatment shifted breast tumor cells to a more aggressive myoepithelial subtype, which is tightly linked to a papillary phenotype.[252]

Nevertheless, the myoepithelial content in tumors and its papillary morphology are tightly correlated, since being papillary intrinsically implies higher presence of myoepithelial cells.[253] It is controversial the relationship between myoepithelial cells and papillary morphology. However, it was published that only a combination of malignant luminal and myoepithelial cells could derive breast tumors to a papillary morphology, whereas only malignant luminal or myoepithelial cells could not generate that morphology.[254] Therefore, a crosstalk between different cell types might be responsible for the generation of papillary tumors.

8. Regulation of tumor composition by Snail1 in endothelial cells

Due to the striking differences we observed in the morphology of the tumors at carcinoma stage, we analyzed the tumor populations of our spontaneous breast mouse model. Regarding epithelial cells, most of them tumoral, they were dramatically reduced under the absence of Snail1 in endothelial cells (see Figure D-2). We hypothesized that this reduction might, in part, be caused by necrosis, since dead cells are not counted in this analysis and necrotic volume was enriched in endothelial Snail1 knocked out tumors. Another plausible explanation is that tumoral cells have a reduced proliferation in endothelial Snail1 knocked out tumors, which we did observed in tumors at carcinoma stage, considering that most of the proliferation at carcinoma stage came from tumoral cells. Moreover, the increased number of myoepithelial cells, characteristic of papillary morphology of endothelial Snail1 knocked out tumors, could reduce the proliferation of epithelial cells. Furthermore, we also considered that the differentially fibroblasts over-activation could be a cause of this epithelial unbalance.

Furthermore, it would be interesting to point out that apart from the proportion of tumoral cells, their expression of ERα and HER2 was also controlled by the expression of Snail1 in the endothelium (see Figure R-31). We found that the usual loss of ERα signal and the gain of HER2 expression in MMTV-PyMT tumoral cells over tumor progression was reduced when Snail1 could not be expressed in endothelial cells, which is considered as a good prognostic value.[255,256] ERα expression can be modulated by several factors, such as DNA methylation, microRNA deregulation or posttranslational modification, among others.[256] In the case of HER2, the main cause of its overexpression is the increase of genomic instability, which might be prevented in the group of tumors lacking endothelial Snail1 (see Figure R-51).[257] In either case, it would be interesting to analyze the gene expression profile of tumoral cells of each animal group to identify the molecular trigger of that difference.

Apart from the epithelial cells, the immune cell population was also reduced in the control group of tumors compared to tumors that did not express Snail1 in the endothelium (see Figure D-2). Recently, it was published that a similar model of ours presented more immune infiltration when Snail1 was knocked out in endothelial cells, in this case after induction of kidney fibrosis;[182] which reinforced our results. We hypothesized that this immune infiltration could be explained by a tumor vascular normalization process. For instance, it has been described that tumor angiogenesis alters the surface molecules of endothelial cells, modulating the extravasation of immune cells and the secretion of cytokines, which may regulate the recruitment of immune cells to the parenchyma of the tumors.[258] Another possibility could rely on the lymphatic vessels, which has been reported to modify immune cell activity and presence in tumors.[259] However, lymphangiogenesis was not altered at carcinoma stage (see Figure R-37); moreover, this process has even been reported to not be key during breast cancer tumorigenesis.[260] A deeper analysis of the composition of the immune cell population in those tumors would be required to completely understand the relevance of this result and their impact on tumor prognosis.

In the cell population classified as ‘others’, we could find several types of cells, being fibroblasts, CAFs and myoepithelial cells the more predominant ones. In the control

group, this group might be governed by CAF, which were more active along tumor progression, compared to the endothelial Snail1 knocked out tumors (Figure R-33). In the endothelial Snail1 knocked out group, myoepithelial cells might be the main component of this category, as commented before. Nevertheless, we cannot assure if, in this model, myoepithelial cells increased their proliferation, survival or escaped less from the tumor. Further research on it might bring light to this phenomenon.

9. Endothelial Snail1 effects on total angiogenesis and vessel morphology

Regarding total angiogenesis, we observed a significant decrease in Matrigel plugs, breast spontaneous tumors and a highly tendentious reduction in breast orthotopic tumors, in endothelial Snail1 knock out mice. Actually, that outcome was supported *in vitro* by a decrease in the proliferation of HUVEC, only significantly different in knock down for Snail1. However, in the case of the spontaneous breast tumor model, when time was prolonged in endothelial Snail1 knock out mice, the amount of angiogenesis was recovered. We hypothesized that it might be explained as an effect of the high amount of necrosis in tumors lacking endothelial Snail1 (see Figure R-40). In fact, necrosis is an inductor of angiogenesis.[261] For instance, necrosis induces an increase of HIF-1α transcription factor, which is a potent activator of angiogenesis by regulating VEGF-A and FGF2 expression.[262] Presumably, that boost of angiogenesis and the additional gap of time needed for tumors to reach carcinoma stage, are the reasons under the recovery of endothelial cell presence in tumors with Snail1 depleted endothelial cells.

One striking phenotype we dealt with was the differential vessel lumen size found in spontaneous and orthotopic breast tumors and Matrigel plugs from our mouse models (see Figure D-2). We analyzed two parameters, lumen size and vessel perimeter. Thanks to both, we could determine the size of vessels and the tortuosity of them, although in each comparison both parameters behave with the same trend. Thus, in this case, they can be considered as overlapping features. In terms of the experiments we used to

evaluate vessel morphology, we can distinguish three types, depending on their duration and exposure time to angiogenic factors: short, middle and long term.

Short ones are the experiments of Matrigel plugs, which entails 7 days (see Figure R-20). In this short period of time, we observed the earliest effects of the presence of Snail1 in endothelial cells. Without any supplemental factor and with FGF2 addition, the lumen size and the vessel perimeter were smaller upon the presence of Snail1 in endothelial cells. Moreover, FGF2 addition provoked a reduction of lumen size and vessel perimeter only when Snail1 was present in the vessels. This data indicated that, at shorter times, FGF2 is responsible for the shrink of vessel size, which is hijacked under the absence of Snail1 in endothelial cells. Previous research indicated that FGF2 and VEGF-A widen vessels.[263,264] Although, these studies were performed in tumors and not in Matrigel plugs; moreover, those experiments had a longer duration compared to our Matrigel plug model.

In the middle-term experiment we found the analysis of tumor vessels at early stages of mice spontaneous breast tumors (see Figure R-23). At early stage of tumorigenesis, Snail1 in endothelial cells already induced a diminished size of vessels; probably due to the formation of new vessels that are smaller than the preexisting ones.[265] Under the lack of endothelial Snail1 it does not occur, presumably due to the angiogenic delay they experimented.

In the long-turn we had the analysis of tumor vessels of 18 and 22 weeks old spontaneous breast tumors and 15 weeks old in the orthotopic murine breast tumors (see Figure R-36, 42). In the case of the spontaneous breast tumors, first we compared the size of vessels before the moment tumorigenesis was induced (6 weeks old breasts) and did not detect any difference regarding the Snail1 status in endothelial cells. However, comparing same age tumors, we found the only case in which the general fashion was disrupted. Snail1 presence in endothelial cells generated bigger vessels, in area and perimeter, compared to Snail1 knocked out tumor vessels. This could be due to the fact that tumorigenesis is delayed in tumors lacking Snail1 in their endothelium; thus, compared vessels are in tumors at distinct histological grades. Another explanation

could be the time factor. We hypothesized that there is a delayed in the angiogenesis when Snail1 is not present in the endothelium. Assuming that *de novo* vessels are smaller due to the angiogenic process, we expected that vessels with Snail1 knocked out endothelial cells were smaller since their angiogenesis is retarded, compared to the control ones. I would like to point out that the vessels were smaller, compared to healthy tissues, due to the compression forces of tumor cells, which is a phenomenon already characterized.[119] When we compared tumors at carcinoma stage at final point (18 weeks old control group and 22 weeks old knocked out group), we observed a dramatic increase in the size of vessels lacking Snail1. We hypothesized that the papillary morphology of those tumors generated low pressure to the vessels by their own constitution, allowing their enlargement.

In general terms, lack of Snail1 in endothelial cells provoked an increase of the vessel size, presumably by the lack of ramification and increase compaction experienced during angiogenesis. In order to explain this differential phenotype in the lumen size, we considered two hypotheses, related to lumen formation through VVO and through intussusception.

The first hypothesis was the presence of vesiculo-vacuolar organelles (VVO), which were reported to be a key agent in the formation of lumen in neo-vessels.[111] Supporting that hypothesis, we observed that Caveolin 1 (the only reliable marker for VVO),[266] was upregulated in Snail1 knocked down HUVEC and downregulated in Snail1 overexpressed HUVEC (Figure R-12). Thus, the less Snail1, the more Caveolin 1, the more VVO. Actually, an electronic microscopy study showed an increase of VVO in tumor endothelial cells lacking Snail1. Other laboratories analyzed the relation between Snail1 and Caveolin 1. The addition of TGF-β, a generally known inducer of Snail1, reduced the levels of Caveolin 1.[267] Moreover, the overexpression of Snail1 in tumoral cells reduces the phosphorylation of Caveolin 1, which is a signal of its activation.[268] Due to all of that, we could confirm our data since Snail1 was shown to have a tight link to Caveolin 1.

The second explanation involved the intussusception process. Sprouting is not the only way vessels can grow; in fact, vessels can split themselves in a process called

intussusception, which plays an important role in the expansion and remodeling of vessel networks in tumors.[269] In the intussusceptive angiogenesis, firstly, there is an enlargement of the vessel due to an inability to sense a directed source of angiogenic factors. Afterwards, there is a protrusion of the vessel or an intraluminal sprouting by tip cells, with filopodia, leading to a split of the vessel in two.[270] In relation to our data, we proposed that Snail1 may be essential for that intraluminal sprouting, since it seemed that lack of Snail1 in endothelial cells provoked its arrest at that stage, being unable to complete the intussusception process. We based this hypothesis in the numerous amounts of filopodia found in the lumen of tumor vessels lacking Snail1 (see Figure R-39). Apart from explaining the differential vessel size of tumors depending on endothelial Snail1 status, this hypothesis could through some light into a molecularly poor understood process that is intussusception.

Finally, bevacizumab treatment showed an increase of vessel lumen area and perimeter (Figure R-45). Supporting our results, previous research on human melanoma metastases treated with bevacizumab showed an increase of vessel diameter, compared to untreated metastases.[264] This effect might be caused by the reduction of Snail1 by bevacizumab in endothelial cells; however, further analysis of Caveolin 1 levels and ultrastructure of tumor vessels upon bevacizumab treatment would be required to shed light on the issue. Nevertheless, the intussusception hypothesis gains relevance, since the abrogation of VEGF-A sensing could potentiate this process, leading to more arrested vessels in the middle of this process being, at the end of the day, bigger in size.[269]

10. Snail1 in tumor endothelial cells: necrosis, vessel localization and permeability

In spontaneous breast mouse tumors at carcinoma stage with no expression of Snail1 in their endothelium, we observed less necrotic areas (Figure R-40). Due to the predominant papillary phenotype of endothelial Snail1 knocked out tumors, we analyzed the necrosis of solid and papillary tumors of the control group to ascertain if necrosis is related to papillary morphology or with Snail1 presence in endothelial cells. Our results indicated that necrosis was induced regardless of the morphology of the

tumor; therefore, the focus was brought to a direct effect of Snail1 in the endothelium. It is accepted that the less angiogenesis a breast tumor has, the more necrotic it is.[271,272] However, other studies indicated an opposite relationship between angiogenesis and necrosis.[273] That reinforces the fact that in our model, the necrosis is not simply related to more or less angiogenesis, but it relies on further alterations.

We hypothesized that vessels that expressed Snail1 could be located closer to tumor cells, hence, providing them with more nutrients and oxygen. To support that hypothesis, we found that surrounding premalignant ducts, vessels were more closed to them when Snail1 could be expressed in the endothelial cells, compared to endothelial Snail1 knocked out vessels. Moreover, we found that at carcinoma stage, tumor vessels were more covered with Collagen, compared to endothelial Snail1 knocked out tumor vessels, which might be due to a higher capability to penetrate in Collagen rich areas. To complement these results, we observed that MMP1, MMP7, MMP9 and MMP13 were tightly regulated by Snail1; the more Snail1, the more expression of those MMP, as previously reported.[274–276] Those MMP have been recognized as regulators of tumor angiogenesis, and curiously, it has been reported that MMP9 released the vast majority of VEGF-A anchored in the ECM, boosting angiogenesis.[277] These set of results laid a strong foundation for this hypothesis.

However, it is necessary to say that the result about Collagen around the vessels might have another interpretation. Snail1 in endothelial cells may control Collagen production, as published previously.[69] Firstly, the Collagen was assessed using a Masson's trichrome staining, which stained fibrillar Collagens, namely types I-III, V and XI.[278] However, it has been reported that Masson's trichrome staining could also detect Collagen IV around tumor vessels, which is the main component of vessels' basal lamina.[279] Even though it has been extensively considered that for angiogenesis, ECM and basal lamina has to be degraded,[277,280] Collagen IV was detected in the sprouting areas of breast tumor vessels, guiding tip cells.[281] Moreover, in breast tumors, the amount of Collagen IV around aberrant tumor vessels is maintained or, even increased.[282] Supporting this theoretical explanation, we observed a controlled

expression of Collagen IV depending on Snail1 in endothelial cells: the more Snail1, the more Collagen IV expression (Figure R-12).

In terms of permeability, we found that Snail1 lack of in the endothelium generated tumor vessels at carcinoma stage with less dismantled lumens (Figure R-39). Interestingly, this could be noticed as a signal of normalization of tumor vasculature, which link the typical features of normal vessels to better prognosis in tumors.[131] Nevertheless, a detailed analysis of tumor vessel permeability might be essential to resolve this issue. Moreover, a pericyte coverage analysis of the tumor vessels would complement the permeability assay, considering that the presence of pericytes is linked to higher vessel integrity and less permeability.[80]

11. Bevacizumab and its effect on tumorigenesis

Due to the fact that bevacizumab reduced the levels of Snail1 in HUVEC by diminishing the effect of VEGF-A over HUVEC, we decided to administrate bevacizumab from 6 weeks old mice to MMTV-PyMT mice, mirroring the time point in which we depleted Snail1 from endothelial cells in spontaneous breast tumor mouse model. The effects we observed were similar to the depletion of Snail1 in endothelial cells, delayed tumor growth and a solid versus papillary dichotomic morphology (Figure R-44).

In the case of the tumor onset, bevacizumab induced a delay of 10 days, instead of 36 days in the endothelial Snail1 depleted spontaneous breast tumor mouse model. This indicates that affecting the angiogenic ability of endothelial cells by only blocking VEGF signaling was not enough to reproduce that remarkable delay. Subsequently, together with our data related to the endothelial contribution to fibroblast activation and the tumor onset delay, a treatment of an antiangiogenic and an antifibrotic drug might be highly relevant to prevent tumor growth. Indeed, recently, the FDA has approved a treatment to delay tumor relapse of ovarian, fallopian tube or primary peritoneal cancers, based on bevacizumab and olaparib.[283] Olaparib is a pharmacological inhibitor of the enzyme poly ADP ribose polymerase (PARP), which, among other effects as an inductor of apoptosis, acts as an antifibrotic agent.[284]

Regarding the amount of angiogenesis, we observed equivalent levels in big tumors regardless of the treatment of bevacizumab (Figure R-45). Although at a first glimpse the expectation was to find a reduction of angiogenesis upon bevacizumab, we had to take into account the development of resistance to antiangiogenic treatments, especially due to the long-term treatment we administrated.[132,285] Since VEGF-A was hijacked by bevacizumab, tumors could generate an adaptive resistance by substituting VEGF-A by other angiogenic factors such as FGF2 or angiopoietins, a recruitment of vascular progenitors or proangiogenic monocytes coming from the bone marrow. Moreover, through vasculogenic mimicry tumor cells organize themselves into vascular-like structures overshadowing angiogenesis. Finally, by vessel co-option tumor cells take advantage of the preexisting vasculature to nourish themselves.[286] We do not have consistent data that supports any of these options; hence, all of them are open possibilities that could be further explored by quantification of cytokine levels in tumors, tumor cell population study, analysis of $CD31^-$ areas in tumor vessels or the disposition of tumor cells along the vessels and their lumen size. Nevertheless, there is a small hint towards the adaptive resistance option, since breast tumors have a wide catalogue of cytokines in their environment and VEGF-A tend to diminish in advanced tumor stages, gaining importance other angiogenic cytokines.[287]

12. Human tumor samples mirroring endothelial Snail1 effects in angiogenesis and tumorigenesis

Our final goal was to recapitulate our results in human samples. For that, we collected NST human breast tumor samples, as a mimic of our control group, and papillary carcinomas, mirroring our endothelial Snail1 knocked out group. NST tumors recapitulated several aspects of the control group in our mouse models, such as a tendency of less intensity of ERα, more proliferation in the tumors, a significant increase of advanced tumorigenic stages, less presence of $p63^+$ cells (myoepithelial), a tendency of higher tumor angiogenesis with significantly smaller vessels with higher proportions of $Snail1^+$ endothelial cells and $Snail1^+$ cells closed to them, compared to papillary tumors (Figure R-46-48).

Continuing the study in human breast tumor samples, we moved to an open access online database containing genomic sequencing profiles of them; specifically, the TCGA Breast Invasive Carcinoma (Firehose Legacy) database.[204,205] There, we observe that CD31, as a marker of angiogenesis, and Snail1, as a marker of cell activation, had a strong positive correlation, supporting our previous data (Figure R-49). Moreover, CD31 and Snail1 had a positive correlation with Vimentin, as a marker of fibroblast activation, reinforcing our results regarding stroma activation via Snail1 in endothelial cells.

To investigate if survival and prognosis differences in our spontaneous mice model could be extrapolated to breast human tumors, we humanized our endothelial Snail1 spontaneous breast mouse model. To achieve it, and due to the lack of morphological data about samples, we used the results collected along the project and translating them to gene expression. For the humanization of PyMT VE-Cadh^{Snail1CT} mice, we chose high angiogenesis, high stroma activation, low myoepithelial content and low immune system presence, as our results indicate. In the case of PyMT VE-Cadh^{Snail1KO} mice, the opposite scheme was followed. Thanks to that, we observed that the survival and the disease-free period followed the same trend as our mouse model.

Finally, we could analyze the main active biological processes of each humanized group by using the GSEA software. In the control group we observed that the main processes upregulated were related to extracellular matrix reorganization, which was expected since endothelial Snail1 had a significant role inducing fibrosis. Moreover, blood vessel morphology appeared in the top ten list, as a signal of the angiogenic process undergoing. Finally, several biological processes related to oxidative metabolism also appeared, which has been linked to tumor progression.[288] Aerobic and oxidative metabolism has been directly linked to extracellular matrix deposition and fibroblast activation, as well as less hypoxia/necrosis, as in our model.[289,290] In the endothelial Snail1 knocked out mimic group, the main topic of the biological processes involved were chromatin remodeling and gene regulation. We are aware that aberrant expression or epigenetic modulation confer a unique ability to tumor cells to reprogram their genome, not only gaining and maintaining oncogenic phenotypes, but also reverting tumor progression.[291] For example, among the genes upregulated in this

analysis we found histone deacetylase SIRT6 and DNA polymerase ε POLE4, which are known as tumor suppressors, supporting the phenotype we observed in our model.[292,293] Based on those results, a highly interesting path to follow would be to perform an RNA-seq of the different tumor population of PyMT tumors, with our without Snail1 in their endothelium, to identify concrete genes that could be amplifying the effect of endothelial Snail1, provoking the differential effects on tumor at advanced stage.

13. Final considerations

Summing everything up, with this thesis, we have thrown some light on the role of Snail1 in endothelial cells. We determined that endothelial Snail1 is key for proper angiogenesis, as well as for breast tumorigenesis, boosting fibroblast activation in a paracrine manner and controlling tumor morphology and composition. These findings are recapitulated in the proposed model (Figure D-2). We expect that future clinical treatments for tumor relapse could be inspired from this study, mainly acting on reducing angiogenesis and fibrosis related to tumor development.

CONCLUSIONS

After concluding this thesis, we reached to these conclusions:

1. Endothelial cells express Snail1 *in vitro*, especially under angiogenic stimuli.
2. Snail1 in endothelial cells is essential for endothelial cell activation, migration, tubulogenesis and sprouting.
3. Endothelial Snail1 is required for adult neo-angiogenesis *in vivo*, but not for quiescent vasculature homeostasis, organ morphology or adult vascularization.
4. Breast tumor cells induce Snail1 dependent angiogenesis *in vitro* through FGF2 and VEGF-A signaling.
5. Snail1 in endothelial cells is key in tumor angiogenesis and vessel morphology in cancer murine models.
6. Snail1 expressing endothelial cells secretome activates stromal fibroblasts through FGF2 and CXCL12 signaling, fostering breast tumor initiation.
7. Endothelial Snail1 modifies the development of luminal breast tumors *in vivo*, by affecting tumor composition, tumor cell differentiation, tumor morphology, necrosis and survival.
8. *In vivo* early antiangiogenic treatment of breast tumors provokes a delay in tumor onset and tumor morphology changes.
9. Papillary human breast tumors mimic the differences in angiogenesis, vessel morphogenesis, profibrotic signaling and tumor development of murine breast tumors lacking Snail1 in endothelial cells.

REFERENCES

1. Hanahan, D. & Weinberg, R. A. Hallmarks of cancer: The next generation. *Cell* **144**, 646–674 (2011).

2. The Global Cancer Observatory. Cancer fact sheet. *https://gco.iarc.fr/today/data/factsheets/cancers/39-All-cancers-fact-sheet.pdf.* (2019).

3. Sociedad Española de Oncología Médica. Las cifras del cáncer en España 2020 Hombres. *Sociedad Española de Oncología Médica* (2020).

4. International, W. *Diet, nutrition, physical activity and breast cancer*. *Continuous Update Project Expert Report* (2018).

5. Benson, J. R. & Jatoi, I. The global breast cancer burden. *Future Oncology* **8**, 697–702 (2012).

6. Bricout, N. & Bricout, N. Anatomy and morphology of the breast. *Breast Surgery* 7–32 (1996).

7. Davies, J. A. Do different branching epithelia use a conserved developmental mechanism? *BioEssays* **24**, 937–948 (2002).

8. Harbeck, N. *et al.* Breast cancer. *Nature Reviews Disease Primers* **5**, 66 (2019).

9. Pierre Denoix. *Le livre de poche pratique*. (1943).

10. Brierley, J. D., Gospodarowicz, M. K. & Wittekind, C. *TNM classification of malignant tumours - 8th edition*. *Union for International Cancer Control* (2017).

11. *AJCC Cancer Staging Manual*. *AJCC Cancer Staging Manual* (2017).

12. Wong, E., Chaudhry, S. & Rossi, M. Breast cancer, McMaster Pathophysiology Review. *McMaster University* (2016).

13. Malhotra, G. K., Zhao, X., Band, H. & Band, V. Histological, molecular and functional subtypes of breast cancers. *Cancer Biology and Therapy* **10**, 955–960 (2010).

14. Elston, C. W. & Ellis, I. O. Pathological prognostic factors in breast cancer. I. The value of histological grade in breast cancer: experience from a large study with long-term follow-up. *Histopathology* **19**, 403–410 (1991).

15. Lester, S. C. *et al.* Protocol for the examination of specimens from patients with invasive carcinoma of the breast. *Archives of Pathology and Laboratory Medicine* **133**, 1515–1538 (2009).

16. Makki, J. Diversity of breast carcinoma: Histological subtypes and clinical relevance. *Clinical Medicine Insights: Pathology* **21**, 23–31 (2015).

17. Pal, S. K. *et al.* Papillary carcinoma of the breast: An overview. *Breast Cancer Research and Treatment* **122**, 637–645 (2010).

18. Lakhani, S. R. *et al.* The pathology of familial breast cancer: Histological features of cancers in families not attributable to mutations in BRCA1 or BRCA2. *Clinical Cancer Research* **6**, 782–789 (2000).

19. DeeAnne. Memorang. link: https://www.memorangapp.com/flashcards/74908/Pathoma+Chapter+16+-+Revised/.

20. Vollenweider-Zerargui, L., Barrelet, L., Wong, Y., Lemarchand-Béraud, T. & Gómez, F. The predictive value of estrogen and progesterone receptors' concentrations on the clinical behavior of breast cancer in women. Clinical correlation on 547 patients. *Cancer* **57**, 1171–1180 (1986).

21. Torregrosa, D. *et al.* Prognostic significance of c-erbB-2/neu amplification and epidermal growth factor receptor (EGFR) in primary breast cancer and their relation to estradiol receptor (ER) status. *Clinica Chimica Acta* **262**, 99–119 (1997).

22. Slamon, D. J. *et al.* Studies of the HER-2/neu proto-oncogene in human breast and ovarian cancer. *Science* **244**, 707–712 (1989).

23. Perou, C. M. *et al.* Molecular portraits of human breast tumours. *Nature* **406**, 747–752 (2000).

24. Sørlie, T. *et al.* Gene expression patterns of breast carcinomas distinguish tumor subclasses with clinical implications. *Proceedings of the National Academy of Sciences of the United States of America* **98**, 10869–10874 (2001).

25. Cheang, M. C. U. *et al.* Defining Breast Cancer Intrinsic Subtypes by Quantitative Receptor Expression. *The Oncologist* **20**, 474–482 (2015).

26. Cardiff, R. D. & Kenney, N. A compendium of the mouse mammary tumor biologist: From the initial observations in the house mouse to the development of genetically engineered mice. *Cold Spring Harbor Perspectives in Biology* **3**, (2011).

27. CO, J. Experimentelle Untersuchungen über Krebs bei Mäusen. *Z Krebs-forsch* **1**, 134–138 (1904).

28. Holen, I., Speirs, V., Morrissey, B. & Blyth, K. In vivo models in breast cancer research: Progress, challenges and future directions. *DMM Disease Models and Mechanisms* **10**, 359–371 (2017).

29. Guy, C. T., Cardiff, R. D. & Muller, W. J. Induction of mammary tumors by expression of polyomavirus middle T oncogene: a transgenic mouse model for metastatic disease. *Molecular and Cellular Biology* **12**, 954–961 (1992).

30. Dennis, J. W., Granovsky, M. & Warren, C. E. Glycoprotein glycosylation and cancer progression. *Biochimica et Biophysica Acta - General Subjects* **1473**, 21–34 (1999).

31. Dankort, D. L. & Muller, W. J. Signal transduction in mammary tumorigenesis: A transgenic perspective. *Oncogene* **19**, 1038–1044 (2000).

32. Gottlieb, K. A. & Villarreal, L. P. Natural Biology of Polyomavirus Middle T Antigen. *Microbiology and Molecular Biology Reviews* **65**, 288–318 (2001).

33. Ponta, H., Kennedy, N., Skroch, P., Hynes, N. E. & Groner, B. Hormonal response region in the mouse mammary tumor virus long terminal repeat can be dissociated from the

proviral promoter and has enhancer properties. *Proceedings of the National Academy of Sciences of the United States of America* **82**, 1020–1024 (1985).

34. Lin, E. Y. *et al.* Progression to Malignancy in the Polyoma Middle T Oncoprotein Mouse Breast Cancer Model Provides a Reliable Model for Human Diseases. *American Journal of Pathology* **163**, 2113–2126 (2003).

35. Kelsey, J. L., Gammon, M. D. & John, E. M. Reproductive Factors and Breast Cancer. *Epidemiologic Reviews* **15**, 36–47 (1993).

36. Cardiff, R. D. & Munn, R. J. Comparative pathology of mammary tumorigenesis in transgenic mice. *Cancer Letters* **90**, 13–19 (1995).

37. Maglione, J. E. *et al.* Transgenic Polyoma middle-T mice model premalignant mammary disease. *Cancer Research* **61**, 8298–305 (2001).

38. Zhang, M., Lee, A. v. & Rosen, J. M. The cellular origin and evolution of breast cancer. *Cold Spring Harbor Perspectives in Medicine* **7**, a027128 (2017).

39. Ma, X. J., Dahiya, S., Richardson, E., Erlander, M. & Sgroi, D. C. Gene expression profiling of the tumor microenvironment during breast cancer progression. *Breast Cancer Research* **11**, R7 (2009).

40. Bombonati, A. & Sgroi, D. C. The molecular pathology of breast cancer progression. *Journal of Pathology* **223**, 307–317 (2011).

41. Boudreau, A., Van't Veer, L. J. & Bissell, M. J. An "elite hacker": Beast tumors exploit the normal microenvironment program to instruct their progression and biological diversity. *Cell Adhesion and Migration* **6**, 236–248 (2012).

42. Bissell, M. J. & Radisky, D. Putting tumours in context. *Nature Reviews Cancer* **1**, 46–54 (2001).

43. McManaman, J. L. & Neville, M. C. Mammary physiology and milk secretion. *Advanced Drug Delivery Reviews* **55**, 629–641 (2003).

44. Keller, P. J. *et al.* Mapping the cellular and molecular heterogeneity of normal and malignant breast tissues and cultured cell lines. *Breast Cancer Research* **12**, R87 (2010).

45. Gudjonsson, T., Adriance, M. C., Sternlicht, M. D., Petersen, O. W. & Bissell, M. J. Myoepithelial cells: their origin and function in breast morphogenesis and neoplasia. *Journal of Mammary Gland Biology and Neoplasia* **10**, 261–272 (2005).

46. Maller, O., Martinson, H. & Schedin, P. Extracellular matrix composition reveals complex and dynamic stromal-epithelial interactions in the mammary gland. *Journal of Mammary Gland Biology and Neoplasia* **15**, 301–318 (2010).

47. Arendt, L. M., Rudnick, J. A., Keller, P. J. & Kuperwasser, C. Stroma in breast development and disease. *Seminars in Cell and Developmental Biology* **21**, 11–18 (2010).

48. Andersen, K. *et al.* The metastasis-promoting protein S100A4 regulates mammary branching morphogenesis. *Developmental Biology* **352**, 181–190 (2011).

49. Paszek, M. J. *et al.* Tensional homeostasis and the malignant phenotype. *Cancer Cell* **8**, 241–54 (2005).

50. Gouon-Evans, V., Lin, E. Y. & Pollard, J. W. Requirement of macrophages and eosinophils and their cytokines/chemokines for mammary gland development. *Breast Cancer Research* **4**, 155–164 (2002).

51. Wang, P., Mariman, E., Renes, J. & Keijer, J. The secretory function of adipocytes in the physiology of white adipose tissue. *Journal of Cellular Physiology* **216**, 3–13 (2008).

52. Bautch, V. L. & Caron, K. M. Blood and lymphatic vessel formation. *Cold Spring Harbor Perspectives in Biology* **7**, (2015).

53. Bissell, M. J. & Hines, W. C. Why don't we get more cancer? A proposed role of the microenvironment in restraining cancer progression. *Nature Medicine* **17**, 320–329 (2011).

54. Sternlicht, M. D. & Barsky, S. H. The myoepithelial defense: A host defense against cancer. *Medical Hypotheses* **48**, 37–46 (1997).

55. Sternlicht, M. D., Kedeshian, P., Shao, Z. M., Safarians, S. & Barsky, S. H. The human myoepithelial cell is a natural tumor suppressor. *Clinical Cancer Research* **3**, 1949–58 (1997).

56. Polyak, K. & Hu, M. Do myoepithelial cells hold the key for breast tumor progression? *Journal of mammary gland biology and neoplasia* **10**, 231–47 (2005).

57. Bani, D., Riva, A., Bigazzi, M. & Bani Sacchi, T. Differentiation of breast cancer cells in vitro is promoted by the concurrent influence of myoepithelial cells and relaxin. *British Journal of Cancer* **70**, 900–4 (1994).

58. Duivenvoorden, H. M. *et al.* Myoepithelial cell-specific expression of stefin A as a suppressor of early breast cancer invasion. *Journal of Pathology* **243**, 496–509 (2017).

59. Nguyen, M. *et al.* The human myoepithelial cell displays a multifaceted anti-angiogenic phenotype. *Oncogene* **19**, 3449–3459 (2000).

60. Kalluri, R. & Zeisberg, M. Fibroblasts in cancer. *Nature Reviews Cancer* **6**, 392–401 (2006).

61. Kalluri, R. The biology and function of fibroblasts in cancer. *Nature Reviews Cancer* **16**, 582–598 (2016).

62. Orimo, A. *et al.* Stromal fibroblasts present in invasive human breast carcinomas promote tumor growth and angiogenesis through elevated SDF-1/CXCL12 secretion. *Cell* **121**, 335–348 (2005).

63. Karnoub, A. E. *et al.* Mesenchymal stem cells within tumour stroma promote breast cancer metastasis. *Nature* **449**, 557–563 (2007).

64. Aboussekhra, A. Role of cancer-associated fibroblasts in breast cancer development and prognosis. *International Journal of Developmental Biology* **55**, 841–9 (2011).

65. Alba-Castellón, L. *et al.* Snail1-dependent activation of cancer-associated fibroblast controls epithelial tumor cell invasion and metastasis. *Cancer Research* **76**, 6205–6217 (2016).

66. Hynes, R. O. The extracellular matrix: Not just pretty fibrils. *Science* **326**, 1216–1219 (2009).

67. Henke, E., Nandigama, R. & Ergün, S. Extracellular Matrix in the Tumor Microenvironment and Its Impact on Cancer Therapy. *Frontiers in Molecular Biosciences* **6**, 160 (2020).

68. Sala, L. *et al.* Abrogation of myofibroblast activities in metastasis and fibrosis by methyltransferase inhibition. *International Journal of Cancer* **145**, 3064–3077 (2019).

69. Stanisavljevic, J. *et al.* Snail1-expressing fibroblasts in the tumor microenvironment display mechanical properties that support metastasis. *Cancer Research* **75**, 284–295 (2015).

70. Gatti-Mays, M.E., Balko, J.M., Gameiro, S. R. et al. If we build it they will come: targeting the immune response to breast cancer. *Breast Cancer* **5**, 37 (2019).

71. Schäffler, A. & Büchler, C. Concise Review: Adipose Tissue-Derived Stromal Cells-Basic and Clinical Implications for Novel Cell-Based Therapies. *Stem Cells* **25**, 818–827 (2007).

72. Zhao, M. *et al.* Mesenchymal stem cells in mammary adipose tissue stimulate progression of breast cancer resembling the basal-type. *Cancer Biology and Therapy* **13**, 782–792 (2012).

73. de Palma, M., Biziato, D. & Petrova, T. v. Microenvironmental regulation of tumour angiogenesis. *Nature Reviews Cancer* **17**, 457–474 (2017).

74. Kolte, D., McClung, J. A. & Aronow, W. S. Vasculogenesis and Angiogenesis. *Translational Research in Coronary Artery Disease, Academic Press.* 49–65 (2016).

75. Kazemi, S. *et al.* Differential role of bFGF and VEGF for vasculogenesis. *Cellular Physiology and Biochemistry* **12**, 55–62 (2002).

76. Risau, W. & Flamme, I. Vasculogenesis. *Annual Review of Cell and Developmental Biology* **11**, 73–91 (1995).

77. Gonzalez-Crussi, F. Vasculogenesis in the chick embryo. An ultrastructural study. *American Journal of Anatomy* **130**, 441–460 (1971).

78. Risau, W. *et al.* Vasculogenesis and angiogenesis in embryonic-stem-cell-derived embryoid bodies. *Development* **102**, 471–478 (1988).

79. B Alberts, et al. Molecular Biology of the Cell, 4th Edition. *New York: Garland Science* (2002).

80. Raza, A., Franklin, M. J. & Dudek, A. Z. Pericytes and vessel maturation during tumor angiogenesis and metastasis. *American Journal of Hematology* **85**, 593–598 (2010).

81. Ribatti, D., Nico, B., Vacca, A., Roncali, L. & Dammacco, F. Endothelial cell heterogeneity and organ specificity. *Journal of Hematotherapy and Stem Cell Research* **11**, 81–90 (2002).

82. Galley, H. F. & Webster, N. R. Physiology of the endothelium. *British Journal of Anaesthesia* **93**, 105–113 (2004).

83. Tahergorabi, Z. & Khazaei, M. A review on angiogenesis and its assays. *Iranian Journal of Basic Medical Sciences* **15**, 1110–1126 (2012).

84. Lenzi, P., Bocci, G. & Natale, G. John Hunter and the origin of the term "angiogenesis." *Angiogenesis* **19**, 255–256 (2016).

85. Papetti, M. & Herman, I. M. Mechanisms of normal and tumor-derived angiogenesis. *American Journal of Physiology - Cell Physiology* **282**, C947-70 (2002).

86. Thiersch, K. der. Epithelialkrebs, namenthlich der Haut mit Atlas. (1865).

87. Ribatti, D. Judah Folkman, a pioneer in the study of angiogenesis. *Angiogenesis* **11**, 3–10 (2008).

88. Greenblatt, M. & Philippe, S. K. Tumor angiogenesis: Transfilter diffusion studies in the hamster by the transparent chamber technique. *Journal of the National Cancer Institute* **41**, 111–124 (1968).

89. Ehrmann, R. L. & Knoth, M. Choriocarcinoma: Transfilter stimulation of vasoproliferation in the hamster cheek pouch—studied by light and electron microscopy. *Journal of the National Cancer Institute* **41**, 1329–1341 (1968).

90. Otrock, Z. K., Mahfouz, R. A. R., Makarem, J. A. & Shamseddine, A. I. Understanding the biology of angiogenesis: Review of the most important molecular mechanisms. *Blood Cells, Molecules, and Diseases* **39**, 212–220 (2007).

91. Huang, Z. & Bao, S. D. Roles of main pro- and anti-angiogenic factors in tumor angiogenesis. *World Journal of Gastroenterology* **10**, 463–470 (2004).

92. Hanahan, D. & Folkman, J. Patterns and emerging mechanisms of the angiogenic switch during tumorigenesis. *Cell* **86**, 353–364 (1996).

93. Ferrara, N., Gerber, H. P. & LeCouter, J. The biology of VEGF and its receptors. *Nature Medicine* **9**, 669–676 (2003).

94. Bikfalvi, A., Klein, S., Pintucci, G. & Rifkin, D. B. Biological roles of fibroblast growth factor-2. *Endocrine Reviews* **18**, 26–45 (1997).

95. Ornitz, D. M. & Itoh, N. The fibroblast growth factor signaling pathway. *Wiley Interdisciplinary Reviews: Developmental Biology* **4**, 215–266 (2015).

96. Conte, C. *et al.* FGF2 translationally induced by hypoxia is involved in negative and positive feedback loops with HIF-1α. *PLoS ONE* **3**, e3078 (2008).

97. Morfoisse, F. *et al.* Hypoxia induces VEGF-C expression in metastatic tumor cells via a HIF-1α-independent translation-mediated mechanism. *Cell Reports* **16**, 155–167 (2014).

98. Zgraggen, S., Ochsenbein, A. M. & Detmar, M. An Important Role of Blood and Lymphatic Vessels in Inflammation and Allergy. *Journal of Allergy* **49**, 672381 (2013).

99. Murakami, M. & Simons, M. Fibroblast growth factor regulation of neovascularization. *Current Opinion in Hematology* **15**, 215–220 (2009).

100. de Smet, F. *et al.* Fibroblast growth factor signaling affects vascular outgrowth and is required for the maintenance of blood vessel integrity. *Chemistry and Biology* **21**, 1310–1317 (2014).

101. Li, D. *et al.* VEGF regulates FGF-2 and TGF-β1 expression in injury endothelial cells and mediates smooth muscle cells proliferation and migration. *Microvascular Research* **77**, 134–142 (2009).

102. Blanco, R. & Gerhardt, H. VEGF and Notch in tip and stalk cell selection. *Cold Spring Harbor Perspectives in Medicine* **3**, a006569 (2013).

103. Gerhardt, H. *et al.* VEGF guides angiogenic sprouting utilizing endothelial tip cell filopodia. *Journal of Cell Biology* **161**, 1163–1177 (2003).

104. Lugano, R., Ramachandran, M. & Dimberg, A. Tumor angiogenesis: causes, consequences, challenges and opportunities. *Cellular and Molecular Life Sciences* **77**, 1745–1770 (2019).

105. Ribatti, D. & Crivellato, E. “Sprouting angiogenesis”, a reappraisal. *Developmental Biology* **372**, 157–165 (2012).

106. Lubarsky, B. & Krasnow, M. A. Tube morphogenesis: Making and shaping biological tubes. *Cell* **112**, 19–28 (2003).

107. Kamei, M. *et al.* Endothelial tubes assemble from intracellular vacuoles in vivo. *Nature* **4422**, 453–456 (2006).

108. Betz, C., Lenard, A., Belting, H. G. & Affolter, M. Cell behaviors and dynamics during angiogenesis. *Development* **143**, 2249–2260 (2016).

109. McDonald, D. M. & Baluk, P. Significance of blood vessel leakiness in cancer. *Cancer Research* **62**, 5381–5385 (2002).

110. Dvorak, A. M. & Feng, D. The vesiculo-vacuolar organelle (VVO): A new endothelial cell permeability organelle. *Journal of Histochemistry and Cytochemistry* **49**, 419–432 (2001).

111. Vasile, E., Qu-Hong, Dvorak, H. F. & Dvorak, A. M. Caveolae and vesiculo-vacuolar organelles in bovine capillary endothelial cells cultured with VPF/VEGF on floating matrigel-collagen gels. *Journal of Histochemistry and Cytochemistry* **47**, 159–167 (1999).

112. Denekamp, J. & Hobson, B. Endothelial-cell proliferation in experimental tumours. *British Journal of Cancer* **46**, 771–720 (1982).

113. Cao, Y. Emerging mechanisms of tumour lymphangiogenesis and lymphatic metastasis. *Nature Reviews Cancer* **5**, 735–43 (2005).

114. Cao, Y. Why and how do tumors stimulate lymphangiogenesis? *Lymphatic Research and Biology* **6**, 145–148 (2008).

115. Vaupel, P., Kallinowski, F. & Okunieff, P. Blood Flow, Oxygen and Nutrient Supply, and Metabolic Microenvironment of Human Tumors: A Review. *Cancer Research* **49**, 6449–65 (1989).

116. Peter, V. Tumor microenvironmental physiology and its implications for radiation oncology. *Seminars in Radiation Oncology* **14**, 198–206 (2004).

117. Yu, L., Chen, X., Sun, X., Wang, L. & Chen, S. The glycolytic switch in tumors: How many players are involved? *Journal of Cancer* **8**, 3430–3440 (2017).

118. Sevick, E. M. & Jain, R. K. Microvascular Architecture in a Mammary Carcinoma: Branching Patterns and Vessel Dimensions. *Cancer Research* **51**, 265–73 (1991).

119. Padera, T. P. *et al.* Cancer cells compress intratumour vessels. *Nature* **427**, 695 (2004).

120. Reymond, N., D'Água, B. B. & Ridley, A. J. Crossing the endothelial barrier during metastasis. *Nature Reviews Cancer* **13**, 858–870 (2013).

121. Schaaf, M. B., Garg, A. D. & Agostinis, P. Defining the role of the tumor vasculature in antitumor immunity and immunotherapy article. *Cell Death and Disease* **9**, (2018).

122. Georganaki, M., van Hooren, L. & Dimberg, A. Vascular Targeting to Increase the Efficiency of Immune Checkpoint Blockade in Cancer. *Frontiers in immunology* **9**, (2018).

123. Cao, Z. *et al.* Targeting the vascular and perivascular niches as a regenerative therapy for lung and liver fibrosis. *Science Translational Medicine* **9**, (2017).

124. Sanchez, B. *et al.* Impact of human dermal microvascular endothelial cells on primary dermal fibroblasts in response to inflammatory stress. *Frontiers in Cell and Developmental Biology* **7**, (2019).

125. Eklund, L., Bry, M. & Alitalo, K. Mouse models for studying angiogenesis and lymphangiogenesis in cancer. *Molecular Oncology* **7**, 259–282 (2013).

126. Baron, U. & Bujard, H. Tet repressor-based system for regulated gene expression in eukaryotic cells: Principles and advances. *Methods in Enzymology* **327**, 401–21 (2000).

127. Wang, Y. *et al.* Ephrin-B2 controls VEGF-induced angiogenesis and lymphangiogenesis. *Nature* **465**, 483–6 (2010).

128. Bergers, G. & Hanahan, D. Modes of resistance to anti-angiogenic therapy. *Nature Reviews Cancer* **8**, 592–603 (2008).

129. Bueno, M. J., Mouron, S. & Quintela-Fandino, M. Personalising and targeting antiangiogenic resistance: A complex and multifactorial approach. *British Journal of Cancer* **116**, 1119–1125 (2017).

130. Al-Husein, B., Abdalla, M., Trepte, M., DeRemer, D. L. & Somanath, P. R. Antiangiogenic therapy for cancer: An update. *Pharmacotherapy* **13**, 345–8 (2012).

131. Jain, R. K. Normalization of tumor vasculature: an emerging concept in antiangiogenic therapy. *Science* **307**, 58–62 (2005).

132. Vasudev, N. S. & Reynolds, A. R. Anti-angiogenic therapy for cancer: Current progress, unresolved questions and future directions. *Angiogenesis* **17**, 471–494 (2014).

133. Grau, Y., Carteret, C. & Simpson, P. Mutations and chromosomal rearrangements affecting the expression of snail, a gene involved in embryonic patterning in Drosophila melanogaster. *Genetics* **108**, 347–360 (1984).

134. Wieschaus, E., Nüsslein-Volhard, C. & Jörgens, G. Mutations affecting the pattern of the larval cuticle in Drosophila melanogaster. *Wilhelm Roux's Archives of Developmental Biology* **193**, 283–295 (1984).

135. Paznekas, W. A., Okajima, K., Schertzer, M., Wood, S. & Jabs, E. W. Genomic organization, expression, and chromosome location of the human SNAIL gene (SNAI1) and a related processed pseudogene (SNAI1P). *Genomics* **62**, 42–49 (1999).

136. Katoh M, K. M. Identification and characterization of human SNAIL3 (SNAI3) gene in silico. *Int J Mol Med.* **11**, 383–388 (2003).

137. Knight, R. D. & Shimeld, S. M. Identification of conserved C2H2 zinc-finger gene families in the Bilateria. *Genome biology* **2**, research0016.1 (2001).

138. Mingot, J. M., Vega, S., Maestro, B., Sanz, J. M. & Nieto, M. A. Characterization of snail nuclear import pathways as representatives of C2H2 zinc finger transcription factors. *Journal of Cell Science* **122**, 1452–1460 (2009).

139. Batlle, E. *et al.* The transcription factor Snail is a repressor of E-cadherin gene expression in epithelial tumour cells. *Nature Cell Biology* **2**, 84–89 (2000).

140. Kataoka, H. *et al.* A novel Snail-related transcription factor Smuc regulates basic helix-loop-helix transcription factor activities via specific E-box motifs. *Nucleic Acids Research* **28**, 626–633 (2000).

141. Peinado, H., Ballestar, E., Esteller, M. & Cano, A. Snail Mediates E-Cadherin Repression by the Recruitment of the Sin3A/Histone Deacetylase 1 (HDAC1)/HDAC2 Complex. *Molecular and Cellular Biology* **24**, 306–319 (2004).

142. Lin, Y. *et al.* The SNAG domain of snail1 functions as a molecular hook for recruiting lysine-specific demethylase 1. *EMBO Journal* **29**, 1803–1816 (2010).

143. Hemavathy, K., Ashraf, S. I. & Ip, Y. T. Snail/Slug family of repressors: Slowly going into the fast lane of development and cancer. *Gene* **257**, 1–12 (2000).

144. Zhou, B. P. *et al.* Dual regulation of Snail by GSK-3β-mediated phosphorylation in control of epithelial-mesenchymal transition. *Nature Cell Biology* **6**, 931–940 (2004).

145. Molina-Ortiz, P. *et al.* Characterization of the SNAG and SLUG domains of Snail2 in the repression of E-cadherin and EMT induction: Modulation by serine 4 phosphorylation. *PLoS ONE* **7**, e36132 (2012).

146. Cano, A. *et al.* The transcription factor Snail controls epithelial-mesenchymal transitions by repressing E-cadherin expression. *Nature Cell Biology* **2**, 76–83 (2000).

147. Moreno-Bueno, G. *et al.* Genetic profiling of epithelial cells expressing E-cadherin repressors reveals a distinct role for snail, Slug, and E47 Factors in epithelial-mesenchymal transition. *Cancer Research* **66**, 9543–9556 (2006).

148. Jiang, R., Lan, Y., Norton, C. R., Sundberg, J. P. & Gridley, T. The slug gene is not essential for mesoderm or neural crest development in mice. *Developmental Biology* **198**, 277–285 (1998).

149. Olmeda, D. *et al.* Snai1 and Snai2 collaborate on tumor growth and metastasis properties of mouse skin carcinoma cell lines. *Oncogene* **27**, 4690–4701 (2008).

150. Hsu, D. S. S. *et al.* Acetylation of snail modulates the cytokinome of cancer cells to enhance the recruitment of macrophages. *Cancer Cell* **26**, 534–548 (2014).

151. Stanisavljevic, J., Porta-de-la-Riva, M., Batlle, R., de Herreros, A. G. & Baulida, J. The p65 subunit of NF-κB and PARP1 assist Snail1 in activating fibronectin transcription. *Journal of Cell Science* **124**, 4161–4171 (2011).

152. Henderson, V. *et al.* Snail promotes cell migration through PI3K/AKT-dependent Rac1 activation as well as PI3K/AKT-independent pathways during prostate cancer progression. *Cell Adhesion and Migration* **9**, 255–264 (2015).

153. Garcia de Herreros, A. Annual report - Common Molecules in Development and Carcinogenesis. *Juan March Foundation* Madrid (2001).

154. Miyoshi, A. *et al.* Snail accelerates cancer invasion by upregulating MMP expression and is associated with poor prognosis of hepatocellular carcinoma. *British Journal of Cancer* **92**, 252–258 (2005).

155. Stemmler, M. P., Eccles, R. L., Brabletz, S. & Brabletz, T. Non-redundant functions of EMT transcription factors. *Nature Cell Biology* **21**, 102–112 (2019).

156. Yang, J. *et al.* Guidelines and definitions for research on epithelial–mesenchymal transition. *Nature Reviews Molecular Cell Biology* **21**, 341–352 (2020).

157. Brenot, A., Knolhoff, B.L., DeNardo, D. G. et al. SNAIL1 action in tumor cells influences macrophage polarization and metastasis in breast cancer through altered GM-CSF secretion. *Oncogenesis* **7**, 32 (2018).

158. Mazzolini, R. *et al.* Snail1 transcription factor controls telomere transcription and integrity. *Nucleic Acids Research* **46**, 146–158 (2018).

159. Kim, N. H. *et al.* Snail reprograms glucose metabolism by repressing phosphofructokinase PFKP allowing cancer cell survival under metabolic stress. *Nature Communications* **8**, 14374 (2017).

160. Lambies, G. *et al.* TGFb-activated USP27X deubiquitinase regulates cell migration and chemoresistance via stabilization of Snail1. *Cancer Research* **79**, 33–46 (2019).

161. Baulida, J., Díaz, V. M. & García de Herreros, A. Snail1: A Transcriptional Factor Controlled at Multiple Levels. *Journal of Clinical Medicine* **8**, 757 (2019).

162. Dave, N. *et al.* Functional cooperation between snail1 and twist in the regulation of ZEB1 expression during epithelial to mesenchymal transition. *Journal of Biological Chemistry* **286**, 12024–12032 (2011).

163. Villarroel, A. *et al.* Src and Fyn define a new signaling cascade activated by canonical and non-canonical Wnt ligands and required for gene transcription and cell invasion. *Cellular and Molecular Life Sciences* **77**, 919–935 (2020).

164. de Craene, B., van Roy, F. & Berx, G. Unraveling signalling cascades for the Snail family of transcription factors. *Cellular Signalling* **17**, 535–547 (2005).

165. Wanami, L. S., Chen, H. Y., Peiró, S., García de Herreros, A. & Bachelder, R. E. Vascular endothelial growth factor-A stimulates Snail expression in breast tumor cells: Implications for tumor progression. *Experimental Cell Research* **314**, 2448–2453 (2008).

166. Barrallo-Gimeno, A. & Nieto, M. A. The Snail genes as inducers of cell movement and survival: Implications in development and cancer. *Development* **132**, 3151–3161 (2005).

167. Smith, D. E., Franco Del Amo, F. & Gridley, T. Isolation of Sna, a mouse gene homologous to the Drosophila genes snail and escargot: Its expression pattern suggests multiple roles during postimplantation development. *Development* **116**, 1033–1039 (1992).

168. Carver, E. A., Jiang, R., Lan, Y., Oram, K. F. & Gridley, T. The Mouse Snail Gene Encodes a Key Regulator of the Epithelial-Mesenchymal Transition. *Molecular and Cellular Biology* **21**, 8184–8188 (2001).

169. Murray, S. A. & Gridley, T. Snail family genes are required for left-right asymmetry determination, but not neural crest formation, in mice. *Proceedings of the National Academy of Sciences of the United States of America* **103**, 10300–10304 (2006).

170. Batlle, R. *et al.* Snail1 controls TGF-β responsiveness and differentiation of mesenchymal stem cells. *Oncogene* **32**, 3381–3389 (2013).

171. Boutet, A. *et al.* Snail activation disrupts tissue homeostasis and induces fibrosis in the adult kidney. *EMBO Journal* **25**, 5603–5613 (2006).

172. Rowe, R. G. *et al.* Hepatocyte-Derived Snail1 Propagates Liver Fibrosis Progression. *Molecular and Cellular Biology* **31**, 2392–2403 (2011).

173. Li, X. he *et al.* Parthenolide attenuated bleomycin-induced pulmonary fibrosis via the NF-KB/Snail signaling pathway. *Respiratory Research* **19**, 111 (2018).

174. Balkwill, F. & Mantovani, A. Inflammation and cancer: Back to Virchow? *Lancet* **357**, 539–545 (2001).

175. Francí, C. *et al.* Snail1 protein in the stroma as a new putative prognosis marker for colon tumours. *PLoS ONE* **4**, 1–7 (2009).

176. Rowe, R. G. *et al.* Mesenchymal cells reactivate Snail1 expression to drive three-dimensional invasion programs. *Journal of Cell Biology* **184**, 399–408 (2009).

177. Kaufhold, S., Bonavida, B. Central role of Snail1 in the regulation of EMT and resistance in cancer: A target for therapeutic intervention. *Journal of Experimental and Clinical Cancer Research* **33**, 62 (2014).

178. Kokudo, T. *et al.* Snail is required for TGFβ-induced endothelial-mesenchymal transition of embryonic stem cell-derived endothelial cells. *Journal of Cell Science* **121**, 3317–3324 (2008).

179. Lomelí, H., Starling, C. & Gridley, T. Epiblast-specific Snai1 deletion results in embryonic lethality due to multiple vascular defects. *BMC Research Notes* **2**, 22 (2009).

180. Gill, J. G. *et al.* Snail Promotes the Cell-Autonomous Generation of Flk1+ Endothelial Cells Through the Repression of the microRNA-200 Family. *Stem Cells and Development* **21**, 167–176 (2012).

181. Wu, Z. Q. *et al.* A Snail1/Notch1 signalling axis controls embryonic vascular development. *Nature Communications* **5**, 3998 (2014).

182. Lovisa, S. *et al.* Endothelial-to-mesenchymal transition compromises vascular integrity to induce Myc-mediated metabolic reprogramming in kidney fibrosis. *Science signaling* **13**, eaaz2597 (2020).

183. Timmerman, L. A. *et al.* Notch promotes epithelial-mesenchymal transition during cardiac development and oncogenic transformation. *Genes and Development* **18**, 99–115 (2004).

184. Armstrong, E. J. & Bischoff, J. Heart valve development: Endothelial cell signaling and differentiation. *Circulation Research* **95**, 459–470 (2004).

185. Sun, J. X. *et al.* SNAI1, an endothelial–mesenchymal transition transcription factor, promotes the early phase of ocular neovascularization. *Angiogenesis* **21**, 635–652 (2018).

186. Park, Jeong Ae., et al. Endothelial Snail Regulates Capillary Branching Morphogenesis via Vascular Endothelial Growth Factor Receptor 3 Expression. *PLoS Genetics* **11**, e1005324 (2015).

187. Daneman, R. & Prat, A. The blood–brain barrier. *Cold Spring Harbor Perspectives in Biology* **7**, a020412 (2015).

188. Kim, B. J. *et al.* Bacterial induction of Snail1 contributes to blood-brain barrier disruption. *Journal of Clinical Investigation* **125**, 2473–2483 (2015).

189. Yang, R. *et al.* Induction of VEGFA and Snail-1 by meningitic Escherichia coli mediates disruption of the blood-brain barrier. *Oncotarget* **7**, 63839–63855 (2016).

190. Welch-Reardon, K. M. *et al.* Angiogenic sprouting is regulated by endothelial cell expression of Slug. *Journal of Cell Science* **127**, 2017–2028 (2014).

191. Jury, D. *et al.* miR-151a enhances Slug dependent angiogenesis. *Oncotarget* **11**, 2160–2171 (2020).

192. Welch-Reardon, K. M., Wu, N. & Hughes, C. C. W. A role for partial endothelial-mesenchymal transitions in angiogenesis? *Arteriosclerosis, Thrombosis, and Vascular Biology* **35**, 303–308 (2015).

193. Zeisberg, E. M., Potenta, S., Xie, L., Zeisberg, M. & Kalluri, R. Discovery of endothelial to mesenchymal transition as a source for carcinoma-associated fibroblasts. *Cancer Research* **67**, 10123–10128 (2007).

194. Potenta, S., Zeisberg, E. & Kalluri, R. The role of endothelial-to-mesenchymal transition in cancer progression. *British Journal of Cancer* **99**, 1375–1379 (2008).

195. Mahmoud, M. M. *et al.* Shear stress induces endothelial-To-mesenchymal transition via the transcription factor Snail. *Scientific Reports* **7**, 3375 (2017).

196. Wei, X. min *et al.* Protein tyrosine phosphatase L1 represses endothelial-mesenchymal transition by inhibiting IL-1β/NF-κB/Snail signaling. *Acta Pharmacologica Sinica* **41**, 1102–1110 (2020).

197. Schindelin, J. *et al.* Fiji: An open-source platform for biological-image analysis. *Nature Methods* **9**, 676–82 (2012).

198. Rueden, C. T. *et al.* ImageJ2: ImageJ for the next generation of scientific image data. *BMC Bioinformatics* **18**, 529 (2017).

199. Larriba, M. J. *et al.* Snail2 cooperates with Snail1 in the repression of vitamin D receptor in colon cancer. *Carcinogenesis* **30**, 1459–68 (2009).

200. Carpentier, G. ImageJ contribution: angiogenesis analyzer. *ImageJ News* **9**, (2012).

201. Heiss, M. *et al.* Endothelial cell spheroids as a versatile tool to study angiogenesis in vitro. *FASEB Journal* **29**, 3076–84 (2015).

202. Murray, S. A., Carver, E. A. & Gridley, T. Generation of a Snail1 (Snai1) conditional null allele. *Genesis* **44**, 7–11 (2006).

203. Mao, X., Fujiwara, Y., Chapdelaine, A., Yang, H. & Orkin, S. H. Activation of EGFP expression by Cre-mediated excision in a new ROSA26 reporter mouse strain. *Blood* **97**, 324–6 (2001).

204. Cerami, E. *et al.* The cBio Cancer Genomics Portal: An open platform for exploring multidimensional cancer genomics data. *Cancer Discovery* **2**, 401–404 (2012).

205. Gao, J. *et al.* Integrative analysis of complex cancer genomics and clinical profiles using the cBioPortal. *Science Signaling* **2**, pl1 (2013).

206. Mootha, V. K. *et al.* PGC-1α-responsive genes involved in oxidative phosphorylation are coordinately downregulated in human diabetes. *Nature Genetics* **34**, 267–273 (2003).

207. Subramanian, A. *et al.* Gene set enrichment analysis: A knowledge-based approach for interpreting genome-wide expression profiles. *Proceedings of the National Academy of Sciences of the United States of America* **102**, 15545–15550 (2005).

208. Ashburner, M. *et al.* Gene ontology: Tool for the unification of biology. *Nature Genetics* **25**, 25–29 (2000).

209. Carbon, S. *et al.* The Gene Ontology Resource: 20 years and still GOing strong. *Nucleic Acids Research* **8**, D330–D338 (2019).

210. Francí, C. *et al.* Expression of Snail protein in tumor-stroma interface. *Oncogene* **25**, 5134–5144 (2006).

211. Pear, W. S., Nolan, G. P., Scott, M. L. & Baltimore, D. Production of high-titer helper-free retroviruses by transient transfection. *Proceedings of the National Academy of Sciences of the United States of America* **90**, 8392–8396 (1993).

212. Ramos-Fernández, E. *et al.* Posttranslational nitro-glycative modifications of albumin in alzheimer's disease: Implications in cytotoxicity and amyloid-β peptide aggregation. *Journal of Alzheimer's Disease* **40**, 643–657 (2014).

213. Tait, L., Russo, J. & Soule, H. D. Ultrastructural and Immunocytochemical Characterization of an Immortalized Human Breast Epithelial Cell Line, MCF-10. *Cancer Research* **50**, 6087–6094 (1990).

214. Owens, R. B. Glandular epithelial cells from mice: a method for selective cultivation. *Journal of the National Cancer Institute* **52**, 1375–1378 (1974).

215. Morita, S., Kojima, T. & Kitamura, T. Plat-E: An efficient and stable system for transient packaging of retroviruses. *Gene Therapy* **7**, 1063–1066 (2000).

216. Boareto M., et al. Jagged mediates differences in normal and tumor angiogenesis by affecting tip-stalk fate decision. *Proceedings of the National Academy of Sciences* **112**, E3836-44 (2015).

217. Jouppila-Mättö, A. *et al.* Transcription factor snail1 expression and poor survival in pharyngeal squamous cell carcinoma. *Histology and Histopathology* **26**, 443–449 (2011).

218. Tomazini Pinto, M. *et al.* Endothelial cells from different anatomical origin have distinct responses during SNAIL/TGF-β2-mediated endothelial-mesenchymal transition. *American Journal of Translational Research* **10**, 4065–4081 (2018).

219. Platel, V., Faure, S., Corre, I. & Clere, N. Endothelial-to-Mesenchymal Transition (EndoMT): Roles in Tumorigenesis, Metastatic Extravasation and Therapy Resistance. *Journal of Oncology* 8361945 (2019).

220. Lee, S. W. *et al.* Snail as a potential target molecule in cardiac fibrosis: Paracrine action of endothelial cells on fibroblasts through snail and CTGF Axis. *Molecular Therapy* **21**, 1767–1777 (2013).

221. de Frutos, C. A. *et al.* Snail1 Is a Transcriptional Effector of FGFR3 Signaling during Chondrogenesis and Achondroplasias. *Developmental Cell* **13**, 872–883 (2007).

222. Lee, J. G., Jung, E. & Heur, M. Fibroblast growth factor 2 induces proliferation and fibrosis via SNAI1-mediated activation of CDK2 and ZEB1 in corneal endothelium. *Journal of Biological Chemistry* **293**, 3758–3769 (2018).

223. Behelgardi, MF., et al. Targeting signaling pathways of VEGFR1 and VEGFR2 as a potential target in the treatment of breast cancer. *Molecular Biology Reports* **47**, 2061–2071 (2020).

224. Heryanto, B., Lipson, K. E. & Rogers, P. A. W. Effect of angiogenesis inhibitors on oestrogen-mediated endometrial endothelial cell proliferation in the ovariectomized mouse. *Reproduction* **125**, 337–346 (2003).

225. Al-Nedawi, K., Meehan, B., Kerbel, R. S., Allison, A. C. & Rak, A. Endothelial expression of autocrine VEGF upon the uptake of tumor-derived microvesicles containing oncogenic EGFR. *Proceedings of the National Academy of Sciences of the United States of America* **106**, 3794–3799 (2009).

226. Nowak-Sliwinska, P. *et al.* Consensus guidelines for the use and interpretation of angiogenesis assays. *Angiogenesis* **21**, 425–532 (2018).

227. Oladipupo, S. S. *et al.* Endothelial cell FGF signaling is required for injury response but not for vascular homeostasis. *Proceedings of the National Academy of Sciences of the United States of America* **111**, 13379–13384 (2014).

228. S., Vainikka, et al. Association of a 85-kDa serine kinase with activated fibroblast growth factor receptor-4. *Journal of Biological Chemistry* **271**, 1270–1273 (1996).

229. S., Vainikka, et al. Signal transduction by fibroblast growth factor receptor-4 (FGFR-4). Comparison with FGFR-1. *Journal of Biological Chemistry* **269**, 18320–18326 (1994).

230. A Peláez-García., et al. FGFR4 Role in Epithelial-Mesenchymal Transition and Its Therapeutic Value in Colorectal Cancer. *PLos One* **8**, e63695 (2013).

231. Dumont, D. J. *et al.* Vascularization of the mouse embryo: A study of flk-1, tek, tie, and vascular endothelial growth factor expression during development. *Developmental Dynamics* **203**, 80–92 (1995).

232. Tang, Y., Harrington, A., Yang, X., Friesel, R. E. & Liaw, L. The contribution of the Tie2+ lineage to primitive and definitive hematopoietic cells. *Genesis* **48**, 563–567 (2010).

233. Kaipainen, A. & Bielenberg, D. R. Hemangiogenesis versus lymphangiogenesis. *Encyclopedia of the Eye. Academic Press.* 227–232 (2010).

234. Mammoto, T. *et al.* Twist1 controls lung vascular permeability and endotoxin-induced pulmonary edema by altering Tie2 expression. *PloS One* **8**, e73407 (2013).

235. Hamada, N. *et al.* Anti-Vascular Endothelial Growth Factor Gene Therapy Attenuates Lung Injury and Fibrosis in Mice. *The Journal of Immunology* **175**, 1224–1231 (2005).

236. Philippeos, C. *et al.* Spatial and single-cell transcriptional profiling identifies functionally distinct human dermal fibroblast subpopulations. *Journal of Investigative Dermatology* **138**, 811–825 (2018).

237. Richardson, A. M. *et al.* Vimentin is required for lung adenocarcinoma metastasis via heterotypic tumor cell–Cancer-associated fibroblast interactions during collective invasion. *Clinical Cancer Research* **24**, 420–432 (2018).

238. Yu, W., Zhang, Y., Ruest, L. B. & Svoboda, K. K. H. Analysis of snail1 function and regulation by Twist1 in palatal fusion. *Frontiers in Physiology* **4**, 12 (2013).

239. Meng, J. *et al.* Twist1 regulates vimentin through Cul2 circular RNA to promote EMT in hepatocellular carcinoma. *Cancer Research* **78**, 4150–4162 (2018).

240. Liefeldt, L. *et al.* Effects of transgenic endothelin-2 overexpression on diabetic cardiomyopathy in rats. *European Journal of Clinical Investigation* **40**, 203–210 (2010).

241. Gallini, R., Lindblom, P., Bondjers, C., Betsholtz, C. & Andrae, J. PDGF-A and PDGF-B induces cardiac fibrosis in transgenic mice. *Experimental Cell Research* **349**, 282–290 (2016).

242. Liu, Z. C. *et al.* AKT/GSK-3β regulates stability and transcription of snail which is crucial for bFGF-induced epithelial-mesenchymal transition of prostate cancer cells. *Biochimica et Biophysica Acta - General Subjects* **1840**, 3096–3105 (2014).

243. Rodríguez-Nieves, J. A., Patalano, S. C., Almanza, D., Gharaee-Kermani, M. & Macoska, J. A. CXCL12/CXCR4 axis activation mediates prostate myofibroblast phenoconversion through non-canonical EGFR/MEK/ERK signaling. *PLoS One* **11**, e0159490 (2016).

244. Mao, S. P. H. *et al.* Loss of amphiregulin reduces myoepithelial cell coverage of mammary ducts and alters breast tumor growth. *Breast Cancer Research* **20**, 131 (2018).

245. Maroulakou, I. G., Oemler, W., Naber, S. P. & Tsichlis, P. N. Akt1 ablation inhibits, whereas Akt2 ablation accelerates, the development of mammary adenocarcinomas in mouse mammary tumor virus (MMTV)-ErbB2/Neu and MMTV-polyoma middle T transgenic mice. *Cancer Research* **67**, 167–177 (2007).

246. Bolós, V. *et al.* Notch activation stimulates migration of breast cancer cells and promotes tumor growth. *Breast Cancer Research* **15**, R54 (2013).

247. Ouderkirk-Pecone, J. L. *et al.* Myosin 1e promotes breast cancer malignancy by enhancing tumor cell proliferation and stimulating tumor cell de-differentiation. *Oncotarget* **7**, 46419–46432 (2016).

248. Williams, T. M. *et al.* Loss of caveolin-1 gene expression accelerates the development of dysplastic mammary lesions in tumor-prone transgenic mice. *Molecular Biology of the Cell* **14**, 1027–1042 (2003).

249. Rose-Hellekant, T. A. *et al.* Prolactin induces ERα-positive and ERα-negative mammary cancer in transgenic mice. *Oncogene* **22**, 4664–4674 (2003).

250. Wechselberger, C. *et al.* Human Cripto-1 overexpression in the mouse mammary gland results in the development of hyperplasia and adenocarcinoma. *Oncogene* **24**, 4094–4105 (2005).

251. Eilon, T. & Barash, I. Distinct gene-expression profiles characterize mammary tumors developed in transgenic mice expressing constitutively active and C-terminally truncated variants of STAT5. *BMC Genomics* **18**, 231 (2009).

252. Gökmen-Polar, Y. *et al.* Gene expression analysis reveals distinct pathways of resistance to bevacizumab in xenograft models of human ER-positive breast cancer. *Journal of Cancer* **5**, 633–645 (2014).

253. Hill, C. B. & Yeh, I. T. Myoepithelial cell staining patterns of papillary breast lesions: From intraductal papillomas to invasive papillary carcinomas. *American Journal of Clinical Pathology* **123**, 36–44 (2005).

254. Bumaschny, V. *et al.* Malignant myoepithelial cells are associated with the differentiated papillary structure and metastatic ability of a syngeneic murine mammary adenocarcinoma model. *Breast Cancer Research* **6**, 116–129 (2004).

255. English, D. P., Roque, D. M. & Santin, A. D. HER2 expression beyond breast cancer: Therapeutic implications for gynecologic malignancies. *Molecular Diagnosis and Therapy* **17**, 85–99 (2013).

256. Kerdivel, G., Flouriot, G. & Pakdel, F. Modulation of Estrogen Receptor Alpha Activity and Expression During Breast Cancer Progression. *Vitamins and Hormones* **93**, 135–160 (2013).

257. Iqbal, N. & Iqbal, N. Human Epidermal Growth Factor Receptor 2 (HER2) in Cancers: Overexpression and Therapeutic Implications. *Molecular Biology International* **2014**, 852748 (2014).

258. Huang, Y. *et al.* Improving immune-vascular crosstalk for cancer immunotherapy. *Nature Reviews Immunology* **18**, 195–203 (2018).

259. Garnier, L., Gkountidi, A. O. & Hugues, S. Tumor-associated lymphatic vessel features and immunomodulatory functions. *Frontiers in Immunology* **10**, 720 (2019).

260. Vleugel, M. M. *et al.* Lack of lymphangiogenesis during breast carcinogenesis. *Journal of Clinical Pathology* **57**, 746–751 (2004).

261. Chen, L., Endler, A. & Shibasaki, F. Hypoxia and angiogenesis: Regulation of hypoxia-inducible factors via novel binding factors. *Experimental and Molecular Medicine* **41**, 849–857 (2009).

262. Semenza, G. L. HIF-1: Using two hands to flip the angiogenic switch. *Cancer and Metastasis Reviews* **19**, 59–65 (2000).

263. Konerding, M. A. *et al.* Impact of fibroblast growth factor-2 on tumor microvascular architecture: A tridimensional morphometric study. *American Journal of Pathology* **152**, 1607–1616 (1998).

264. Yu, J. L., Rak, J. W., Klement, G. & Kerbel, R. S. Vascular endothelial growth factor isoform expression as a determinant of blood vessel patterning in human melanoma xenografts. *Cancer Research* **62**, 1838–1846 (2002).

265. Klagsbrun, M. & Moses, M. A. Molecular angiogenesis. *Chemistry and Biology* **6**, 217–224 (1999).

266. Shannon, R. P. Microvascular Research: Biology and Pathology. *Circulation* **113**, e763–e764 (2006).

267. R Strippoli, et al. Caveolin-1 deficiency induces a MEK -ERK 1/2-Snail-1-dependent epithelial–mesenchymal transition and fibrosis during peritoneal dialysis. *EMBO Molecular Medicine* **7**, 102–123 (2015).

268. T Tomoro, et al. Snail-Induced Epithelial-to-Mesenchymal Transition Enhances P-gp-Mediated Multidrug Resistance in HCC827 Cells. *Journal of Pharmacological Sciences* **106**, 2642–2649 (2017).

269. de Spiegelaere W., et al. Intussusceptive angiogenesis: a biologically relevant form of angiogenesis. *Journal of Vascular Research* **49**, 390–404 (2012).

270. Paku, S. *et al.* A new mechanism for pillar formation during tumor-induced intussusceptive angiogenesis: Inverse sprouting. *American Journal of Pathology* **179**, 1573–1585 (2011).

271. Mazumdar, S. *et al.* CoREST1 promotes tumor formation and tumor stroma interactions in a mouse model of breast cancer. *PloS One* **10**, e0121281 (2015).

272. Hillers-Ziemer, L. E. *et al.* Obesity promotes cooperation of cancer stem-like cells and macrophages to enhance mammary tumor angiogenesis. *Cancers* **12**, 502 (2020).

273. Delfortrie, S. *et al.* Egfl7 promotes tumor escape from immunity by repressing endothelial cell activation. *Cancer Research* **71**, 7176–7186 (2011).

274. Stetler-Stevenson, W. G. Matrix metalloproteinases in angiogenesis: A moving target for therapeutic intervention. *Journal of Clinical Investigation* **103**, 1237–1241 (1999).

275. Kudo, Y. *et al.* Matrix metalloproteinase-13 (MMP-13) directly and indirectly promotes tumor angiogenesis. *Journal of Biological Chemistry* **287**, 38716–38728 (2012).

276. Deryugina, E. I. & Quigley, J. P. Tumor angiogenesis: MMP-mediated induction of intravasation- and metastasis-sustaining neovasculature. *Matrix Biology* **44**, 94–112 (2015).

277. M Mongiat., et al. Extracellular Matrix, a Hard Player in Angiogenesis. *International Journal of Molecular Sciences* **17**, 1822 (2016).

278. Huijbers IJ., et al. A Role for Fibrillar Collagen Deposition and the Collagen Internalization Receptor Endo180 in Glioma Invasion. *PLoS One* **5**, e9808 (2010).

279. Maehira H., et al. Vimentin Expression in Tumor Microenvironment Predicts Survival in Pancreatic Ductal Adenocarcinoma: Heterogeneity in Fibroblast Population. *Annals of Surgical Oncology* **26**, 4791–4804 (2019).

280. Hewitt, R. E. *et al.* Laminin and collagen IV subunit distribution in normal and neoplastic tissues of colorectum and breast. *British Journal of Cancer* **75**, 221–229 (1997).

281. Exposito, J. Y., Valcourt, U., Cluzel, C. & Lethias, C. The fibrillar collagen family. *International Journal of Molecular Sciences* **11**, 407–426 (2010).

282. P Baluk., et al. Abnormalities of Basement Membrane on Blood Vessels and Endothelial Sprouts in Tumors. *The American Journal of Pathology* **163**, 1801–1815 (2003).

283. U.S. Food & Drug Administration. Link: https://www.fda.gov/drugs/drug-approvals-and-databases/fda-approves-olaparib-plus-bevacizumab-maintenance-treatment-ovarian-fallopian-tube-or-primary (2020).

284. P Mukhopadhyay., et al. PARP inhibition protects against alcoholic and non-alcoholic steatohepatitis. *Journal of Hepatology* **66**, 589–600 (2017).

285. Kong, D. H., Kim, M. R., Jang, J. H., Na, H. J. & Lee, S. A review of anti-angiogenic targets for monoclonal antibody cancer therapy. *International Journal of Molecular Sciences* **18**, 1786 (2017).

286. Qian CN., et al. Revisiting tumor angiogenesis: vessel co-option, vessel remodeling, and cancer cell-derived vasculature formation. *Chinese Journal of Cancer* **35**, 10 (2016).

287. Relf, M. *et al.* Expression of the angiogenic factors vascular endothelial cell growth factor, acidic and basic fibroblast growth factor, tumor growth factor β-1, platelet-derived endothelial cell growth factor, placenta growth factor, and pleiotrophin in human primary br. *Cancer Research* **57**, 963–969 (1997).

288. Maiuri, M. C. & Kroemer, G. Essential role for oxidative phosphorylation in cancer progression. *Cell Metabolism* **21**, 11–12 (2015).

289. Eales, K. L., Hollinshead, K. E. R. & Tennant, D. A. Hypoxia and metabolic adaptation of cancer cells. *Oncogenesis* **5**, e190 (2016).

290. Vallée, A., Lecarpentier, Y. & Vallée, J. N. Thermodynamic aspects and reprogramming cellular energymetabolism during the fibrosis process. *International Journal of Molecular Sciences* **18**, 2537 (2017).

291. Nair, S. S. & Kumar, R. Chromatin remodeling in Cancer: A Gateway to regulate gene Transcription. *Molecular Oncology* **6**, 611–619 (2012).

292. Sebastián, C. *et al.* The histone deacetylase SIRT6 Is a tumor suppressor that controls cancer metabolism. *Cell* **151**, 1185–1199 (2012).

293. Bellelli, R. *et al.* Polε Instability Drives Replication Stress, Abnormal Development, and Tumorigenesis. *Molecular Cell* **70**, 707–721 (2018).

ACKNOWLEDGEMENTS

Primero de todo, me gustaría agradecer a Antonio haberme dado la oportunidad de trabajar en su laboratorio y siempre tener la puerta de su despacho abierta. A Raúl, muchas gracias por enseñarme un millón de técnicas, conceptos e ideas y probarlas de un montón de formas diferentes para sacar el proyecto adelante. Pero, sobre todo por estar 24/7 conectado para cualquier tipo de duda. Estos cuatros años han supuesto un tiempo de aprendizaje enorme, muchas gracias a los dos.

Bea, la alegría del Sur. Me llevo solo salados recuerdos de ti. Eres como el vino, cuánto más años pasan, más vales. A Willy (x2), Marina, Héctor, Aida, Rubén y la recién 'diamante' llegada al lab, Laura, por vuestra compañía, los pedidos de Groupon y por aguantar mi música en el lab. ¡Muchos ánimos con todo! A Laura (grado), muchas gracias por colaborar en el proyecto.

Asya, I hope only the BEST for such a powerful woman like you are. Sara, te como la cara, que joyita que eres.

Al Chromatin Team, por el tiempo compartido estos años. Habéis dejado huella en el laborotario.

Al pasillo del IMIM: Cristina, Jeni, Laura (Mañas), Anna, *Moon*, Budour… muchas gracias por todo. Marta Garrido, tienes la fuerza de mil huracanes y un terremoto. Un modelo vital a seguir.

Laura y Marta (máster), fuisteis como una brisa de aire fresco frente a la playa. Solo os puedo decir que las coincidencias del destino están por algún motivo, y eso me alegra.

Nayomi, eres un ángel en la tierra, y poco más se puede añadir a un ser de semejantes dimensiones de amor. Cati, el ser buena persona se nota y se siente. Iván, tienes un gran futuro por delante, ole tú.

Agradecer obviamente a los Bigas, Jessica siempre un amor, David y Violeta que son unos cachos de pan, Luis que es un rayito de sol e Irene la loca, reina de Castilla.

Pilar y Rosi, me habéis alegrado muchísimo las tardes y me habéis hecho sentir parte de una familia allí.

Marisol, me has regañado como un hijo, pero también cuidado como un hijo. Eres un Sol.

¡Sin olvidarme de los niños de las prácticas! Ha sido un honor y una alegría estar con vosotros. Mil gracias por demostrar que las nuevas generaciones valen y mucho.

Realmente pensar en cómo he vivido en Barcelona es pensar en 'EL' piso. Literalmente los mejores momentos en Barcelona los he vivido allí, o relacionados con él. Me encantaba que el piso fuera siempre una caja de sorpresas… *Roomie* y Judith, sois lo mejor en todos los sentidos posibles. Solo os puedo agradecer que cuando buscabais compañero/a de piso, contaseis conmigo. Ha sido un verdadero DISFRUTE vivir con vosotras.

Y Judith, tú has sido lo mejor que me llevo de Barcelona. Realmente, una hermana adoptiva. Que alegría de habernos encontrado en el camino.

Estelaaaaa y Álvaro, mil gracias por todo lo que me habéis ayudado y por hacerme sentir que os tenía en Barcelona.

Desi, eres una ARTISTAZA y un cachito de pan azucarado. Gracias por todo y por las mejoras en la portada de la tesis.

Por supuesto a Spotify, que ha puesto la banda sonora a toda esta aventura.

Y por supuesto, no podía faltar un ¡Arriba ANDALUCÍA y DOS HERMANAS!

Y mención especial a mi familia, abuelas… y a mis padres, que me han apoyado en cada paso que he dado y en cada decisión, aunque ello supusiera estar a cientos de kilómetros e incluso durante una pandemia. Os quiero mucho y os agradezco todo lo que me habéis dado y enseñado.

Esta tesis va dedicada a todos aquellos que han, están o van a emigrar para labrarse un mejor futuro. Diferentes tiempos, mismas razones.

Erratum

After presenting the thesis to the PhD Commission and the members of the Evaluation Board we realized that the cell line used in this work and named immortalized HUVEC indeed corresponded to ECV-304. Since some reports indicate that these cells are not endothelial cells, we have repeated the most relevant experiments of the in vitro cell culture part with the human microvascular endothelial cells 1 (HMEC-1) obtained from ATCC through Dr. Diaz-Ricart. The results obtained with these cells are compatible with the main conclusions of our work.